Qualitative Analysis for

Dynamic Behavior of Railway Ballasted Track

vorgelegt von

Dipl.-Ing. Jungyoul, Choi

aus Seoul, Süd Korea

Von der Fakultät V - Verkehrs- und Maschinensysteme

der Technischen Universität Berlin

Zur Erlangung des akademischen Grades

Doktor der Ingenieurwissenschaften

- Dr.-Ing. -

genehmigte Dissertation

Promotionsausschuss:

Prof. Dr.-Ing. Jürgen Thorbeck (Vorsitzender)

Prof. Dr.-Ing. habil. Jürgen Siegmann (Erstberichter)

Prof. Dr.-Ing. habil. Danuta Bryja (Zweitberichterin)

Tag der wissenschaftliche Aussprache: 06. Januar 2014

Berlin 2014

D 83

Qualitative Analysis for

Dynamic Behavior of Railway Ballasted track

By

M.Sc. Jungyoul, Choi

from Seoul, South Korea

A Thesis

Submitted to Faculty of Mechanical Engineering and Transport Systems

Department of Track and Railway Operations - TU Berlin - Berlin - Germany

TU Berlin (Berlin Institute of Technology)

in Fulfillment of the Requirement for the Degree of

Doctor of the Railway Engineering

Approved Dissertation

Promotion Committee:

Chairman: Prof. Dr.–Eng. Jürgen Thorbeck (TU Berlin, Germany)

Referee: Prof. Dr.–Eng. habil. Jürgen Siegmann (TU Berlin, Germany)

Referee: Prof. Dr.–Eng. Danuta Bryja (TU Wrocław, Poland)

Day of scientific debate: 06 .01. 2014

Berlin 2014

D 83

ACKNOWLEDGEMENTS

This work could not have been completed without the support of a number of people to whom I am deeply grateful. I thank all of my Dissertation Committee members for their advice and suggestions.

Especially to my supervisor, Prof. Dr.–Eng. habil. Jürgen Siegmann, I greately appreciate his excellent guidance, inspiration and supervision throughout this thesis; without his support, this thesis would not have been possible.

I would also like to express my gratitude to my examiners, Prof. Dr.–Eng. habil. Danuta Bryja and Prof. Dr.–Eng. Jürgen Thorbeck, for their invaluable advice.

All colleagues in the Department of Track and Railway Operations of TU Berlin, in particular Dr. Yin-Hung Lin, Dr. Mahmoud Mousa Ali, Dipl. Reinhold Wassmann and Dipl. Christian Weise for their encouragement and friendship.

I truly appreciate the help and valuable research resource support I received from Prof. Yong-gul Park of Seoul National University of Science and Technology throughout this thesis. I am also thankful for the assistance with measurement from all colleagues in Seoul National Unisversity of Science and Technology.

Finally, I want to extend my most gracious and special thanks to my family. Without their endless support, belief and encouragement, this could not have been completed.

Jungyoul Choi

January 2014

TABLE OF CONTENTS

ABSTRACT

Because track structures subjected to dynamic loading are usually constructed from different materials and components, their behavior cannot be easily verified or predicted. The design, repair, and effective maintenance of tracks are therefore critical for ballasted track performance assessment. Moreover, low reliability of input variables used in ballasted track analysis can have a potentially large effect on the solution. If the uncertainty in input data could be considered by a range of values rather than a single value, a more reliable design and satisfactory maintenance measures for the entire range of input values could be achieved.

In this study, theoretical, experimental, analytical, and statistical evaluations were performed to predict and assess the track support stiffness, track impact factor, dynamic wheel-rail forces, and subgrade modulus. Field measurements for evaluating the dynamic characteristics of a ballasted track and its components were performed; their results reveal a correlation between track support stiffness and the corresponding track response. The track support stiffness directly affects the track response and the entire ballasted track system, implying that the response should ideally be a function of the stiffness.

A qualitative analysis–based dynamic behavior prediction model for ballasted tracks (qualitative prediction model) was developed to predict and assess track performance as a function of dynamic vehicle loading and track support stiffness variation. The prediction model consists of a two-degrees-of-freedom dynamic track model and modified track properties, which define the rail pad and ballast stiffness ranges, based on designed and measured values. The qualitative prediction model for dynamic track behavior, capable of simulating the complex interaction between the track's component properties and track responses, was developed in this study. The qualitative analysis results are presented as a discrete space area of various track responses and parameters, instead of single values. The dynamic behavior of in-service ballasted tracks can be qualitatively predicted by the proposed qualitative analysis map as a function of the rail pad and ballast stiffnesses, and a simple field test. This new approach is expected to facilitate track behavior assessment by owners based on more realistic track conditions, as well as reduce inaccuracies and deliver results that are consistent with the prediction results of in-service track responses using single design values.

KURZFASSUNG

Schottergleise sind infolge ihrer dynamischen Belastungen und weil sie aus verschiedenen Materialien und Komponenten bestehen, nicht leicht zu prüfen und in ihrem Verhalten vorherzusagen. Für die Beurteilung der Schotteroberbauqualität sind daher Gleisdesign, Instandsetzung und effektive Wartung wichtig. Zudem kann eine unzureichende Zuverlässigkeit der Input-Variablen, die in der Beurteilung von Schotteroberbaukonstruktionen und deren Zustandsprognosen im Betrieb verwendet werden, eine große Wirkung auf das Ergebnis haben.

In dieser Studie wurden theoretische, experimentelle, analytische und statistische Analysen durchgeführt, um Gleissteifigkeit, Gleis-Impaktfaktor, dynamische Rad-Schiene-Kräfte und Gleisbettmodul zu modellieen und ihr Langzeitverhalten im Betrieb vorherzusagen. Es wurde festgestellt, dass eine gewisse Korrelation zwischen der Gleissteifigkeit und der entsprechenden Gleisreaktion besteht. Die Gleissteifigkeit wird hauptsächlich von der Gleisreaktion und dem gesamten Schottergleissystem beeinflusst. Die Schottergleisreaktion sollte daher idealerweise eine Funktion der Gleissteifigkeit sein.

In dieser Studie wird ein Vorhersagemodell zum dynamischen Verhalten des Schottergleises entwickelt unter Anwendung einer qualitativen Analysemethode, das der Vorhersage und Beurteilung der Gleislebensdauer unter dynamischer Fahrzeugbelastung und sich verändernder Gleissteifigkeit dient. Das vorgeschlagene qualitative Vorhersagemodell besteht aus einem dynamischen Gleismodell mit zwei Freiheitsgraden (2DOF) und modifizierbaren Gleiseigenschaften, die den Bereich von Schienenunterlage und Schottersteifigkeit, basierend auf Anfangsswerten und im späteren Verlauf gemessenen Werten definieren.

Das qualitative Modell zur Vorhersage dynamischen Verhaltens des Gleises, das die komplexe Interaktion zwischen den Eigenschaften der Gleiskomponenten und der entsprechenden Gleisreaktion zu simulieren vermag, wurde innerhalb der vorliegenden Studie erarbeitet und verifiziert. Die Ergebnisse der qualitativen Analyse werden als diskrete Fläche der verschiedenen Gleisreaktionen und Parameter dargestellt. Das dynamische Betriebsverhalten von belasteten Schottergleisen kann durch die Analysenkarten und den dynamischen Gleisreaktionen vorhergesagt werden. Es ist zu erwarten, dass sich hiermit die Qualität der Prognose der zu erwartetenden Qualität von Schottergleisen unter Betrieb erhöht und die Auswirkungen von Instandhaltungsmaßnahmen noch besser beurteilt werden können.

LIST OF FIGURES

LIST OF TABLES

1 INTRODUCTION

A railway ballasted track was inevitably affected by various parameters such as environmental and mechanical conditions during a service, thus it is degrading and deteriorating. Because railway ballasted track structures subjected to dynamic loading are usually constructed from different materials and components, their behavior cannot be easily verified or predicted. It is important to assess that the strategic planning of maintenance or renewal work for the ballasted track concerned with the actual condition of track and deterioration. However, the structural conditions of railway ballasted tracks are typically not confirmed either before or after maintenance procedures. In addition, the experimental or numerical method would be lead to unreliable results due to a lot of unpredictable problems in the actual ballasted track such as nonlinearity and irregularity that is attributed to voided sleeper, track irregularity, wheel-rail surface roughness and degraded rail pad and ballast (gravel). The structural integrity and current condition of railway ballasted tracks is limited to finding the information. The design, repair, and effective maintenance of tracks are therefore critical for ballasted track performance assessment. Moreover, low reliability of input variables used in ballasted track analysis can have a potentially large effect on the solution. The dynamic characteristics of the in-service ballasted track were higher and more roughly distributed over a wider range than the design value used for the design and construction. If the uncertainty in input data could be considered by a range of values rather than a single value, a more reliable design and satisfactory maintenance measures for the entire range of input values could be achieved.

The dynamic response of railway ballasted track would be affected by several parameters such as rail pad and ballast stiffness, rail surface roughness, track components condition and the other things. Among of these parameters, the principal parameter was the rail pad and ballast stiffness that was related in the track support stiffness. Therefore, a qualitative analysis, which define the rail pad and ballast stiffness ranges based on the measured and initial design values, would be more suitable in simulating the track behavior, because the current assessment method which use a single value as there is a significant difference between the initial design values and field measurement results.

In this study, prior to developing the qualitative prediction model, theoretical, experimental, analytical, and statistical evaluations were performed to predict and assess the track support stiffness, track impact factor, dynamic wheel-rail forces, track displacement, and subgrade modulus. Field measurements for evaluating the dynamic characteristics of a ballasted track and its components were performed.

A qualitative analysis–based dynamic behavior prediction model for ballasted tracks (qualitative prediction model) was developed to predict and assess track performance. The qualitative prediction model consists of a two-degrees-of-freedom (2DOF) dynamic track model and modified track properties, which define the rail pad and ballast stiffness ranges, based on designed and measured values. The qualitative prediction model for dynamic track behavior, capable of simulating the complex interaction between the track's component properties and track responses, was developed in this study.

The qualitative analysis results are presented as a discrete space area of various track responses and parameters, instead of single values. The dynamic behavior of in-service ballasted tracks can be qualitatively predicted by the proposed qualitative analysis map as a function of the rail pad and ballast stiffnesses, and a simple field test.

An outline of the rest of the research is as follows.

In Section 2, the fundamental information of typical railway ballasted track, its structural components and track dynamics in the literature are overviewed. This section is focused on identifying principal functions of track components. And it provides the fundamental information for typical resonance frequencies and the associated modes of ballasted track vibrations.

In Section 3, an overview of the theoretical background for numerical simulation of the ballasted track focused on track support stiffness (track receptance) and mechanical ballasted track models in the literature are presented.

In Section 4, the influence of typical track defects on the stiffness and damping of track components (the rail and ballast) is presented. The methodology presented in Section 4 is adopted from literature (the mothod proposed by Kaewunruen and Remennikov). It is possible to determine experimentally the fundamental track parameters which are required in numerical simulations of track vibrations, and also are useful for an assessment of track response using the qualitative analysis. To extract the stiffness and

damping parameters of the ballast and rail pad, a 2DOF model of the track is introduced. And, the curve fitting technique is applied to frequency response functions expressed analytically in terms of physical parameters and modal parameters of 2DOF model.

In Section 5, the relationship between track impact factor and track support stiffness are evaluated using field measurement. The track impact factor of ballasted tracks (with good and bad ballast conditions) and slab tracks (elastic fastening system, rail floating system, and sleeper floating system) were measured and compared to evaluate the effects of track structure and dynamic wheel load on the service line. In addition, it is suggested that the track impact factor of actual tracks should be evaluated in terms of the track support stiffness of different types of tracks.

In Section 6, the results of prediction of displacement on the ballasted track using finite element analysis and field measurement are presented. The measured track impact factor was applied to the derived time history function of the finite element analysis in order to predict the train-induced track displacement under real conditions, which included curved and the track conditions.

In Section 7, the relationship between dynamic wheel-rail forces, rail surface roughness and track support stiffness are evaluated using field measurement and qualitative analysis. Theoretical, empirical, and statistical analyses were performed and a prediction equation for the peak dynamic forces was developed.

In Section 8, the results of prediction of subgrade modulus on the in-service ballasted track using field measurement, finite element analysis and qualitative analysis are presented. The subgrade modulus of in-service ballasted tracks was calculated by measuring the dynamic response of a tested track using an empirical conventional equation, and this value was compared with the design value obtained from a plate load test. The subgrade modulus was further predicted from a proposed subgrade modulus map developed from the results of field tests and empirical equations for comparison with the design value.

In Section 9, the qualitative prediction model for dynamic track behavior, capable of simulating the complex interaction between the track's component properties and track responses, is developed. The qualitative prediction model consists of a 2DOF dynamic track model and modified track properties, which define the rail pad and ballast stiffness ranges, based on designed and measured values. In the qualitative analysis, the

measurement results of the variable parameter of track components and track response of Section 5–8 was used. The qualitative analysis results are presented as a discrete space area of various track responses and parameters, instead of single values.

In Section 10, conclusions are drawn and further research is discussed.

This thesis consists of 4 appended papers that peer-reviewed and published during the period of dissertation work. The appended papers are:

• PAPER A (Section 5) : Jungyoul Choi, Influence of track support stiffness of railway tracks on track impact factor. ASCE, *Journal of Engineering Mechanics*, 10.1061/EM.1943-7889.0000744 (2013).

• PAPER B (Section 6) : Jungyoul Choi, Prediction of displacement induced by tilting trains running on ballasted tracks through measurement of track impact factors. *Engineering Failure Analysis* 31 (2013) 360–374.

• PAPER C (Section 7) : Jungyoul Choi, Influence of track support stiffness of ballasted track on dynamic wheel-rail forces. ASCE, *Journal of Transportation Engineering*. 139 (2013) 709–718.

• PAPER D (Section 8) : Jungyoul Choi, Experimental study on estimation of subgrade modulus of in-service ballasted tracks. Submitted 2013 for publication in ASCE, *Journal of Transportation Engineering*.

2 FUNDAMENTAL INFORMATION OF TYPICAL BALLASTED TRACK -LITERATURE REVIEW

2.1 Introduction

The dynamic parameters of railway tracks, such as natural frequency, damping constant, and corresponding vibration mode shape, are of substantial importance in the procedures needed for analysis and design of railway tracks [40, 41, 86]. In several countries, the traditional railway track system is the ballasted track, i.e., consists of rail, rail pad, and concrete or wooden sleeper on ballast and subgrade [41, 86]. Recently, the increase in frequency of traffics, the heavier loads, and the higher vehicle speed have a significant factor increasing to the deterioration or damage and maintenance or repair of the track system [41, 86].

Recently, several railway engineers have focused on the actual bearing capacity of track components under realistic load to develop the advances in design of railway infrastructure [41, 85–88]. At present, researchers over the world have investigated and studied that the knowledge related to the dynamic behaviors of ballasted track's components; prestressed concrete sleepers, rail pads, and others [41, 85–88]. The better findings for the static and dynamic responses of track component have researched to improve the capacity of existing railway ballasted tracks and the economical analysis and design [41, 58, 60, 61, 63, 64, 85–88, 93, 94, 153].

Railway track is a fundamental part of railway infrastructure and its components are divided into superstructure and substructure [41, 86, 114]. The most observable parts such as the rails, rail pads, sleepers, and rail fastening systems are referred to as the superstructure while the substructure is associated with a geotechnical system consisting of ballast, sub-ballast and subgrade [41, 86, 114]. Several researchers over the world have investigated and introduced that various dynamic testing approaches for railway tracks and its components, especially focused on the rails, sleepers, rail fastering systems including rail pads and ballasts [41, 58, 60, 61, 63, 64, 85–88, 93, 94, 153].

In this section, the structural component of ballasted track was introuduced and briefly the dynamics of its components have reviewed. And, a part of the technical procedures and testing methodology for dynamic characteristics of track components such as rail

pads, prestressed concrete sleepers have been reviewed and summarized. Previous analytical vibration model of railway track have also reviewed.

2.2 Components of ballasted track

Railway track is a fundamental part of railway infrastructure can be classified by superstructure and substructure [41, 86, 114]. The most primary parts of the track as the rails, rail pads, sleepers (ties), and rail fastening systems (fastenings) are referred to as the superstructure, while the substructure is consisted with a geotechnical layer consisting of ballast (gravel), sub-ballast and subgrade (formation and base) [41, 86, 114]. The typical shape and construction profiles of a ballasted track are shown in Fig. 2.1.

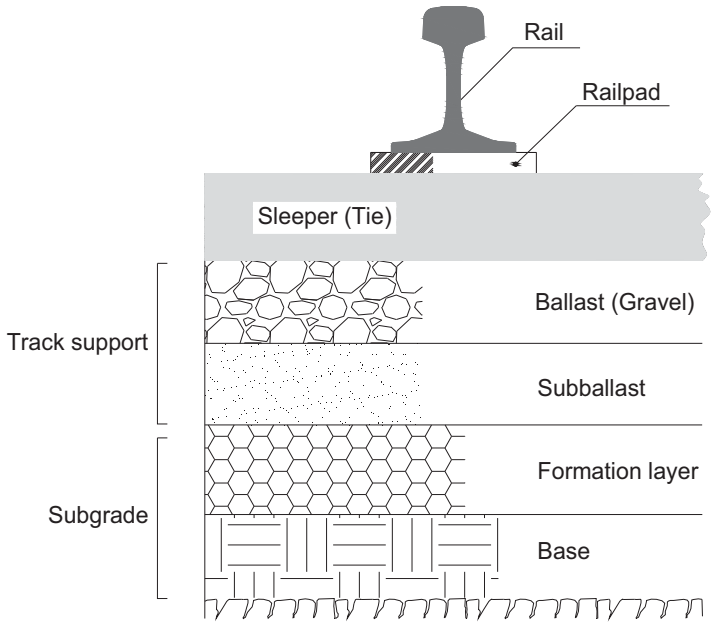

Fig. 2.1 Schematie of typical railway ballasted track

2.2.1 Rails

Rails are longitudinal members made by steel that are placed on spaced sleepers to guide the rolling stock [41, 86]. Their strength and stiffness must be sufficient to maintain a steady shape and smooth track configuration, and resist various forces by vehicles [41, 86, 114, 160]. The principal function of the rail is to accommodate and transfer the wheel loads onto the supporting sleepers. Esveld presented that a modern rail track also conveys signals and acts as a conductor on an electrified line [41, 86, 114].

Table 2.1 describes typical rail profiles and their applications [41, 86]. The most commonly used profile is flat-bottom rail, also called Vignole rail, and the rail is divided into three parts according to its geometrical and mechanical fuctions: rail head (the top surface that contact with the wheel), rail web (the middle part that supports the rail head) and rail foot (the bottom part that distributes the wheel load from the web to the underlying superstructure components) [41, 86, 114].

Table 2.1 Types of rail and their applications [41, 86]

Shape	Profile type	Applications
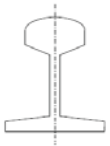	Flat-bottom rail	Standard railway track
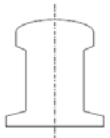	Construction rail	Manufacturing of automobiles and switch parts
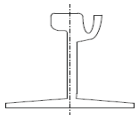	Grooved rail	Railway track embedded in pavements, roads, yards
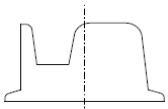	Block rail	Railway track used in concrete slab as part of Nikex-structure
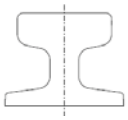	Crane rail	Heavy load hoisting cranes with high wheel loads

2.2.2 Rail fastening systems

The rail fastening system or fastenings includes every component that connects the rail to the sleeper including fastener and rail pad. Fastenings clamp the rail gauge within acceptable tolerances and then absorb forces from the rails and transfer them to the sleepers [41, 86, 114]. Vibration and impact are also dampened and decelerated by fastenings [41, 86, 114]. Fastenings also act as electrical insulation between the rail and the sleepers [41, 86, 114]. The principal components of the fastenings are fastener and rail pad [41, 86]. A typical fastening system for concrete sleeper used in Republic of Korea is shown in Fig. 2.2. The typical fastening system for concrete sleeper is consisting of rail pads, fasteners (clip), Y-type shoulders.

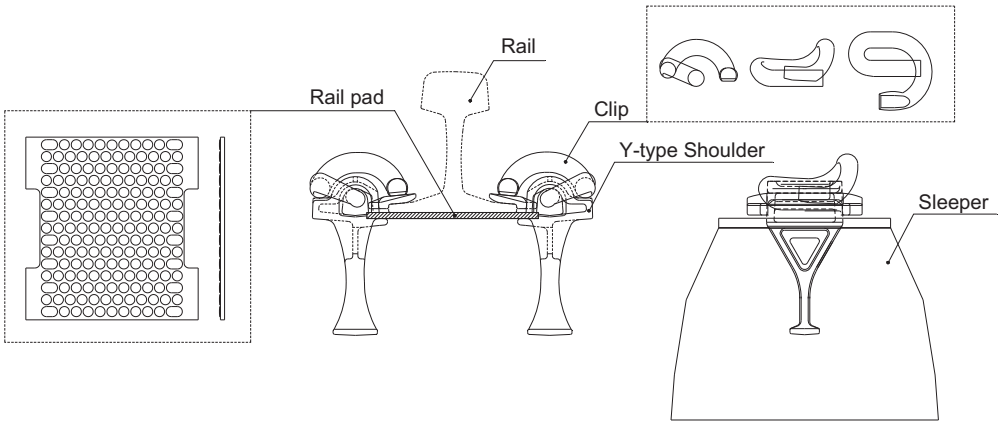

Fig. 2.2 Typical fastening systems

As shown in Fig. 2.3, there are a number of different types of fasteners which was depend on the geometrical characteristics of fastener and the sleeper types [41, 86, 114, 164, 171]. The fasteners withstand the vertical, lateral, and longitudinal forces on the rails, and keeping the place of the rails [41, 86, 114]. The fastener especially transfers the longitudinal forces due to the change of temperature to the adjacent sleepers [41, 86, 114].

(a) Pandrol clip (PR-type)

(b) Pandrol clip (e-type)

(c) Pandrol clip (fast clip)

(d) Vossloh tension clamp

Fig. 2.3 Types of fasteners for concrete sleepers

Rail pads are usually installed on rail supporting points to reduce and transfer the stress and dynamic forces from rails to the sleepers [41, 86, 114]. Rail pads are very important

because they reduce the interaction force between the rail and the sleepers [41, 86, 114]. Further, the rail pads provides a resilience function between rail and sleeper that helps absorb shock and impact from the wheels to the rails, and reduce a damage of rail supporting point and contact abrasion [41, 86, 114]. Several models of rail pads had been reviewed and introduced in the time or frequency domain, and the dynamic parameters of the rail pad were investigated experimentally [41, 86, 174, 175].

2.2.3 Sleepers

Sleepers are transverse beams resting on ballast and support [41, 86]. Wooden sleepers were used in the past because timber was used in several cuntries [41, 86]. However, pre-stressed or reinforced concrete sleepers, and to a limited extent steel sleeper, have been adopted in modern railway tracks over the past decades because of their durability and long service life [41, 86]. Esveld have introduced that classified of timber sleepers into two types: softwood (pinewood) and hardwood (beech, oak, tropical tree) [41, 86]. Concrete sleepers are described as either twin-block or mono-block, and are shown in Fig. 2.4 [41, 52, 86]. The concrete sleepers are widely used, because they are relatively not affected by environmental effect (including circumstance effect) [41, 86].

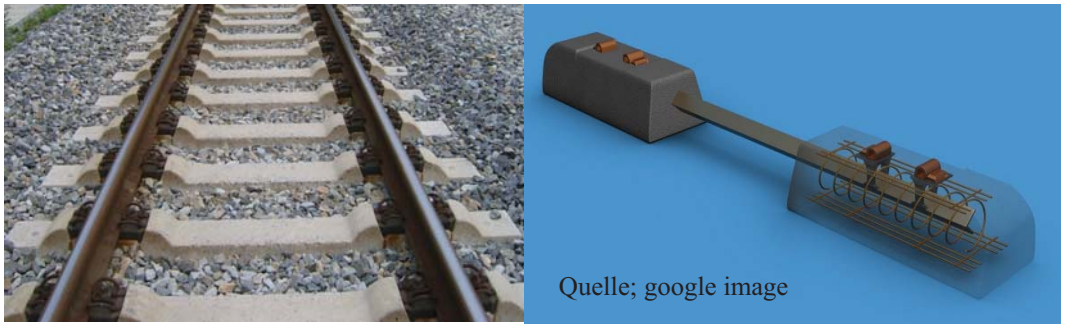

(a) Mono block concrete sleeper (b) Twin block concrete sleeper

Fig. 2.4 Types of concrete sleepers

The important functions of sleepers are [41, 86, 114]:

• To uniformly transfer and distribute loads from the rail to the ballast bed [86];

• To provide an anchorage for the fastening system that holds the rails at their correct gauge and preserves inclination, and [86]

• To support the rail and restrain longitudinal, lateral and vertical movement by embedding itself onto the substructures [86].

2.2.4 Ballast

Ballast is an elastic support layer to support sleepers and transfer the forces from the rail and sleeper to the sub-ballast [41, 86]. This layer comprises graded crushed stone, gravel, and crushed gravel such as granite and basalt and it also drains water from the rails and sleepers [41, 86].

Thus, ballast provides a stability of sleeper by distributing uniformly over the sub-ballast and subgrade (as shown in Fig. 2.5) [41, 86]. According to previous researches, the basic functions of ballast have summarised as follows [41, 73, 86, 160].

• Resist vertical, lateral and longitudinal forces applied to the sleepers, to retain the track in its position because the interlocking of irregularly shaped ballast tends to confine the sleepers [86];

Fig. 2.5 Photographs of in-situ ballasts

• Absorb impact from the rough particles as a spring element with limited action [86];

• Give resiliency and energy absorption to the sleeper [86];

• Reduce bearing stresses from the sleeper to acceptable stress levels [86];

• Allow suitable global and local track settlement [86];

• Avoid freezing and melting (thawing) problems by frost [86];

• Provide an insulating layer and fast drainage of fluid [86];

• Absorb airborne noise, and facilitate reconstruction of the track [86].

2.2.5 Sub-ballast

Sub-ballast is a layer of granular material between the ballast and underlying subgrade [41, 86]. According to [86], sub-ballast is composed of broadly graded slag or crushed aggregate, although a broadly graded sand-gravel compound is used [41, 86]. General functions of sub-ballast are presented in [41, 86]:

• Reduce stress at the bottom of the ballast layer to a reasonable level for the top of the subgrade [86];

• Prevent inter-penetration from the upward migration of fine particles from the layer of subgrade to the upper layer of ballast [86];

• Provide drainage that is ascribed to the non-obstructed voids by inter-penetration [86];

• Act as a shedding layer to keep water away from subgrade [86];

• Protect the subgrade from attrition by the hard ballast; and [86]

• Inhibit freezing and thawing problems in the subgrade [86].

2.2.6 Subgrade

Subgrade is also referred to as the formation [86]. It includes the existing soil and rock, which possess slopes, ditches and other structures or materials within [86]. The subgrade is the last support, i.e., bearing and distributing the dynamic loading resultant downward [86]. This layer must have sufficient bearing capacity, provide good drainage and provide a smooth settlement to ensure track serviceability [86]. Recently, some synthetic materials (e.g, geotextile, fabric, etc.), have applied to improving the subgrade performance [86].

2.3 Dynamics of rail pads

The standard rail pads used in the railway ballasted track are usually made from rubber and polymeric compound materials (EVA; Ethylene vinyl acetate, TPU; Thermoplastic polyurethane, etc.) [41, 86, 87, 100, 114]. Rail pads are installed on rail supporting points to reduce the dynamic stress from vehicle loads and dynamic wheel impact force [41, 86, 114]. These rail pads are very important because of it have reduce the dynamic effect between rail and sleepers [41, 86, 114]. Inappropriate or inadequate uses of rail pads increase the damage and defect of sleeper such as cracks at rail seat [41, 86, 114]. Further, the wrong use of rail pads increases high settlements of tracks, and ballast/subgrade breakage [41, 86, 87]. This negative effect affects on the capacity and integrity of an entire railway ballasted track system [41, 86, 114].

Several researches have demonstrated the dynamic behaviour of rail pads mathematically (linear or nonlinear models) [41, 50, 86–88, 100, 114, 174, 175]. Dynamic rail pad models are usually on both time and frequency domain [41, 50, 78, 86, 90, 97–100, 114, 174, 175]. The previous studies show the frequency domain model implicates dynamic properties such as resonant frequencies and damping [41, 49, 50, 78, 86, 90, 97–100, 114, 174, 175]. According to Fenander, a suitable fractional derivative model with a linear relationship was developed and adopted to a linear model [50, 51, 86].

A time domain model with compressive actions has developed at the frequency and dynamic amplitude [86, 163]. The developed various rail pad models have provided the nonlinear shape factor, neo-Hookean hyper-elastic model, fractional derivative element model, and Coulomb forcing function [86, 100, 163]. According to Knothe et al., the equivalent complex stiffness of rail pads with a frequency dependent model can be approximated by a bi-linear function [86, 100].

According to Grassie, the properties of a number of rail pads with different materials (synthetic and natural rubber, plastics, and composites) and surfaces (plain, grooved and studded surfaces) have investigated in the laboratory and on a track [59, 86]. The dynamic stiffness of rail pad is higher than the tangent stiffness from the load deflection curves [59, 86]. Further, the damping of rail pad has almost no affect on the dynamic response of a well compacted ballasted track, while higher damping of rail pad causes the rail pad to excite itself [59, 86, 100]. According to Fenander and Verheij, the

vertical stiffness and damping of several rail pads on a complete track including studded rail pad have investigated [50, 86, 184]. The stiffness of rail pad tends to increase with preload and excitation frequency [50, 86, 184].

According to Van't Zand, the dynamic characteristics of rail pad was assessed by performing fast fourier transform (FFT) technique using impact load tests [86, 183]. The curve fitting method was used for a single-degree-of-freedom (SDOF) equation of motion to the measured data, i.e., at a specific frequency of 400–2,000 Hz [86, 183]. Recently, this method was applied and extended to the urban track structures [40–42, 86]. Thompson et al. developed an indirect method for measuring the high frequency dynamic stiffness of resilient elements by applying the theory of 2DOF system [86, 174].

Another rail pad test have constructed based on the SDOF model, to examine their dynamic properties are considered to the elastic components (tuned masses, preloading springs and elastic supports) in the laboratory [35, 36, 86]. Recently, according to Knothe et al., the quasi-static and dynamic measurements of resilient rubber pads were performed in the low frequency (0–40 Hz) and high frequency range (100–2,000 Hz) [86, 100]. The equivalent stiffness of rail pad increased with increasing preload and decreasing amplitude [86, 100]. These test results showed the hyper-elastic action (visco-plastic action) of the rubber in the quasi-static test in the low frequency, and high frequency cyclic load test [86, 100].

2.4 Dynamics of concrete sleepers

Several researches have demonstrated that the dynamic strength of sleepers was assessed by their response to various dynamic loading tests [30, 35, 52–54, 63, 64, 85, 86, 93, 94, 96, 104, 151, 153, 165, 166]. According to Standards Australia, AS1085.14 for analysing and designing concrete sleepers has developed that provides the testing methods for static, quasi-static, and cyclic loading and the allowable limits and serviceability of sleepers [86, 165, 166].

According to Ford and Vincent, a modal analysis on a concrete sleeper was performed by laboratory test [53, 54, 86, 186]. The tested sleeper was suspended at each ends by soft springs which allowed for "free-free" support and ecited by an electro-dynamic shaker [53, 54, 86, 186]. From this test, the natural frequencies and corresponding mode

shapes were estimated by the obtained FRFs using the measured acceleration of the sleeper [53, 54, 86, 186].

The influence of various boundary conditions on the sleeper such as free-free, perfectly coupled to the subsoil, and voided sleepers, were investigated [86, 139]. FRFs were obtained and became a means to study the effects of various boundary conditions on their response to vibration [86, 139].

2.5 Dynamics of railway tracks

One of the first analytical models, i.e., the rail was considered as an infinite uniform Euler beam laid on a continuous damped elastic Winkler foundation, of railway ballasted track dynamics was developed by Timoshenko [86, 176]. A number of researchers found that there are only two dominant resonances in the frequency range of interest for railway ballasted track experimentally [13, 15, 20, 21, 41, 63, 64, 86, 89–92, 95, 98, 99, 110, 114, 153, 195]. The first resonance is an in-phase mode at about 100 Hz, which was moved together with the sleeper and rail on the ballast [41, 62–65, 86, 98, 99]. The second resonance is the out-of-phase mode at the frequency approximately between 300–500 Hz [41, 62–65, 86, 98, 99]. It is depending on the rail pad parameters, and it was moved to the opposite vibration direction of sleepers on ballast and rails over the rail pad [41, 62–65, 86, 98, 99].

The dynamic response and impact were subsequently observed from various researchs that a rail pad could be resilient at several hundred frequencies, and it would substantially reduce the dynamic loads on sleepers [41, 62–65, 86, 98, 99]. Thus, the rail pads could be reduced the dynamic bending stress in concrete sleepers about more than 50% [41, 62–65, 86, 98, 99]. A stiffness of the rail pad has a greater effect on reducing strain in a sleeper than its thickness [59, 60, 86].

The dynamic loading exerted on sleepers was also studied and revealed that the poor condition of ballast, such as loosely and voided [59, 60, 86]. In case of poor ballast condition, the dynamic loads increase significantly higher and the resilient effect of the rail pads should be decrease [59, 60, 86]. Selig and Waters found that the subgrade is the important component of the substructure, and it affect on track stiffness greatly [86, 160]. Raymond also found that hardened tracks have smaller differential settlements and it cause lower track impact effect than those of softer tracks [86, 150]. Further,

Liang and Zhu found the higher deformation and unstability of the track structure including the ballast occurred by the reduction of subgrade stiffness [86, 113].

Field measurements for determining the behavior of ballasted track were usually performed by the instrumented sensors and impact hammer technique because an impact hammer is mobile and self-supporting and the attached sensors such as strain gages and LVDT were easy to instrumented [6, 13, 22–26, 34–36, 40–44, 48, 55, 62, 67, 77, 79–81, 85–95, 110, 126, 127, 142]. The FRF measurements can be obtained through a computer package and automatically extracted for such modal properties as resonant frequency, damping constant, and corresponding mode shape [85–95].

Dynamic track modelling is needed to allow more accurate prediction of track degradation and associated railway track maintenance [41, 86]. In the mechanical models for railway tracks, the track components have simulated as a specified elements (classified according to their properties) as follows [41, 86]:

• Components with mass and geometrical properties (rail and sleepers) [86]

• Components with elastic properties (rail pads) and [86]

• Component with mass, geometrical and elastic properties (ballast) [86]

The dynamic responses of ballasted track depend on the track component properties, the contact condition between components, and the dynamic loads [86]. Rail and sleepers with mass and geometrical (inertia) properties keep the track stable under vehicle loads [86]. Rail pads and ballast with elastic properties reduce the impact energy and dampen the dynamic frequency [86]. However, in a well-ballasted track structure, the rail pad does not plays significant role in softening transient load action and dampen the vibration of sleeper [86, 96]. And, the dynamic behavior of ballasted track with the ballast damping over 100kNs/m (typical of well-compacted ballast) affected little by the damping of rail pad [86].

The imposed forces on a railway track can be divided into three categories corresponding to the direction of loading: vertical, lateral and longitudinal [41, 86, 114]. The vertical loading on the track consists of the static load of the vehicle and any additional dynamic contribution (dynamic impact), i.e., imposed into the static load [41, 86, 114]. These dynamic contributions are often the dynamic impact forces due to track defects and vehicle parameters, such as [41, 86, 114]:

• Irregularities in the geometry of the track structure; [86]

• Irregularities on the surface of the rail and wheel; [86]

• The vehicle speed and the mass and suspension characteristics of the vehicle (sprung and unsprung mass) [86].

The structural vibration mode of track structures consists depending on the resonant frequencies on the vertical, lateral and longitudinal direction in response of the physical properties such as a mass and stiffenss [86, 87, 89–92, 95, 98, 99].

The lowest vertical resonant frequency of the track is the full track resonance that include both in-phase and out-of-phase vibrations [86, 87, 89–92, 95, 98, 99].

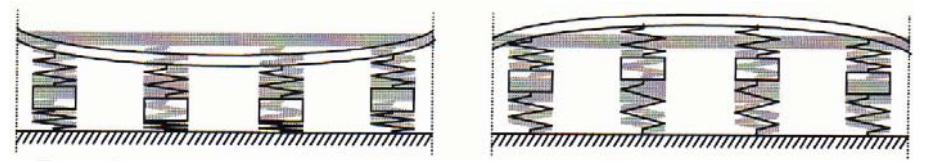

(a) Full track vertical resonant

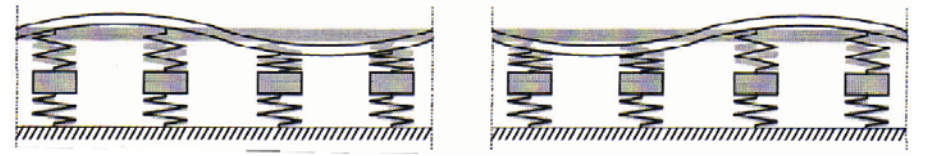

(b) Rail resonant

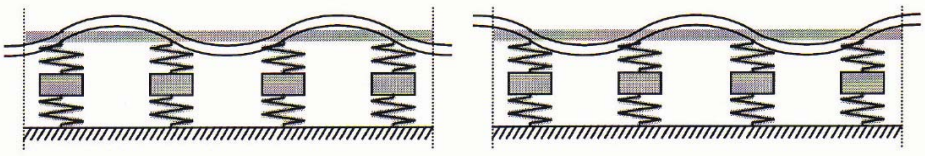

(c) First order pin-pin resonant

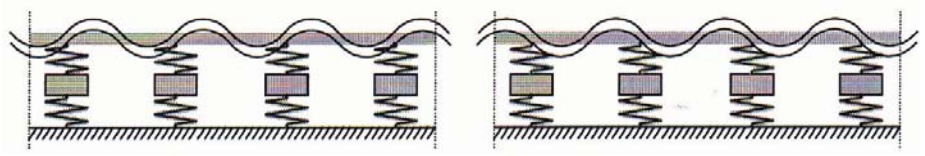

(d) Second order pin-pin resonant

Fig. 2.6 Resonant frequency mode shape of ballasted track [86]

For ballasted tracks in good conditions, the full track resonant frequencies (first vibration mode), second and third vertical vibration mode are 40–140 Hz, 100–400 Hz, and 250–1,500 Hz, respectively [86, 87, 89–92, 95, 98, 99].

Fig. 2.6(a) shows the typical full track vibrations [86]. In addition, the rail resonant frequency whereas the rail vibrating to the supports and is highly dependent on the rail pad properties, but is independent to the sleeper and ballast properties, as shown in Fig. 2.6(b) [86, 95, 98, 99]. The vibration modes and shapes are dependent on the sleeper support spacing [86, 95, 98, 99]. These vibration modes are so-called '*pin-pin*' resonant modes, corresponding to pin-pin resonant frequencies [86, 95, 98, 99].

The first pin-pin resonant frequencies (Fig. 2.6(c)) occur between 400–1,200 Hz and the second (Fig. 2.6(d)) at slightly less than 4 times higher frequencies [86, 95, 98, 99].

Kaewunruen and Remennikov reported that the frequency range has varying effects on the railway track as a structure and on each component [86, 95]. According to the frequency ranges, the low (0–40 Hz), mid (40–400 Hz), and high (400–1,500 Hz) lead to damage to the substructure (subgrade, sub-ballast and ballast), and superstructure (sleepers, fasteners, and rail pads), and rail and fastener [41, 86, 95, 98, 114].

Also, rail corrugation, and wheel defects would be produced periodical loading [41, 86, 95, 114, 152]. The longitudinal vibration modes produced the compression waves in the rails, and it affects the fatigue performance in minor axis of the rails, and its fastener [86].

The track substructure has a direct influence on the dynamic factor of wheel load, track stiffness, and roughness [41, 86]. The substructure components have a very strong non-linear stress-strain relationship with non-homogeneous properties [20, 86]. The most important duties of the track substructures are supporting and distributing the dynamic load from the sleepers to the ground, and providing suitable drainage and resilience for the track system [41, 86, 114].

The major failure mode of the ballasted track is produced in the track substructures (such as ballast and subgrade) [20, 73, 86]. The successful method to obtaining dynamic characteristics of the ballast and subgrade materials was assessed by performing triaxial testing [20, 86]. The test represents basic informations of ballast and subgrade materials such as resilient or elastic behaviour, plastic or permanent strain, breakage, and failure stress level, and these are used to design and maintenance for the track substructure [20, 86, 106].

The frequency response function (FRF) of the ballasted track shows two resonance peaks because of the ballasted track has a discrete continuous support with two mass of

the rail and the sleeper [143]. To prevent excitation by a train running with high speed, these resonance peaks have to sets sufficiently high [143].

For the rail is excited between two sleepers, the rail vibrates easily corresponding to a resonance peak [143]. In a case of excitation on the sleeper the FRF shows anti-resonance [143]. The FRF of ballasted track shows two other resonances that were correspond to respectively movement of rail and sleepers in phase and in anti-phase [31, 95, 98, 99, 143]. The stiff behaviour of the track at certain frequencies increases the possibility to the formation of corrugation [143]. The first natural frequency of the ballasted track is relatively low [143]. The excitation frequency increases with the train speed according to equation (2-1).

$$f = \frac{v}{\lambda} \tag{2-1}$$

Where, f is the frequency [Hz], v is the train speed [m/s] and λ is the wave length [m] [143].

The first natural frequency of the track must be sufficiently higher to prevent rapid track deterioration [143]. The track stiffness of the ballasted track can not be chosen to low as to prevent excitation by a train running at high speed of the excitation frequency [143]. Contrary, the slab track structure has a continuous support and has only one mass, the rail [143]. Therefore the slab track structure with a continuously supported rail has only one resonance peak and no anti-resonance peaks [143].

The track may be excited by an impact load to investigate the track response at higher frequencies, for example from a sledge-hammer [31, 86, 88–92, 95, 152]. The receptance is the ratio of the track deflection and the force act on the track, and define a deflection per the load (m/N) [31, 98, 99, 143].

The receptance is the inverse of the track stiffness [31]. As shown in Fig. 2.7, the receptance and the track stiffness depend on the load frequency, and the maximum frequency indicates the resonance frequencies for the track [31, 98, 99, 143]. The typical receptance also depends on the preload because of most tracks have a non-linear relationship between load and deflection [31, 98, 99, 143]. Therefore the phase of track receptance is significantly changed at the frequency of 1,000 Hz according to the

loading point on the rail, i.e., between two sleepers (full-line) and above one sleeper (dashed line) [31, 98, 99, 143].

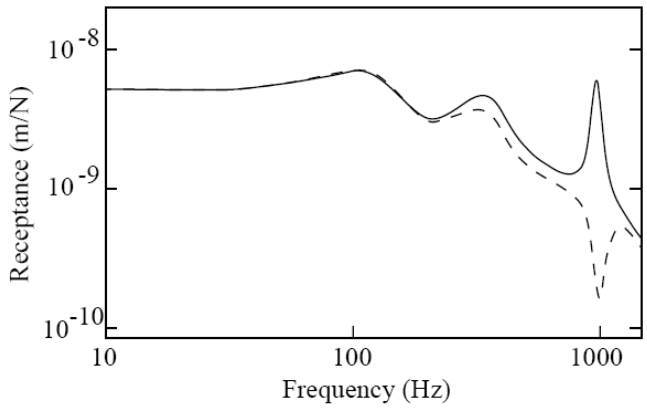

Fig. 2.7 Typical track receptances with a sinusoidally varying force [31]

Track resonance is usually obtained in the frequency range of 50–300 Hz [31, 98, 99, 143]. This resonance is obtained when the track structure (rails and sleepers) vibrates on the ballast [31, 98, 99, 143]. The rails and the sleepers provide the mass element, and the ballast provides the spring-damper element for the resonance [31, 98, 99, 143]. The resonance at a frequency of less than 100 Hz is found that the constant receptance due to a sufficient damping capacity of the ballast and is well damped as shown in Fig. 2.7 [31, 98, 99, 143].

As shown in Fig. 2.7, the highest resonance frequency, i.e., the resonance peak is narrow and less damped, is the pinned-pinned resonance frequency at less than 1,000 Hz (200–600 Hz) [31, 98, 99, 143]. In this frequency, the rail pad play a role of a spring element inserted between the mass of rail and sleeper [31, 98, 99, 143]. The pinned-pinned frequency is obtained when the rail vibrating on the rail pads and the wavelength of the rail bending is twice as long as the sleeper spacing, i.e., the rail supporting point [31, 98, 99, 143]. The pinned-pinned frequency is relatively less damped due to depending on mainly the material damping of the rail; therefore, this frequency leads to increase a highest deflection of the rail at 800–1,000 Hz (the peak of full-line in Fig. 2.7) [31, 98, 99, 143].

In contrast, the anti-resonance is obtained when the rail vibrating on a sleeper, i.e. the supporting point of the pinned-pinned vibration, and it lead to increase the track stiffness [31, 98, 99, 143]. At this frequency, the track deflection is balanced to a

vertical direction of the loading point, and the slope of the rail is zero at the loaded sleeper [31, 98, 99, 143].

In Euler-Bernoulli beam theory, the pinned-pinned frequency is easy to estimate. The frequency f (Hz) (or angular frequency ω, radians/sec) is the same as the fundamental frequency of a simply supported beam of length L [31].

$$f = \frac{\omega}{2\pi} = \frac{1}{2\pi}\pi^2\sqrt{\frac{EI}{mL^4}} \tag{2-2}$$

Where, EI is the bending stiffness of the rail, m is the mass of the rail per unit length, and L is the sleeper spacing [31]. For a UIC60 rail (assumed, m=60 kg/m and EI=6.4 MNm^2, L=0.65 m, an estimated pinned-pinned frequency is obtained f=1,214 Hz [31].

In practice, this resonance frequency will be lower than the calculated due to the real pinned-pinned frequency is lower than the frequency given by equation (2-2) [31]. For the short wavelength λ, the Euler-Bernoulli beam theory is not suitable, thus it can be obtained when the wavelength is longer than the height of the beam [31].

3 THEORETICAL BACKGROUND FOR NUMERICAL SIMULATION OF BALLASTED TRACK

3.1 Introduction

This section presents a result of literature reviews and investigates the effect of track components and vertical track support stiffness, and its effect on the track performance [31, 98, 99, 143]. The Ballasted track can be divided into three groups of discrete support models, as shown in Fig. 3.1 [98, 99]. Two approaches for calculating global track stiffness, a static approach based on Zimmermann's theory and a dynamic one based on the dynamic vehicle–track interaction model are discussed [31, 90, 98, 99, 110, 111, 137, 143].

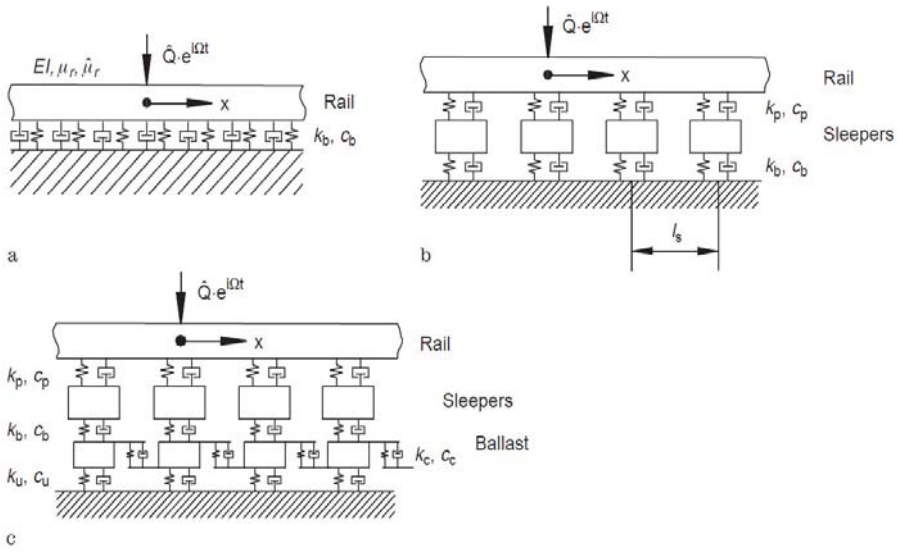

Fig. 3.1 Ballasted track model (a: on an elastic support, b: on a discrete support, c: taking account of ballast mass and shear stiffness) [99]

Most of the ballasted track models are based on the model of an elastic foundation for ballast and subgrade proposed by Winkler [31, 41, 90, 98, 99, 110, 111, 114, 137, 143]. Winkler's original model is usually used in civil engineering to investigate stresses in the structural members [31, 41, 90, 98, 99, 110, 111, 114, 137, 143]. According to Zimmermann, it was investigated that dealing with Winkler's model [99].

The first dynamic extension of the model was by Timoshenko [176]. Researchers over the world have investigated the track model and its applications and produced various

numerical track models using finite or infinite element [31, 41, 90, 98, 99, 110, 111, 114, 137, 143]. Recently, the track models with discretely supported sleepers are common type of the numerical track model [21, 31, 41, 98, 99, 114, 195].

As shown in Fig. 3.2, the measured and calculated receptances of a track are compared to identifying the unknown track parameters [31, 98, 99]. The track model was exerted by a harmonic load, and the displacement at the point of excitation was measured [31, 98, 99].

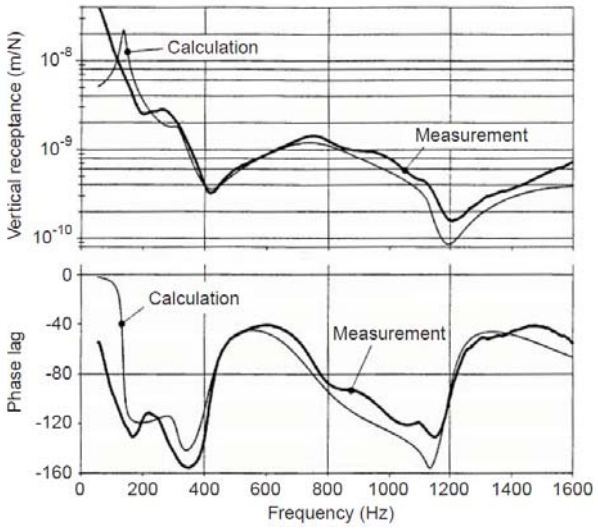

Fig. 3.2 Comparison between measured and calculation result for Fig. 3.1(c) [99]

The dynamic amplitude of displacement and load is defined as the receptance or dynamic flexibility [31, 98, 99]. The rail pad and ballast parameters have to be chosen such as a designed value, and then the measured and calculated receptances is obtained [31, 98, 99]. According to previous researches, a finite number of sleepers (in most cases seven) are based on the subgrade [99].

3.2 Mathematical models

As shown in Fig. 3.3, the track-subgrade model is excited by a vertical harmonic force to investigate the dynamic response of the ballasted tracks [99]. To simplify the model, the sleeper is assumed to a rigid mass, and the rail pad is modelled as a visco-elastic element [98, 99]. The ballast is modelled as a short length of elastic link [98, 99]. The subgrade under the ballast can be either an elastic link or a layer of elastic halfspace [98,

99]. The interaction force between ballast link and the subgrade one is assumed to be uniform [98, 99]. The ballast link consisted on elastic stiffness and a damping value [98, 99]. The elastic stiffness of the ballast and a mass can be estimated by experiment and calculation [98, 99].

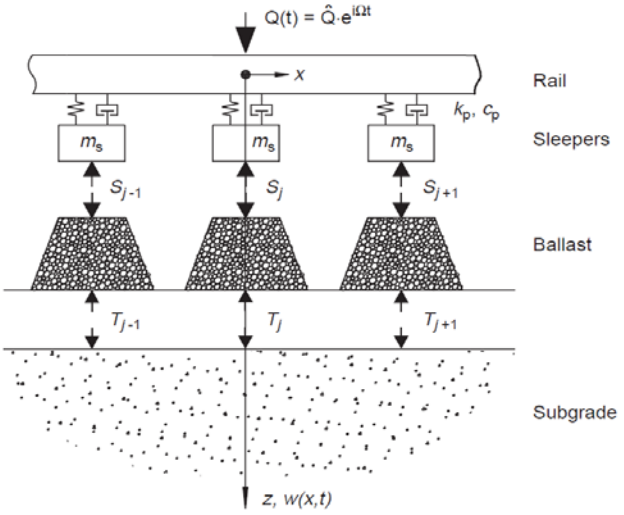

Fig. 3.3 Track-subgrade model [99]

The rail is modelled as a Timoshenko beam [98, 99]. Therefore, two partial differential equations are obtained [99]:

$$EI\frac{\partial^2\beta(x,t)}{\partial x^2}-GA\left[\beta(x,t)+\frac{\partial w_r(x,t)}{\partial x}\right]-\hat{\mu}_r\frac{\partial^2\beta(x,t)}{\partial t^2}=0 \tag{3-1}$$

$$\begin{aligned}&GA\left[\frac{\beta(x,t)}{\partial x}+\frac{\partial^2 w_r(x,t)}{\partial x^2}\right]-\mu_r\frac{\partial^2 w_r(x,t)}{\partial t^2}=\\&-Q(t)\delta(x)+\sum_{j=-\infty}^{\infty}\delta(x-jl_s)\left\{k_p[w_r(x,t)-w_s(jl_s,t)]+c_p\left[\frac{\partial w_r(x,t)}{\partial t}-\frac{\partial w_s(jl_s,t)}{\partial t}\right]\right\}\end{aligned} \tag{3-2}$$

Where, $w_r(x, t)$ is the vertical displacement of the rail, $\beta(x, t)$ is the slope of the cross section of the rail and $w_s(jl_s,t)$ is the vertical sleeper displacement [99].

The sleeper spacing is denoted as l_s, and the distance between sleeper '0' and sleeper *'j'* is jl_s, $\delta(x)$ and $\delta(x- jl_s)$ are Dirac functions [99]. A second-order ordinary differential equation is obtained for the rigid sleeper mass [99]:

$$
\begin{aligned}
&-m_s \frac{\partial^2 w_s(jl_s,t)}{\partial t^2} + k_p[w_r(jl_s,t) - w_s(jl_s,t)] \\
&+ c_p\left[\frac{\partial w_r(jl_s,t)}{\partial t} - \frac{\partial w_s(jl_s,t)}{\partial t}\right] - S_j(jl_s,t) = 0 \quad \text{for} \quad -\infty \le j \le \infty
\end{aligned} \tag{3-3}
$$

The vertical forces between sleeper and ballast are denoted by $S_j(jl_s, t)$ and the resultant vertical forces acting on the subgrade surface by $T_j(jl_s,t)$ [99]. A system of differential equations has to be formulated for the ballast link [99]:

$$
\mathbf{M}_j \ddot{\mathbf{w}}_j(t) + \mathbf{D}_j \dot{\mathbf{w}}_j(t) + \mathbf{K}_j \mathbf{w}_j(t) = \begin{Bmatrix} S_j \\ -T_j \end{Bmatrix} \tag{3-4}
$$

Where, $\mathbf{M}_j$, $\mathbf{K}_j$ and $\mathbf{C}_j$ are the mass, stiffness and damping matrix, respectively [99].

It is sufficient to use only two displacements, $\mathbf{w}_j^T(t) = \{w_s, w_f\}_j$, where w_s is the vertical displacement of the sleeper and w_f is the mean displacement of the subgrade under the ballast link [99]. The behavior of the subgrade is described by the vertical receptances in frequency-dependent [99]. For a track model used in the low-frequency range ($f \le$ 40Hz) or in the medium-frequency range (40Hz $\le f \le$ 400Hz), the coupling between two ballast links through the subgrade is significant [99].

The dynamic model for simulating the vertical track–vehicle interaction that can be divided into three sub systems: track, vehicle, and wheel-rail contact as shown in Fig. 3.4 [111].

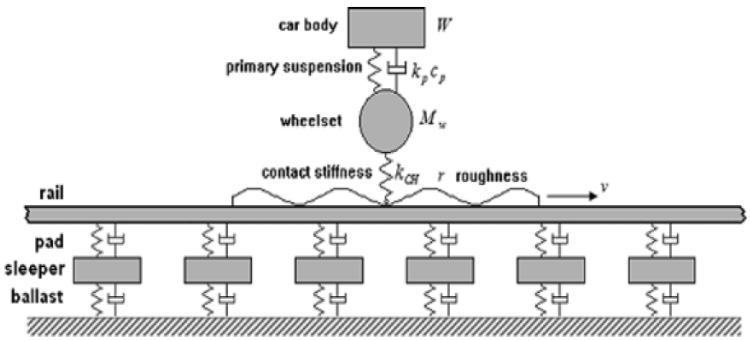

Fig. 3.4 Dynamic model for vertical track–vehicle interaction [111]

The track model is conducted as an infinitely long Timoshenko beam on the supported by discrete rail pads, sleepers, ballast, and subgrade [31, 98, 99, 111]. The vehicle model includes wheelset and carbody as masses and linear primary suspension, respectively [31, 98, 99, 111]. The wheels are connected with the rail by an element of Hertzian contact spring. And the vertical rail roughnesses are introduced as dynamic excitations and the entire track system is solved in the frequency domain [31, 111].

3.2.1 General model

It is necessary to formulate coupling conditions to combine track and subgrade [99]. This can either be done by stiffness or by flexibility matrices [99]. For a track with an infinite number of sleepers, the mathmetical model can be transformed to the other using the inversion of the specific matrices [99]. The displacements of rigid foundations have to be described to determine the dynamic stiffness matrix [99]. And the resultant forces, i.e., a component of the dynamic stiffness matrix, are obtained by integration of the general pressure distribution over the foundation area [99]. A uniform load distribution is acted on the foundation area, i.e., no rigidity assumed, to determine the flexibility matrix [99]. The flexibilities are derived by integrating the vertical displacements over the foundation area [99]. As shown in Fig. 3.5, the stiffness and flexibility method were indicated by black filled and white open arrows, respectively [99].

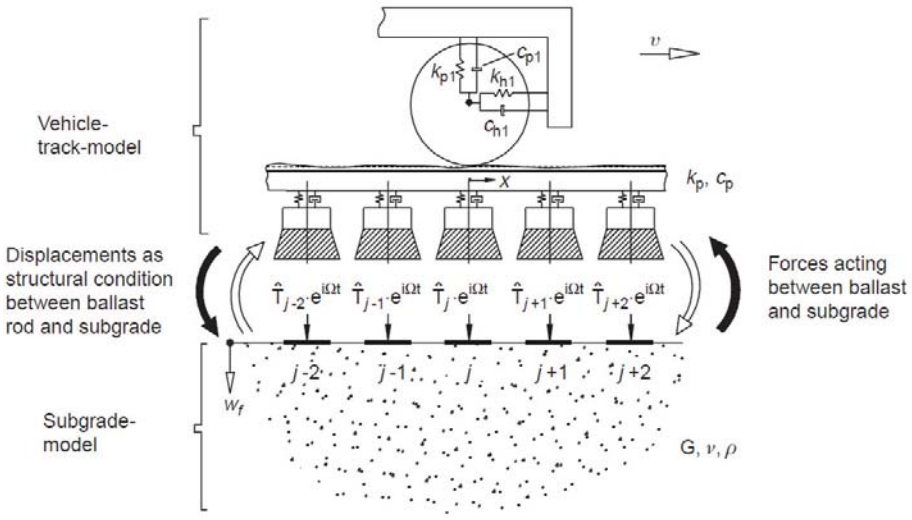

Fig. 3.5 Vehicle-track-subgrade model [99]

The receptances, i.e., for prescribed pressure distributions, are softer than the dynamic stiffnesses for prescribed displacements [99]. Therefore, it is easy to find analytical estimations for the receptances, i.e., transformed into a time-domain model [99].

3.2.2 Track dynamics

The rail is consisted with the Young's modulus E, shear modulus G, density ρ, cross-sectional area A, second moment of area of section I, and shear coefficient κ [111]. The bending stiffness is represented by $B=EI$ and the shear stiffness by $K=GA\kappa$ [111]. The sleeper is conducted by mass m_s, whereas the rail pad and the ballast are modelled by stiffness and loss factor k_{pad} and η_{pad}, k_{bal} and η_{bal}, respectively [111]:

$$\widetilde{k}_{pad} = k_{pad} + i\eta_{pad}, \quad \widetilde{k}_{bal} = k_{bal} + i\eta_{bal} \tag{3-5}$$

Both of the wheel force and point force exerted on each support of the rail [111]. The dynamic stiffness (impedance) $S(\omega)$ is introduced to the relationship between the force $\hat{F}_n$ at each support point and corresponding displacement $\hat{u}_n$ [111]:

$$\hat{F}_n = -S(\omega)\cdot\hat{u}_n \tag{3-6}$$

$$S(\omega) = \frac{\widetilde{k}_{pad}\cdot(\widetilde{k}_{bal} - \omega^2 m_s)}{\widetilde{k}_{pad} + \widetilde{k}_{bal} - \omega^2 m_s} \tag{3-7}$$

The identical supports at $x_n = nl$ with $S(\omega)$ are considered and an external force per unit length $\hat{f}(x,\omega)$ is included [111]. The general governing equations of motion for the track in the frequency domain can be derived as [111]:

$$\begin{aligned}&\left(\frac{d^2}{dx^2}+k_p^2\right)\left(\frac{d^2}{dx^2}-k_d^2\right)\hat{u}(x,\omega)+\frac{S(\omega)}{B}\left[1-\frac{B}{K}\left(\frac{d^2}{dx^2}+k_c^2\right)\right]\cdot\sum_{-\infty}^{+\infty}\hat{u}(x,\omega)\delta(x-nl)\\&=\frac{1}{B}\left[1-\frac{B}{K}\left\{\frac{d^2}{dx^2}+k_c^2\right\}\right]\hat{f}(x,\omega)\end{aligned} \tag{3-8}$$

Where,

$$k_p^2 = \frac{1}{2}\left[\sqrt{(k_c^2 + k_t^2)^2 + 4(k_B^4 - k_c^2 k_t^2)} + (k_c^2 + k_t^2)^2\right] \tag{3-9}$$

$$k_d^2 = \frac{1}{2}\left[\sqrt{(k_c^2 + k_t^2)^2 + 4(k_B^4 - k_c^2 k_t^2)} - (k_c^2 + k_t^2)^2\right] \tag{3-10}$$

$$k_c = \omega\sqrt{\frac{\rho}{E}},\ \ k_t = \omega\sqrt{\frac{\rho}{G\kappa}}, \text{ and } k_B = \left(\frac{\omega^2 \rho A}{EI}\right)^{1/4} \tag{3-11}$$

To calculate the vertical track receptance, the Green's function $\hat{G}_\omega^T(x, x_0)$ that corresponds to the rail response at a specific point x to a unit point force acting at the excitation point x_0, i.e., the solution of equation (3-8) for $\hat{f}(x,\omega) = \delta(x - x_0)$ [111]. Further, a free Timoshenko beam $\hat{G}_\omega^f(x, x_0)$ should be solved as to obtaining $\hat{G}_\omega^T(x, x_0)$ [111]:

$$\hat{G}_\omega^f(x, x_0) = -\frac{1}{B}\left[F_d e^{-k_d|x-x_0|} + iF_p e^{-ik_p|x-x_0|}\right] \tag{3-12}$$

$$F_d = \frac{1 - B/K(k_d^2 + k_c^2)}{2k_d(k_p^2 + k_d^2)}, \qquad F_p = \frac{1 - B/K(-k_p^2 + k_c^2)}{2k_p(k_p^2 + k_d^2)} \tag{3-13}$$

The first terms of equation (3-12) on the right side means that a near-field bending wave, which decays exponentially away from the excitation point with a given decay rate [111]. The second terms of equation (3-12) on the right side represent a free bending wave, which reproduce from the excitation point and its wavelength is $2\pi/k_p$ [111]. The Floquet theorem can be applied that the solution has the periodicity of the sleeper spacing and can be derived as [111]:

$$\hat{u}(x + nl, \omega) = \hat{u}(x, \omega)e^{-n\gamma l} \tag{3-14}$$

Where, n is the integer, and the quantity γ is the propagation constant related with the free bending wave of the discretely supported rail [111]. By substituting equation (3-14)

into equation (3-8), letting $\hat{f}(x,\omega)=0$ and using equation (3-12), the associated solution for free bending waves of the supported rail can be obtained for $0 \le x < l$ [111]:

$$\hat{u}(x,\omega)=-\hat{u}(0,\omega)\frac{S(\omega)}{B}\times\left[F_p\frac{\sin k_p(l-x)+e^{-\gamma l}\sin k_p x}{\cos k_p l-\cosh\gamma l}-F_d\frac{\sinh k_d(l-x)+e^{-\gamma l}\sinh k_d x}{\cosh k_d l-\cosh\gamma l}\right] \quad (3\text{-}15)$$

The solution for the outside of $0 \le x < l$ can be obtained by equation (3-14) [111]. The propagation constant γ are determined by the dispersion relation by letting x=0 in equation (3-15) [111].

$$1=-\frac{S(\omega)}{B}\left[F_p\frac{\sin k_p l}{\cos k_p l-\cosh\gamma l}-F_d\frac{\sinh k_d l}{\cos k_d l-\cosh\gamma l}\right] \quad (3\text{-}16)$$

From equation (3-16), two complex values $\pm\gamma_p$ and $\pm\gamma_d$ for the propagation constant correspond to each solution of $\cosh\gamma_p l$ and $\cosh\gamma_d l$ [111].

The homogeneous differential equation for the free supported rail has four solutions, and the general solution is a linear combination [111].

$$Y(\tilde{x},\gamma)=F_p\frac{\sin k_p(l-\tilde{x})+e^{-\gamma l}\sin k_p\tilde{x}}{\cos k_p l-\cosh\gamma l}-F_d\frac{\sinh k_d(l-\tilde{x})+e^{-\gamma l}\sin k_d\tilde{x}}{\cosh k_d l-\cosh\gamma l} \quad (3\text{-}17)$$

The Green's function of the discretely supported rail, i.e., the solution of equation (3-8), can be derived as a linear superposition of the solutions on each side of x_0 as [111]:

$$\begin{aligned}&\hat{G}^T_\omega(x,x_0)=a_1Y(\tilde{x},-\gamma_d)e^{n\gamma_d l}+a_2Y(\tilde{x},-\gamma_p)e^{n\gamma_p l}\\&x=\tilde{x}+nl<x_0,\quad n=0,-1,-2,...\end{aligned} \quad (3\text{-}18)$$

$$\begin{aligned}&\hat{G}^T_\omega(x,x_0)=b_1Y(\tilde{x},\gamma_d)e^{-n\gamma_d l}+b_2Y(\tilde{x},\gamma_p)e^{-n\gamma_p l}\\&x=\tilde{x}+nl>x_0,\quad n=0,1,2,...\end{aligned} \quad (3\text{-}19)$$

The coefficients a_1, a_2, b_1, and b_2 are determined from the conditions for the Green's function and its derivatives at the point $x=x_0$ [111]:

$$\begin{bmatrix} -Y(x_0,-\gamma_d) & -Y(x_0,-\gamma_p) & Y(x_0,\gamma_d) & Y(x_0,\gamma_p) \\ -\dot{Y}(x_0,-\gamma_d) & -\dot{Y}(x_0,-\gamma_p) & \dot{Y}(x_0,\gamma_d) & \dot{Y}(x_0,\gamma_p) \\ -\ddot{Y}(x_0,-\gamma_d) & -\ddot{Y}(x_0,-\gamma_p) & \ddot{Y}(x_0,\gamma_d) & \ddot{Y}(x_0,\gamma_p) \\ -\dddot{Y}(x_0,-\gamma_d) & -\dddot{Y}(x_0,-\gamma_p) & \dddot{Y}(x_0,\gamma_d) & \dddot{Y}(x_0,\gamma_p) \end{bmatrix} \cdot \begin{bmatrix} a_1 \\ a_2 \\ b_1 \\ b_2 \end{bmatrix} = \begin{bmatrix} 0 \\ -1/K \\ 0 \\ 1/B[1+(B/K)k_t^2 \end{bmatrix} \quad (3\text{-}20)$$

Where, $\dot{Y}$, $\ddot{Y}$, and $\dddot{Y}$ are the derivatives of order 1, 2, and 3 with respect to $\tilde{x}$. In case of $x=x_0$, the direct point receptance of track $\alpha_r = \hat{G}_\omega^T(x_0,x_0)$ [111].

3.2.3 Vehicle and wheel–rail contact

The governing equations of the vehicle model can be written as [111]:

$$\begin{bmatrix} M_c & 0 \\ 0 & M_w \end{bmatrix} \begin{bmatrix} \ddot{u}_c \\ \ddot{u}_w \end{bmatrix} + \begin{bmatrix} C_p & -C_p \\ -C_p & C_p \end{bmatrix} \begin{bmatrix} \dot{u}_c \\ \dot{u}_w \end{bmatrix} + \begin{bmatrix} K_p & -K_p \\ -K_p & K_p \end{bmatrix} \begin{bmatrix} u_c \\ u_w \end{bmatrix} = \begin{bmatrix} M_c g \\ M_w g - f_{wr} \end{bmatrix} \quad (3\text{-}21)$$

Where, u_c and u_w are the vertical displacements of carbody and wheelset, respectively [111]. And, M_c is the mass of a carbody, M_w is the mass of wheelset (half), K_p and C_p are the stiffness and damping of the primary suspension system, and f_{wr} is the wheel–rail contact force [111].

In the frequency domain, the equations (3-21) can be simplified as [111]:

$$H_v(\omega) \cdot U_v(\omega) = F_v(\omega) \quad (3\text{-}22)$$

Where, $H_v(\omega)$ is the complex frequency response transfer function [111]:

$$H_v(\omega) = K_v + i\omega C_v - \omega^2 M \quad (3\text{-}23)$$

From equation (3-23), the direct point receptance of the wheel $\alpha_w(\omega)$ can be calculated [111]. The wheel–rail contact force is defined according to the Hertz theory as [111]:

$$f_{wr} = C_H (u_w - u_r - r)^{3/2} \tag{3-24}$$

Where, C_H is the Hertzian contact spring stiffness and r is the vertical track irregularities [111].

The Hertzian contact spring stiffness should be linearized because of the solution in the frequency domain requires that all components should be linear [111]. The relationship between the force and displacement was performed by increasing the static wheel–rail force Q_0 [111]. The receptance of the wheel–rail contact α_c *(ω)* at the constant point is obtained as [111]:

$$\alpha_c(\omega) = \frac{1}{k_{CH}} = \frac{2}{3} C_H^{-2/3} Q_0^{-1/3} \tag{3-25}$$

In contact condition betwwen the wheel and rail, the continuity at the contact point requires [111]:

$$u_r + u_{wr} - u_w = r \tag{3-26}$$

By introducing the each receptances of vehicle α_w, track α_r, and Hertz contact α_c into equation (3-26), the vertical dynamic wheel–rail force in the frequency domain can be derived as [111]:

$$Q_{dyn}(\omega) = -\frac{R(\omega)}{\alpha_w(\omega) + \alpha_r(\omega) + \alpha_c(\omega)} \tag{3-27}$$

Where, *R (ω)* is the track irregularities expressed in the frequency domain [111].

3.3 Track support stiffness

3.3.1 Definition and calculation theory

Track support stiffness (wheel load divided by track deflection) is an important parameter of track design and maintenance that influence the bearing capacity of track, vehicle dynamics, and the quality and life of track components [31, 33, 41, 55, 67, 77, 110, 114]. The high track stiffness is generally effective that it provides sufficient track resistance to applied loads and reduced the track deflection, i.e., affect track deterioration [31, 110, 114]. However, dynamic forces on wheel–rail contact surface and sleepers and ballast increase with track stiffness increased [14, 22, 31, 43, 110]. The variation of the track support stiffness along the track lead to variations in vehicle–track interaction forces and differential settlement, and therefore it could be lead to the differential track deterioration problems [108–114].

Many research works and literature surveys on track support stiffness have been published over the years [31, 33, 41, 55, 67, 77, 81, 110,]. Hence, further research and studies are required to developing a reasonable approach to the track design and maintenance [31, 77, 110]. Therefore, the technical method for the track support stiffness is important to measure and predict the track performance of existing lines [31, 77, 110]. And it can be evaluated and suitable making a decisions regarding to track maintenance works [31, 77, 110].

According to [110], two approaches for calculating global track stiffness, a static one based on Zimmermann's theory and a dynamic one based on the track model used in the dynamic vehicle–track interaction program Dynamisk Interaktion mellan Fordon och Farbana (DIFF) in this section was investigated by [110]. DIFF is also used to investigate the track stiffness and its associated dynamic track responses by parametric excitations [110].

The variations in ballast/subgrade stiffness derived by the measured datas from the rolling stiffness measurement vehicle (RSMV) were used to the input data in DIFF simulations [110]. Input data for ballast/subgrade have determined by a complex work for simulating vehicle–track interaction problems [110]. Recently, several techniques for vertical track stiffness measuring continuously have been developed [13, 14, 55, 77, 110]. The RSMV is a rebuilt two-axle freight wagon and can measure dynamic stiffness up to 50 Hz [110].

Track support stiffness k (precisely global vertical track stiffness) can be defined as the ratio between the vertical force Q on rail and the vertical track displacement w as [110]:

$$k(t) = \frac{Q(t)}{w(t)} \quad \text{or} \quad k(f) = \frac{Q(f)}{w(f)} \tag{3-28}$$

Therefore, the dynamic track stiffness is dependent on the applied load or a function of excitation frequency f and time t domain [110].

1) Static approach

Conventional track calculations are based on a static approach developed by Zimmermann [110]. For the static approach, it was considered an infinite long beam (rail) with a bending stiffness EI, which is loaded by a vertical force Q at x=0 and is supported by a continuous elastic foundation with distributed stiffness k_c ($k_c = k_s/a$) [31, 41, 110, 114]. Where, a is the sleeper spacing and k_s is the total of support stiffness in series of rail pad, ballast, and subgrade [31, 41, 110, 114].

Governing differential equation for the problem combining with boundary conditions derives the solutions for rail displacement w, sectional moment of the rail M, and pressure load on sleeper F as follows [41, 110]:

$$w(x) = \frac{QL^3}{8EI} e^{-(x/L)} \left(\cos\frac{x}{L} + \sin\frac{x}{L} \right) \tag{3-29}$$

$$M(x) = \frac{QL}{4} e^{-(x/L)} \left(\cos\frac{x}{L} - \sin\frac{x}{L} \right) \tag{3-30}$$

$$F(x) = \frac{Qa}{2L} e^{-(x/L)} \left(\cos\frac{x}{L} + \sin\frac{x}{L} \right) \tag{3-31}$$

Where, L is the characteristic length of the track and is determined by [41, 110]:

$$L = \sqrt[4]{\frac{4EI}{k_c}} = \sqrt[4]{\frac{4EIa}{k_s}} \tag{3-32}$$

And, k_s is determined as the series stiffness of pad stiffness k_{pad} and ballast/subgrade stiffness k_{bs} by [41, 110]:

$$\frac{1}{k_s} = \frac{1}{k_{pad}} + \frac{1}{k_{bs}} \tag{3-33}$$

Therefore, from the definition of equation (3-28), the global static track stiffness according to Zimmermann's theory can be obtained as [41, 110]:

$$k = \frac{8EI}{L^3} = 2\sqrt{2}\sqrt[4]{EIk_c^3} \tag{3-34}$$

The global track support stiffness is a function of the structural properties of the rail, rail pad, sleeper, and ballast/subgrade [41, 110].

Numerical results are presented in this section was investigated by [110]. As listed in Table 3.1 [110], the calculated results using the static approach are presented for three typical track structures, i.e., classified with the global track stiffness; soft (31.6 kN/mm), normal (78.0 kN/mm) and stiff (171.5 kN/mm) according to the stiffness of rail pad and ballast/subgrade [110]. The tracks are loaded by a same vertical force Q=100 kN, which is used as the reference wheel load in the International Union of Railways (UIC) project [77, 81, 110].

Low track stiffness leads to increase the rail displacement and bending moment [77, 81, 110]. In contrast, high track stiffness leads to increase higher pressure force on sleepers [77, 81, 110]. According to [77, 81, 110], the general vertical rail displacement should be in a range of 1–2 mm for a wheel load of 100 kN, and it would be leads to the track stiffness in a range of 50–100 kN/mm.

For the high-speed line, the optimal track stiffness of 70–80 kN/mm has proposed by López Pita *et al.* [81, 110]. According to Table 3.1, it was agreed with the results of previous researches having a global vertical track stiffness of 78.0 kN/mm [81, 110].

Table 3.1 Static behavior of tracks according to static approach [110]

	Track A 'soft'	Track B 'normal'	Track C 'stiff'
Stiffness of rail pad k_{pad} (kN/mm)	70	70	500
Stiffness of ballast/subgrade k_{bs} (kN/mm)	10	50	100
Stiffness of discrete support k_s (kN/mm)	8.75	29.2	83.3
Characteristic length L (m)	1.175	0.870	0.669
Global track stiffness (static) k (kN/mm)	31.6	78.0	171.5
Rail displacement (mm)	3.16	1.28	0.58
Rail sectional moment (kN m)	29.4	21.7	16.7
Pressure load on sleeper (kN)	27.7	37.4	48.6

2) Dynamic approach

Recently, most of the track models presented for dynamic vehicle–track interaction have demonstrated and used for investigating the global vertical dynamic track stiffness [110, 111]. In the previous study, the finite element (FE) model for tracks consists of one rail of finite length and discretely supported rail pads by sleepers on ballast were conducted by using the commercial program DIFF [110, 111].

The FE model is conducted by the half of track model, and the rail is modelled by Rayleigh–Timoshenko beam element and the sleepers are considered as rigid masses [110, 111]. The rail pad and ballast/subgrade is modelled as an in series of elastic spring and viscous damper [110, 111]. The structural dynamic equations can be derived as:

$$\boldsymbol{M}\ddot{u} + \boldsymbol{C}\dot{u} + \boldsymbol{K}u = F \tag{3-35}$$

Where, M, C, and K are the mass, damping, and stiffness matrices of the track, respectively, and F is the applied load vector [110]. In the frequency domain, the equation (3-35) can be derived as [110]:

$$(-\omega^2 \boldsymbol{M} + i\omega \boldsymbol{C} + \boldsymbol{K}) \cdot U(\omega) = F(\omega) \tag{3-36}$$

By assuming F be a unit load vector acting at an excitation position on the rail, the track receptance is the solution of U at the loading position [110]. And, the global dynamic

track stiffness is calculated by inverse of the track receptance [110]. Further details about numerical models and solutions of DIFF can be found in reference [110].

3.3.2 Simulation results of track support stiffness

Numerical results are presented in this section was also investigated by [110]. Fig. 3.6 shows the calculated global dynamic track stiffness for the three tracks [110]. The dynamic track stiffness increase with the frequency increases, therefore the tracks of higher frequency range was stiffer than those of low frequency range [110].

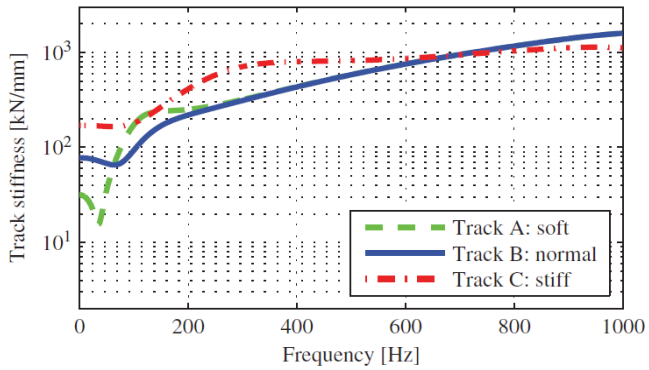

Fig. 3.6 Analyzed dynamic track stiffness [110]

In the low frequency range, resonances can be observed that implies that rail and sleepers are moving in phase on the ballast [110]. And the global static track stiffness was obtained at the frequency of 0 [110].

According to [110], dynamic responses of the track due to parametric excitations are presented in Fig. 3.7 [110]. The high track stiffness leads to increase the dynamic forces both in wheel–rail interface and on sleepers [110]. Further, the low track stiffness leads to also increase rail moment, rail displacement, and sleeper acceleration [110]. However, the dynamic contribution could be amplificated by other excitations such as track irregularities, wheel-rail contact surface roughness [110].

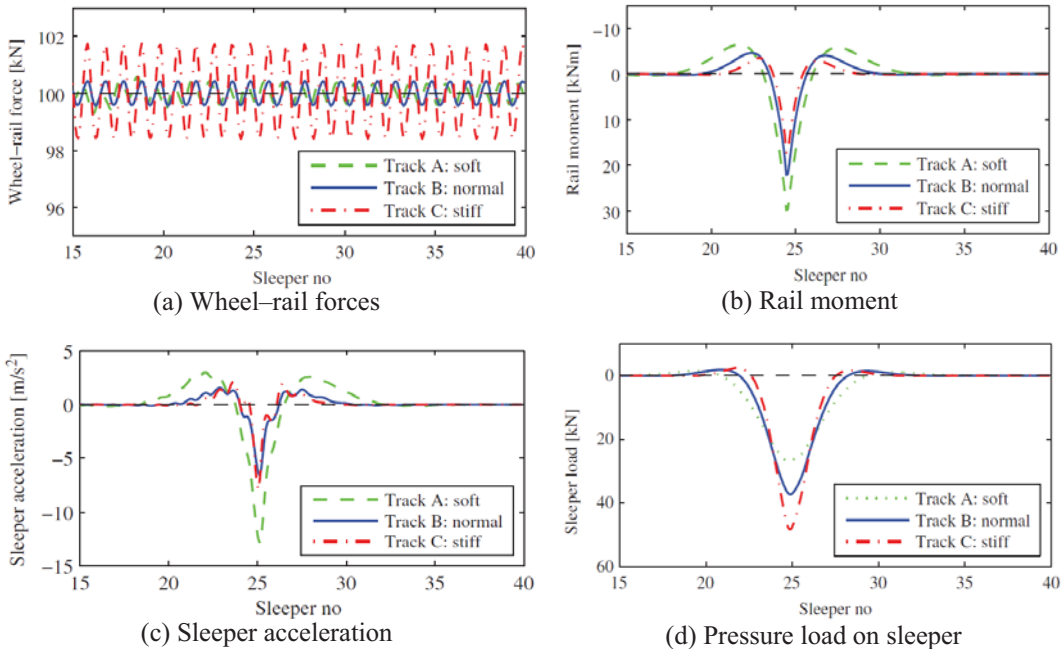

(a) Wheel–rail forces (b) Rail moment

(c) Sleeper acceleration (d) Pressure load on sleeper

Fig. 3.7 Dynamic responses of tracks for different track stiffness [110]

According to [110], the softer ballast/subgrade, the lower global track stiffness leads to increased track responses. In contrary, in case of both rail pads and ballast/subgrade are hardend, higher global track stiffness leads to increased dynamic responses of the track such as dynamic wheel–rail forces, dynamic forces on sleepers and wheel vibrations [110].

3.4 Track receptances

The track receptance (dynamic flexibility) is defined as the ratio of the rail displacement to the exciting force [99]. Using the frequency-dependent receptance of the rail, the static and dynamic properties of the track in response to the point of the displacement could be estimated regarding to the subgrade as a homogeneous elastic half-space [99]. It is also possible to consider a half-space layer with dependent parameters (e.g. Young's modulus, mass density etc.) [99].

Fig. 3.8 shows the track receptance calculated depends on the number of sleeper couplings [99]. Maximum amplitude of the receptance of the subgrade was found at the frequency of approximately 60 Hz [99].

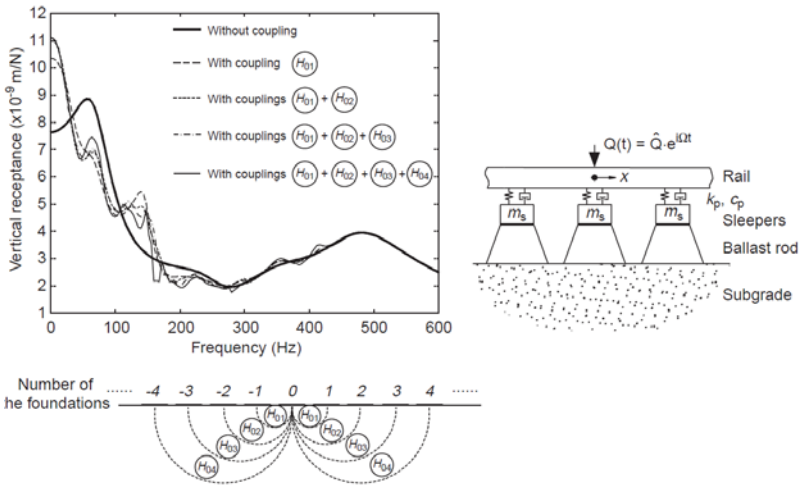

Fig. 3.8 Influence of the number of sleeper couplings on rail receptances [99]

As shown in the lower part of Fig. 3.8, this coupling is valid for every sleeper regardless a number of sleeper couplings [99]. Relatively similar results are obtained at the curves for different types of coupling [99]. The static receptance has always the higher than dynamic receptance and the dynamic receptance decreases with excitation frequnecy increases at 70 Hz, 135 Hz and 225 Hz [99]. The maximum at approximately 135 Hz has a half level of the static receptance, and then the dynamic receptance increases up to approximately 470 Hz, i.e., as the same type of resonance peaks appearred in a Winkler's foundation [99]. The resonance responses are a result of wave propagation effects at frequencies of 70 Hz, 135 Hz and 225 Hz, evidently [99]. Fig. 3.9 shows the results of calculation for stiff, medium and soft soil of tracks in the different wave propagation speeds v_s [99].

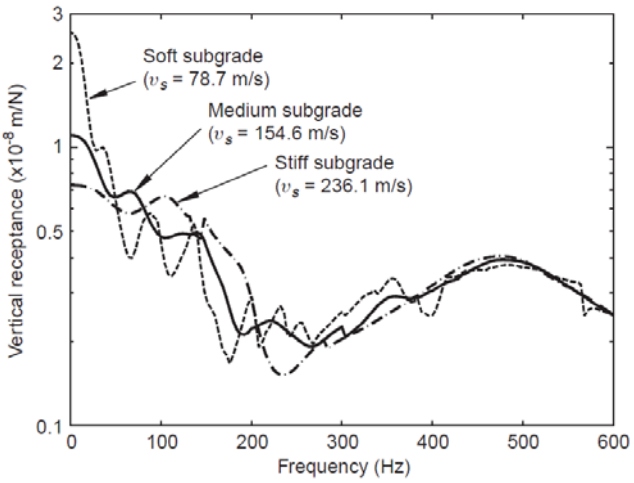

Fig. 3.9 Influence of soil subgrade properties on track receptances [99]

For soft soil, a variation of peak response was fluctuated [99]. In all three cases, the receptances are nearly similar in frequencies over than 400 Hz [99]. It is found that the receptances are dependent on the soil properties in the low and medium frequency range between 0 Hz and 400 Hz [99]. However, the property of rail pad is dominant in the high frequency range of over 400 Hz [99].

As shown in Fig 3.10, the receptance for the discretely supported track model and the continuously supported track model are similar in the entire frequency range [99]. According to the rail bending effect, the receptances of the discrete supported track are slightly higher than those of the continuously supported track model [99]. The resonance mode of the rail, i.e., pinned-pinned-mode, was found at 1,070 Hz of the discretely supported track model [99].

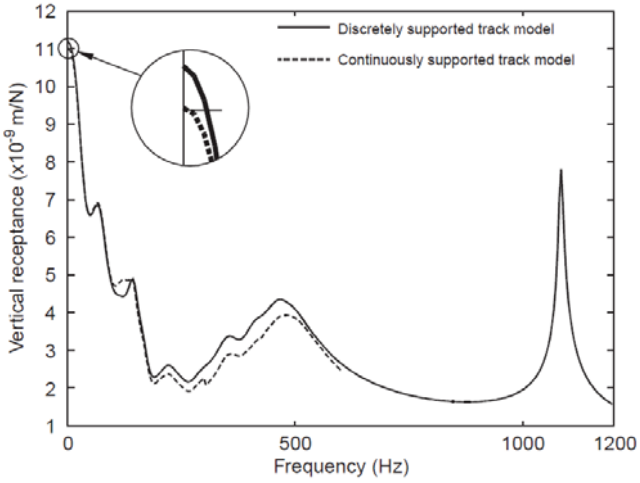

Fig. 3.10 Receptance for discretely and continuously supported track model [99]

Track deflection is possible to measure in the frequency from 0 Hz to some hundreds Hz [99]. Several researchers have been measured the deflections of rail and sleeper and in the subgrade for an electric locomotive running [31, 99]. According to these results, the ballast stiffness was investigated and the agreement between measured and calculated results is good in frequencies over 100 Hz [31, 99].

The receptance of Timoshenko beam on Winkler's foundation decreases in the low frequencies [99]. However, the measured receptance increases for decreasing frequency [99]. Krupp Industrieund Stahlbau (KIS) developed and represented the special equipment for measuring receptance [99]. According to KIS, the receptance increase

below 50 Hz and the peak displacement found at near 120 Hz, i.e., the resonance frequency of rail and sleeper mass due to moving on a Winkler foundation [99]. Therefore, a maximum of the receptance (resonance) is found between 100 Hz and 200 Hz in the foundation model [99]. However, the receptance of halfspace model increases below 100 Hz [99]. Therefore, a resonance response is usually obtained for the static condition [99].

Differences between measured and calculated results for receptances based on foundation models could be not sufficiently estimated by measurements only [99]. To avoid a numerical error, the appropriate numbers of overlapping sleeper coupling for the static and dynamic analysis were three and five, respectively [99]. In the frequency of over 250 Hz, the influence of the subgrade reduced and the influence of the rail pad increased [99].

Determining input data for rail pads and ballast is difficult to get the information because of their material properties can be changed according to various factors and a complex constitutive relation [111]. Further, the property of rail pad is dependent on preload and frequency [111]. According to a number of researchers, the properties of the Pandrol pad (5877D, studded, 10 mm thick, rubber) have investigated [111].

Fig. 3.11 shows the frequency dependent stiffness k_b and damping loss factor η_b of rail pad under a preload of 40 kN increased by frequency increasing [111, 137].

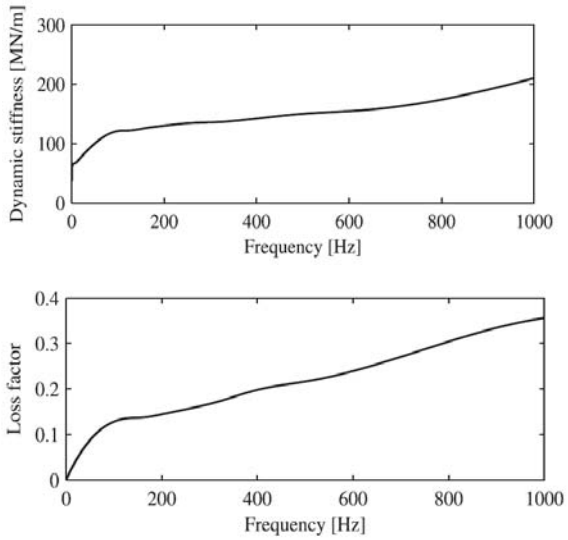

Fig. 3.11 Dynamic stiffness and loss factor of rail pad [137]

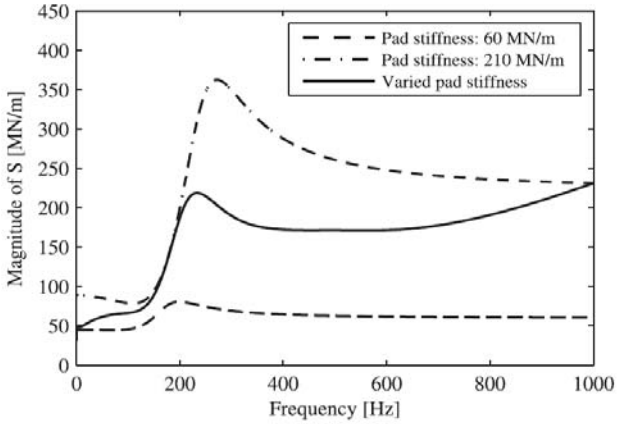

Fig. 3.12 Variations in dynamic receptance for different stiffness of rail pad [111]

As shown in Fig. 3.12, the influence of dynamic parameters of the rail pad on the track receptance $S(\omega)$ is clearly, and it is found that the rail pad affects $S(\omega)$ strongly [111].

3.5 Modelling of in-situ ballasted track

For design and maintenance, modelling of in-situ ballasted tracks should be constructed to considering the actual field condition [41, 95]. Finite element (FE) models calibrated using experimental data are capable of providing reliable predictions of railway track response [95].

Researchers over the world have developed and demonstrated the FE models of railway tracks, such as Grassie's model based on discrete support model and Cai's model based on Timoshenko beam [21, 64, 95, 176]. Among of them, Cai's model, i.e., modeled as Timoshenko beam for the rail and sleeper, provides the optimized analytical results [21, 95]. For the FE model, both ends of the rail are usually conducted as hinges, and the springs of ballast connected the ground using rigid link elements [21, 95]. According to previous findings [93–95, 98], the results of FE model of ballasted track have three dominant resonances. The resonance frequencies represent the in-phase, out-of-phase, and pin–pin vibration modes of a track [95].

As shown in Table 3.2, both the in-phase and out-of-phase modes can be simplified with a 2DOF mass–spring system [95]. The 2DOF models have been widely used to identify the dynamic behavior and conditions of ballasted tracks [34, 89–92, 95].

Table 3.2 Dynamic modeling of ballasted tracks [95]

Finite element model	2DOF mass-spring system
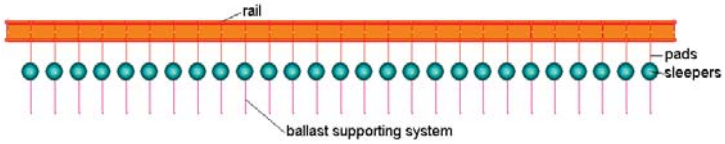	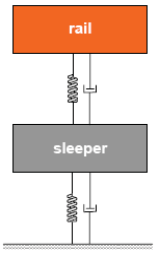
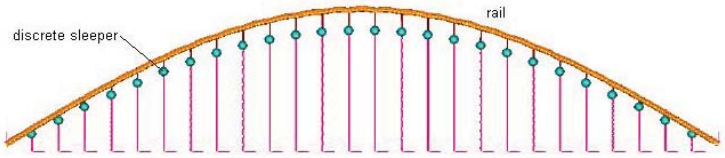 in-phase vibration	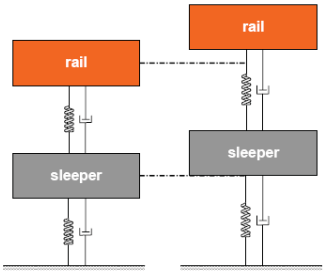
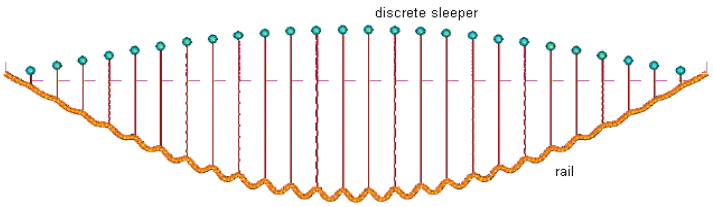 out-of-phase vibration	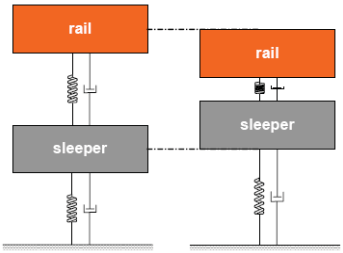

The track geometry quality is evident that almost all railway operators make use of automatic track recording cars (TRCs) to routinely collect track geometric datas and to assess the track quality with limit values in terms of the standard deviations of track irregularities [111]. European standards (EN 13848-1, prEN 13848-5, and EN 14363) have been developed to meet the requirements of European railway interoperability and also to improve track maintenance procedures [111].

Track defects with short wavelength (e.g. rail welds, dipped joints, hanging sleepers, and so on) are difficult to detect by evaluating the measured track geometry data [111]. Track safety, maintenance costs, and passenger comfort are depends on highly the track–vehicle system dynamics [111]. Thus, it is important to develop an assessment system that can effectively identify the in-situ ballasted tracks [111]. Accordingly, a planning for track maintenance should be decided that the combination of the track geometry quality and dynamic track responses [111].

Several researchers have investigated and devoted to this topic [17, 109, 111, 172, 185]. The dynamic model of track–vehicle interactions is reviewed and discussed in detail in [98, 111, 130, 140, 141]. Using commercial computer packages, it is possible to carry out simulations of the dynamic behaviour of track–vehicle; however it requires the sophisticated vehicle models [111]. To considering vehicle–track interaction problems such as rail and wheel corrugations, impact loads due to out-of-round wheels, and so on, the DIFF has been developed at CHARMEC could be performed to evaluate the vertical wheel–rail forces and track responses at high frequencies (up to 2,000 Hz) [92, 109, 111].

According to Berggren *et al.*, an evaluating system of dynamic wheel–rail forces for long track sections have recently developed and reviewed its application [13, 14, 111]. The model included that a vehicle (wheelset, carbody, and primary suspension) and a track (two layer continuously supported beams (introduced by Grassie and in TWINS) [65, 111, 180]. The track irregularities of short wavelengths (λ=0.5–3 m) can be generated high dynamic wheel–rail forces, and the level of irregularity amplitudes should be limited below the specifications [14, 111].

According to [14, 111], the track model, i.e., a finitely long beam resting on discrete rail pads/sleepers/ballast supports, provides the sleeper-passing frequency and pinned–pinned resonance. By several researchers, numerical track model have investigated that focused on wheel–rail interaction forces due to track irregularities and ballast condition in the mid and high frequency ranges [65, 72, 75, 111, 131].

According to [111], the dynamic track–vehicle model is produced for evaluating a long ballasted track section with 50kg rail and wooden sleepers on the Swedish line. Track irregularities measured by Banverket's TRC Strix with a wavelength of 0.5–25 m are used in the numerical analysis [111]. As shown in Fig. 3.13, the results of measured track irregularities and calculated dynamic wheel–rail forces were estimated for a 1.5 km long tested section [111]. To estimate the short track waves, the measured irregularities were high-pass filtered at a wavelength of 3 m [111].

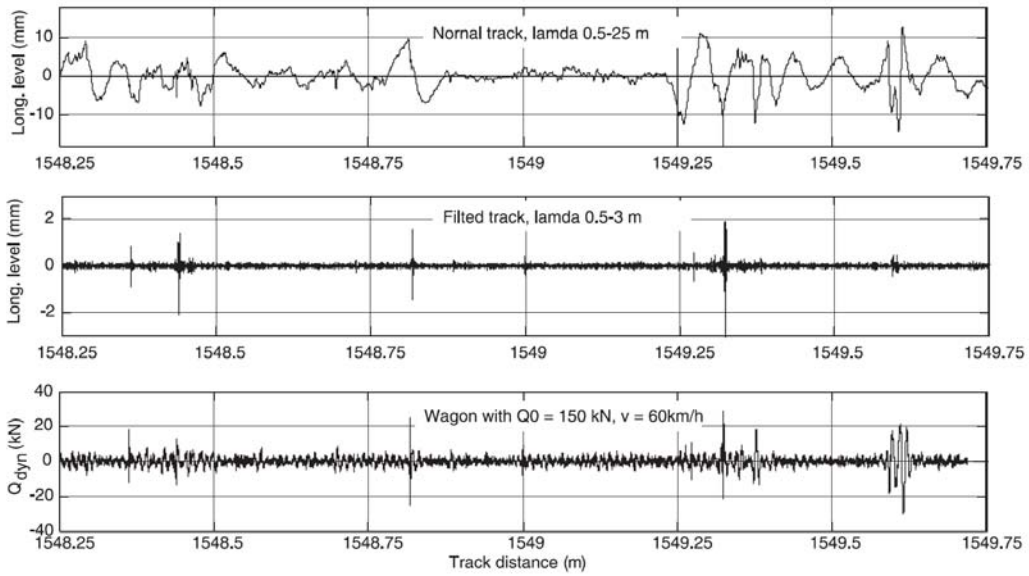

Fig. 3.13 Track geometry quality and calculated vertical dynamic wheel–rail forces [111]

As shown in Fig. 3.14, dynamic wheel–rail force over 40 kN are plotted with corresponding defect values [111]. According to the simulation using the wavelengths 0.5–3 m, the defect (vertical track irregularity) directly affects the dynamic wheel–rail force with a linear relationship [111].

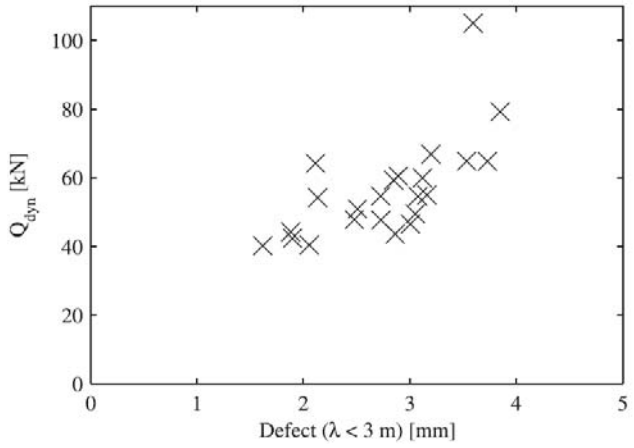

Fig. 3.14 Relationship between defects and dynamic force with short defects [111]

4 FIELD MEASUREMENT FOR TRACK CONDITION ASSESSMENT

4.1 Introduction

Most track engineers and designers usually estimate the dynamic response of the ballasted track based on the static loading specified in the design standards and apply dynamic factors [31, 41, 83, 87, 89, 90]. Nevertheless these results lead to extremely unreliable results due to unpredictable parameters in the track (e.g., the nonlinearity attributed to voided sleepers, rail irregularities, corrugation, deterioration of rail pads, etc) [31, 41, 95, 114]. The field measurement is the most effective method that accepted for determining the dynamic parameters of track components and for assessing the in-situ ballasted track [41, 85–92, 95, 127].

Experimental modal analysis is the most significant methodologies to solve the dynamic problems and analyse the track structures [85–92, 95]. It promises mechanical practical procedures and a reasonable solution to structural dynamics for the railway tracks [85–92, 95]. The structural track parameter such as stiffness and damping constant is depending on factors which were the time invariant properties [31, 85–92, 95]. The frequency response function (FRF) method is currently the common one to use for assessing and predicting modal parameters [31, 85–92, 95, 98, 99].

According to Sadeghi, the natural frequencies obtained from a test in the laboratory are higher than those obtained from the in-situ track test by performing modal testing [31, 89, 90, 95, 154]. These results indicated that ballast and subgrade cause a slight reduction in the natural frequencies of sleepers [31, 89, 90, 95, 154].

According to Plenge and Lammering, the dynamic behaviour of a segment track with voids between the sleepers and underlying ballast was assessed by performing full scale laboratory experiments [31, 89, 90, 95, 139]. The effects of partially unsupported sleepers lead to especially remarkable changes in the dynamic behavior [31, 41, 74, 90, 95, 139].

The discretely supported continuous rail system represent two effective masses of rail and sleeper, as well as two dynamic stiffness and two dashpots of rail pad and ballast/formation, respectively [34, 36, 95, 98]. Based on FRF measurements and FFT, the modal parameters of the track were extracted by an automatic curve fitting

optimisation procedure [85–92, 95]. Two resonance frequencies were clearly obtained and the first 'pin-pin' resonance was noticed in the FRFs measured [31, 41, 85–92, 95, 98, 99]. However Knothe et al. reported that the values obtained from the field could only be reliable in the frequency range of the second resonance peak [31, 95, 98–100].

The measured dynamic properties of track component can provide a reasonable input parameter for predicting and determining the dynamic behavior of ballasted track [31, 34, 35, 85–92, 95]. This section presents a non-destructive testing approach to evaluate the dynamic parameters of in-situ ballasted track components using the field testing and experimental modal analysis [85–92, 95].

Several researchers currently have investigated the dynamic parameter and condition assessment methods for the ballasted track, and produced various empirically and experimentally determined results [31, 34, 35, 85–92, 95]. According to Kaewunruen S and Remennikov A, the motion equations of a 2DOF model of ballasted track was developed using Fast Fourier Transform (FFT) technique based on the discrete support model [89, 90, 95].

Further, the modal properties of track components could be extracting from the field testing results obtained using an instrumented hammer impact technique [89, 90, 95]. Experimental modal testing is a very effective, mobile, and non-destructive testing, however, the measured response would be indicated the local track behaviours only [87, 89, 90, 95].

4.1.1 Overview of test sites

The field measurements were carried out on the ballasted track of a conventional line in Republic of Korea as shown in Fig.4.1.

The tested track provides a complex service to the passenger and freight trains. The ballasted tracks in the existing line currently under use were selected (R400 PCT). The test section was the curved and consisted of 50 kg long rails. Based on the visual inspection, the rail gauge and cant was found normal in general.

Fig. 4.1 Photographs of tested track and vehicles (Freight and passenger trains)

At the test sites, visual inspection for observable defects was carried out. The overall conditions of track were relatively found in good. There is less irregularity found on the railhead surface, such as dip-joints, squats, wheel burns, wears and so on. However, a damage of rail fastening system, and cracks in concrete sleepers was detected in some section as shown in Fig. 4.2.

(a) Cracked sleeper (b) Loosening fastener

Fig. 4.2 Photographs of tested track

In this section, the measured data are recorded to enhancing the non-destructive testing and its evaluation [89, 90, 95]. A total of four sections of a ballasted track were considered in this study (classified according to the good condition, loosening fastener, poor ballast condition and a track with cracked sleeper), i.e., had been classified by Kaewunruen S and Remennikov A [89, 90, 95].

4.1.2 Field test method

Experimental modal analysis (EMA) or modal testing is a non-destructive testing based on vibrations of the track structures using the instrumented hammer impact technique was introduced by Kaewunruen S and Remennikov A [89, 90, 95]. This technique has a lot of advantages such as mobililty and self-supporting, further the analytical models and the results has led to integrity evaluations of the part or entire of track structures [34, 35, 40–42, 89, 90, 95]. The EMA is used in this study as a non-destructive testing technique, i.e, as a same of the proposed method by Kaewunruen S and Remennikov A [74, 89, 90, 95].

Frequency response functions (FRFs) obtained by field test was used to predict the dynamic parameters of track components, i.e., dynamic stiffness, damping constant and mass, in the actual condition [31, 89, 95, 99]. Modal testing is useful to assess and predict the structural conditions of rail assemblages, i.e., concrete sleepers, rail pads, and ballast [31, 89, 95, 99]. The FRFs were recorded by vibration analyser in a frequency domain between 0 and 1,600 Hz [31, 89, 90, 95, 98, 99]. The frequency of interest was up to 600 Hz [89, 90, 95]. The measured data were optimised using a best curve fitting method to investigate the dynamic parameters of tested track components [89, 90, 95].

In this study, a large sledge impact hammer (5kg mass) was employed to measure the dynamic properties of the ballasted track [89, 95]. The impact hammers were used to hit at rail and sleeper to give excitation to the track [89, 95]. An accelerometer was installed on the specific part of rail and sleeper. Both the impact hammer and accelerometer were connected to the dynamic analyser system i.e., the FRFs could be investigated [89, 95]. To extracting the dynamic properties of the track components, the analytical models of the 2DOF model based on the FFT method depicted in Fig. 4.4 were developed by Kaewunruen S and Remennikov A [89, 95].

4.2 Track condition assessment

On the 2DOF system, a system identification of the ballasted track is important on account of the actual global track vibration of the ballasted track may not be identical to the model assumed [89, 95, 98, 99]. Five point test technique, i.e., was introduced by

Kaewunruen S and Remennikov A, is the effective alternative to estimate the system vibrations as shown in Fig. 4.3 [89, 90, 95].

The dynamic responses were processed by the dynamic analyser package to produce FRFs [89, 90, 95]. The FRFs have been employed in modal testing analysis package to identify the resonance frequencies and corresponding dynamic parameters of the tested track [89, 90, 95].

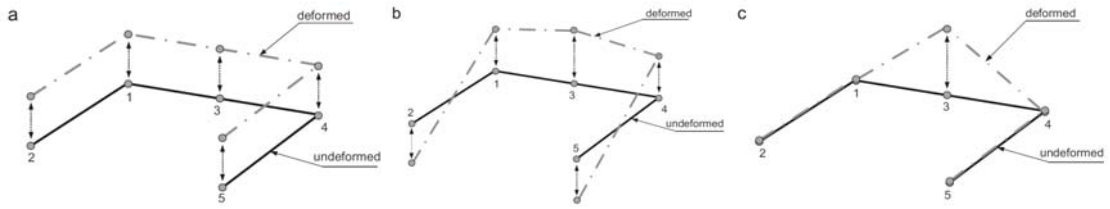

Fig. 4.3 Modal results from 5-point tests of track; (a) in-phase mode, (b) out-of-phase mode, (c) pin–pin mode [95]

As shown in Fig. 4.3(a), the resonance frequency between 150 and 250 Hz is related on the in-phase mode of vibration [89, 95]. The frequency range between 400 and 600 Hz is associated with the out-of-phase mode of vibration (Fig. 4.3(b)), and the pin–pin vibration is found that over the frequency range of 700–850 Hz (Fig. 4.3(c)) [89, 95].

According to previous studies, the 2DOF model of ballasted tracks has been proved by the field tests [88–92, 95]. Therefore, the ballasted track was simplified as a model of 2DOF discretely supported rail as shown in Fig. 4.4 [88–92, 95].

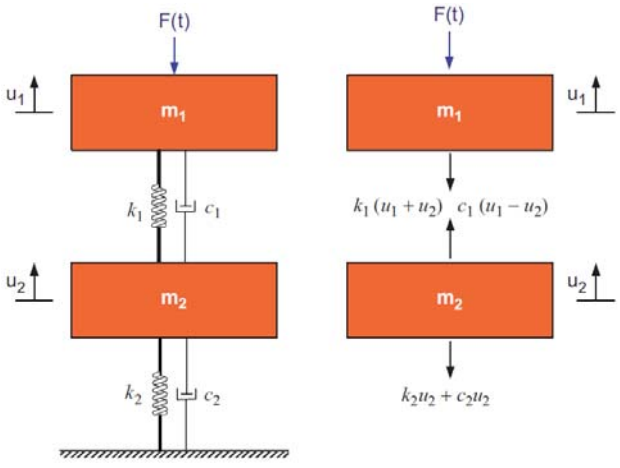

Fig. 4.4 2DOF dynamic model of railway track [95]

According to Kaewunruen S and Remennikov A, the 2DOF model has been developed based on the FFT and Mode Superposition (MS) methods which are given in equations (4-1) and (4-2), respectively [89, 95, 132].

$$H_{11}(f)=\frac{\sqrt{[k_1+k_2-4\pi^2 f^2]^2+[2\pi f(c_1+c_2)]^2}}{\sqrt{[(k_1-4m_1\pi^2 f^2)(k_2-4m_2\pi^2 f^2)-4\pi^2 f^2(k_1m_1+c_1c_2)]^2+4\pi^2 f^2[k_1c_2+k_2c_1-(m_1(c_1+c_2)+c_1m_2)4\pi^2 f^2]^2}} \quad (4\text{-}1)$$

$$H_{11}(f)=\left|\frac{1}{m_1}\frac{4\pi^2(m_1/k_1)f^2}{\sqrt{[1-4\pi^2(m_1/k_1)f^2]^2+[4\pi^2(m_1/k_1)(c_1^2/k_1m_1)f^2]}}+\frac{1}{m_2}\frac{4\pi^2(m_2/k_2)f^2}{\sqrt{[1-4\pi^2(m_2/k_2)f^2]^2+[4\pi^2(m_2/k_2)(c_2^2/k_2m_2)f^2]}}\right| \quad (4\text{-}2)$$

where, m_1 and m_2 are masses of rail and sleeper, k_1 and c_1 represent stiffness and damping coefficients of the rail pad and k_2 and c_2 represent stiffness and damping coefficients of ballast [89, 95, 132]. The parameters in equation (4-1) represent the actual stiffness, actual damping and actual mass value [89, 95, 132]. On the contrary, those of equation (4-2) were represented the modal stiffness, modal damping and modal mass based on the MS method [89, 95, 132]. These equations are to be used in least square method for the evaluation of the dynamic parameters of track components [89, 95, 132].

Fig. 4.5 shows the sensor instruments on the tested track in this study. Each point was hitted by the impact hammer. The accelerometers were installed at the rail and sleeper, which provides clearly the dynamic responses to impact excitations [89, 95].

Fig. 4.5 Photogrpahs of sensors instrumentation (Accelerometer and LVDT)

4.2.1 Good condition tracks

The FRF data to be processed for assessing the conditions of the tested track was assessed by performing field measurements [89–91, 95]. Fig. 4.6 shows the example of FRF measured in a frequency range of 0–600 Hz of the tested tracks [89–91, 95]. It shows good agreement with the experimental results of the previous researches [89–91, 95]. The FRF measured represents the dynamic responses of ballasted track system to given excitation, while the coherence provides the quality level of the measured signals [89–91, 95].

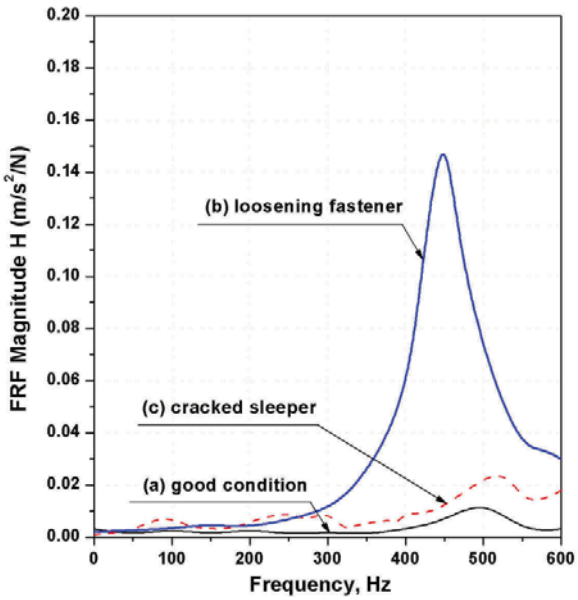

Fig. 4.6 Measured FRF on a site according to the condition of track component

In the frequency range of 0–600 Hz, it is found that the response quality is very good and acceptable in FRFs [89–91, 95]. According to the previous experimental works, the corresponding frequency range was of practical interest in this study, this frequency range is associated to the identified 2DOF system vibrations [74, 87, 89–91, 95].

The in-phase vibration tends to break and reshape the ballast granular, while the out-of-phase vibration is likely to accelerate the cracks on the railway sleepers [21, 31, 89, 95].

The data sets obtained from the field tests were processed using both of FFT and MS [89, 95]. The curve fitting algorithms were developed on the basis of least square optimization technique, and calculated by using a curve-fitting package Origin^{TM}

according to equation (4-1) and (4-2) [87–92, 95]. The FRFs obtained were tuned for the dynamic parameters [87–92, 95].

Dynamic parameters of the ballasted track can be predicted from the curve fitting as shown in Fig. 4.7 and Table 4.1 [87–92, 95]. In the frequency range of interest (0–600 Hz), the good condition tracks provide the dynamic responses in a good agreement with theoretical simulations as shown in Fig. 4.7 [88–92, 95]. According to the previous studies, typical ballasted tracks would behave like a 2DOF dynamic model, and the FRFs of this model consist of more than two apparent resonance peaks [88–92, 95] as shown in Fig. 4.7.

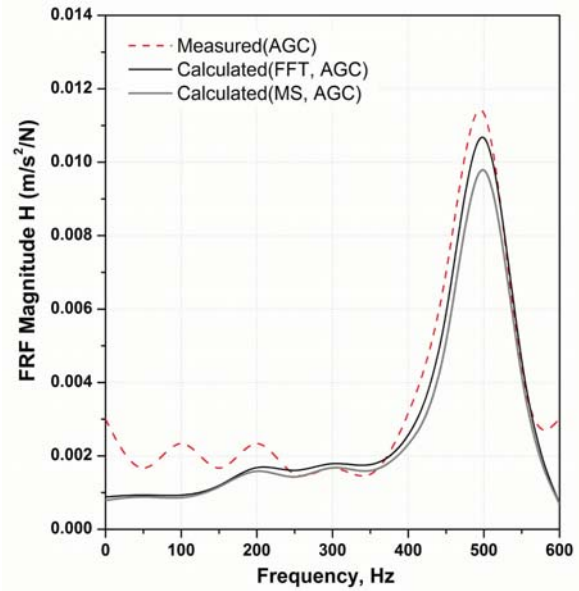

Fig. 4.7 Comparison of FRF for the good condition (AGC: All good condition)

Table 4.1 Summary of dynamic properties for tested track (using FFT)

Section (0–600Hz.)	Correlation (r^2)	Superstructure (Upper Part)		
		C_{pad} (kNs/m)	K_{pad} (kN/mm)	M_{rail} (kg)
A	0.99	1.4	963.4	168.9
B	0.99	17.0	570.4	72.5
C	0.88	5.0	524.5	115.5
Section	Correlation (r^2)	Substructure (Lower Part)		
		$C_{ballast}$ (kNs/m)	$K_{ballast}$ (kN/mm)	$M_{sleeper}$ (kg)
A	0.99	254.3	282.2	204.4
B	0.99	0.0	0.0	0.0
C	0.88	94.3	50.2	94.7

A: Good condition track, B: Track with loosening fastener, C: Track with cracked sleeper

The first low peak is the natural frequency of substructure, i.e., sleeper on ballast, and the second high peak is the frequency of superstructure, i.e., rail on rail pad [88–92, 95]. After curve fitting, the dynamic properties of the tested track were found close to the previous works [88–92, 95].

The actual dynamic properties of the tested track at section A (good condition) are listed in Table 4.2 using FFT and MS approaches, respectively [88–92, 95]. It was found that the correlation error of the curve fitting is less than 3% for FFT and 4% for MS approaches [88–92, 95]. The results obtained in this study using both approaches were in a good agreement with the previous experimental work [74, 88–92, 95].

Table 4.2 Comparison of dynamic properties for FFT and MS (good condition)

No.	Correlation (r^2)		Upper Part					
			C_{pad} (kNs/m)		K_{pad} (kN/mm)		M_{rail} (kg)	
	FFT	MS	FFT	MS	FFT	MS	FFT	MS
1	0.99	0.96	6.6	6.8	1,045.4	1,418.2	179.9	231.5
2	0.97	0.96	6.9	6.5	956.9	1,277.2	177.3	223.7
3	0.99	0.97	1.4	1.3	963.4	1,292.6	168.9	215.1
4	0.97	0.96	1.5	12.6	892.7	1,188.3	146.1	179.6
5	0.99	0.97	7.2	7.3	865.4	1,203.1	161.9	210.9
No.	Correlation (r^2)		Lower Part					
			$C_{ballast}$ (kNs/m)		$K_{ballast}$ (kN/mm)		$M_{sleeper}$ (kg)	
	FFT	MS	FFT	MS	FFT	MS	FFT	MS
1	0.99	0.96	239.8	234.2	362.2	474.1	227.0	316.9
2	0.97	0.96	241.6	214.8	284.0	356.1	194.2	263.0
3	0.99	0.97	254.3	234.2	282.2	366.5	204.4	285.5
4	0.97	0.96	254.8	237.7	271.5	306.3	184.2	264.7
5	0.99	0.97	204.8	209.5	191.0	261.5	183.9	261.5

Using FFT technique, the stiffness of rail pads was found to be about 865–1,045 kN/mm, while the MS technique resulted in 1,188–1,418 kN/mm. And, using FFT technique, the ballast stiffness was found to be approximately 191–362 kN/mm, and the MS technique resulted in approximately 261–474 kN/mm [90, 91, 95]. The damping constants for rail pads varied between 1–7 and 1–12 kNs/m based on FFT and MS technique, respectively [90, 91, 95]. Further, the damping of ballast varied from approximately 205–250 kNs/m based on both FFT and MS technique [74, 90, 91, 95].

The average parameters of track components determined by the field tests are listed in Table 4.3. Regarding to the stiffness and damping characteristics of rail pads (EVA), the conditions of track components can be considered reasonable and acceptable [95].

Table 4.3 Summary of dynamic properties for tested track (good condition)

Track components	Methodologies	Average parameters	
		Damping (kNs/m)	Stiffness (kN/mm)
Rail pad	FFT	4.7	944.7
	MS	6.9	1,275.8
	FFT+MS	9.3	1,021.5
Ballast	FFT	245.0	278.2
	MS	226.1	352.9
	FFT+MS	223.1	310.7

4.2.2 Loosening fastener

In a case of the fastener in a part of rail fastening system (e-Clip) was loosen and did not hold the rail to the concrete sleeper perfectly, the FRFs shows clearly that a defect in the local track system in the frequency range of up to 600 Hz [88–92, 95]. The FRFs of the track with loosening fastener looks similar to that found in a single-degree-of-freedom (SDOF) dynamic model [88–92, 95]. There is only one dominant peak in the frequency range of interest as shown in Fig. 4.8 [88–92, 95].

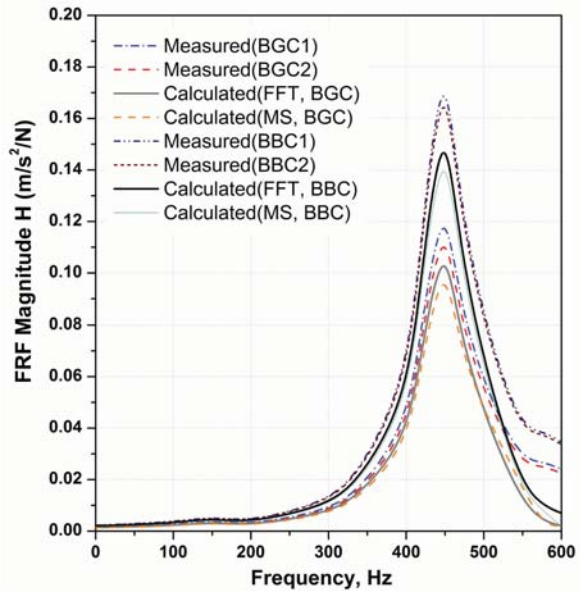

Fig. 4.8 Comparison of FRF for the loosening fastener

The dynamic responses of substructure in low frequency range reduced dramatically as a reason of there is no connection between superstructure (upper part) and substructure (lower part) [89, 95]. The curve fitting results with loosening fasener shows a poor integrity of substructure as listed in Table 4.4 [89, 95]. The average dynamic stiffness and damping constant of rail pad were 502 kN/mm and 16 kNs/m, respectively [89, 95].

Table 4.4 Summary of dynamic properties for tested tracks (loosening fastener)

Track components	Methodologies	Average parameters	
		Damping (kNs/m)	Stiffness (kN/mm)
Rail pad	FFT	17.0	580.7
	MS	13.4	415.2
	FFT+MS	16.1	502.0
Ballast	FFT	-	-
	MS	-	-
	FFT+MS	-	-

4.2.3 Cracked sleeper

The cracked sleeper significantly reduces the dynamic mass and stiffness of sleeper and ballast as listed in Table 4.5 [90, 91, 95]. The average stiffness of rail pad and ballast were approximately 720 kN/mm and 74 kN/mm, respectively. These values were lower than those of good conditioned track [90, 91, 95]. The ballast damping is also much lower than that of the good conditioned track [90, 91, 95].

Table 4.5 Summary of parameters of the ballasted track components with cracked sleeper

Track components	Methodologies	Average parameters	
		Damping (kNs/m)	Stiffness (kN/mm)
Rail pad	FFT	4.0	504.9
	MS	4.3	973.3
	FFT+MS	5.1	720.1
Ballast	FFT	91.4	48.9
	MS	73.4	98.1
	FFT+MS	83.6	74.5

As shown in Fig. 4.9, the FRFs with cracked sleeper shows that a lot of peaks with irregularities between the first and second peak [90, 91, 95]. In a case of the cracked

sleeper, the FRF signal presents less information for the detection on any defects [90, 91, 95]. However, the FRFs shows that a number of significant peaks with low amplitude and irregularities in the frequency range of up to 600 Hz [90, 91, 95].

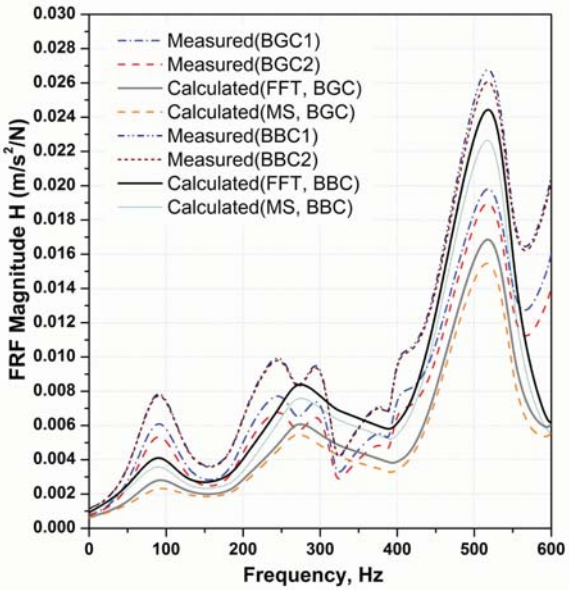

Fig. 4.9 Comparison of FRF for the cracked sleeper (BGC: Ballast good condition, BBC: Ballast bad condition)

4.3 Conclusions

The degradation and damage of the components for ballasted track could be caused a serious problem. Threfore, the integrity evaluation of ballasted track condition is important to ensure and predict that the track safety and track maintenance. The current condition of ballasted track was assessed by performing field measurement. The methodology presented in this section is adopted from the literature by Kaewunruen S and Remennikov A [88–92, 95].

(1) In this section, the experimental modal analysis was performed by the non-destructive testing, i.e., proposed by Kaewunruen S and Remennikov A [88–92, 95]. Modal test results were obtained from the field test and used to assess the condition of the track components. A total of four sections of a ballasted track were considered in this study (classified according to the good condition, loosening fastener, poor ballast condition and a track with cracked sleeper), i.e., had been classified by Kaewunruen S

and Remennikov A [88–92, 95]. For practical purposes, this section integrates field measurements and experimental modal analysis to evaluate the dynamic integrity of in-situ ballasted track.

(2) From the field test, the system of ballasted track was found to be simplified as a two-degree-of-freedom (2DOF) dynamic system. The dynamic properties of track components were assessed by performing the field test using hammer impact technique. The measured data in the frequency range of interest (up to 600 Hz) have been analyzed using least-square curve fitting to determine the dynamic stiffness and damping of the tested track components. The analysis results obtained using two approaches, i.e., FFT and MS, were in a good agreement with the previous experimental results [88–92, 95]. Therefore, the condition of track component was found to directly affect the dynamic response of ballasted tracks (e.g. the frequency response function).

(3) As the results, the dynamic properties of the track component was depend on the track condition and was distributed more roughly and over a wider range than its initial design values. Therefore, the dynamic property of ballasted track is more suitable to assess by the range of properties.

Further, the methodology presented in this section is possible to determine experimentally the fundamental track parameters which are required in the numerical analysis of track vibration, and also are useful for the assessment of track condition.

5 RELATIONSHIP BETWEEN TRACK IMPACT FACTOR AND TRACK SUPPORT STIFFNESS

5.1 Introduction

Track support stiffness (TSS) is used as a quality index of rail tracks to assess their performance and bearing capacity. The TSS is measured in terms of the amount of deformation in tracks subjected to a passing train load. TSS directly depends on the elastic stiffness of the elastic elements and the structural characteristics of the track system. Therefore, TSS is an important factor affecting both the tracks and the vehicles [22, 25, 26, 83]. Further, the TSS values vary with the track structure (e.g., ballasted and slab tracks) and the structural characteristics of the slab track (elastic fastening system, rail floating system, and sleeper floating system) [25, 26].

TSS can be regarded as a unique characteristic of a track system. The TSS of track structures has been investigated by performing theoretical and experimental studies related to the dynamic behavior of tracks with variations in the track stiffness between tunnels, bridges, and earthwork joints, and it has been shown that the TSS directly depends on the variations in the dynamic wheel load and deflections in the tracks [13, 20, 22, 25, 26, 124].

However, only a few studies have been conducted on the TSS of various types of tracks used in domestic railways, and therefore, in this study, the empirical TSS for different track structures was compared with the experimentally measured value to show that the TSS of different track structures should be taken into account during track designing and evaluation [25, 26]. In the Republic of Korea, the track impact factor (TIF) currently used in designing ballasted and slab tracks is estimated according to the specifications of American Railway Engineering Association (AREA) (1+0.513V/100; V=train speed, km/h) [26, 57, 177, 178]. However, the TIF is not detailed enough to describe various track types and TSS; for instance, the structural behaviors of a ballasted track and rail floating track are significantly different.

The relationship between the TSS and the TIF for various types of tracks currently employed in Korean urban transit was assessed by performing field tests using actual vehicles running along the service lines [25, 26]. In this section, field tests were performed on ballasted tracks (with good and bad ballast conditions) and three slab

track types, i.e., sleeper-embedded track (elastic fastening system), rail floating track, and sleeper floating track, as done in the author's previous studies [25, 26].

The theoretically designed TIF and TSS were compared with the corresponding TIF and TSS measured through field tests for the various track types on the service line.

5.2 Literature review of dynamic wheel load

Dynamic force is a time-dependent external force that includes inertial, damping, and elastic forces acting on a structure, and it could be converted to a single static force, called pseudo-static force [31, 41, 67, 77, 114]. Therefore, dynamic force could be defined simply by the relationship between the dynamic stiffness and the displacement [67, 77]. The structural dynamic force can be derived from the equation of motion (5-1):

$$\{F(t)\} = [M]\{d''(t)\} + [C]\{d'(t)\} + [K]\{d(t)\} \tag{5-1}$$

Where, $[M]$ is the mass matrix, $[C]$ is the damping matrix, $[K]$ is the stiffness matrix, and $\{F(t)\}$ is the dynamic force as a time-dependent external force. $\{d''(t)\}$, $\{d'(t)\}$, and $\{d(t)\}$ are the acceleration, velocity, and displacement of the rail, respectively [67]. When the displacement d of node i is at its maximum at $t = t_{(i)\max}$, the pseudo-static force is defined by rearranging the equation of motion (5-1) [67]:

$$\{F_{pseudo}(t_{(i)\max})\} = [K]\{d(t_{(i)\max})\} = [M]\{d''(t_{(i)\max})\} + [C]\{d'(t_{(i)\max})\} - \{F(t_{(i)\max})\} \tag{5-2}$$

From equation (5-2), the maximum pseudo-static force of node i throughout time with the maximum displacement at $d'(t)=0$ is defined more accurately by equation (5-3) [67]:

$$F_{pseudo\ (i)\max} = [K_{(i)}]\{d_{(i)\max}\} \tag{5-3}$$

Where, $[K_{(i)}]$ is the i-th row of $[K]$ and $\{d_{(i)max}\}$ is the displacement of node i at its maximum [67]. In equation (5-3), $[K_{(i)}]$ is a known value and the theoretically designed value in a linear system. $F_{\text{pseudo(i)max}}$ and $d_{\text{(i)max}}$ can be estimated by a field test or

numerical analysis. Thus, equation (5-3) represents the equivalent stiffness of node *i* with respect to the displacement [67]. Therefore, the equivalent stiffness directly affects the dynamic force.

Track geometrical irregularities, unsprung and sprung masses, vehicle suspension stiffness and damping variations in track flexibility, wheel flats, and corrugations on wheels and rails exert dynamic forces on the track; train speed is another important parameter [22, 41, 83, 114, 127, 144]. The influence of rail surface roughness and TSS of a ballasted track on dynamic forces, i.e., dynamic wheel-rail force such as P1 and P2 force, was assessed by performing numerical analysis and field tests along the in-service high speed railway lines [22]. For a constant rail surface roughness, an increase in the TSS caused the dynamic force to increase.

Therefore, the TSS directly affects the dynamic force of the track [22]. The TIF, i.e., dynamic factor or dynamic amplification factor, converts a static wheel load to an equivalent dynamic wheel load [22, 67]. In track design, the vertical wheel load is multiplied by the TIF to account for the dynamic force of the track [7, 41, 67, 114, 127, 148]. The TIF is determined under the assumption that the static wheel load is known [67, 127].

Several approaches have been developed to estimate the dynamic forces and the TIF on a track. One approach is to measure the dynamic wheel loads using specially designed wheels or vehicles. Another approach is to perform computer simulations using appropriate numerical models of the vehicle and the track. The vertical wheel loads exerted by a standard Swedish RC locomotive on a tangent track of good quality were estimated using different models in a study by Johan Öberg [83].

Fig. 5.1 shows the differences when using the different models of dynamic force contributions [83].

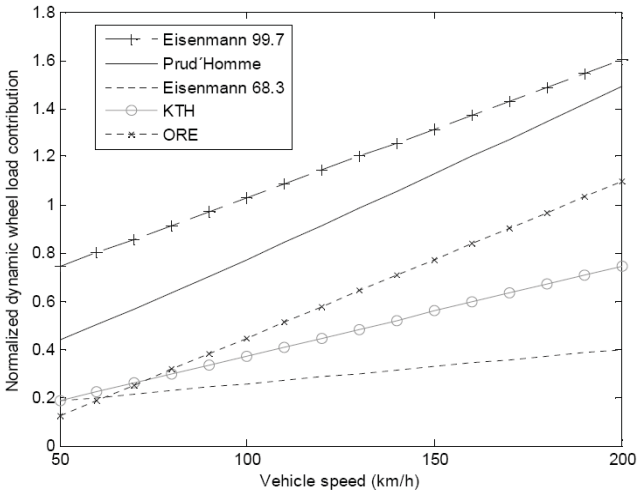

Fig. 5.1 Dynamic wheel load contribution for different models [83]

Further, Naudé et al. have investigated different dynamic factors such as the ratio of the total dynamic wheel load to the static wheel load [127]. They compared the results of different models with those of empirical tests on dynamic forces, and the ratio was found to range from 1.0 to 2.4 for train speeds ranging from 0 to 140 km/h. It is obvious that the different models consider different aspects and different conditions for trains and tracks [83].

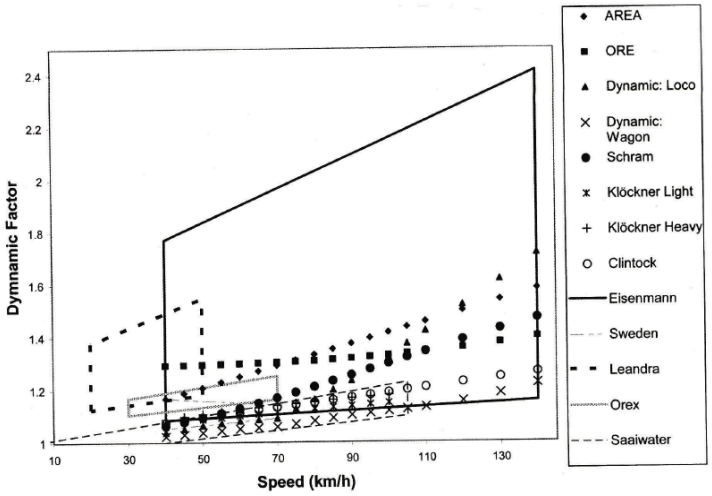

Fig. 5.2 Dynamic factors in a comparative study made by Naudé et al. [83, 127]

Gu & Choi have investigated the relationship between dynamic impact factors and the stiffness for the rail support, including damping of the rail support materials [67]. They proposed a simplified analysis method for the rail support response and compared the

results of proposed numerical models with those of experimental tests on dynamic forces for various rail support stiffnesses [67]. According to them, the dynamic impact force of the track is governed by the stiffness and damping of the rail support materials [67].

In order to investigate the magnitude of typical dynamic factors, i.e., TIF, current widely accepted empirical formulas were investigated and compared to measurements. According to Esveld, it is common practice to carry out strength or fatigue calculations for a static system in which the dynamic effects are taken into account by a speed coefficient or a dynamic amplification factor, i.e., dynamic factor or TIF [41]. Further, Esveld proposes multiplication of the static wheel load by an additional factor to account for the increase in wheel loads at the curved tracks as caused by cant deficiency or excess [41].

Researchers over the world have investigated the magnifying effect of dynamic wheel loads and produced various empirically determined formulas demonstrated that the measured results and static wheel loads as input [115, 126].

As shown in Table 1, a number of empirical formulas for the calculation of the TIF were investigated according to the train speed and geometric conditions in different countries, e.g., those of Eisenmann, Schramann, Klöchkener, Clarke, ORE, and AREA [7, 41, 67, 115, 126, 127, 177, 178, 188]. However, these empirical formulas are not detailed enough to describe various track types and TSSs [67, 126].

Table 5.1 Empirical formulas for calculation of track impact factor [67]

Proposer	Formula	Proposer	Formula
AREA	$1+5.21(V/D)$	BR	$8.784(\alpha_1+\alpha_2)V\left(P_jP_u/g\right)^{1/2}/P_s$
Republic of Korea	$1+0.513(V/100)$	South Africa	$1+4.92(V/D)$
Eisenmann (V≤60km/h)	$1+\delta\,\eta\,t$	Schramann	$1+45\times10^{-6}V+15\times10^{-8}V^3$
Eisenmann (60≤V≤200km/h)	$1+\delta[1+(V-60)/140]t'$	Klöchkener (light traffic)	$1+20\times10^{-4}V+7\times10^{-6}V^2$
Sadeghi	$1.098+8\times10^{-4}V+10^{-6}V^2$	Clarke	$1+\left(19.65V/Du^{1/2}\right)$

5.3 Theoretical track support stiffness

As shown in Fig. 5.3, the analytical model of a general track structure is a linear spring model wherein each track component is connected to spring elements having different spring stiffnesses. The stiffness of the track components such as rails and sleepers was excluded from the calculations of the elastic stiffness of the track structure; only the configuration of elastic-resilience materials was considered.

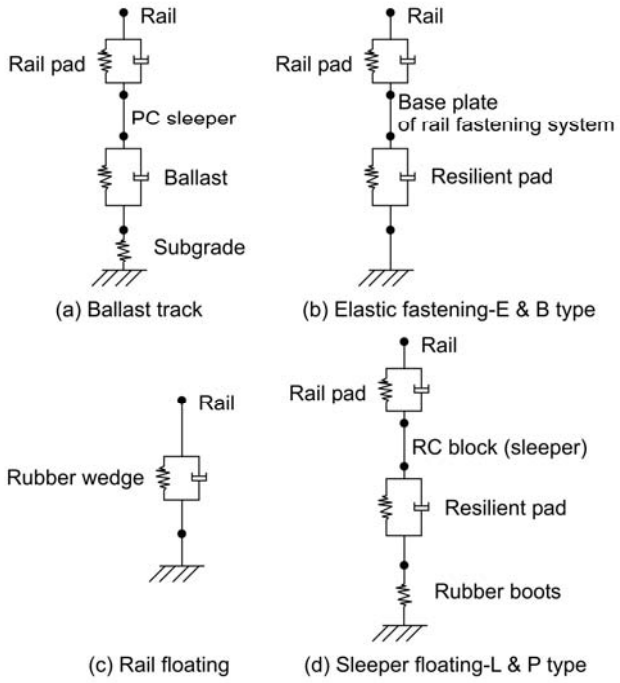

Fig. 5.3 Analytical models of different track structures

Many researchers have assumed that k can be expressed as a series of linear spring elements with different spring stiffnesses placed at the rail supporting point composed of a rail pad, sleeper, and roadbed (subsoil) connected in series following equation (5-4) [13, 20, 25, 41, 57, 98, 102, 114, 127, 144].

$$k = \frac{1}{\frac{1}{k_p} + \frac{1}{k_b} + \frac{1}{k_s}} \tag{5-4}$$

Where, k_p: rail pad stiffness, k_b: ballast stiffness and k_s: subsoil stiffness.

In this study, the spring stiffness of the supporting point of the track structure, i.e., the track spring coefficient *k*, was calculated by considering the structural characteristics of the track, and the TSS was calculated by considering the sleeper spacing, as shown in Table 5.2 [25, 26].

Table 5.2 Theoretical track support stiffness of different track structures [25, 26]

		Ballasted track	Slab track				
			Elastic fastening		Rail floating	Sleeper floating	
			E type	B type		L type	P type
Spring stiffness of elastic materials (kN/mm) (static/dynamic)	Rubber wedge	-	-	-	4.2/6.3	-	-
	Rail pad	400	600	600	-	400	450
	Resilience pad	-	14.9 /22.3	17.5 /26.25	-	20/30	15/22.5
	Rubber boots	-	-	-	-	2,000	2,000
	Ballast	200	-	-	-	-	-
Spring stiffness of rail supporting point (kN/mm), (static/dynamic)		133.3	14.54 /21.55	16.77 /25.15	4.2/6.3	18.9 /27.5	14.14 /21.21
Sleeper spacing (mm)		625	618	625	634	625	625
Theoretical track support stiffness (kN/mm), (static/dynamic)		213.28	23.53 /34.87	26.83 /40.24	6.63/9.94	30.20 /44.0	22.62 /33.94

The spring stiffness of the different elastic spring materials used for the rail supporting point was obtained by referring to the design data of each track structure [25, 57, 67, 177, 178]. Further, the theoretically designed TSS was compared with the TSS measured by considering the sleeper spacing at the test site.

5.4 Field measurements

5.4.1 Overview of test sites

A total of seven track sections of a subway line in Seoul, Korea, were considered in this study: two sections of a ballasted track (classified according to the ballast condition, i.e., good or bad) and five sections of a slab track (classified according to the type of elastic fastening system, rail floating system, and sleeper floating system) [25, 26].

All the sections were 60-kg straight, continuous welded rail tracks. The gauge and cant of the track segments obtained from the field measurements appeared to meet the specifications of a straight track, and therefore, it was considered that there was no significant difference between the wheel load acting on the inner and outer rail tracks. The parameters and photographs of the test sites are shown in Table 5.3 and Fig. 5.4, respectively [25, 26].

Table 5.3 Parameters of test sites [25, 26]

	Ballasted track		Slab track				
			Elastic fastening system		Rail floating system	Sleeper floating system	
	Bad	Good	E type	B type		L type	P type
Passing tonnage (MGT)	3.5	6.6	0 (test line)	0.3	0 (test line)	2.5	3.1
Curve radius (R)	∞ (straight)		∞ (straight)	∞ (straight)	∞ (straight)	∞ (straight)	∞ (straight)
Cant[2] (mm)	0		0	0	0	0	0
Track gauge[2] (mm)	1,435		1,435	1,435	1,435	1,435	1,435
Rail	continuous welded rail, 60 kg		continuous welded rail, 60 kg	continuous welded rail, 60 kg	continuous welded rail, 60 kg	continuous welded rail, 60 kg	continuous welded rail, 60 kg
Spring stiffness of rail supporting point[1] (kN/mm)	133.3		14.54	16.77	4.2	18.9	14.14
Sleeper type	PC sleeper		RC block	Precast slab panel	-	RC block	PC sleeper
Sleeper spacing[2] (mm)	625		618	625	634	625	625

[1] Spring stiffness of rail supporting point considered during track designing. (Reference design data)

[2] Data measured at test site

Fig. 5.4 Photographs of test tracks

5.4.2 Dynamic track response measurement

The dynamic wheel load acting on track segments subjected to a passing train load was measured by installing a two-axis strain gauge on the rail web between sleepers [25, 26, 79]. The measured signal was recorded on a data acquisition system (MGC-Plus) and was analyzed using the Origin™ program [25, 26, 79]. To eliminate the interference from other passing trains and obtain a reliable measure of the wheel load of the current

passing train, the dynamic wheel load at the site was measured by attaching a wheel load gauge wired to eight strain gauges at an angle of 45° along the neutral axis of the rail web and at a distance of 100 mm from the center point between sleepers, as shown in Fig. 5.5 [25, 26]. The vertical wheel loads were measured using shear strain gauges coupled to a full Wheatstone bridge circuit [25, 26, 79]. The strain gauge bridges were calibrated using a hydraulic ram and a load cell to obtain measurements with an accuracy of 2%. The shear strain bridges were mounted on both rails between two consecutive sleepers. In order to prevent data distortion and loss, the sampling rate was set to 1 kHz [22, 25, 26].

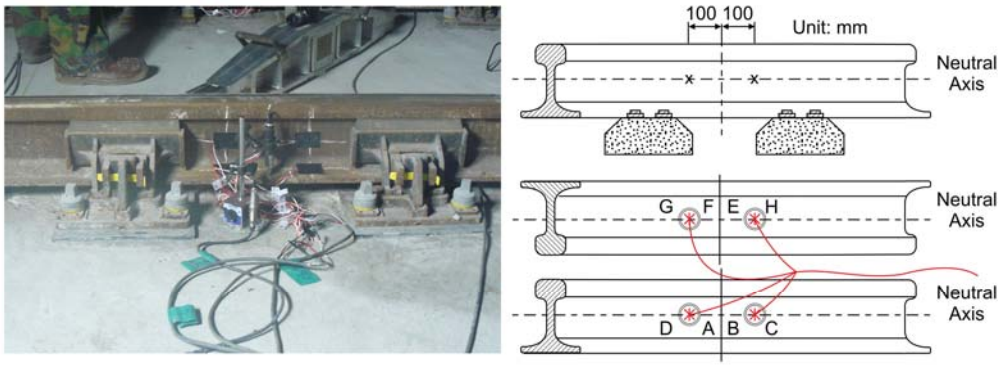

Fig. 5.5 Photograph of wheel load gauge and positions

By measuring the vertical displacement of tracks subjected to a passing train load, the effect of the dynamic load on the track section can be evaluated and used to calculate the TSS of the track [25]. Vertical rail displacements were measured using displacement transducers such as linear variable differential transformers (LVDTs) mounted on a jig anchored at the concrete layer of the subway structure, as shown in Fig. 5.6 [25, 26].

Fig. 5.6 Photographs of displacement transducers and strain gauges

In the case of the ballasted track, to avoid interference due to the displacement of the ballast and measure only the displacement of the track, the jig was firmly fixed to below the ballast layer at the concrete surface of the tunnel, i.e., tunnel invert concrete. The concrete structure, i.e., a part of substructure or subgrade, does not deform. Therefore, the resultant displacement of the ballasted track on the tunnel is dependent only on the displacement of the elastic components, i.e., the rail pad and the ballast (gravel), between the rail and the bottom concrete surface of the tunnel.

In the case of the slab track, the displacement transducer was mounted on the upper surface of the slab track, assuming that the slab layer does not deform when subjected to a passing train load. Although both vertical and lateral displacements were measured during the field tests, only the vertical displacement was used to calculate the TSS.

TSS is measured as the ratio of the maximum vertical displacement to the maximum dynamic wheel load. TSS (k) can be defined as follows [67]:

$$k = \frac{F_{railmid}}{d_{railmid}} \tag{5-5}$$

Where, k is the TSS (kN/mm), $d_{railmid}$ is the vertical displacement of the rail between two consecutive sleepers (mm), and $F_{railmid}$ is the vertical dynamic wheel load at the same point (kN). This definition assumes that load and displacement have a linear relationship [67].

The bending strain of rail was measured by longitudinally attaching a one-axis strain gauge to the bottom flange of the rail, as shown in Fig. 5.6 [22, 25, 127]. The strain gauge was placed between sleepers, at the centre.

In this section the effect of track support stiffness of railway tracks on track impact factor has been evaluated based on the field test performed in the author's previously published studies [25, 26].

5.4.3 Field measurement results and analysis

The dynamic wheel load measured for the different track segments is shown in Fig. 5.7 [25, 26]. The train speed and number of measurements for each test section are listed in Table 5.4 [25, 26].

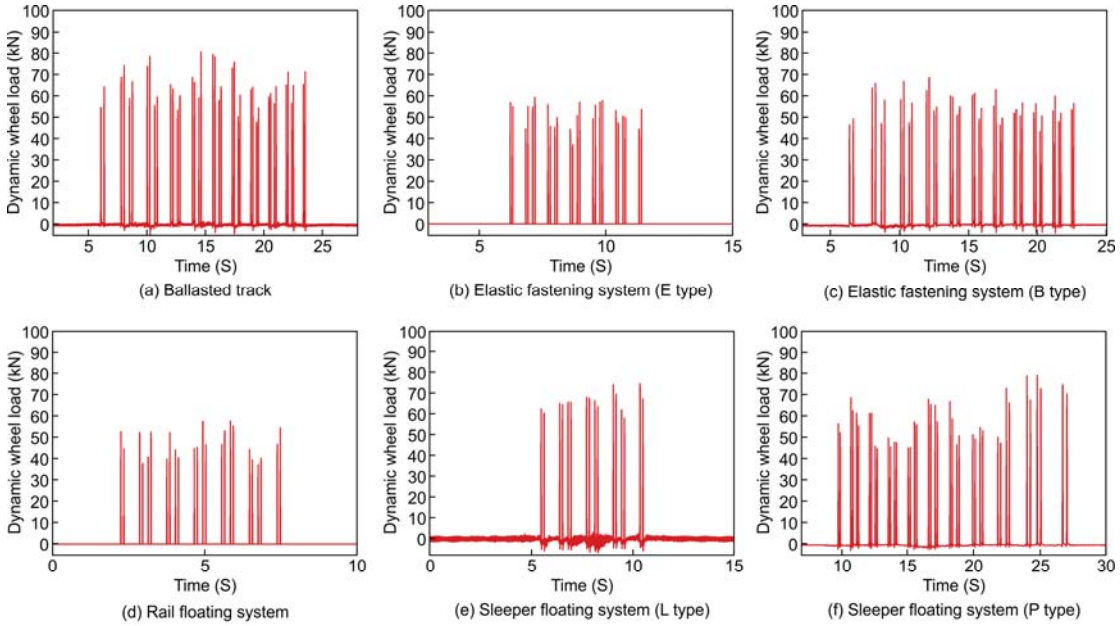

Fig. 5.7 Measured dynamic wheel load

Table 5.4 Number of measurements and train speed [25, 26]

Track type	Number of measurements	Train speed (km/h)	
		Min	Max
Ballasted track (Bad)	38	41	59
Ballasted track (Good)	44	28	47
Elastic fastening system (E type)	18	5	80
Elastic fastening system (B type)	36	31	39
Rail floating system	18	5	80
Sleeper floating system (L type)	32	32	45
Sleeper floating system (P type)	45	38	73

Fig. 5.8 (a)–(d) show the variations in the wheel load acting on the track segments at different train speeds. In the case of elastic fastening (E type) (Fig. 5.8 (b)) and rail floating systems (Fig. 5.8 (c)), the variations were distributed on a low level, i.e., approximately 10 kN for the dynamic wheel load was 50–60 kN, over a wide range of speeds, i.e., 5–80 km/h [25, 26].

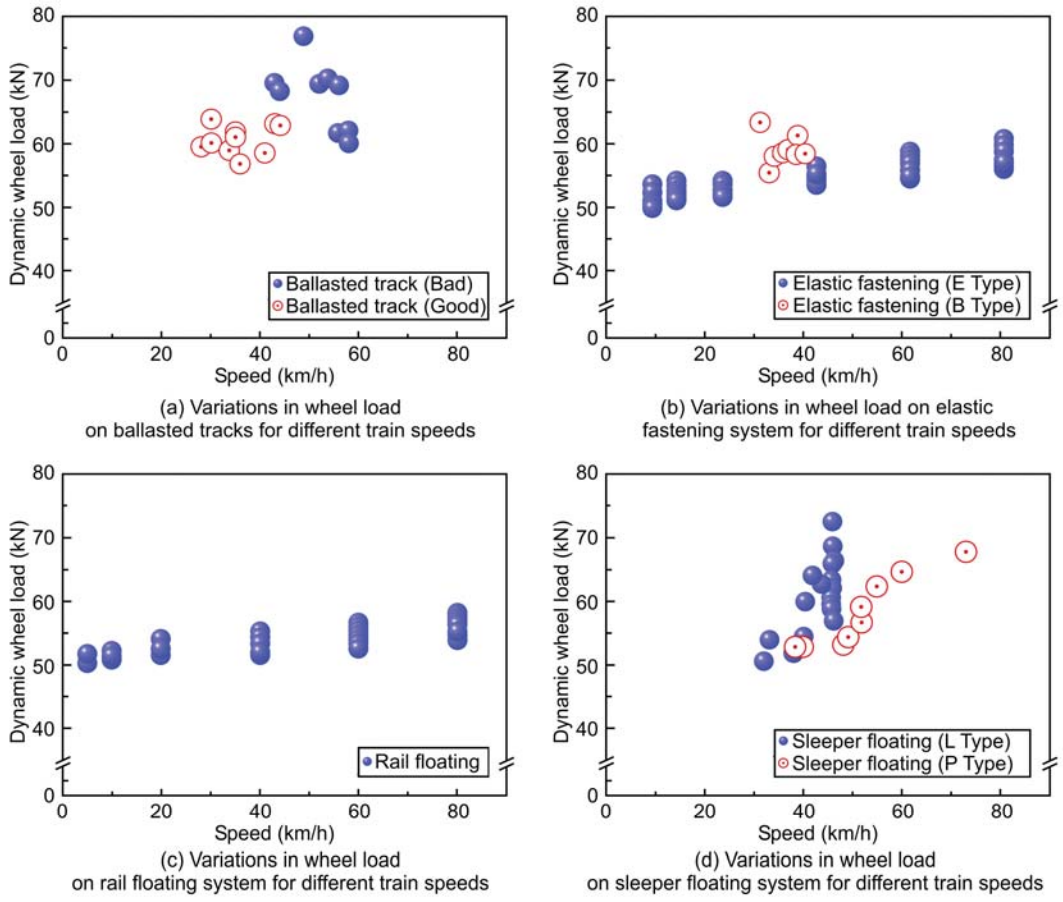

Fig. 5.8 Variations in dynamic wheel load vs. train speed on different track systems

As shown in Fig. 5.8 (a), in the case of the ballasted track in bad condition, the variation was distributed on a higher level, i.e., approximately 20 kN for the dynamic wheel load of 59–78 kN, over a narrow range of speeds, i.e., 41–59 km/h, as compared to the case of the ballasted track in good condition i.e., approximately 8 kN over the same range of speeds [25].

Further, as shown in Fig. 5.8 (d), the distribution of wheel load for the L-type sleeper floating system was relatively larger over a narrow range of speeds than that for the P-type sleeper floating system [25]. The vertical displacements in the track sections subjected to a passing train load are shown in Fig. 5.9 [25, 26].

Fig. 5.9 shows that the rail floating system showed the highest vertical displacement and the ballasted track showed the lowest vertical displacement [25, 26]. The reason for this difference was that the rail web in the case of the rail floating system was supported by a relatively soft resilience material, and therefore, the track structure itself was floated [25, 26].

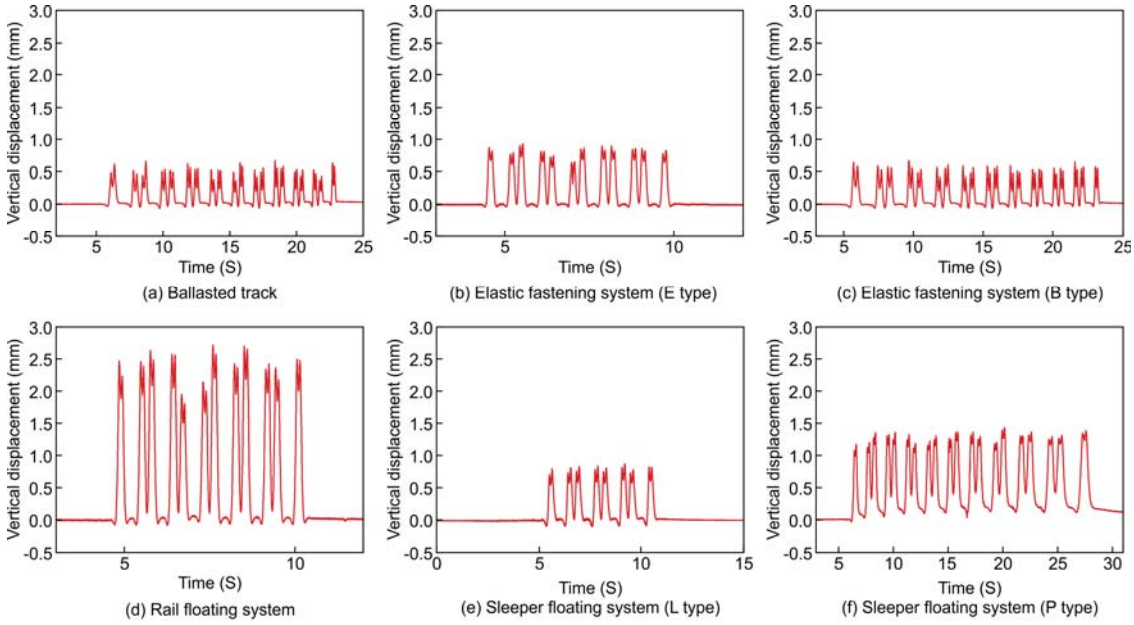

Fig. 5.9 Measured vertical displacements in track segments

However, because the large vertical displacements in the rail floating system were not due to flexural deformation of the track itself, this track showed the lowest bending stress, as shown in Fig. 5.10 [25, 26]. The ballasted track showed the largest bending stress [25].

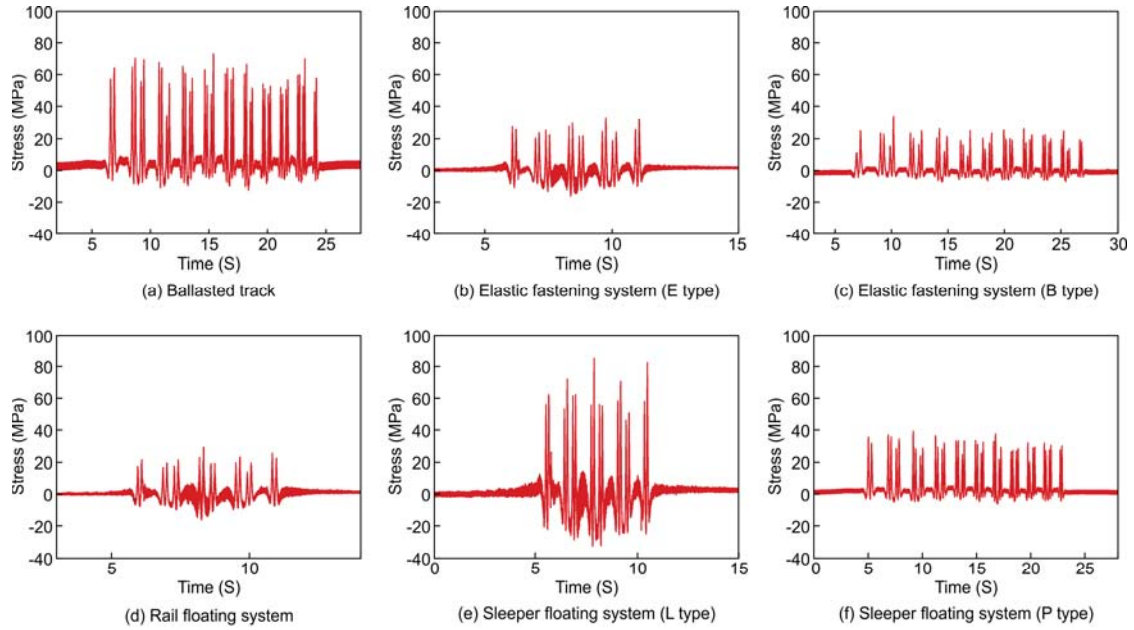

Fig. 5.10 Measured bending stress of rail bottom in track segments

5.5 Measured track support stiffness

As discussed before, the dynamic response of the ballasted tracks differed according to the condition of the ballast, i.e., good or bad. Therefore, prior to the measurement of the TSS, the ballast was sieved and its condition was evaluated by conducting an abrasion test (KS F 2502, for 5610-1058 A). The ballast was graded as good or bad according to its abrasion resistance. The ballast was sieved three times, and the average weight of the three samples was used in the evaluation [25, 26].

Table 5.5 lists the results of sieving, and Table 5.6 shows the results of the abrasion test [25, 26]. Fig. 5.11 shows the particle size distribution of the ballast on the basis of sieving results; the standard particle size distribution is also shown for reference [25, 26].

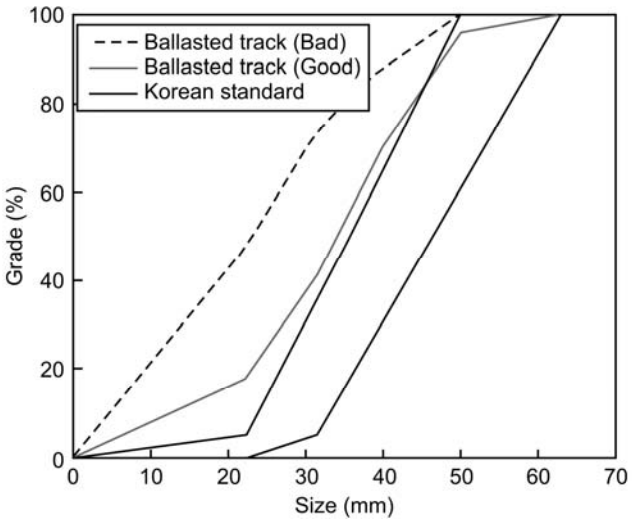

Fig. 5.11 Particle size distribution of ballast

Table 5.5 shows that the grades of almost all the samples exceeded the reference values [25, 26]. On the other hand, Table 5.6 shows that the abrasion resistance of all the samples was below the reference value, and therefore, it was inferred that the abrasion resistance of the ballast in the ballasted track can be ignored [25, 26]. TSS is measured as the ratio between the maximum vertical displacement and the maximum dynamic wheel load. The estimated TSS for each track is shown in Fig. 5.12 [25].

Table 5.5 Results of sieving [25, 26]

Sieve size (mm)	Grade (%)		Korean standard
	Ballast (Bad)	Ballast (Good)	
22.4	48	18	0–5
31.5	74	41	5–35
40	88	70	30–65
50	100	96	60–100
63	100	100	100

Table 5.6 Results of abrasion test [25, 26]

	Ballast (Bad)	Ballast (Good)	Korean standard
Abrasion rate (%)	15.2	8.2	<25

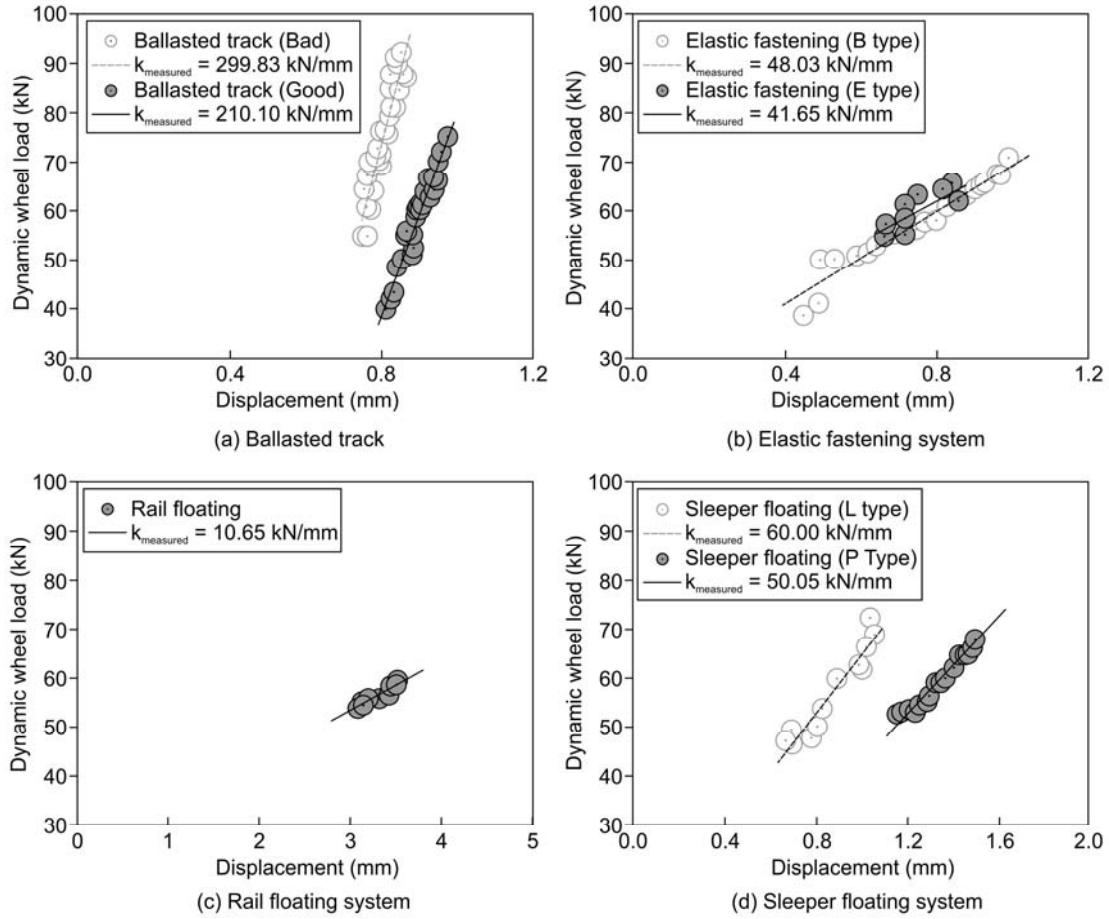

Fig. 5.12 Measured track support stiffness

A linear regression analysis of the measured TSS values was conducted by excluding the maximum and minimum values and the values corresponding to abnormal signals (noise component) or measurement errors [25]. The coefficient of correlation was

approximately in the range of 0.89–0.92 for each test section, and thus, the reliability of the linear regression analysis was confirmed [25]. As shown in Fig. 5.12(a), the condition of the ballast appeared to directly affect the TSS of the ballasted track and the slope of the curve was fairly larger than that of the other tracks [25]. This reason for this difference was attributed to the deterioration of the ballast [25].

In the case of the ballasted tracks, the TSS for the bad ballasted track was approximately 30% higher than that for the good ballasted track [25]. In the case of the slab tracks, the TSS for the sleeper floating systems was approximately 28% higher than that for the elastic fastening systems and the TSS for the rail floating system was approximately 4 times lower than that for the elastic fastening systems [25].

In the case of the ballasted track in bad condition, the measured TSS value was 29% higher than the theoretical value [25]. In the case of the sleeper floating tracks (L and P type), the measured value was 32% higher than the theoretical value [25]. On the other hand, the theoretical and measured values were almost similar for both the rail floating system and the good ballasted track [25].

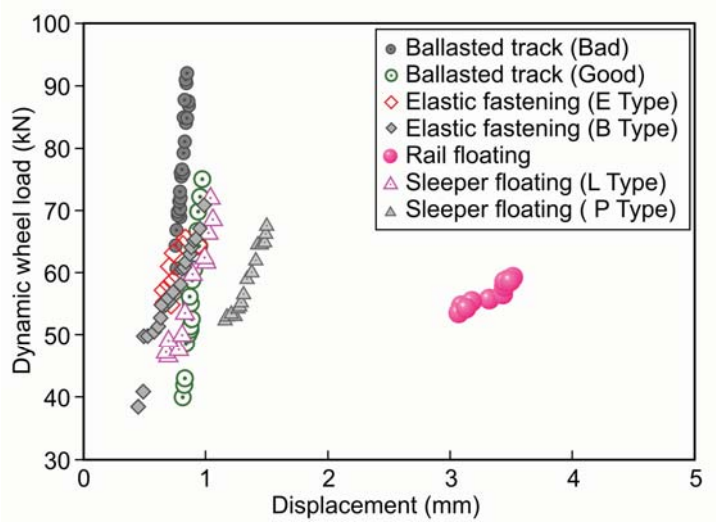

Fig. 5.13 Comparison of measured track support stiffness values for seven track segments

The sleeper floating tracks (L and P type) consist of soft resilient pads embedded under the sleepers, and therefore, the design specifications of TSS values for these tracks are low [25]. Further, the theoretical TSS was estimated considering only the vertical stiffness of the tracks, whereas the measured TSS was estimated considering both the longitudinal and the vertical stiffness of the tracks [25]. Therefore, the measured value

was higher than the theoretical value [25]. This suggests that the longitudinal stiffness of the tracks should also be considered in the evaluation of the TSS [25].

5.6 Measured track impact factor

The dynamic wheel load exerted on a track by a moving train includes the impact load caused by an increase or a decrease in the train speed and other dynamic load amplification factors, in addition to the static wheel load [26]. Therefore, the wheel load obtained by the field measurements was a dynamic value, and the TIF was calculated by comparing the dynamic load with the static load of a train. The measured TIF converts the static wheel load to an equivalent dynamic wheel load. Moreover, to consider the increase in weight due to boarding passengers, the static wheel load was measured when the trains were in motion. In reality, it is difficult to estimate the static load of a train and the exact number of passengers boarding the train. Therefore, the variations in the total wheel load were measured during peak hours [26].

The passenger load was assumed to be 62 kg per person, and the passengers were classified into three groups according to the level of congestion: highly congested, moderately congested, and less congested [26, 57]. Table 5.7 lists the passenger load in the middle and lead cars of a train, and Table 5.8 lists the static wheel load on each test track segment [26].

Table 5.7 Passenger load in middle and lead cars

	Scoring criteria	Number of passengers		Passenger load (kN)	
		Lead car	Middle car	Lead car	Middle car
Highly congested	More than 60% of car is occupied	148	160	92	99
Moderately congested	60% of car is occupied	89	96	55	60
Less congested	All seats are occupied	54	54	33	33

Table 5.8 Static wheel load on each test track

	Ballasted track	Slab track				
		Elastic fastening		Rail floating	Sleeper floating	
		E Type	B Type		L Type	P Type
Static wheel load(kN)	53.7	48.2	54.3	48.2	48.2	37.7

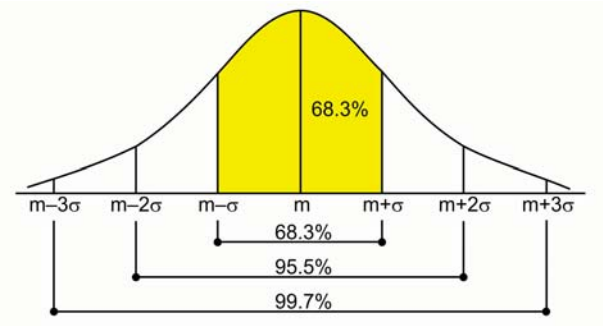

Fig. 5.14 Normal distribution curve of track impact factor [26]

For calculating the TIF using a dynamic wheel load, the probability density in Gaussian probability distribution is found to be more than 68% (Fig. 5.14) by considering twice the standard deviation (σ) of the measured wheel load [26, 148, 157], which is expressed as $(P_{dyn} - P_{sta})/P_{sta}$. This normal distribution has the maximum probability value at the average value (m), and as the distribution becomes distant from m, the probability is inflected as $x = m \pm \sigma$ and approaches 0 [26]. As shown in Fig. 5.14, the probability becomes 68.3% in the range of $x \pm m$, 95.5% in the range of $m \pm 2\sigma$, and 99.7% in the range of $m \pm 3\sigma$ [26]. The TIF values were calculated for different standard deviations of the dynamic wheel load by considering twice the standard deviation (σ) of the measured wheel load [26, 148].

The equation of the Korean standard for urban transit used by AREA or the Japanese railway for TIF for a train speed of 100 km/h is shown as equation (5-6) [26, 148, 177, 178], and that for a train speed of 80 km/h is shown as equation (5-7). In this study, equation (5-7), i.e., a maximum train speed of 80 km/h, was used to calculate the TIF [26].

$$i = 1 + 0.513\frac{V}{100} \tag{5-6}$$

$$i = 1 + 0.410\frac{V}{80} \tag{5-7}$$

The measured TIF for different standard deviations of the dynamic wheel load are shown in Fig. 5.15 [26].

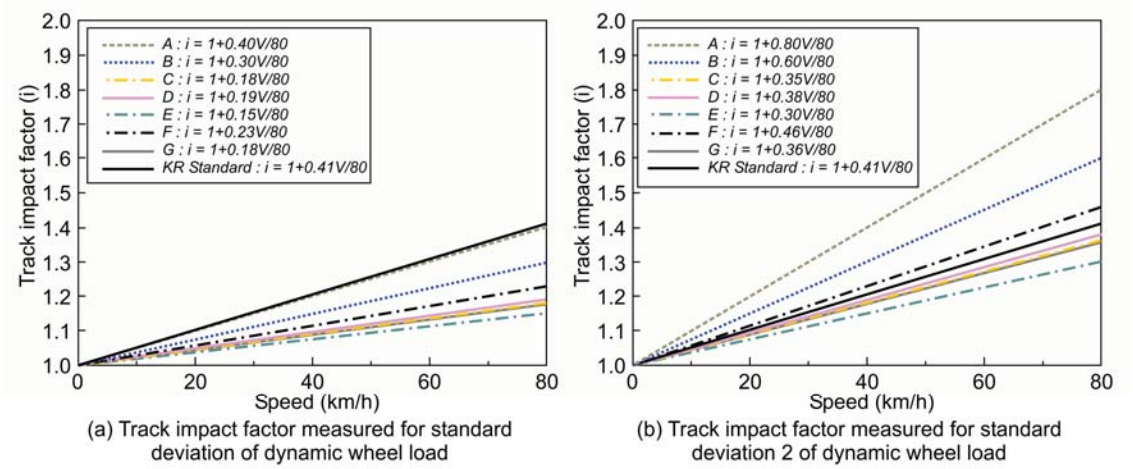

Fig. 5.15 Track impact factor measured for different standard deviations of dynamic wheel load

For a standard deviation of 2σ, the measured TIF for the ballasted track in bad condition (A) was calculated as 0.8V/80, and that for track in good condition (B) was calculated as 0.6V/80 [26]. In the case of the elastic fastening systems, the TIF was 0.35V/80 for the E-type track (C) and 0.38V/80 for the B-type track (D) [26]. The TIF for the rail floating system (E) was calculated as 0.30V/80, which was the lowest among all the measured values [26]. In fact, it was lower than the Korean standard for railways (adopted from AREA) [26, 177, 178], i.e., 0.410V/80 [26]. The TIF for the L-type sleeper floating system (F) was calculated as 0.46V/80; this value exceeded the Korean standard for railways [26]. The TIF for the P-type sleeper floating system (G) was calculated as 0.36V/80 [26].

For a standard deviation of σ, all the seven track segments satisfied the design specifications of TIF [26]. However, for a standard deviation of 2σ, the TIF for the ballasted tracks was estimated to be higher than the Korean standard for railways [26]. Then, in the case of the slab tracks, except the L-type sleeper floating system (F), the TIF was lower than the Korean standard [26].

As shown in Table 5.9, the TIF for a standard deviation of σ was generally lower than the Korean standard [26]. For a standard deviation of 2σ, although dynamic amplification factors such as track conditions and the roughness of rails and wheels were taken into consideration, the measured TIF of almost all the slab tracks was estimated to be lower than the design specifications [26]. Further, the TIF of the service

line appeared to increase with the TSS, and therefore, it was concluded that the TSS directly affects the TIF [26].

Table 5.9 Comparison of track support stiffness and track impact factor measured from standard deviations of dynamic wheel load

	Ballasted track		Slab track					Korean standard
			Elastic fastening		(E) Rail floating	Sleeper floating		
	(A) Bad	(B) Good	(C) E Type	(D) B Type		(F) L Type	(G) P Type	
Measured track impact factor (1σ)	0.4V /80	0.3V /80	0.18V /80	0.19V /80	0.15V /80	0.23V /80	0.18V /80	0.41V/80 (Design track impact factor)
Measured (1σ)/Design track impact factor (%)	98	73	44	46	37	56	44	
Measured track impact factor (2σ)	0.8V /80	0.6V /80	0.35V /80	0.38V /80	0.30V /80	0.46V /80	0.36V /80	
Measured (2σ)/Design track impact factor (%)	195	146	85	93	73	112	88	
Theoretical track support stiffness (kN/mm)	213.28	213.28	34.87	40.24	9.94	44.0	33.94	(Design track support stiffness)
Measured track support stiffness (kN/mm)	299.83	210.10	41.65	48.03	10.65	60.00	50.05	
Theoretical /Measured track support stiffness (%)	28.9	1.5	16.3	16.2	6.7	26.7	32.2	

Fig. 5.16 shows that the TIF increases with increase in the TSS [26]. The correlation between the TIF and the TSS was investigated by linear regression analysis of the TIF and the TSS measured through field measurements, and was calculated by the least-squares method [26]. The value of R-square is a measure for the goodness of fit, 0 indicates no correlation and 1 indicates a perfect correlation. It is clear from the R-square value, which is close to 1, that the regression line is a near perfect fit with our data. Therefore, the trend of the correlation between the TIF and the TSS obtained experimentally in this study is similar to that predicted by numerical analysis in recent studies [22, 67, 127, 188].

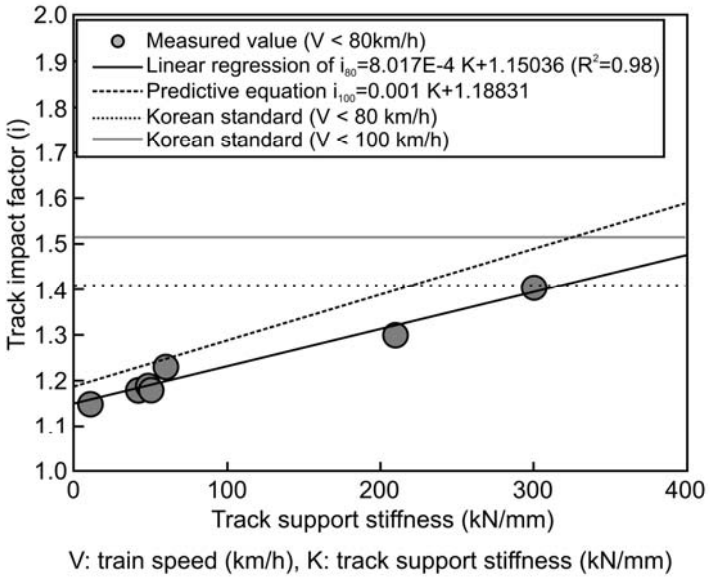

Fig. 5.16 Relationship between track support stiffness and track impact factor

For train speeds of both 80 and 100 km/h, the predictive TIF with the TSS of 300–320 kN/mm was estimated to be higher than the Korean standard for railways. Therefore, it was concluded that the estimating the appropriate TSS was important to prevent exceeding the TIF over the design specifications.

5.7 Conclusions

The relationship between the track support stiffness and track impact factor for various track types currently employed in Korean urban transit was assessed by performing field measurements. The theoretically designed TSS was compared with the TSS measured through field measurements. The effects of track conditions and types on the TIF were evaluated for a dynamic wheel load. Further, the TIF measured using a dynamic wheel load was compared with the TIF used in the design specifications. The analytical and experimental results obtained in this study are summarized below.

(1) In the case of the ballasted track, the condition of ballast (gravel) was found to directly affect the TSS. Moreover, the slope of the wheel load-displacement curve and the amplitude of the initial-to-peak dynamic wheel load were found to be significantly greater than those on the slab tracks. The displacement of ballasted tracks was relatively lower than even that of the slab tracks. Therefore, it assumed that the stiffness of the

ballast was higher than those of the slab tracks; then, the lower displacement and higher stiffness of the track could amplify the dynamic wheel load on the ballasted tracks. The ballast is the only elastic component in a ballasted track, and its elasticity reduces with time. Therefore, the deterioration of the ballast (such as ballast hardening) could affect the reduction of track settlement and absorbing capacity. Therefore, for the ballasted track in bad condition, the dynamic wheel load was not distributed effectively over the ballast, and then, the stiffness of the ballast increased by increasing the dynamic impact forces in proportion to the amplification of the dynamic reaction forces between the wheel and the rail.

The calculated and measured TSS values of the rail floating system and the ballasted track in good condition were found to be similar, and in the case of the sleeper floating systems, the difference between the theoretical and measured values was largest among all the track segments. Further, the theoretical TSS was calculated considering only the vertical stiffness of the tracks.

(2) The TIF was calculated for standard deviations of the measured dynamic wheel load. For a standard deviation of σ, all the seven track segments satisfied the design specifications. However, for a standard deviation of 2σ, the TIF of the ballasted track was estimated to be higher than the Korean standard for urban railways (adopted from AREA). In addition, except for the L-type sleeper floating system, the TIF of the slab tracks was lower than the Korean standard. For a standard deviation of σ, the calculated TIF was generally lower level than the Korean standard. For a standard deviation of 2σ, although dynamic amplification factors such as track conditions and the roughness of rails and wheels were taken into consideration, the measured TIF of almost all the slab tracks was lower than the design specifications. Further, the TIF for the service line appeared to increase with the TSS, and therefore, it was inferred that the TSS directly affects the TIF.

(3) It is reasonable to consider the actual TSS, in addition to the structural and resilience characteristics, of various types of tracks for determining the design specifications of TIF. Therefore, it was concluded that the TIF could be controlled by designing an appropriate TSS, where such a design could be achieved by designing the spring stiffness of the rail support material.

6 PREDICTION OF DISPLACEMENT ON BALLASTED TRACKS

6.1 Introduction

Since a tilting train (Tilting Train eXpress, TTX) can travel a curve much faster without decreasing passenger comfort, it is suitable for increasing train schedule speeds in the mountainous areas of Korea. The effective center of gravity of a tilting train is lower than that of an upright vehicle and the wheel load correspondingly decreases; the track forces for a tilting train traveling on existing tracks are expected to be lower than those of a normal vehicle and thus, stability when traversing the curve can be secured [187].

However, to convert main arterial railways to high-speed rail (HSR) lines by increasing the train speed through the use of a tilting car, it is necessary to consider the track components and the condition of existing tracks to estimate and predict track safety levels when running trains at speeds about 20–30% higher than normal vehicles.

This section focuses on four existing ballasted track sections with track curvatures of 400 and 600 m and with wooden ties (WTs) or prestressed concrete ties (PCTs). The vertical rail and sleeper (tie) displacement and the dynamic wheel load, which depend on the track condition and train characteristics, are measured and the measured track impact factor, which will be used on the numerical simulation by the derived time history function using the empirical dynamic wheel load, is investigated.

The important parameters in a numerical simulation to evaluate and predict the speedup effect and behavior characteristics of a ballasted track is the practical wheel load, which reflects the characteristics of the train and the track components, and the establishment of an analytical model that represents the condition of the actual ballasted track being used is also necessary.

The procedure of prediction of train-induced track displacement using the measured track impact factor is shown in Fig. 6.1.

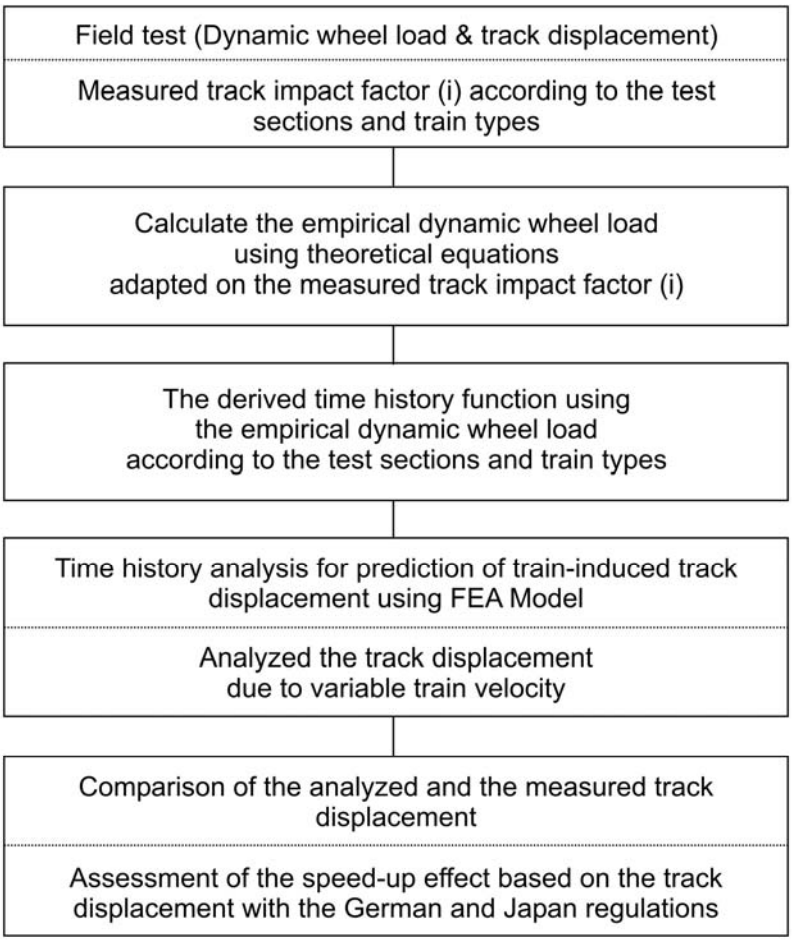

Fig. 6.1 Procedure of prediction of train-induced track displacement

A prediction of the track displacement using the empirical dynamic wheel load can account for static train properties and track curvature but actual track conditions are difficult to include. Therefore, a representative dynamic wheel load is calculated by using track impact factors measured at the test sites in the theoretical expression of the wheel load. This is then used to calculate a time history function that is applied to a finite element analysis (FEA) model of the track behavior. The results of the FEA simulations are compared with the measured rail and sleeper displacements and simulation are performed for train speeds that would be impossible on a service line.

The speed increase associated with a tilting train is evaluated and compared with the speed for a normal vehicle (an electricity motor unit, EMU) through a comparative consideration of the bearing capacity of the track (the rail and sleeper displacement) and the German and Japanese regulation base limits for the vertical track displacement when increasing speed by the use of tilting trains.

6.2 Theoretical background

6.2.1 Wheel load equation

The wheel load for a tilting train is expressed as the sum of the component normal to the rail and a variable contribution to the train load. As shown in Fig. 6.2, the normal components of the inner and outer rail wheel loads can be calculated from the sum of moments centering on the wheel-rail contact points taking into account the inclination of the car body [148, 187].

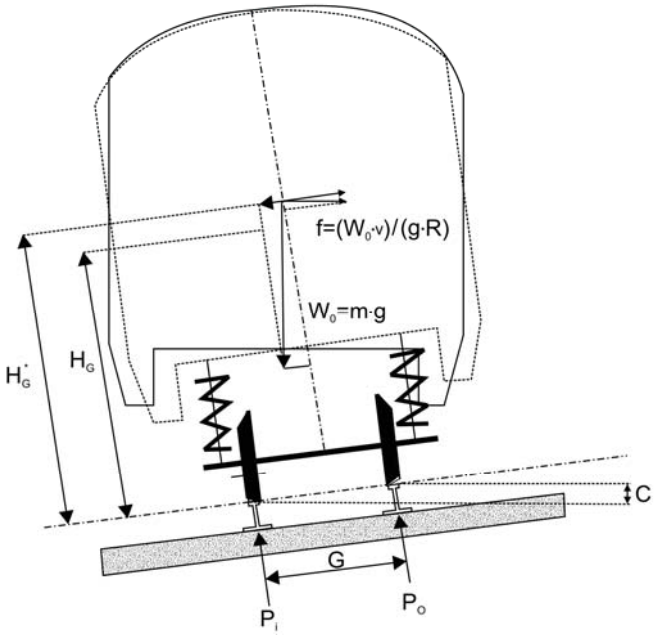

Fig. 6.2 Schematic wheel load on a curved track

The center of gravity of the train changes according to the inclination and since the slope of the car body is proportional to the excessive centrifugal force (cant deficiency C_d), it is considered to be equivalent to the height of the center of gravity H_G increasing to an effective height $H^*_{G.}$ The wheel load normal to the rail can be expressed as:

$$P_{low} = \frac{W_o}{2}[(1 + \frac{(V/3.6)^2}{gR}\frac{C}{G}) - \frac{H^*_G}{G/2}(\frac{(V/3.6)^2}{gR} - \frac{C}{G})] \tag{6-1}$$

$$P_{high} = \frac{W_o}{2}[(1 + \frac{(V/3.6)^2}{gR}\frac{C}{G}) + \frac{H^*_G}{G/2}(\frac{(V/3.6)^2}{gR} - \frac{C}{G})] \tag{6-2}$$

Where,

P_{low}	Normal component of the inner rail wheel load (kN)
P_{high}	Normal component of the outer rail wheel load (kN)
W_o	Static axis load (kN)
V	Speed (km/h)
g	Acceleration of gravity (m/s^2)
R	Radius of track curvature (m)
C	Cant (m)
G	Track gauge (m)
H^*_G	Valid height of the center of the vehicle (m)

The variable contribution to the wheel load [148] is based on the value of the track impact factor *i*. The variable contribution of the inner and outer rail wheel loads are:

$$\Delta P_{\text{low or high}} = 3(0.5 \times P_{\text{low or high}} \times (i-1)) \tag{6-3}$$

Here, the empirical values of the impact factor *i* are calculated as 1 + 0.3V/100 (*V*: train speed, km/h) for continuous welded rail and as 1 + 0.5V/100 for joint rail [148, 178].

In the track design and the behavior prediction, the variable contribution of wheel load was considered by design load for the tracks. Further, the track impact factor *i* of the equation (6-3) had been use to calculated the dynamic wheel load as a single value uniformly which was chosen by the rail type (i.e., continuous welded rail or joint rail) and the design speed (*V*), and does not consider to the track conditions (i.e., the ballast condition good or bad), the train type (i.e., tilting train and EMU) and the track components (i.e., sleeper type and fastening type).

6.2.2 Track impact factor

Past studies of the dynamic behavior of ballasted track have assumed that both the rails and wheels are flat with little irregularity. However, the dynamic wheel load is commonly used when designing the track and the surface roughness of the wheels and rails and any track irregularities are considered to be more important than the condition of the track. Any track irregularity will affect the vehicle motion characteristics and wheel-rail contact; it is also a source of additional dynamic loading that can reach up to

50% of the wheel load. Therefore, recent studies of dynamic track behavior have considered the total load (dynamic and static load) and not only the static wheel load [148].

The load on the track is higher for a traveling train than a stationary train because of the dynamic effects caused by various factors such as the surface roughness of the wheels and rails, track irregularity, track stiffness, and track condition. The track impact factor expresses this dynamic wheel load increase as a function of train speed. Dynamic wheel load includes the effects of impact loading from an increase or decrease in train speed and other dynamic load amplification factors, i.e., the track condition and the track components, as well as the static load. Therefore, the wheel load measured on-site is the dynamic load and the speed dependent the track impact factor can be calculated by comparing this with the static load. The static wheel loads for the EMU and tilting trains considered in this study are 110 and 75 kN, respectively.

Generally, in calculating the track impact factor the 2σ value of the dynamic wheel load variation ratio $(P_{dyn} - P_{sta})/P_{sta}$, where P_{dyn} is the dynamic load and P_{sta} is the static load, is considered. The results of the impact factor test can be assumed to obey a Gaussian probability distribution. To calculate the track impact factor using the dynamic wheel load, the method used in Japan and by the American Railway Engineering Association (AREA) is applied in Korea [148, 157, 178].

The track impact factor values were calculated for different standard deviations of the dynamic wheel load by considering twice the standard deviation (σ) of the measured wheel load [108]. The equation used by AREA or the Japanese railway for track impact factor for a train speed of 100 km/h is shown as the following equation [148, 178]:

$$i = 1 + 0.548\frac{V}{100} \quad V\text{: train speed (km/h)} \tag{6-4}$$

6.3 Field measurement

6.3.1 Overview of test sites

A total of four sections of the ballasted tracks in the existing line currently under use were selected (R400 PCT, R400 WT, R600 PCT, and R600 WT). These test section,

which was the curved and the deteriorative tracks, are planned to increasing the train speed for approximately 20–30% of existing train speed.

Two different radii of curvature and sleeper types were used for the comparison, and all the measured sections consisted of 50 kg long rails. The properties of the measured tracks are listed in Table 6.1 with accompanying photographs in Fig. 6.3.

Table 6.1 Properties of field measurement site

	R400 PCT	R400 WT	R600 PCT	R600 WT
Track curvature (R)	400 m	400 m	600 m	600 m
Cant (mm)	120	120	100	100
Rail	25 m long rail, 50 kg	25 m long rail, 50 kg	25 m long rail, 50 kg	25 m long rail, 50 kg
Rail fastening	Pandrol e-clip	Spike	Pandrol e-clip	Spike
Sleeper	PC sleeper	Wooden sleeper	PC sleeper	Wooden sleeper
Sleeper spacing (mm)	600	600	600	600

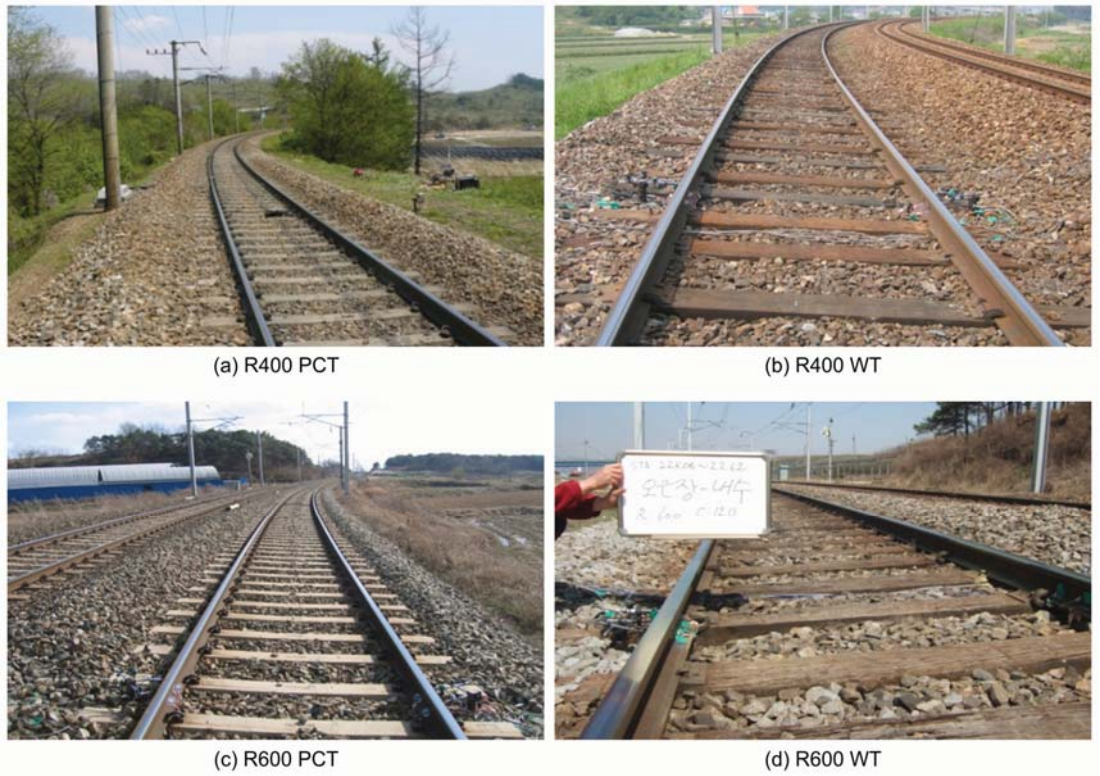

Fig. 6.3 Photographs of the test sites

6.3.2 Dynamic track response measurement

The dynamic wheel load acting on track segments subjected to a passing train load was measured by installing a two-axis strain gauge on the rail web between sleepers [79]. The measured signal was recorded on a data acquisition system (MGC-Plus) and was analyzed using the Origin™ program. To eliminate the interference from other passing trains and obtain a reliable measure of the wheel load of the current passing train, the dynamic wheel load at the site was measured by attaching a wheel load gauge wired to eight strain gauges at an angle of 45° along the neutral axis of the rail web and at a distance of 100 mm from the center point between sleepers, as shown in Fig. 6.4. The vertical wheel loads were measured using shear strain gauges coupled to a full Wheatstone bridge circuit [79]. The strain gauge bridges were calibrated using a hydraulic ram and a load cell to obtain measurements with an accuracy of 2%. The shear strain bridges were mounted on both rails between two consecutive sleepers. In order to prevent data distortion and loss, the sampling rate was set to 1 kHz.

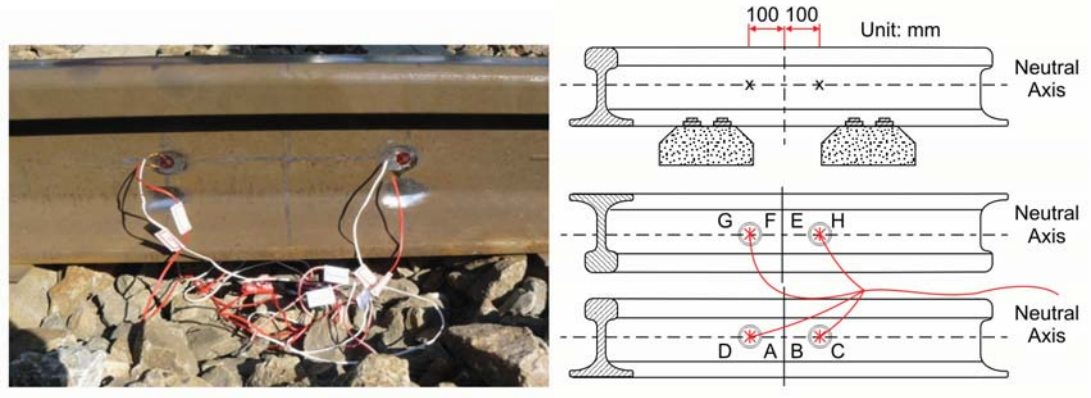

Fig. 6.4 Photograph and schematic of the wheel load sensor installation

By measuring the vertical displacement of tracks subjected to a passing train load, the effect of the dynamic load on the track section can be evaluated and used to compare with the FEA results of the track. Vertical rail displacements were measured using displacement transducers such as linear variable differential transformers (LVDTs) mounted on a jig anchored at the under ballast layer of the tracks, as shown in Fig. 6.5. The displacement transducer is shown in Fig. 6.5.

Fig. 6.5 Photographs of the displacement transducer

6.3.3 Field measurement results

The examples of the measurement results of dynamic wheel load, rail and sleeper displacement of the R400 WT section are shown in Fig. 6.6, and the train speed and number of measurements are listed in Table 6.2.

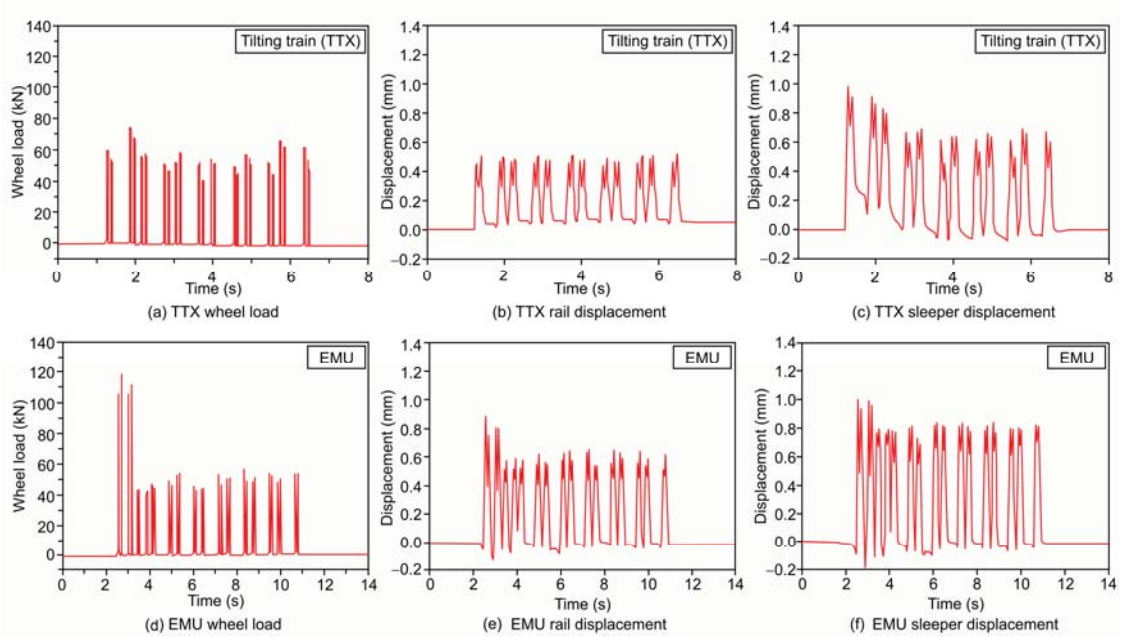

Fig. 6.6 Measured dynamic wheel loads and rail and sleeper displacements

Table 6.2 Number of measurements and train speed at each test site

Test site	Number of measurements	Train speed (km/h)	
		Min	Max
R400 PCT	38	30	89
R400 WT	44	42	85
R600 PCT	36	48	99
R600 WT	26	36	95

6.4 Measured track impact factor

The dynamic response of the ballasted track will depend on the condition of the ballast, and so therefore, an evaluation of the ballast condition was conducted prior to evaluating the track impact factor. Therefore, prior to the measurement of the track impact factor, the ballast was sieved and its condition was evaluated by conducting an abrasion test (KS F 2502, for 5610-1058 A). The ballast was graded as good or bad according to its abrasion resistance. The ballast was sieved three times, and the average weight of the three samples was used in the evaluation. Table 6.3 presents the results of the gradation and abrasion tests, and Fig. 6.7 shows the sieve-size distribution curve for each sample with the standard sieve-size distribution curve also plotted for reference.

Table 6.3 Results of the gradation and abrasion tests

Sieve size (mm)	Grade (%)				Korean standard
	R400 PCT	R400 WT	R600 PCT	R600 WT	
22.4	13	25	8	10	0–5
31.5	41	50	34	47	5–25
40	67	72	58	72	30–65
50	92	96	88	98	60–100
63	100	100	100	100	100
Abrasion rate (%)	10	18	8	12	<25

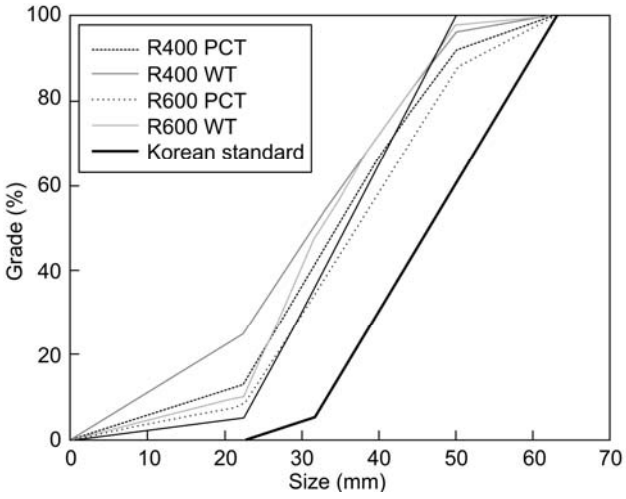

Fig. 6.7 Particle size distribution of ballast

The results of the gradation test show that fouling has progressed to some degree because the percentage passing by weight for all samples exceeds the reference values

for the 22.4 and 31.5 mm sieves. For the 40 mm sieve, only the R600 PCT section satisfies the reference values. On the other hand, the results of abrasion test show that all samples are in accordance with the reference value, and therefore, weakening of the ballast at the test sections was not estimated to be serious. The measured track impact factors at each test site calculated using the results of the measured dynamic wheel load are shown in Fig. 6.8.

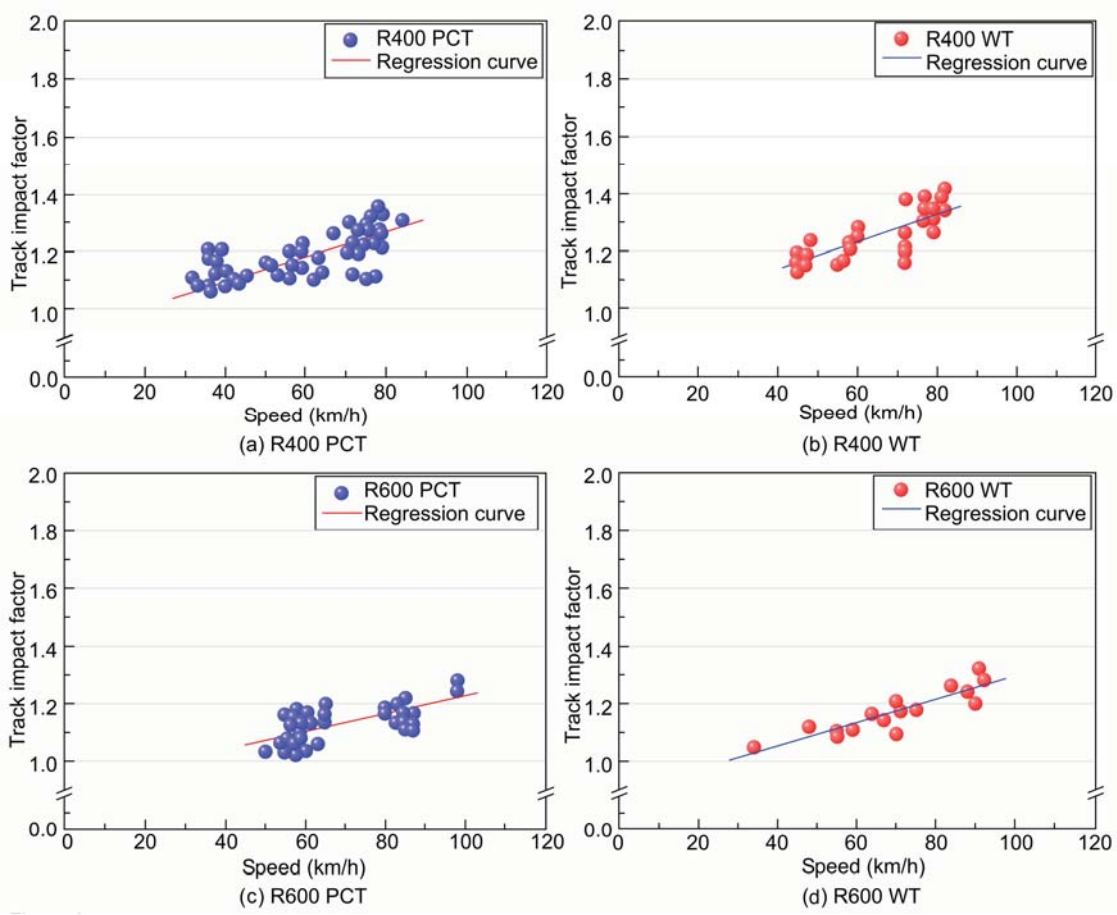

Fig. 6.8 Results of the measured track impact factor at each test site

The track impact factors of 0.38V/100 and 0.48V/100 were calculated for the R400 PCT and R400 WT sections, respectively, while the R600 PCT section has the track impact factor of 0.31V/100 and that of the R600 WT section is 0.40V/100. For the same curvature, the WT section track impact factors are approximately 21–23% higher than those of the PCT section. The measured track impact factors are compared for different track curvatures using the same sleeper in Fig. 6.9. The R400 sections recorded higher track impact factors than the R600 sections. In the case of the WT sections, the

difference between the track impact factors for different curvatures was approximately 17%, and it was approximately 18% in the PCT section case.

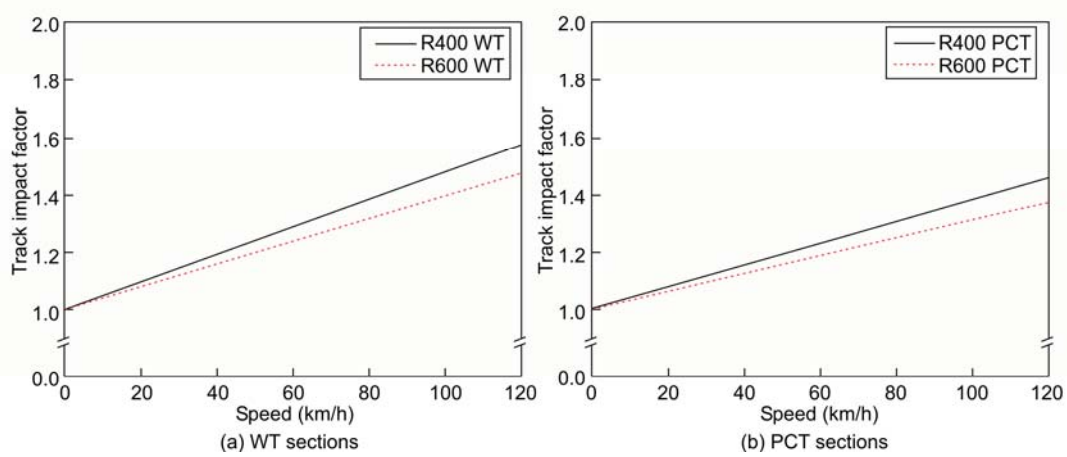

Fig. 6.9 Effect of track curvature on impact factor

The track impact factors for different sleeper types and the same track curvature are compared in Fig. 6.10. The track impact factor is higher in the WT sections than in the PCT sections. As shown in Fig. 6.10 (a), there is a 21% difference in the case of the R400 sections and a 23% difference in the case of the R600 sections (Fig. 6.10 (b)).

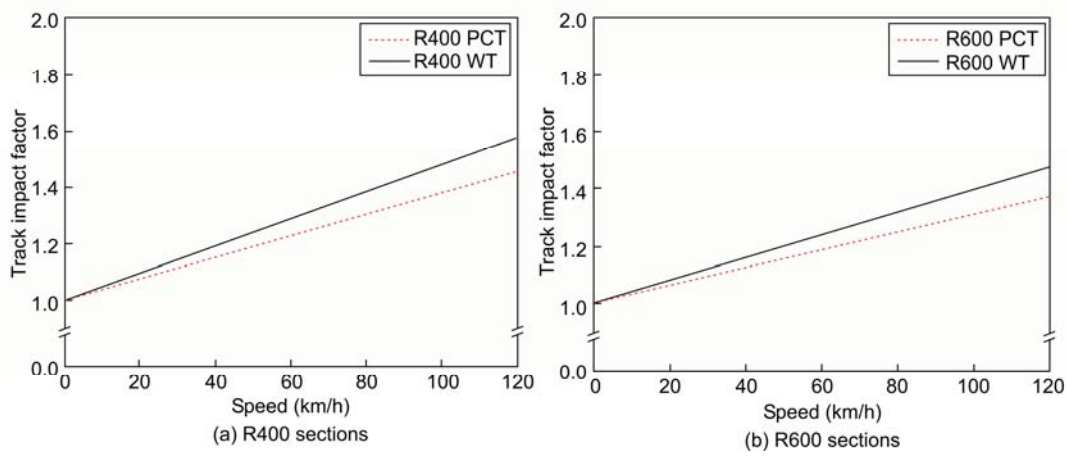

Fig. 6.10 Effect of sleeper type on track impact factor

A comparison of the track impact factors at 100 km/h is presented in Table 6.4. It was estimated that the effect of the ballast condition on the track impact factor to be approximately 2% based on the relative difference of the R600 PCT sections, which

was the ballast condition is relatively good, being higher than the other differences as well as the effects of track curvature and sleeper type.

Table 6.4 Comparison of measured track impact factor for track curvature and sleeper type (at 100 km/h)

Sleeper type / Track curvature	PC sleeper (PCT)	Wooden sleeper (WT)	Relative deviation, PCT/WT (%)
R400	1.38	1.48	20.8
R600	1.31	1.40	22.5
Relative deviation, R400/R600 (%)	18.4	16.7	-

The track impact factors for two different train types at each test site compared with the Korean standard are shown in Fig. 6.11.

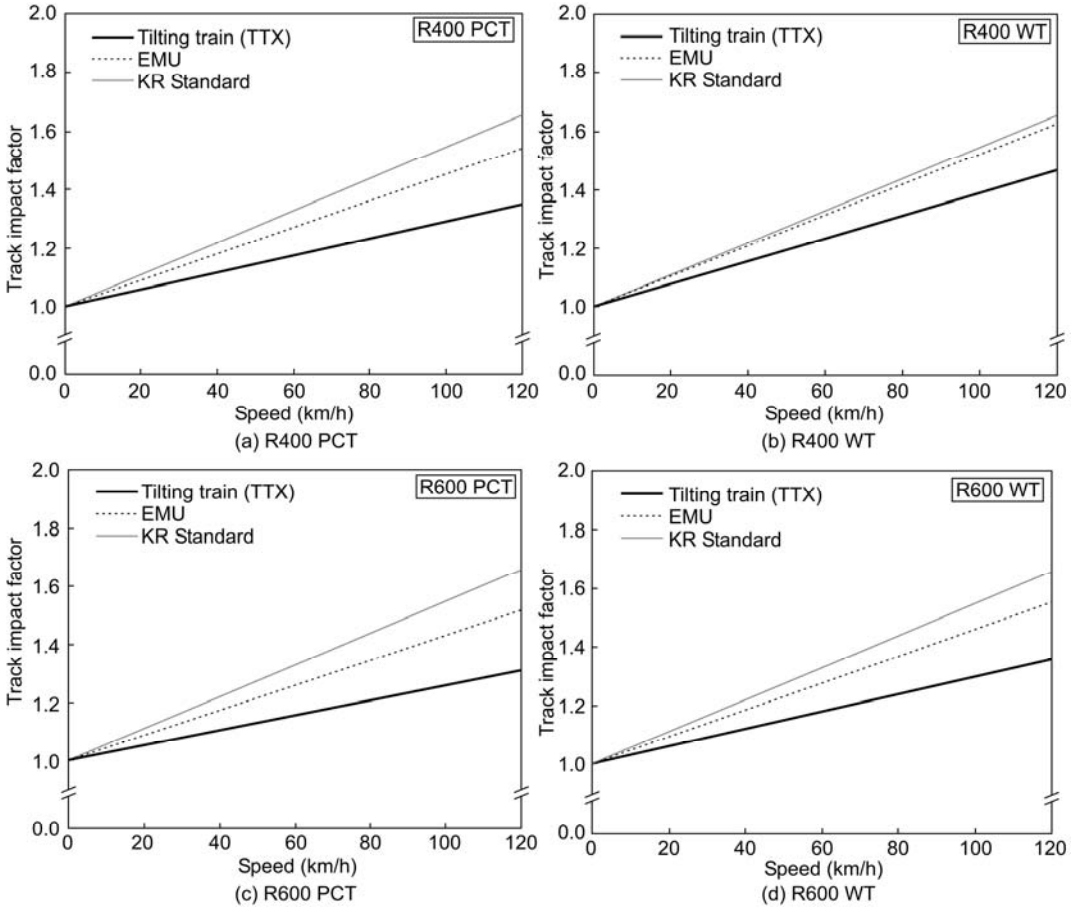

Fig. 6.11 Track impact factors for different train types

The measured track impact factor for a tilting train at a velocity of 90 km/h is approximately 10–12% lower than that for an EMU, and although there was a 30% increase in the speed by running the tilting vehicle (up to 90 km/h), the impact on the track was similar or lower than the impact from the EMU.

6.5 Measured track support stiffness

Track support stiffness (TSS) is measured as the ratio between the maximum vertical displacement and the maximum dynamic wheel load. The estimated TSS for each track is shown in Fig. 6.12.

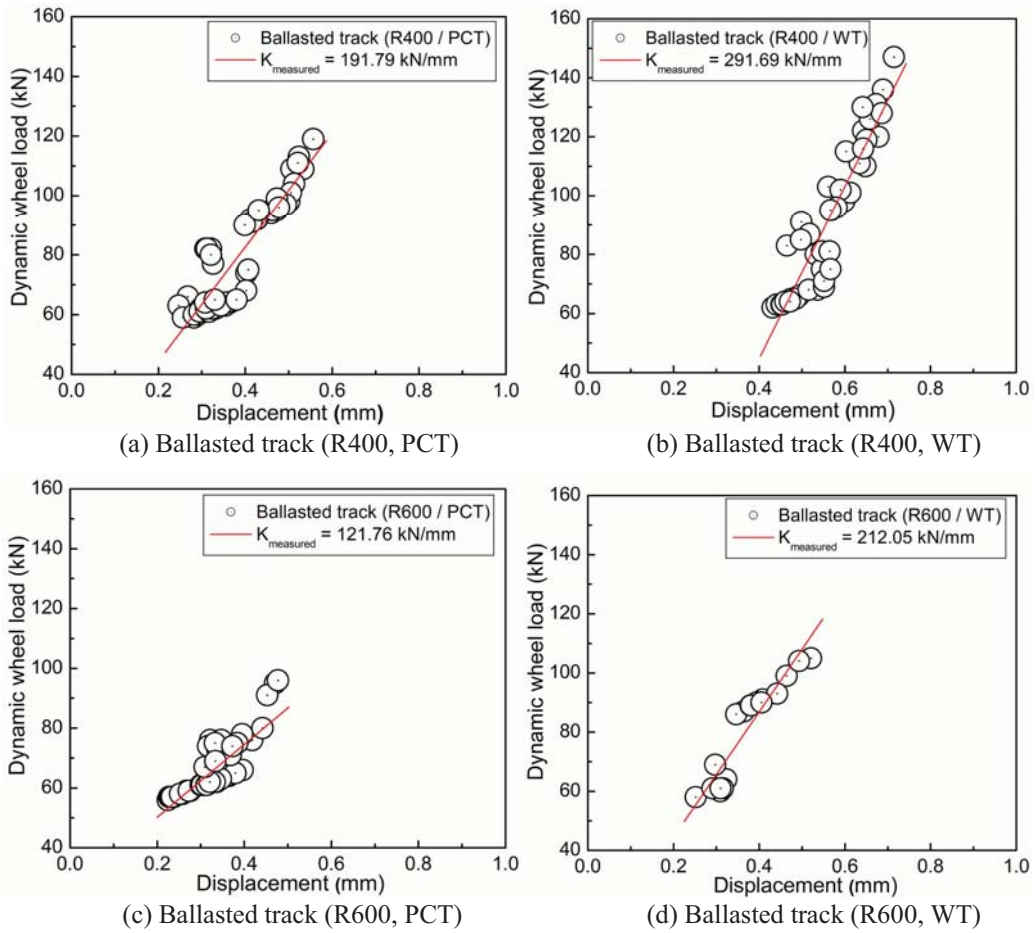

(a) Ballasted track (R400, PCT) (b) Ballasted track (R400, WT)

(c) Ballasted track (R600, PCT) (d) Ballasted track (R600, WT)

Fig. 6.12 Measured track support stiffness

A linear regression analysis of the measured TSS values was conducted by excluding the maximum and minimum values and the values corresponding to abnormal signals (noise component) or measurement errors. The coefficient of correlation was

approximately in the range of 0.91–0.93 for each test section, and thus, the reliability of the linear regression analysis was confirmed. The track support stiffness is higher in the WT sections than in the PCT sections. As shown in Fig. 6.12, in the case of the R400 and R600 section, the TSS for the WT section was approximately 1.5–1.7 times higher than that for the PCT section, respectively.

As shown in Fig. 6.12(b) and (d), the condition of the ballast appeared to directly affect the TSS of the R400 and R600 WT section and the slope of the curve was fairly larger than that of the other tracks. This reason for this difference was attributed to the deterioration of the ballast (see Fig. 6.7). Table 6.5 shows a comparison of the TSS and TIF calculated through field measurements for the each track segments.

Table 6.5 Comparison of track support stiffness and track impact factor

Type of track structure	Track support stiffness (kN/mm)	Track impact factor (i_{100})
(a) Ballasted track (R400 / PCT)	191.79	1.38
(b) Ballasted track (R400 / WT)	291.69	1.48
(c) Ballasted track (R600 / PCT)	121.76	1.31
(d) Ballasted track (R600 / WT)	212.05	1.40

Fig. 6.13 shows that the TIF of service line increases with increase in the TSS. Therefore, it was concluded that the TSS directly affects the TIF. The correlation between the TIF and the TSS was investigated by linear regression analysis of the TIF and the TSS measured through field measurements, and was calculated by the least-squares method. It is clear from the R-square value, which is close to 1, that the regression line is a near perfect fit with measured data.

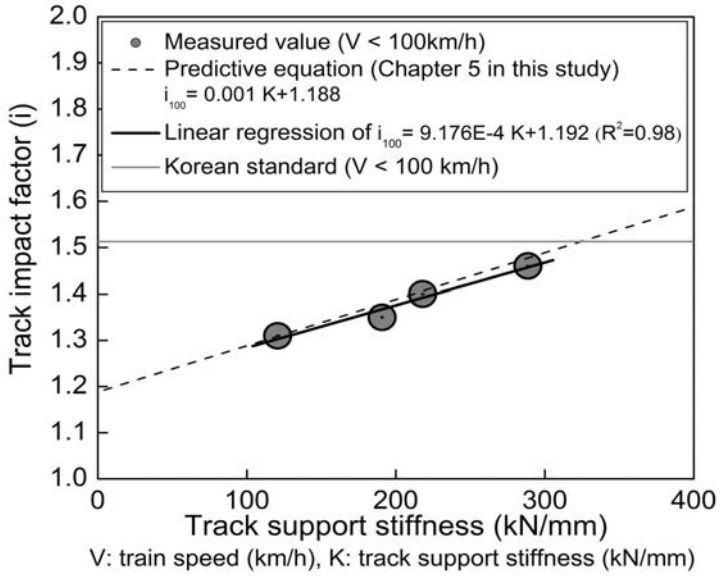

Fig. 6.13 Relationship between track support stiffness and track impact factor

As shown in Fig. 6.13, the linear regression analysis results for the TIF showed good agreement within about 2–5% with the predictive equation of Section 5 in this study (see Fig. 5.16). Therefore, it is considered that the derived predictive equation in this study obtained using measured data in the various tested tracks such as TIF and TSS are suitable for predicting the TIF acting on a ballasted track.

6.6 Finite element analysis

6.6.1 The derived time history function using the measured TIF

The measured track impact factors for each train and section, listed in Table 6.6, are used to calculate the empirical dynamic wheel load that was applied on the derived time history function. Table 6.7 gives an example of the estimated representative dynamic wheel load at 70 km/h based on these measured track impact factors.

Table 6.6 Measured track impact factor for train type (at 100 km/h)

	R400 PCT	R400 WT	R600 PCT	R600 WT
Tilting train	1.29	1.39	1.26	1.30
EMU	1.45	1.53	1.43	1.46

Table 6.7 Example of the empirical dynamic wheel load (at 70 km/h)

	R400 PCT (kN)	R400 WT (kN)	R600 PCT (kN)	R600 WT (kN)
Tilting train	111.74	123.42	106.04	110.61
EMU	191.67	205.40	184.21	189.24

To investigate the train-induced track displacement of the ballasted track, a time-history analysis was performed. In the case of the EMU, one motor car and five passenger cars (where the two types of cars exert different wheel loads) traveling at speeds of 20–300 km/h were considered in the analysis. For the tilting train, six cars with same wheel loads, i.e., two motor cars, two motor-passenger car and two passenger cars), were considered over the same speed range. The train loads compositions for the dynamic analysis are illustrated in Fig. 6.14. Multiple concentrated loads with variable, element length dependent impact load shapes were used in the analysis [24]. The position of the train load in an element can be obtained from:

$$x_n = \frac{V_T \times T_n}{L_e} \tag{6-5}$$

Where, x_n is the distance from the i_{th} node, V_T is the train speed, T_n is the arriving time, L_e is the length of an element, and n is the time step. The nodal load acting on element P_i is given by the product of the train load Q_V and the shape functions N_i (where, i = 1, 2, 3, and 4) as follows:

$$\begin{aligned} P_i &= Q_V \times N_i \\ N_1 &= 2x_n^{\,3} - 3x_n^{\,2} + 1 \\ N_2 &= x_n \times L_e \times (x_n - 1)^2 \\ N_3 &= -2x_n^{\,3} + 3x_n^{\,2} \\ N_4 &= x_n^{\,2} \times L_e (x_n - 1) \end{aligned} \tag{6-6}$$

The example of the time history function for the vehicles at 200 km/h and taking into account the axle distance of the bogie is shown in Fig. 6.14.

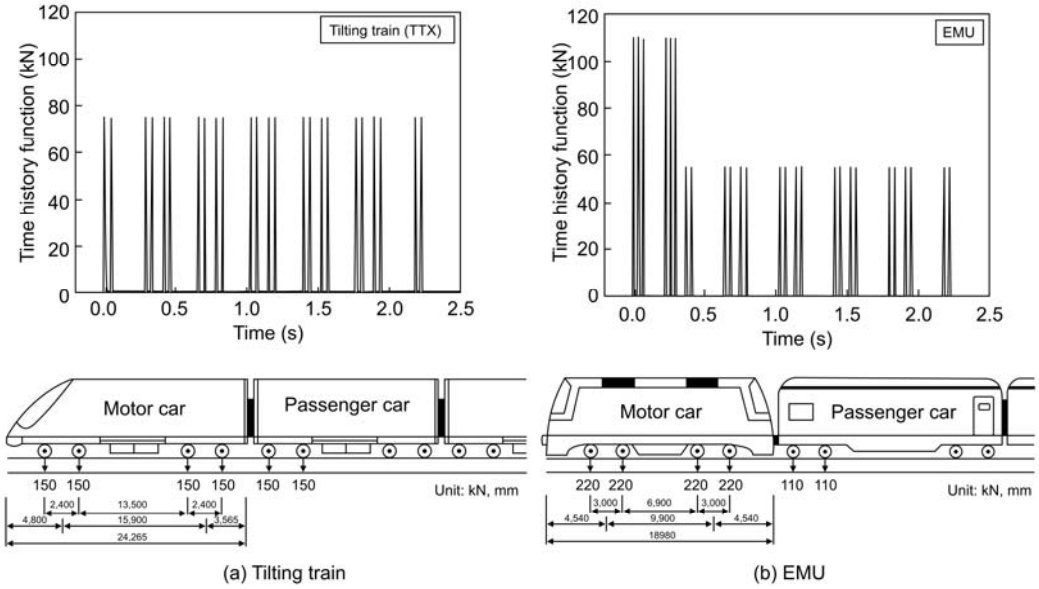

Fig. 6.14 Example of time history function at a train speed of 200 km/h and load combination of each train

6.6.2 Numerical simulation

The derived time history function was estimated considering both the train load composition and the measured track impact factor of each test section. The measured track impact factor was applied to the time history function of the FE analysis in order to predict the track displacement. The peak value of wheel load applied to the time history function was calculated by theoretical equation considering the measured track impact factor. The derived time history function was used in the numerical simulation, i.e., time history analysis, in order to predict the vertical displacements in the track sections subjected to a passing train load at high speed in the near future. Further, a time history analysis was used to compare with the measured track displacement, i.e., the rail and sleeper displacement, and to predict allowable speed increases while considering that the track displacement satisfied the German and Japan regulations.

The FEA was developed using the general commercial FEA package MIDAS [119]. The ballast track model for the numerical simulation was configured as shown in Fig. 6.15. The rails and sleepers are composed of frame elements, and the rail pad and ballast are composed of spring damper elements. The nodal points between the rail and sleeper elements were connected with spring-damper elements with the same properties as the rail pad. The ballast conditions are imposed under the sleeper base by using a spring-damper element with the properties of the ballast.

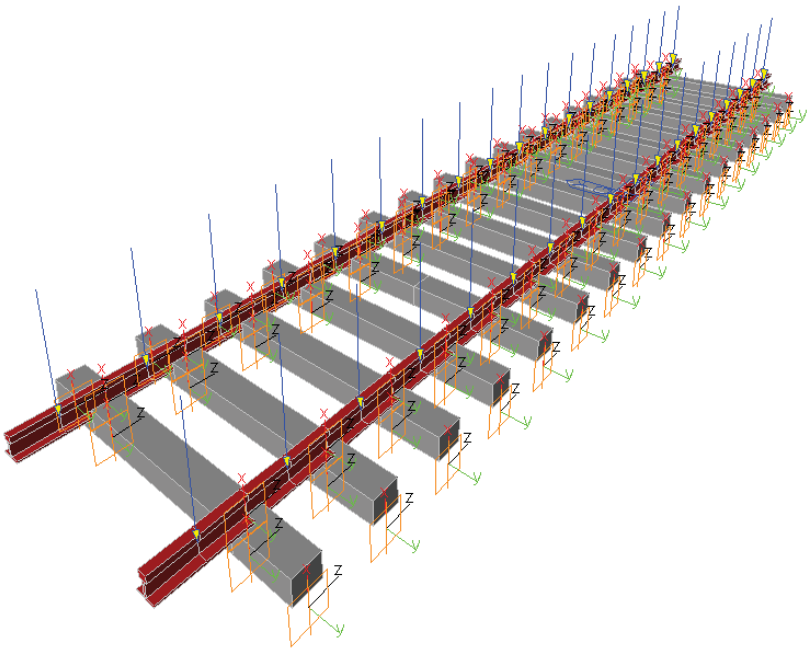

Fig. 6.15 FEA model of ballast track

In this study, the boundary conditions are imposed at the base of the horizontal ballast of the FEA model. The boundary condition of the FEA model of the subgrade medium should be such that the elastic waves, which propagate through the medium, do not reflect back from these boundaries to the vibrating medium [12, 37, 38, 108, 109]. The spring stiffness of the rail pad is 400 kN/mm with a damping coefficient of 15.683 kNs/m, and those for the ballast are 200 kN/mm and 77.877 kNs/m, respectively [15, 104]. And the elastic stiffness of subgrade is 600 kN/mm with the density of subgrade medium of 18×10^{-6} N/mm^3 and the Poisson's ratio of 0.33 [104]. The properties of the rails and sleepers in the FEA model are listed in Table 6.8.

Table 6.8 Properties of the rails and sleepers in the FEA model

	Properties	Rail (50 kgN)	PC Sleeper (PCT)	Wooden sleeper (WT)
Section Properties	Section area (cm^2)	64.2	516.75	360
	Moment of inertia (cm^4)	1,968	16,375	6,750
	Elastic modulus (kN/cm^2)	21,000	4,000	1,000
Material Properties	Weight density (kN/cm^3)	7.85×10^{-5}	2.5×10^{-5}	0.75×10^{-5}
	Poisson ratio (υ)	0.30	0.18	0.33

An example of the FEA results (at 120 and 200 km/h) for the vertical displacement of the rails and sleepers for the two train types of the R600 PCT section is shown in Fig. 6.16.

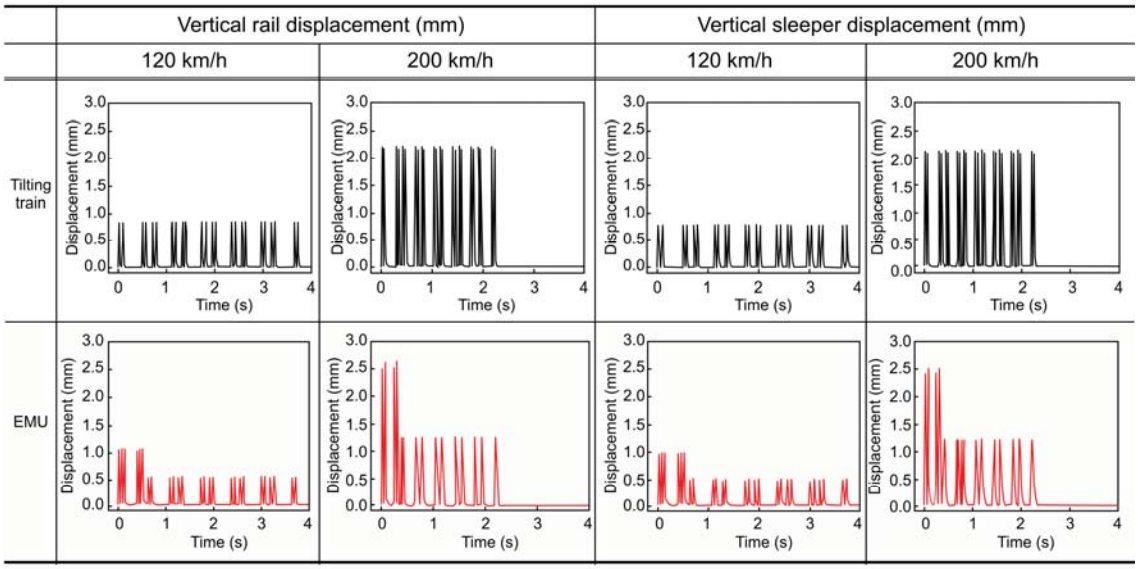

Fig. 6.16 Results of the time history analysis of the R600 PCT section

6.7 Results and discussion

The displacement was analyzed every 20 km/h up to a maximum speed of 300 km/h. The results are shown in Figs. 6.17–18. The FEA results of the track displacement (rail and sleeper) as a function of velocity show good agreement with the experimental results to within about 2–5% for both train types on the R400 PCT section. The agreement was to within about 2–4%, 3–5%, and 2–6% for trains on the R400 WT, R600 PCT, and R600 WT sections, respectively. Therefore, applying time history function based on the measured track impact factors are considered to give sufficiently reliable FEA results in investigating the behavior of the ballasted track.

The difference between the maximum displacements for both train types on all sections was about 15–20%. The results show that both the rail and sleeper displacement exceed the German regulations at velocities greater than 100 km/h on the R400 PCT section, 80 km/h on the R400 WT section, 120 km/h on the R600 PCT section, and 110 km/h on the R600 WT section. The Japanese regulations were only satisfied for the R600 sections. The Japanese regulations on the sleeper displacement were exceeded for an EMU

traveling at velocities between 170 and 200 km/h on the R400 PCT section and for an EMU traveling at velocities greater than 160 km/h on the R400 WT section.

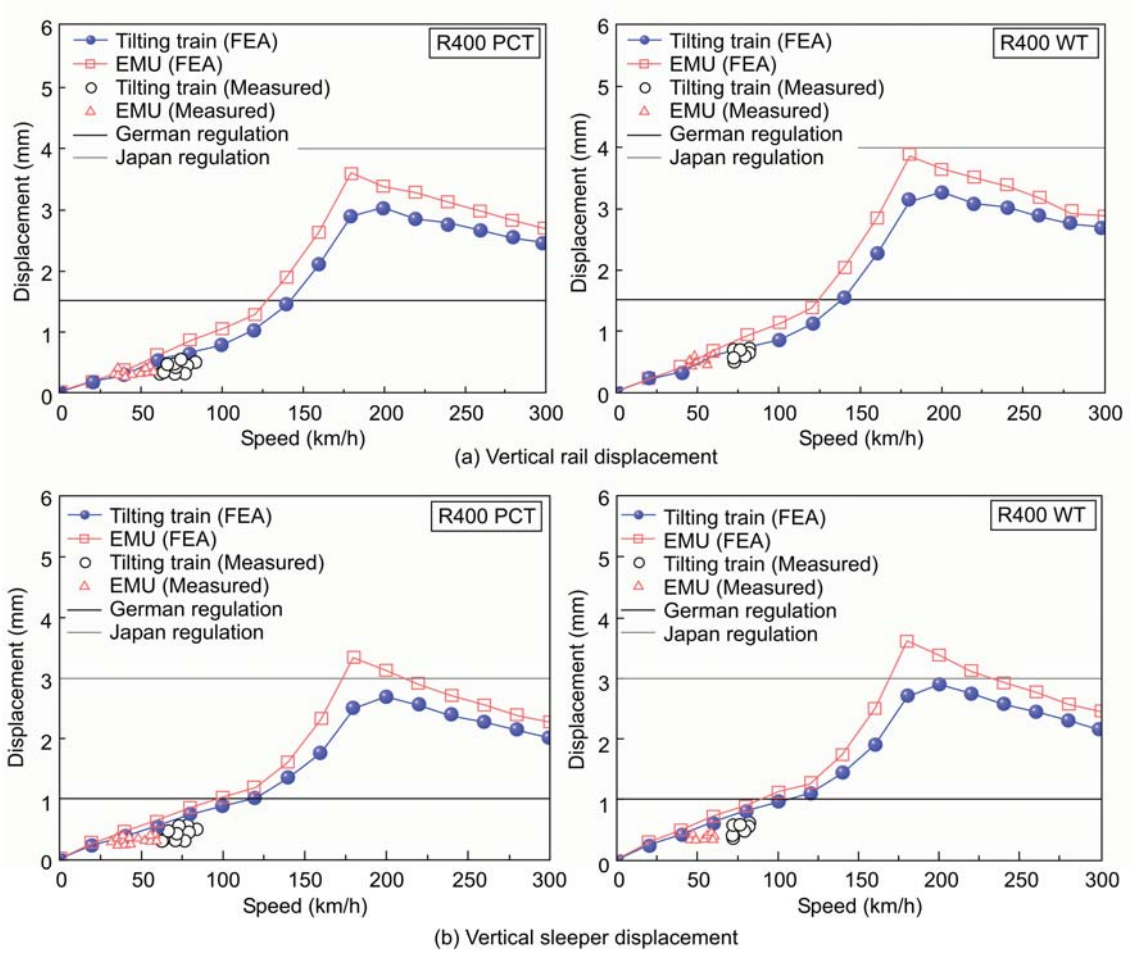

Fig. 6.17 Numerical simulations and measurements of the vertical track displacement of the R400 section

For the R400 PCT section, the lower limit of the German sleeper displacement regulations is satisfied at speeds of 120 km/h for the tilting train and 100 km/h for the EMU. These values decrease to 100 and 80 km/h for the tilting vehicle and EMU, respectively, on the R400 WT section.

However, the lower limits are satisfied at higher speeds on the R600 sections: 140 and 120 km/h for the titling vehicle and EMU, respectively, for the R600 PCT section and 130 and 110 km/h, respectively, for the R600 WT section.

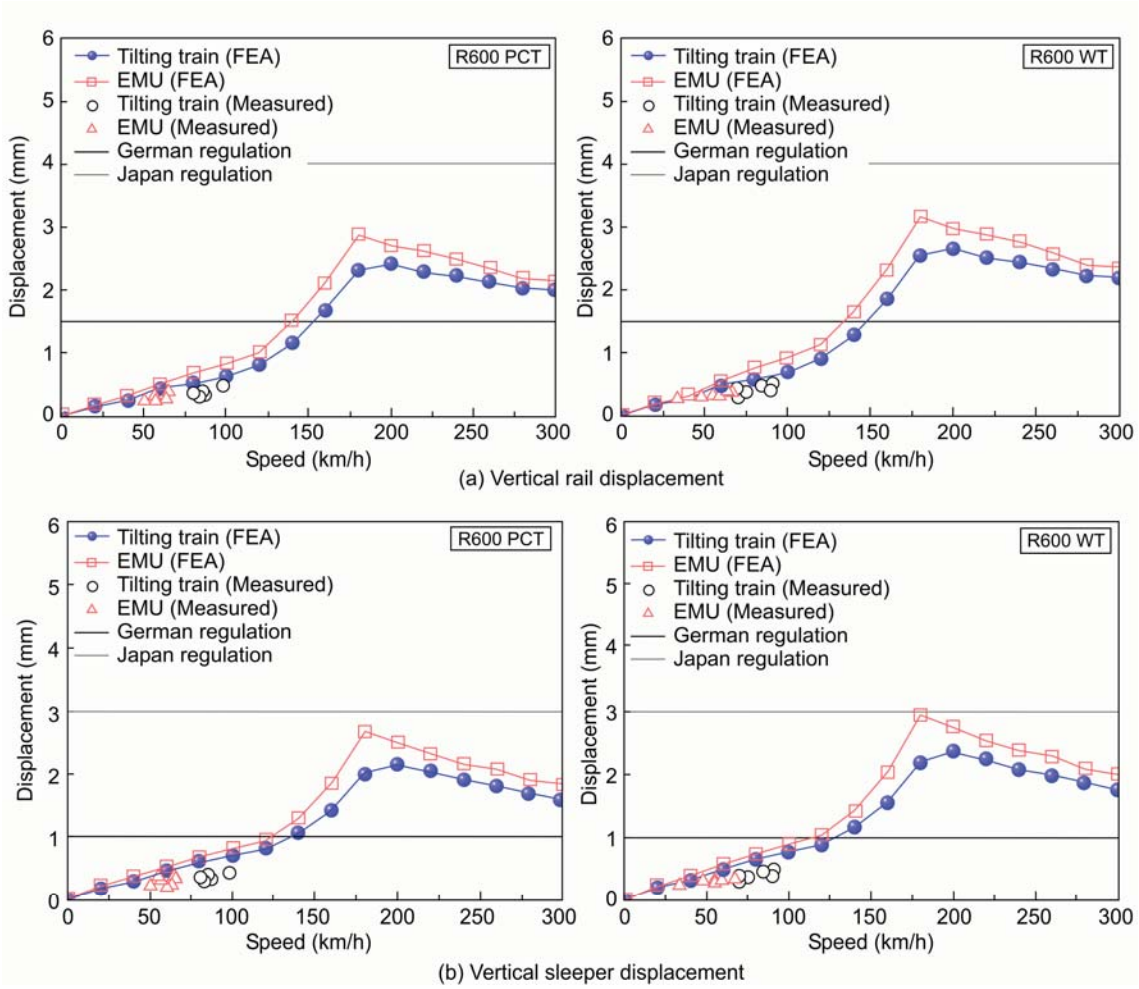

Fig. 6.18 Numerical simulations and measurements of the vertical track displacement of the R600 section

Although there is a small difference between the train types, the maximum displacement (of both the rails and sleepers) occurred at speeds of approximately 170–200 km/h. The response decreased gradually as the speed increased above 200 km/h, indicating resonance of the ballast track. Mode superposition of the sleeper passing frequency in the FEA model and that of the results of an eigenvalue analysis in which the mass and stiffness of the rail-sleeper-ballast system are reflected in the results of time history analysis occurs, and the 1st excitation frequency of the analytical model depends on the train speed and sleeper spacing.

The results of the eigenvalue analysis and the frequency analysis of the time history responses showed that the natural frequency of the analytical model was approximately 74–76 Hz, though there are some differences depending on sleeper type [31, 95]. The sleeper spacing (0.600 m) gives the 1st excitation frequency (sleeper-passing frequency)

as 75 Hz in the 170–175 km/h speed range. Thus, resonance of the ballast track is induced because the sleeper-passing frequency and the natural frequency based on the mass and stiffness of the rail coincide in the frequency band of 70 Hz [6, 31, 95]. In addition, since the difference between the measured and analytical results was approximately 5%, the analytical results that considered the measured track impact factor reflected the measured track displacement results well.

Table 6.9 Comparison of speedup effect for each test site and vehicle type

		R400 PCT		R400 WT		R600 PCT		R600 WT	
		Peak value (mm)	V (km/h)	Peak value (mm)	V (km/h)	Peak value (mm)	V (km/h)	Peak value (mm)	V (km/h)
Tilting train	Rail displacement (1.5–4 mm)	3.03	142	3.27	138	2.42	153	2.66	147
	Sleeper displacement (1–3 mm)	2.69	118	2.90	106	2.15	134	2.37	124
	A Speed limit (km/h)	*	118	*	106	*	134	*	124
EMU	Rail displacement (1.5–4 mm)	3.59	128	3.87	124	2.87	140	3.16	134
	Sleeper displacement (1–3 mm)	3.34	95	3.60	88	2.67	123	3.00	116
	B Speed limit (km/h)	†	95	†	88	†	123	†	116
Speedup effect of tilting train (B/A)		19%		17%		9%		7%	

* Exceeds lower limit (German regulation). Satisfies upper limit (Japan regulation).

† Exceeds upper and lower limits.

As a result of numerical simulation, it showed that the derived time history function using the measured track impact factor which on a smaller track curvature with wooden sleepers is higher than other test section. Therefore, it would be advantageous to increase the weight of sleepers on existing lines to increase the train speed through the speedup effect without the improved track curvature.

The Japanese regulations used by the maximum response limit (upper limit), which is defined based on the material allowable stress of the track components (rail and sleeper), to secure the structural safety [148]. And the German regulations used by the lower

limit are the minimum required levels (appropriate level) to secure stability of running vehicles [187]. The limit of rail displacement is higher than the limit of sleeper displacement. Therefore, the speed limit of each test site was estimated by considering the limit of sleeper displacement.

The results of the speedup effect evaluation are shown in Table 6.9; the lowest speed limits of the tilting train and EMU were in the R400 WT section. This is due to the dynamic load amplification effect (the track impact factor) according to the deterioration of the ballast and the use of WT on a track with small curvature. On the other hand, the highest speed limits of the tilting train and EMU were in the R600 PCT section. As shown in Table 6.9, the track curvature affects the speedup by approximately 10%, while the type of sleeper affects the tilting train speedup by approximately 2%. Therefore, a smaller track curvature leads to a greater speedup effect of the tilting train.

6.8 Conclusions

On-site measurements at four general railway service lines were conducted to calculate the empirical dynamic track impact factor for two different trains while taking into account the track condition and the track component, i.e., sleeper type including fastening, and to evaluate the train-induced track displacement, the derived time history function using the measured track impact factors were applied to a numerical analysis. The results obtained from this study are summarized below.

(1) The empirical track impact factors were 17–18% higher in the R400 sections than in the R600 sections. As the track curvature decreases the impact on the track increases. The track impact factors were 21–23% higher in the WT sections than in the PCT sections, further the measured track impact factor had been influenced by the ballast condition. The impact on the track from a tilting train was 7–11% less than that from EMU at 70 km/h. Although the tilting train is running by speeding up 30% (90 km/h) on the track, the response level was similar to or less than that of the EMU.

(2) The analytical results reproduced the experimental results well within about 2–5% difference in the values. Therefore, applying the derived time history function based on

the measured track impact factors are considered to give sufficiently reliable FEA results in investigating the behavior of the ballasted track. The difference between the maximum track displacements for both train types on all sections was about 15–20%. The analytical results show that both the rail and sleeper displacement exceed the German regulations, i.e., lower limit, at velocities greater than 100 km/h on the R400 PCT section, 80 km/h on the R400 WT section, 120 km/h on the R600 PCT section, and 110 km/h on the R600 WT section.

(3) The Japanese regulations, i.e., upper limit, were only satisfied for the R600 sections. The Japanese regulations on the sleeper displacement were exceeded for an EMU traveling at velocities between 170 and 200 km/h on the R400 PCT section and for an EMU traveling at velocities greater than 160 km/h on the R400 WT section, i.e., the train speeds corresponded with the each track resonance speed.

It showed that the derived time history function using the measured track impact factor which on a smaller track curvature with wooden sleepers is higher than other test section. Therefore, it would be advantageous to increase the weight of sleepers on existing lines to increase the train speed through the speed-up effect without the improved track curvature. The increase in speed by using a tilting train with a small track curvature is much better than that of a larger track curvature approximately 10%.

7 RELATIONSHIP BETWEEN DYNAMIC WHEEL-RAIL FORCES, RAIL SURFACE ROUGHNESS AND TRACK SUPPORT STIFFNESS

7.1 Introduction

Track forces exerted by vehicles on tracks are the most important parameters that determine the condition of tracks and, of course, ride safety and quality. These forces can be classified as static forces (nominal forces), quasi-static forces, dynamic forces, and forces contributed by factors such as asymmetries in the vehicle. Quasi-static forces include additional average forces due to curve negotiation, i.e., the force due to a load shift from one wheel to the other. Static forces are exerted by a stationary vehicle on an ideal and straight track. For a vehicle running along a curve on a perfect track at a constant speed, quasi-static forces due to the cant and radius of the track contribute to the static forces. Dynamic forces are generated when a vehicle is subjected to dynamic motions primarily due to track irregularities and changes in the track geometry. Geometrical irregularities in tracks, unsprung and sprung masses, track stiffness, damping variations in track flexibility, wheel flats, and corrugations on wheels and rails generate dynamic forces on the tracks.

Several approaches have been developed to estimate the dynamic forces exerted by a vehicle running on rails. One approach is to measure the forces using specially designed wheels or rails. Another approach is to perform computer simulations using appropriate models of the vehicle and the rail. The normal load between the wheel and the rail is a very important parameter to be considered in the analysis of the dynamic behavior of coupled vehicle-rail systems. It plays a key role in maintaining vehicle stability and the quality of the vehicle and track components. When a vehicle is subjected to dynamic motions primarily due to rail irregularities and changes in the rail geometry, dynamic forces are generated. These forces can be distributed over a large frequency range. Vehicle velocity is another decisive parameter.

Dynamic forces can be limited to very low frequencies (typically up to 20 Hz as specified in UIC Code 518) or may contain high-frequency components (herein referred to as P1 and P2 forces). P1 and P2 are vertical forces due to unsprung masses, vehicle velocity, and track stiffness, among other parameters. When a wheel travels across a

dipped rail joint or a dipped weld, the two peak forces can be identified. In previous studies on dynamic wheel-rail forces, the causes of P1 and P2 were evaluated by measuring the vertical and horizontal versines at the rail welds [44, 168–170]. However, this approach considers only the quality of roughness of normal rail welds and does not account for that of the entire rail surface. Therefore, it is difficult to use these results for rail maintenance and to predict the dynamic wheel-rail forces.

In this section, an empirical prediction model for P2 is developed to translate the dynamic wheel-rail forces into a multiple regression equation, which includes first-order derivatives of the quality index of rail surface roughness (herein referred to as QI), vehicle velocity, and vertical track stiffness measured using field tests. Digital straightedges (RAILPROF) [43, 147, 168] are used to obtain the QI according to the defined standards and to predict the dynamic wheel-rail forces.

7.2 Dynamic wheel-rail forces: P1 and P2 force

Dynamic wheel-rail forces may be distributed over a large frequency range. They can be limited to very low frequencies (typically up to 20 Hz as specified in UIC Code 518) or may contain high-frequency components, i.e., P1 and P2. As shown in Fig. 7.1, P1 is a high-frequency (very short duration) force [83].

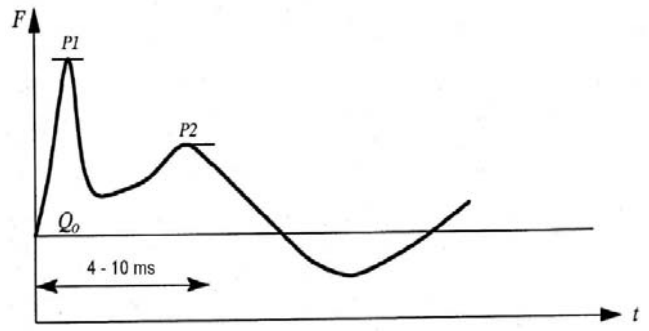

Fig. 7.1 Dynamic wheel–rail forces (P1 and P2) at an interface irregularity [83]

The magnitude of P1 is larger but its duration is less than that of P2 [31, 41, 83, 114]. P1 is generated when a wheel is forced to change direction owing to a “dip”; the wheel and rail masses act against each other through the contact stiffness between the wheel and the rail [41, 83, 114]. This force affects the rails mainly as a contact stress. P2 is

generated after P1, wherein the wheel mass acts against a greater portion of the track mass through the stiffness of the entire track (i.e., not only the contact stiffness) [31, 41, 83, 114]. P2 causes ballast damage and increases the geometric irregularities in the track, which is referred to as settlement [41, 83, 114, 168]. This force may be estimated using Prud'Homme's equation (7-2):

$$Q = Q_0 + \Delta Q_d \tag{7-1}$$

Where, Q is the vertical wheel load according to Prud'Homme (kN), Q_0 is the static wheel load (kN), and ΔQ_d is the dynamic contribution (kN).

$$\begin{aligned} &\Delta Q_d = 2\sqrt{\sigma^2(\Delta Q_s) + \sigma^2(\Delta Q_{os})} \\ &\sigma(\Delta Q_s) \cong Q_0 \cdot k_\sigma, where\, k_\sigma = 0.11 \sim 0.16 \\ &\sigma(\Delta Q_{os}) = \alpha_1 \cdot V \cdot \frac{1}{\sqrt{1000}} \cdot \sqrt{m_{u,w} \cdot g \cdot K} \end{aligned} \tag{7-2}$$

Where, σ denotes the standard deviation, $\triangle Q_{os}$ is the load resulting from imperfections in the wheel and rail geometrical irregularity, unsprung track properties, and vehicle velocity (kN); α_1 represents the geometrical irregularity in tracks and wheels, V is the vehicle velocity (km/h), $m_{u,w}$ is the unsprung mass per wheel (kg), K is the vertical stiffness of track (N/mm), and g is the acceleration of gravity (m/s^2) [83, 114]. Recommended values of α_1 range between 0.00042 and 0.00084 [83]. K depends on the type of track and subgrade and can vary between approximately 50,000 and 300,000 N/mm, according to Sahlin and Sundquist [83].

7.3 Relationship between QI and P1 and P2

Delft University of Technology, in cooperation with the Dutch Rail Infra Manager, ProRail, has developed new technical standards for the geometrical deviations in the metallurgic rail welds employed in the Netherlands [43, 44]. As with most standards

adopted worldwide, the previous Dutch standards for vertical weld geometry were based on the principle of deviations in the vertical geometry measured as a versine on a 1-m base [41, 43, 44, 168, 170]. In this approach, only the maximum irregularity in the longitudinal rail surface is considered and the geometrical shape of the rail is ignored [41, 44, 168, 170]. However, this shape is directly related to the dynamic wheel-rail contact forces, and therefore, it cannot be ignored [43, 44, 168, 170]. The power spectrum of dynamic wheel-rail contact forces indicates that these forces cause track deterioration and degradation of vehicle and track components [41, 43, 44, 168, 170]. Further, in approaches based on geometrical deviations, the vehicle velocity is not considered [44, 168, 170]. However, it is known that contact forces depend on the vehicle velocity [44, 168, 170].

Comparative studies have been carried out to assess the zeroth-, first-, and second-order spatial derivatives of the measured weld geometry [41, 44, 168, 170]. It has been found that an approach based on the first-order derivative shows the best performance, and the approach based on the second-order derivative is extremely sensitive to short indentations but not very sensitive to irregularities with a long wavelength [41, 43, 44, 168, 170]. The following values, proposed by TU Delft [170], were adopted in the Dutch standards [41, 44, 168, 170]:

- $V \leq 40$ km/h: 3.2 mrad
- $40 \leq V \leq 80$ km/h: 2.4 mrad
- $80 \leq V \leq 140$ km/h: 1.8 mrad (7-3)
- $140 \leq V \leq 200$ km/h: 0.9 mrad
- $200 \leq V \leq 300$ km/h: 0.7 mrad

The value of 0.7 mrad for high-speed rail (HSR) lines is used to define the quality of new rails [43, 44, 168, 170]. A sample set of 100 rail segments having a length of 1 m was analyzed, and 0.7 mrad was found to be the upper limit of the 95% reliability interval [43, 44, 168, 170]. For assessment purposes, the QI of the weld is introduced as a dimensionless ratio of the actual value for the first-order derivative of the weld geometry and the velocity-dependent standard value [43, 44, 168, 170]. A value smaller than or equal to 1 implies that the weld quality is high and can be accepted for use,

whereas a value larger than 1 indicates that the weld quality is low and hence it should not be used [43, 44, 168, 170]. For a given vehicle velocity, QI can be expressed as follows [43]:

$$QI = \frac{\left|\frac{dz(x)}{dx}\right|_{\max,actual}}{\frac{dz}{dx}_{norm}} (\leq 1: \text{acceptance}; > 1: rejection) \tag{7-4}$$

The geometry of rail welds is commonly measured using a digital straightedge with a basis of 1 m and a sample interval of 5 mm [43, 44, 168, 170]. For assessment purposes, the signal was averaged by increasing the sample interval to 25 m [43, 44, 168, 170]. Then, wavelengths from 0.1 m to 2 m were measured [43, 44, 168, 170]. From this wavelength range and a velocity range of 80–140 km/h for conventional passenger trains and freight trains, a frequency range 10–400 Hz was estimated [43, 44, 168, 170]. Generally, in this frequency range, several stiffnesses and masses affect the train-track dynamics [41, 43, 44, 168, 170]. The most important masses are the unsprung wheelset mass and the equivalent track mass; the primary suspension stiffness, wheel-rail Hertzian contact stiffness, and equivalent track stiffness are the most important stiffnesses [41, 43, 44, 168, 170].

At each frequency, a combination of a mass and the related stiffness strongly affect the magnitude of wheel-rail contact forces [43, 44, 168, 170]. Assuming that the combination of a dominating mass (*M*) and stiffness (K) shows a quasi-static response and that the vertical rail irregularity is a function of the longitudinal coordinate z(x) at train velocity *V*, the dynamic component of the wheel-rail contact force is equal to the inertia force originating from *M*, which follows the vertical irregularity [43, 168]:

$$F_{dyn}(t) = \alpha m_e \ddot{z}(t) = \alpha m_e \frac{d}{dt}\left(\frac{dz(t)}{dt}\right) \text{ where } m_e = \frac{ML_n}{L_o} \tag{7-5}$$

In this expression, m_e represents a frequency-dependent equivalent mass, which is calculated as a product of the dominant mass in the wheel-rail system multiplied by the

wavelength L_n. L_0 is the reference wavelength [43, 168]. Each measurement signal of a rail weld in the longitudinal direction z(x) can be decomposed into a finite number of harmonics using the discrete Fourier transform (DFT) [43, 168]:

$$Z(x) = \sum_{n=1}^{N} Z_n \sin\frac{2\pi x}{L_n} \;\rightarrow\; Z(t) = \sum_{n=1}^{N} Z_n \sin\frac{2\pi v t}{L_n} \tag{7-6}$$

In the following equation, a single harmonic is considered (N = 1) [43, 168]. The final result can be easily extended for larger N [43, 168]. Then, substitution of equations (7-5) and (7-6) yields

$$F_{dyn}(t) = \alpha m_e \frac{d}{dt}\left(Z_1 \frac{2\pi v}{L_1}\cos\frac{2\pi v t}{L_1}\right) = \alpha 2\pi v \frac{M}{L_0}\frac{d}{dt}\left(Z_1 \cos\frac{2\pi v t}{L_1}\right) \tag{7-7}$$

For $x = V \cdot t$ in the space domain,

$$F_{dyn}(x) = \alpha 2\pi v^2 \frac{M}{L_0}\frac{d}{dx}\left(Z_1 \cos\frac{2\pi x}{L_1}\right) \tag{7-8}$$

Because only the maximum magnitude of the dynamic force was considered and its position was ignored, the cosine terms in the above expression may be replaced with sine terms [43, 168]:

$$F_{dyn,\max} = \alpha 2\pi v^2 \frac{M}{L_0}\left|\frac{dz(x)}{dx}\right|_{\max} \quad or\; F_{dyn,\max} = \beta \frac{Mv^2}{L_0}\left|\frac{dz(x)}{dx}\right|_{\max} \tag{7-9}$$

Thus, the maximum dynamic component of the wheel-rail contact force, corresponding to a specific sampled weld, is expressed in terms of its maximum spatial first-order derivative or, equivalently, in terms of its QI [43, 168]:

$$F_{dyn,\max} = \beta \frac{Mv^2}{L_0}\left.\frac{dz}{dx}\right|_{norm} \cdot QI \tag{7-10}$$

7.4 Field measurements

In this section, six sections of a ballasted track used for the HSR line in South Korea were selected to measure the dynamic wheel-rail forces, track support stiffness and the rail surface roughness.

The ballast state of each test section was relatively good. All the test sections were UIC 60-kg straight tracks with continuous welded rails. The track gauge and cant were measured to be 1,435 and 0 mm, respectively, confirming that the test sections were straight. Therefore, there was no significant difference between the wheel-rail forces acting on the inner and outer rails.

(a) RAILPROF instrumentation used for measuring rail surface roughness

(b) Wheel-rail force sensors instrumentation used for measuring dynamic wheel-rail forces

Fig. 7.2 Photographs of field test site and instrumentation

Fig. 7.2 (a) shows the RAILPROF instrumentation [43, 147, 168] used to measure the rail surface roughness and estimate the QI of each test section. All the test sections were not rail welds and had some irregularity on their surface. The vertical dynamic wheel-rail forces were measured using shear strain gauges coupled to a full Wheatstone bridge circuit, as shown in Fig. 7.2 (b) [79].

The strain gauge bridges were calibrated using a hydraulic ram, and a load cell was used to obtain measurements with an accuracy of 2% [79]. To measure the dynamic wheel-rail forces exerted on each test section by a high-speed vehicle, the shear strain gauges were mounted on both rails between two consecutive sleepers, in line with the six test sections (Fig. 7.2 (b)). The measured signals were recorded on a data acquisition system (MGC-Plus) and were analyzed using the Origin™ program. In order to prevent data distortion and loss, the sampling rate was set to 1 kHz.

The QI-based approach requires a high measurement accuracy of at least 0.18 mrad at a vehicle velocity of 140 km/h and 0.07 mrad at a vehicle velocity of 300 km/h [43, 147, 168]. Therefore, considering the influences of various factors such as rust, dirt, moisture, and temperature, testing and certification procedures should be highly accurate [43, 147, 168]. In particular, capacitive measurement techniques are very susceptible to these influences. RAILPROF uses a 1.5 m reference rail with a milled surface, a cosine-shaped indentation of 0.3 mm in the centre, and a length of 500 mm, corresponding to a QI of 1.034 [43, 147, 168].

Fig. 7.3 shows the photographs and rail surface roughness of each test section, measured in terms of vertical negative and positive versines (herein referred to as NV and PV, respectively) and QI using RAILPROF.

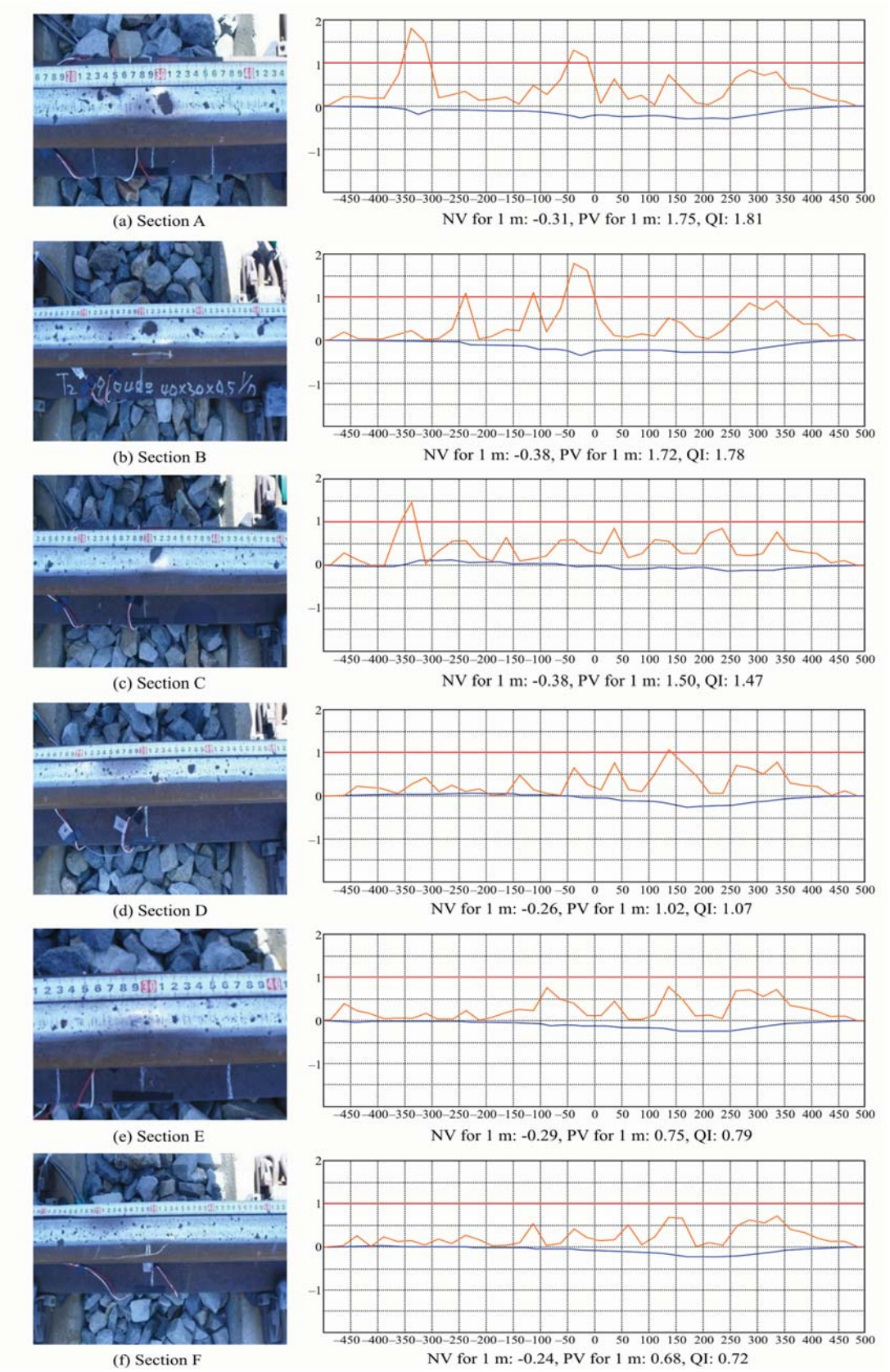

Fig. 7.3 Photographs and measurement results for rail surface roughness of each test section

Fig. 7.4 shows the time history of the dynamic wheel-rail forces measured for the first two axles of a train traveling at a velocity of 200 km/h; the measured signals were low-pass-filtered at 10, 20, and 30 Hz. The peak values of P2 can be limited to very low frequencies (typically up to 20 Hz as specified in UIC Code 518) and those of P1 can include high-frequency components (350 and 750 Hz in this study) [43, 83].

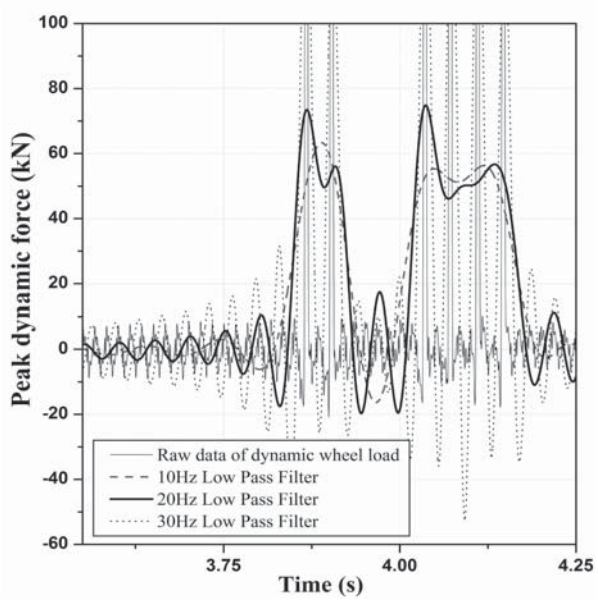

Fig. 7.4 Time history of dynamic forces measured at different low-pass-filter frequencies (*V*=200 km/h)

Fig. 7.5 shows the measurement results for the peak dynamic forces on each test section, measured at a train velocity of 200 km/h and low-pass-filtered at 20 Hz.

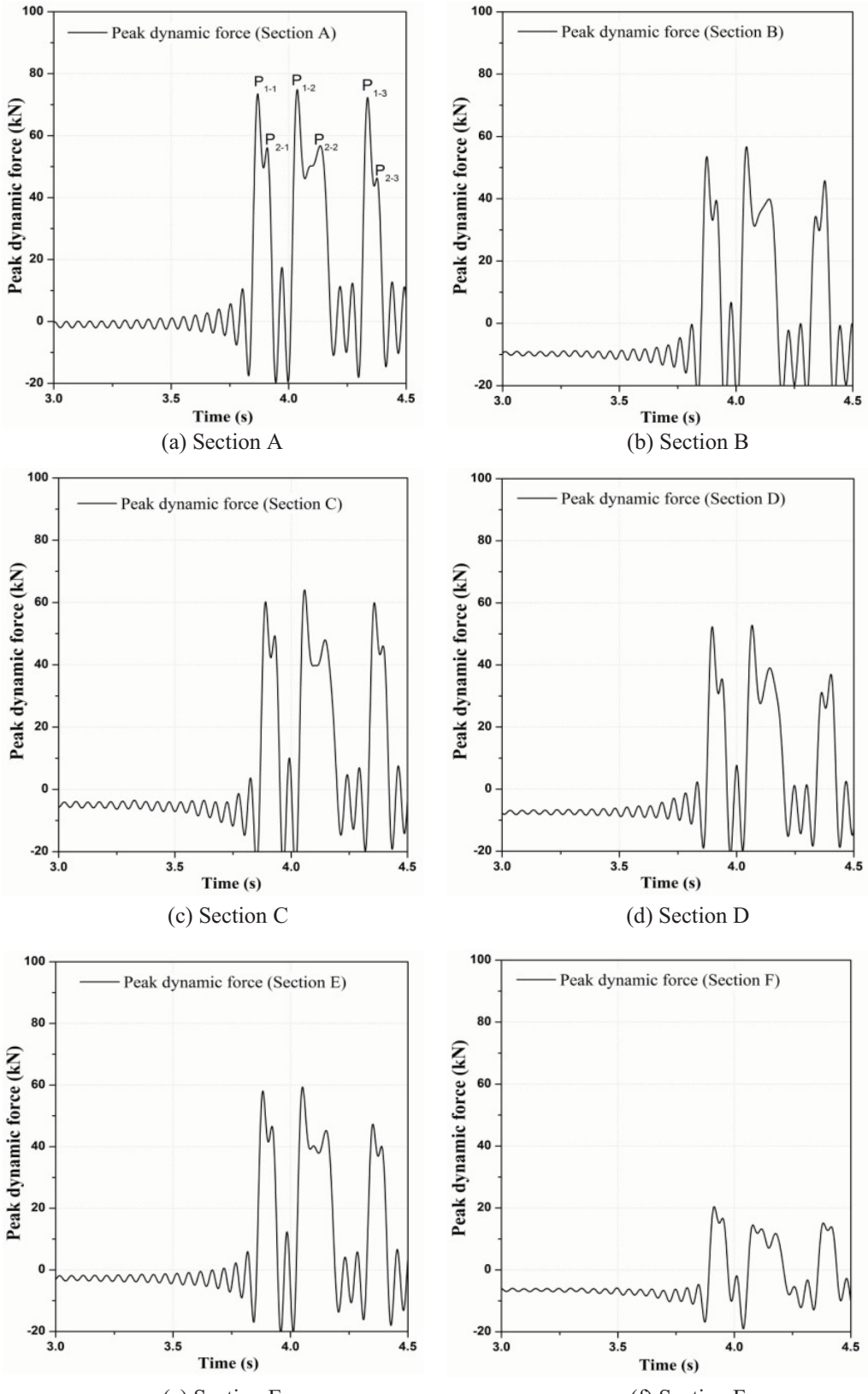

Fig. 7.5 Dynamic forces P1 and P2 exerted by wheel traveling across irregular rail surface

(*V*=200 km/h, low-pass-filter frequency of 20 Hz)

Fig. 7.6 shows the measured peak dynamic forces as a function of the measured rail surface roughness (which is directly related to QI) at train velocities of 200–260 km/h; the measured dynamic wheel-rail forces were fitted according to the QI of each test section. The peak dynamic forces show direct correlation with QI. Moreover, the correlation of the measured peak dynamic wheel-rail forces with the measured QI can be approximated as a linear relationship [43, 169].

The coefficient of determination (R^2) is a measure of the goodness of fit, where 0 indicates no correlation and 1 indicates a perfect correlation. As shown in Fig. 7.6, the correlation between the peak dynamic forces (P1 and P2) and QI was considerably high (0.92–0.99).

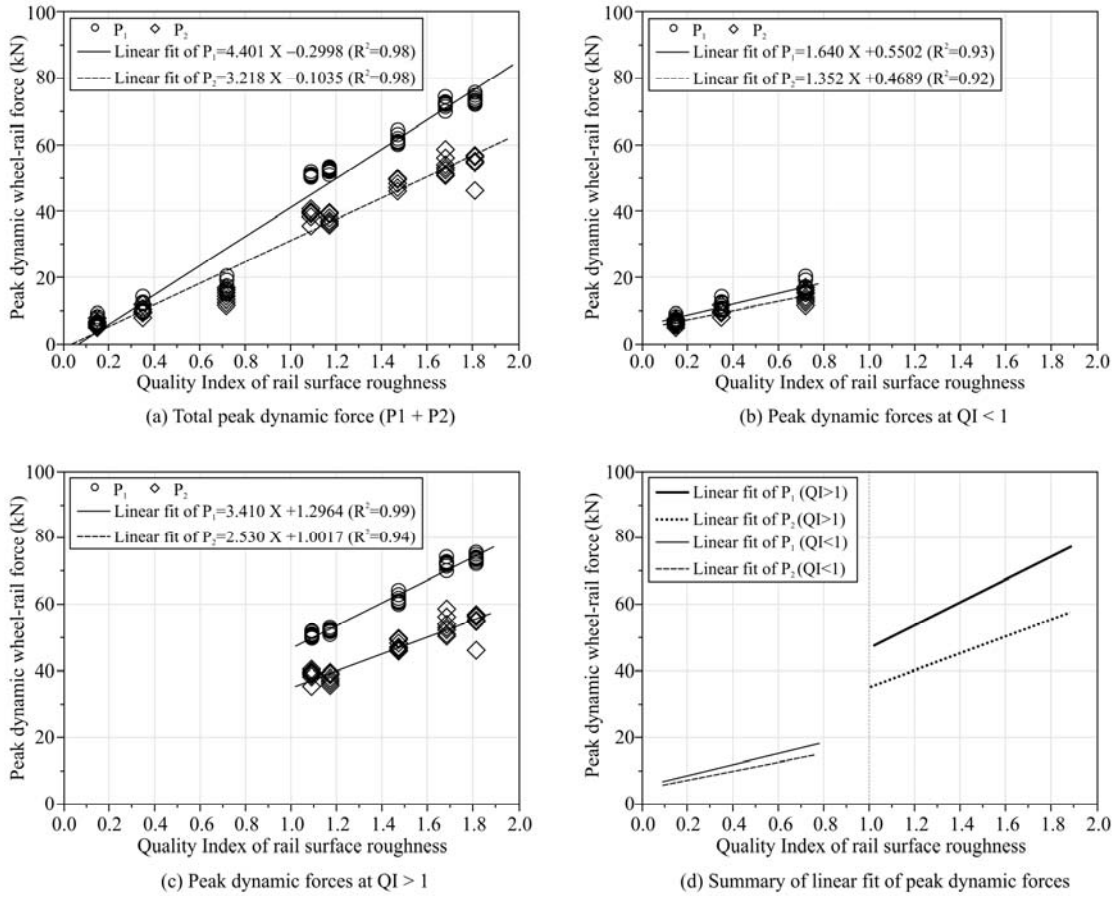

Fig. 7.6 Measured dynamic forces (P1 and P2) and their linear fits according to QI

In Fig. 7.6 (a), P1 and P2 show R^2 values greater and less than 1. For QI < 1 (Fig. 7.6 (b)), neither P1 nor P2 was not significantly affected by changes in QI, and both these forces were lower than 20 kN (dynamic peak forces were in the range of 8–19 kN). For

QI > 1 (Fig. 7.6 (c)), P1 showed a better correlation with QI than did P2. Further, both P1 and P2 were significantly affected by changes in QI, and they were higher than approximately 35 kN. Therefore, P1 (approximately 50–79 kN) showed higher initial and peak values than did P2 (approximately 38–57 kN).

In Fig. 7.6 (d), the peak dynamic forces are fitted according to QI=1. Thus, it was found that the initial values of both P1 and P2 for QI > 1 were more than four times those for QI < 1.

7.5 Multiple regression analysis for prediction of peak dynamic forces

In a multivariate analysis, i.e., when there is more than one independent variable, the regression line cannot be visualized in a two-dimensional space but can be computed very easily. The general purpose of multiple regressions is to learn more about the relationship between several independent or predictor variables and a dependent or criterion variable. A multiple regression analysis can be used to derive a linear prediction equation as follows [105, 149]:

$$\mathrm{Y} = b_0 + b_1 x + b_2 u \tag{7-11}$$

Where, x and u are independent (predictor) variables.

Note that in this equation, the regression coefficient (or partial regression coefficient) represents the independent contribution of each independent variable to the prediction of the dependent variable [105, 149]. In other words, the correlation of variable X with variable Y can be established by controlling all the other independent variables [105, 149]. This type of correlation is also referred to as a partial correlation [105, 149].

In the case of general scatter plots obtained from the field tests, P1 and P2 are the independent variables and QI is the dependent variable. Each point in the plot represents a test section, that is, the correlation between P1 (or P2) and QI for the respective test section. However, linear multiple regression analysis could be employed to convert independent variables to dependent variables and other variables such as train velocity and vertical track stiffness could be considered. Therefore, the measured QI, train

velocity (V) and vertical track stiffness (K) can be considered independent variables and the measured P1 (or P2) can be considered dependent variables [105, 149].

The goal of linear multiple regression procedures is to fit a linear curve through the observed points [105, 149]. The linear regression curve such that the points show minimum squared deviations from the calculated line [105, 149]. The linear regression curve in a two-dimensional or two-variable space is defined by equation (7-11). The constant (b_o) is referred to as the intercept, and the slope (b_1 and b_2) represents the regression coefficient or the partial regression coefficient [105, 149]. The regression line expresses the best prediction of the dependent variable for the given independent variables [105, 149]. However, it is rarely (if ever) perfectly predictable, and usually, there is substantial variation of the observed points around the fitted regression line [105, 149]. The deviation of a particular point from the regression line (its predicted value) is called the residual value [105, 149].

In this study, least squares estimation was used for the linear regression analysis. This estimation method is used to obtain an approximate solution for an over determined system of linear equations, wherein the best approximation is defined as that which minimizes the sum of squared differences between the data values and their corresponding modeled values [105, 149]. For a random sample from the given population, the population parameters were estimated and the sample linear regression model was defined using equation (7-11) [105, 149].

The residual value, $\varepsilon_i = y_i - Y_i = y_i - (b_0 + b_1 x_i + b_2 u_i)$, was calculated as the difference between the true value (measured by the field tests) of the dependent variable, y_i, and the value of the dependent variable predicted by the model, Y_i [105, 149]. The subscript i denotes an observed point. The sum of squared residuals (SSE) was estimated using the ordinary least squares method, as follows [105, 149]:

$$SSE = \sum_{i=1}^{n} \varepsilon_i^2 = \varepsilon_1^2 + \varepsilon_2^2 + \varepsilon_3^2 + \cdots \varepsilon_n^2 \tag{7-12}$$

$$SSE = \{y_1 - (b_0 + b_1 x_1 + b_2 u_1)\}^2 + \{y_2 - (b_0 + b_1 x_2 + b_2 u_2)\}^2 + \cdots + \{y_n - (b_0 + b_1 x_n + b_2 u_n)\}^2$$

Minimization of this function results in a set of normal equations, i.e., a set of simultaneous linear equations of parameters, which are solved to estimate the population parameters [105, 149]. R^2, i.e., the coefficient of determination, is commonly used to evaluate the model fit [105, 149]. When the variability of the residual values around the regression line is small relative to the overall variability, the predictions from the regression equation are good [105, 149]. The R^2 value is an indicator of how well the model fits the data (e.g., an R^2 close to 1.0 indicates that almost all the variability of the variables specified in the model has been accounted for.) [105, 149].

The procedure of multiple regression analysis for the prediction of peak dynamic forces using QI is shown in Fig. 7.7. In this study, QI, the train velocity *V*, and the vertical track stiffness *K* were defined as independent variables and the peak dynamic forces were defined as dependent variables.

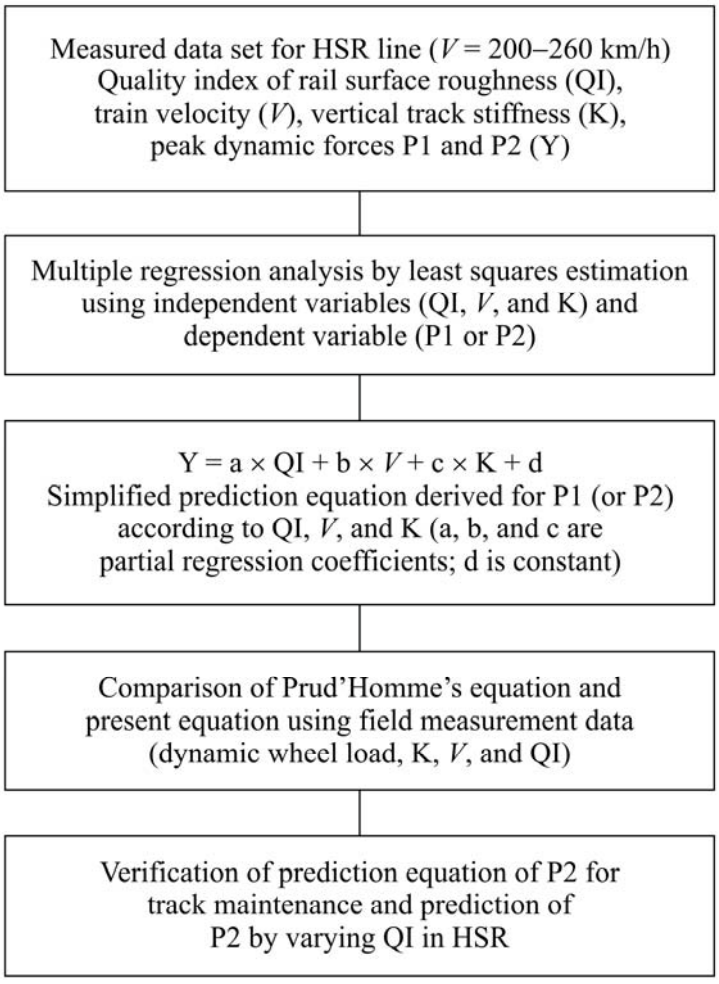

Fig. 7.7 Procedure of multiple regression analysis for prediction of peak dynamic forces according to QI

Table 7.1 and Fig. 7.8 show that QI and V had a larger effect on P1 than on P2, and the R^2 values for P1 and P2 individually were much higher than those for a combination of P1 and P2. Further, the vertical track stiffness affected P2 to a greater extent than it did P1.

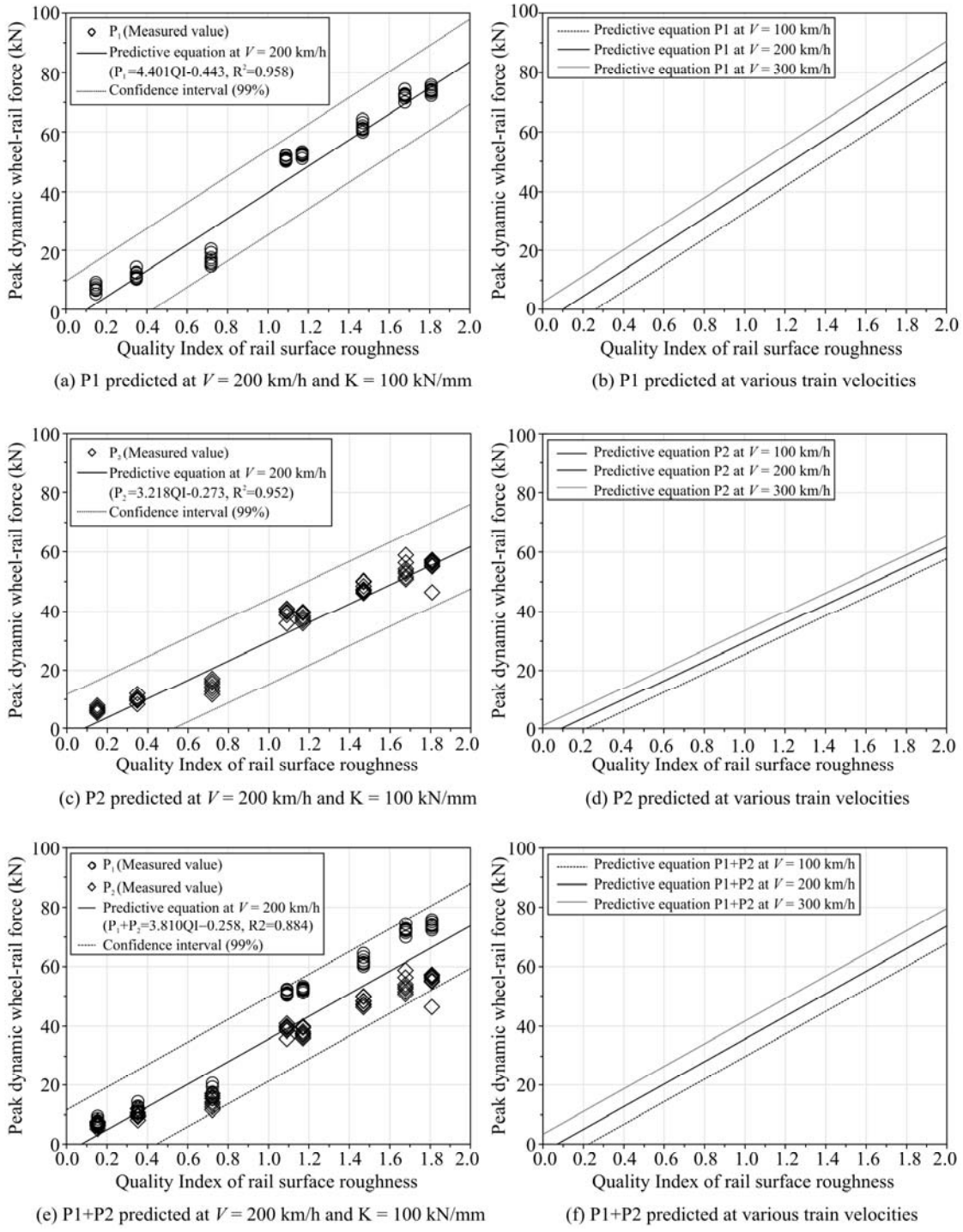

Fig. 7.8 Dynamic forces P1 and P2 and their values predicted by multiple regression analysis at confidence intervals of 99%

The R^2 values obtained from the multiple regression analysis for each test section were more than 0.9 except in the case of combined P1 and P2 (Table 7.1), indicating that the predictions from the regression equation were good and the derived equation fit the measured data well [149, 168].

Table 7.1 Results of multiple regression analysis performed using measured data

Prediction equation of peak dynamic force (kN)	Correlation coefficient	Coefficient of determination (R^2)	Standard error of estimate
$P1 = 4.401QI + 0.007V + 0.001K - 1.943$	0.979	0.958	0.529
$P2 = 3.218QI + 0.004V + 0.002K - 1.273$	0.977	0.952	0.412
$P1 + P2 = 3.810QI + 0.006V + 0.003K - 1.758$	0.941	0.884	0.787

QI: Quality index of rail surface roughness, *V*: Train velocity (km/h), *K*: Vertical track stiffness (kN/mm)

7.6 Numerical simulations for space solution of Prud'Homme's equation

P1 affects the rails mainly as a contact stress. The other force generated after P1 is P2, where the wheel mass acts against a greater portion of the rail mass because of the stiffness of the entire track (i.e., not only the contact stiffness). P2 causes damage to the ballast and increases the geometric irregularities in the rail, which is referred to as settlement [43, 83]. P2 was estimated using equation (7-2) (Prud'Homme's equation) at various vertical track stiffnesses and geometrical quality indexes (as defined by Prud'Homme and here after referred to as QI′) as a function of the peak dynamic forces. The numerical results for a train velocity of 200 km/h are shown in Fig. 7.9. The following parameter values were used in the numerical simulations of the space solution of Prud'Homme's equation for peak dynamic forces: static wheel load of 85 kN, wheel mass (half unsprung mass) of 970 kg, sleeper mass of 300 kg, UIC 60 rail, primary suspension stiffness of 1.8e6 N/m (per wheel), and using the boundary paramenters for vertical track stiffness of 50–300 kN/mm, train velocity of 200–260 km/h, and a geometrical quality index (QI′) of 0.00042–0.00084 (as defined by Prud'Homme).

In the present numerical simulations, a tangent track was considered. The effect of vertical track stiffness, different vehicle velocities, and QI′ was investigated. Some of the other values for the numerical simulations were obtained from previous numerical

and experimental studies [83, 168]. The variation in P2 was measured as a function of the variations in the vertical track stiffness and QI′ at a train velocity of 200 km/h.

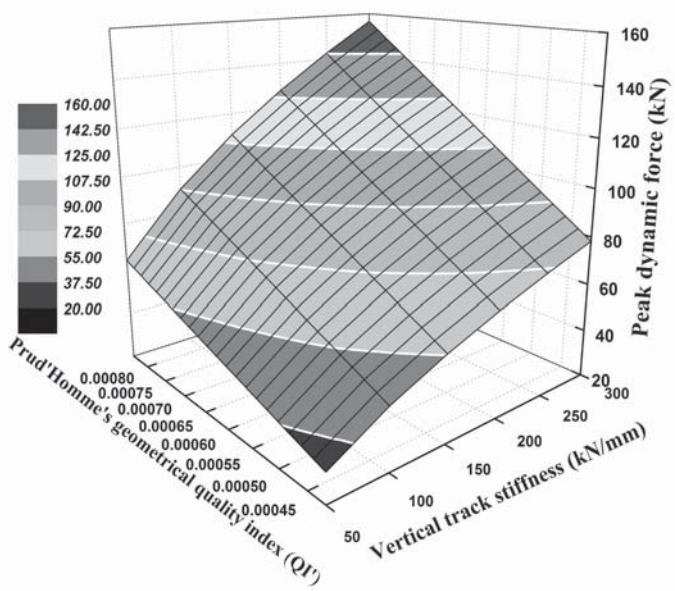

(a) Peak dynamic forces vs. Prud'Homme's geometrical quality index and vertical track stiffness

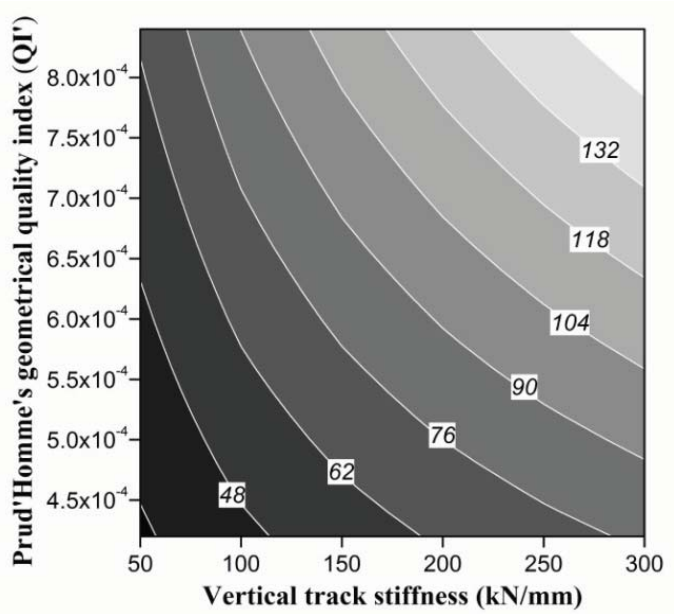

(b) Space solution of peak dynamic forces (kN, values in white box)
vs. Prud'Homme's geometrical quality index and vertical track stiffness

Fig. 7.9 Numerical results of peak dynamic force P2 according to Prud'Homme's equation (train velocity: 200 km/h); as a function of QI′ and vertical track stiffness

Fig. 7.9 shows that P2 increased with an increase in the vertical track stiffness. The discrete space area of P2 increased with an increase in the vertical track stiffness and QI′ (Fig.6 (b)). At vertical track stiffnesses of 150 and 200 kN/mm, the rate of increase

in the peak dynamic force was high. P2 showed a maximum value of 160 kN when QI′ was 0.0008 and vertical track stiffness was 300 kN/mm. This maximum value of P2 was approximately 1.8 times that of the static wheel load.

To ensure that the peak dynamic force is less than the static wheel load, the vertical track stiffness was held constant at 120 kN/mm while varying the geometrical quality of the rail. When the vertical track stiffness exceeded 250 kN/mm, holding the geometrical quality of the rail at a constant value was all the more critical to prevent the peak dynamic force from exceeding the static wheel load. As a result, the vertical track stiffness is directly correlated to the peak dynamic force P2. The vertical track stiffness of 120 kN/mm can be expressed as a track support stiffness of 192 kN/mm with the sleeper spacing of 0.625 m.

7.7 Validation of predicted peak dynamic force P2

In this study, the measured vertical track stiffness of 80–100 kN/mm (which indicates the coverage of the discrete surface area along the X-axis of the P2 map), vehicle speed of 200 km/h (i.e., the general train speed in the test site), and the measured QI (which is shown along the right Y-axis of the P2 map), where the measurements were performed using RAILPROF, were defined as independent variables.

Fig. 7.10 shows the diagram, i.e., the qualitative P2 map of the predicted dynamic force (P2). Fig. 7.10 shows the plot of the variation in the dynamic force (P2) versus the variations in the vertical track stiffness and both QI′ (as defined by Prud'Homme) and QI (as defined by the field measurement performed using RAILPROF). The predicted peak dynamic forces (P2) map was drawn using the empirical equation based on the assumed range of the track support stiffness and QI.

Fig. 7.10 shows that P2 increased with an increase in the vertical track stiffness and QI′ and its corresponding QI. The correlation between QI′ (as defined by Prud'Homme) and the corresponding QI was evaluated from the multiple regression analysis. For a constant QI, the high vertical track stiffness caused the peak dynamic force (P2) to increase. For instance, at QI=1, the peak dynamic force (P2) at a vertical track stiffness of 200 kN/mm was much larger than that at a vertical track stiffness of 100 kN/mm, i.e., larger by a factor of approximately 1.6.

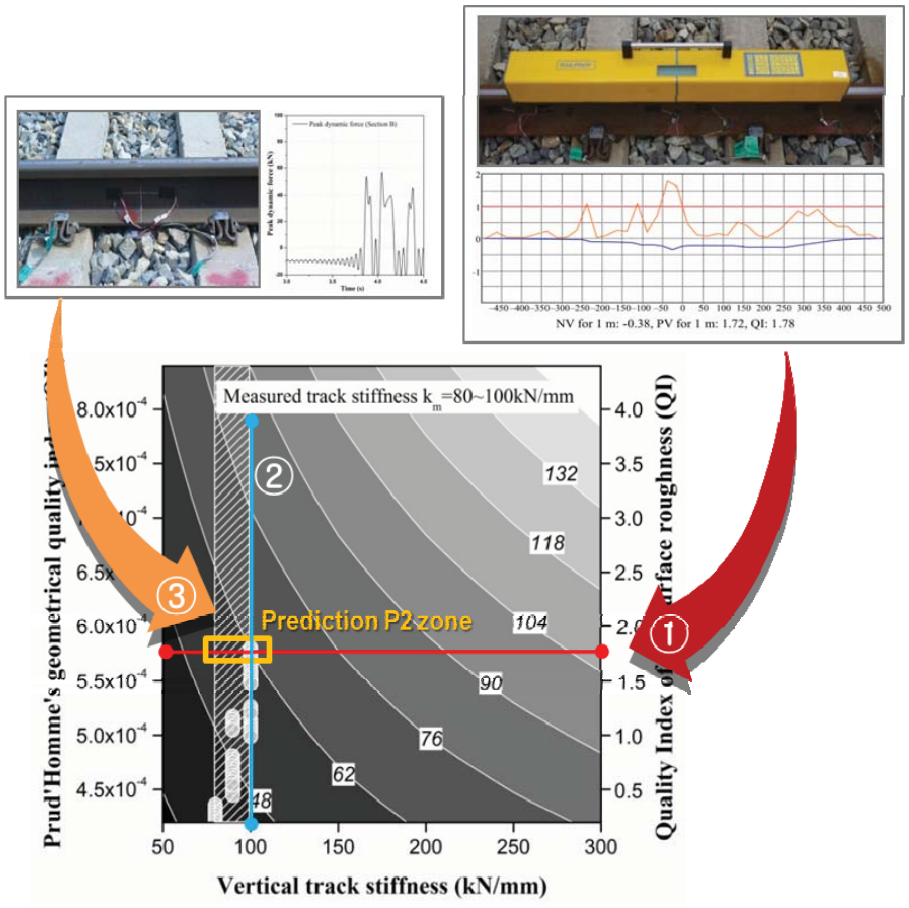

Fig. 7.10 Peak dynamic force P2 map of in-service ballasted track

; Comparison of peak dynamic force P2 estimated using multiple regression analysis (circles) with that estimated using Prud'Homme's geometrical quality index QI′, measured QI, and vertical track stiffness (k_m=80~100kN/mm) can be expressed as a track support stiffness (TSS) of 128~160 kN/mm with the sleeper spacing of 0.625 m

According to the procedure of Fig. 7.10, the peak dynamic forces (P2) of the in-service ballasted track could be predicted from the intersection region of the P2 map and the range of the measured QI in both the vertical and horizontal directions. In other words, the intersection region of a duplicated zone between the vertical and horizontal directions represented the predicted peak dynamic forces (P2) of the in-service ballasted track. The discrete space area of the peak dynamic forces (P2) increased with increasing QI and track support stiffness.

The qualitative analysis using by multiple regression analysis results for the predicted peak dynamic forces (P2) showed good agreement within about 2–5% with the space solution of Prud'Homme's equation. Therefore, it is inferred that multiple regression analysis results obtained using measured data (such as QI, track support stiffness and

dynamic wheel-rail forces) can be used to predict the peak dynamic forces (P1 and P2) acting on a ballasted track and should be of practical use in track maintenance.

7.8 Conclusions

The influence of rail surface roughness and track support stiffness of an in-service ballasted track on dynamic wheel-rail forces currently employed in Korean high-speed lines was assessed by performing field measurements. The theoretical dynamic wheel-rail force determined using Prud'Homme's theory was compared with the dynamic wheel-rail force measured through field measurements. The study performed a comparison between conventional theory and results of the field measurement, and the results contributed toward the development of simple maintenance and assessment methods for the entire rail and not just the welded section. The analytical and experimental results obtained in this study are summarized below.

(1) Numerical simulations and measurements of peak dynamic wheel-rail forces (P1 and P2) for an HSR line with an irregular rail surface showed that the vertical track stiffness affects P2 more strongly than P1. Hence, P1 is more affected by QI and train velocity than P2. The multiple regression analysis results were used to derive an empirical prediction equation for the dynamic wheel-rail forces. For a constant QI, an increase in the vertical track stiffness caused the peak dynamic force to increase. Therefore, it is obvious that keeping the vertical track stiffness of ballasted tracks constant is important to reduce P2.

(3) The multiple regression analysis results showed good agreement within 2–5% with the space solution of Prud'Homme's equation. Therefore, it is inferred that the multiple regression analysis results obtained using measured data (such as QI, track support stiffness and dynamic wheel-rail forces) can be used to predict the peak dynamic forces acting on ballasted tracks, and the prediction equation should be of practical use for track maintenance. If the vertical track stiffness can be known approximately, the peak dynamic force could be qualitatively predicted using the proposed prediction model and QI, which can be measured through a simple test using RAILPROF. Thus, the proposed equation is easy to implement using digital straightedges (such as RAILPROF).

8 PREDICTION OF SUBGRADE MODULUS ON BALLASTED TRACKS

8.1 Introduction

The terms “subgrade modulus,” “ballast modulus,” and, “coefficient of ballast” are used interchangeably to describe the same physical parameter, which is the surface pressure load per unit displacement of the loading surface [77]. The subgrade modulus is an important parameter in investigating track deterioration, maintenance, and settlement, and the critical speed of ballasted tracks [31, 41, 77, 114, 133]. It is estimated by a plate load test (PLT) during the preparation of the railway substructure, or subgrade, before the construction of the track. Whereas the characteristics of the subgrade of in-service tracks have not been extensively studied, it is possible to gather relevant information by field measurements [31]. It is difficult to experimentally estimate the subgrade modulus of in-service tracks because the track components such as rails, fastenings, sleepers, and ballast are installed on top of the subgrade. However, there have been recent attempts to develop a method for measuring the stiffness of the railway subgrade. A novel cyclic penetration test based on the California bearing ratio test was developed for assessing the stiffness of subgrade soils [77, 133]. The test facilitates the measurement of the resilient properties and permanent deformation of subgrade soils, which can be used to estimate the subgrade settlement and determine the ballast depth [77, 133]. However, this method requires several field tests and a special test machine and vehicle, which make it very expensive. Moreover, it does not sufficiently consider the behavior of in-service ballasted tracks.

In this study, the subgrade modulus was determined by an experimental field test on a conventional Korean railway line and compared with that obtained by empirical equations. The subgrade modulus was thus calculated from the subgrade spring stiffness. Furthermore, a finite element (FE) model of the ballasted track was developed by finite element analysis (FEA). The track displacement (i.e., the rail and sleeper displacement) was analyzed and predicted using the FE model. The predictions were compared with the field test results.

The theoretically designed subgrade modulus was first calculated using an empirical equation that had been previously developed from the specifications of the railway subgrade. The measured rail and sleeper displacement, dynamic wheel load, and rail

bending stress were substituted into the empirical equation and the result was compared with that estimated from a map of the subgrade modulus of in-service ballasted tracks developed from the results of field tests. The subgrade modulus map gives the subgrade modulus as a function of the dynamic wheel load and vertical rail displacement. The estimated subgrade modulus was also compared with the design value obtained by the PLT.

8.2 Literature review of subgrade modulus

8.2.1 Definition of subgrade modulus

In a ballasted track, the forces generated by the train axle loads are transmitted from the rails, through the sleepers, and to the ballast, foundation, and subgrade. The theoretical model developed by Zimmermann was used to determine the rail displacement [33, 41, 81, 114]. The model considers the rail as a longitudinal beam that is uniformly and elastically supported at the sleeper support points by the assembly of independent springs that depict the ballast, foundation, and subgrade [33, 41, 81, 114]. It is also assumed that the deflection of each spring is directly proportional to the generated force [33, 77, 114, 133]. It is therefore important to indicate the exact path of a spring when the force and deflection of a ballasted track are discussed [33, 81]. The term “spring” is used in different ways. It sometimes consists of several components of entirely different mechanical properties and is used in different structures [33, 41, 81, 114].

DB AG, a German national railway company, classifies springs in terms of the so-called “ballast modulus” (N/mm³), which is dependent on the rail displacement and surface pressure between the sleeper and the ballast bed (subgrade) [33]. On the other hand, a UIC project report classifies springs in terms of the “subgrade modulus” C (N/mm³), which is a measure of the vertical surface stiffness of the track support substructure, considering the pressure load and the load-bearing area, which includes the ballast and earthwork layers [81].

Furthermore, the track compendium classifies springs in terms of the “coefficient of ballast” (N/mm³), which is also a measure of the vertical surface stiffness of the track support substructure determined by the PLT using the prescribed pressure load and surface area of the loading plate on the earthwork layers [114]. The coefficient of ballast indicates the surface pressure load at which the sleeper subsides by 1 mm [114].

As noted earlier, the terms “ballast modulus,” “subgrade modulus,” and “coefficient of ballast” are used interchangeably to describe the same physical parameter, which is the surface pressure load per unit displacement at the loading surface. In this study, the term “subgrade modulus” is used. When the subgrade modulus is discussed by track engineers, the criteria and positions of the components (whether below the sleeper and subgrade or only below the ballast) should be identified. The subgrade modulus is called the equivalent surface stiffness in track engineering [33, 41, 81, 114]. In this sense, the modulus can be defined more accurately as

$$C = \frac{p}{z} \tag{8-1}$$

Where, p is the surface pressure on a hypothetical load-bearing area (N/mm²) and z is the vertical rail displacement (mm) induced by the surface pressure.

To determine the subgrade modulus of a particular section of a track, the vertical rail displacement is measured and substituted into equation (8-1), together with the value for p, which is computed from the relevant wheel load and the hypothetical load-bearing area of the sleeper [33, 81, 114].

The subgrade modulus describes the stiffness of a support point taking into account the rail bending stiffness and the hypothetical load-bearing area [81]. The vertical stiffness of the subgrade C_{sub} (N/mm) is therefore considered as the spring constant [81]. Generally, the subgrade modulus or surface stiffness is determined from the PLT, and the subgrade stiffness is obtained by dividing the subgrade modulus by the hypothetical load-bearing area [33, 81, 114].

$$C_{sub} = \frac{C}{A} \tag{8-2}$$

Where, C is the subgrade modulus (N/mm³) and A is the hypothetical load-bearing area (mm²). Considering that the total elasticity of the ballasted track is the sum of the elasticity of its various components, the total support point stiffness C_{tot}, which

characterizes the total elasticity below the rail, can be computed by adding the spring constants of the several springs connected in series [33, 81, 114].

$$C_{tot} = \frac{S_i}{z} \tag{8-3}$$

Where, S_i is the force at the support point of the ith sleeper (N) and z is the corresponding vertical rail displacement (mm).

Because C_{tot} takes into account all the elastic components of the rail support [81] shown in Fig. 8.1, rigid components such as the steel plate, concrete sleepers, and concrete structures of the subgrade are not considered in this study.

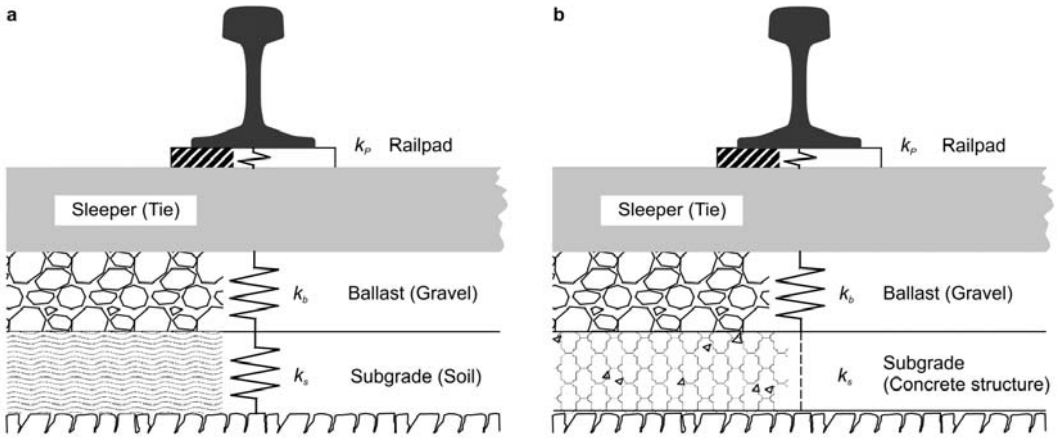

(a) ballasted track on soil (earthwork)

(b) ballasted track on concrete structure (tunnel or bridge)

Fig. 8.1 Elastic spring composition of ballasted track on different substructures

Only flexible elastic components such as the rail pad, ballast, and subgrade earthwork, which govern the displacement of the ballasted track, are considered. For example, in the case of a ballasted track running through a tunnel or over a bridge, the concrete ground surface, which acts as the subgrade, is not considered. Therefore, the resultant displacement of the ballasted track running through a tunnel or over a bridge is only affected by the displacement of the elastic components between the rail and the concrete surface below.

To compare the support point stiffness (C_{tot}) and the track stiffness (k), the relationship between the two is determined using equation (8-4) [33, 81]. Practical values of the track stiffness are often used to simplify the relationship [81]:

$$k = \frac{C_{tot}}{a} \quad \text{or} \quad C_{tot} = \left(\frac{1}{k_p} + \frac{1}{k_b} + \frac{1}{k_s} \right)^{-1} \tag{8-4}$$

Where, a is the spacing of the support points (m), k_p is the rail pad stiffness (kN/mm), k_b is the ballast stiffness (kN/mm), and k_s is the subgrade (soil) stiffness (kN/mm).

8.2.2 Subgrade modulus of ballasted track

DB and the French national railway corporation SNCF estimate the settlement and critical speed of ballasted tracks from the subgrade modulus using design values [33, 114]. The track settlement depends on the sleeper spacing, bending stiffness of the rail, spring stiffness of the rail pad, subgrade type, and subsoil properties. If the settlement is too low, the ballast pressure would drastically increase [33, 114].

The consequences of this increase are the so-called white spots on DB AG high-speed lines, which can be destructive to the ballast [114]. The high-speed ballast tracks of DB AG are highly compacted, and their properties are similar to those of a concrete track [114]. The compaction is carried out using a dynamic track stabilizer (DTS), and the track settlement has been found to be only 0.3–0.45 mm [114]. The stiffness of the subgrade is improved by the insertion of soft elastic rail pads, resulting in a settlement of 0.8 mm [114]. The proposed optimum subgrade modulus of DB AG is within the very narrow range of 0.05–0.1 N/mm^3 [33, 114].

Based on the results of a recent study, the optimum ballasted track stiffness is within the range of 50–100 kN/mm [33, 77, 114]. The optimum range of the subgrade modulus should therefore be estimated to control the settlement of ballasted tracks [33, 114]. Various empirical equations have been developed for this purpose [33, 77, 114].

The typical subgrade modulus has been determined by considering different load-bearing capacities and service conditions [33, 114]. Because the subgrade modulus is based on design values, the results of analyses using the theoretically designed subgrade

modulus do not reflect the performance of in-situ ballasted tracks [31, 33, 77, 81, 114, 133]. This has made it necessary to develop a method for estimating the subgrade modulus and stiffness of in-service ballasted tracks to predict their behavior [77, 81, 114, 133].

In 1994, Cai et al. described the track modulus (k, N/mm) of a ballasted track as the ratio of the rail vertical displacement to the vertical contact pressure between the rail bed and the foundation beam comprising the underlying components [18, 155]. Selig and Li proposed a simplified definition of the coefficient of ballast (c, N/mm^3) in their calculation, namely, the support pressure force exerted on the rail per unit vertical rail displacement [159]. In addition, the main difference between the track modulus k and subgrade modulus *c* is that *k* depends on the rail dimensions and material properties (bending stiffness), whereas *c* depends on the properties of the underlying components (ballast, sub-ballast, and underlying soil layers) and the support subgrade, and is also independent of the rail type [97, 159].

The subgrade modulus is directly related to the overall track performance, safety, serviceability, and the amount of repair and maintenance required. Ebersohn et al. concluded that if the subgrade modulus is low, the settlement along a track could vary and therefore increase the required maintenance [39]. Zarembski and Palese also concluded that a significant variation of the subgrade modulus in, for example, bridges, tunnels, and slab tracks, increases the dynamic forces exerted on the tracks [193].

Different methods have been proposed for the measurement and calculation of the subgrade modulus and stiffness [77, 97, 114, 133]. Moreover, there have been many attempts to estimate the subgrade modulus and control settlement for various types of railway tracks, ballast layer thicknesses, and subgrade types [77, 97].

Subgrade modulus estimation methods are of three major types: theoretical, theoretical-experimental, and experimental [77, 97, 193]. Hay (1953), Birmann and Luber (1965–1966), Prause et al. (1974), Ahlf (1975), and West Australia Railway (1976) analyzed track stiffness by theoretical and experimental methods [97]. The effects of the ballast thickness and conditions of the track subgrade have also been generally considered [97]. Various factors affect track stiffness, and their variability and interaction as well as the dynamic forces determine the subgrade modulus.

For this reason, an estimation of the subgrade modulus is complex and difficult and requires an extensive experimental case study [77, 97, 142, 159]. Priest and Powrie analyzed dynamic track stiffness by experimental methods involving the measurement of the sleeper velocity [142]. They found that the stress and deflection were greater than those determined analytically under perfect track conditions but less than conventional empirical values [142].

8.2.3 Determination of subgrade modulus from track response

The empirical equations used to determine the subgrade modulus consider different factors such as rail displacement, rail bending stress, length of the bending wave, and spring stiffness at the rail supporting point, as well as different train and track conditions [114]. Table 8.1 shows the typical subgrade modulus for subgrade soils with different load-bearing capacities [114].

The subgrade moduli of old sections range between 0.05 and 0.15 N/mm³, whereas those of newly constructed sections range between 0.3 and 0.4 N/mm³ [33, 77, 114].

Table 8.1 Typical subgrade modulus for different subgrade soils [114]

Subsoil	Subgrade modulus (N/mm^3)
Very poor quality subgrade soils (marshy ground, fine-grained sand, etc.)	0.02
Poor quality subgrade soils (cohesive to soft to stiff) (loam, clay, etc.)	0.05
Good quality subgrade soils (coarse sand, gravel, etc.)	0.10
Very good quality subgrade soils (gravel, rock, etc.)	≥0.15
Concrete bottom (tunnel, bridge, etc.), stony soil, rocky subsoil	≥0.30

Table 8.2 lists the various empirical equations used to determine the subgrade modulus [114]. The rail displacement is determined by considering the rail as a longitudinal beam that is uniformly and elastically supported [114]. The ballast, foundation, and sub-base at all the discrete supporting points are considered as being uniformly large and independent springs with a spring path proportional to the applied force [33, 114].

The stiffness of the sleepers is excluded from the calculations of the subgrade modulus of the ballasted track; only the bending stiffness (E and I) and the bending performance

of the rails (y, L, and σ_m) are considered [114]. This makes the subgrade modulus dependent on the rail displacement and surface pressure between the sleeper and the ballast bed [114].

Table 8.2 Empirical equations used to determine subgrade modulus [114]

	Methodology	Empirical equation	Related equation
1	Settlement measurements (rail displacement)	$C = \frac{Q}{4 \cdot b \cdot y} \cdot \sqrt[3]{\frac{Q}{E \cdot I \cdot y}} = \frac{Q \cdot a}{2 \cdot A \cdot y} \cdot \sqrt[3]{\frac{Q}{E \cdot I \cdot y}}$	
2	Rail bending stress	$C = \frac{4 \cdot E \cdot I}{b} \cdot \left(\frac{Q}{4 \cdot \sigma_m \cdot W} \right)^4$	
3	Length of bending wave	$C = \frac{4 \cdot E \cdot I}{b \cdot L^4} = \frac{8 \cdot E \cdot I \cdot a}{A \cdot L^4}$	
4	Spring rate of supporting point	$C = \frac{F_s}{A \cdot y} = \frac{c}{A}$	$c = \frac{F_s}{y} = \frac{1}{4} \cdot \sqrt[3]{\frac{Q^4}{E \cdot I \cdot y^4}}$

Notation
Q: static vertical force acting on rail (N)
E: modulus of elasticity of rail (N/cm^2)
I: moment of inertia of rail (cm^4)
y: displacement of rail (cm)
b: theoretical rail width (cm)
A: half-sleeper support surface area (cm^2)
σ_m: bending stress at centre of rail foot (N/cm^2)
W: section modulus of rail (cm^3)
L: length of bending wave (cm)
F_s: supporting point force acting on rail fastening element (kN)
c: spring rate (kN/mm)
a: sleeper spacing (cm)

The simplest method to determine the subgrade modulus is to measure the rail displacement and use equation (1) shown in Table 8.2 [114]. It is also possible to determine the subgrade modulus from the bending stresses generated under load at the middle of the rail foot using equation (2) in Table 8.2 [114].

Determining the subgrade modulus from the bending wave using equation (3) in Table 8.2 requires very sophisticated equipment and an expensive experiment [114].

The elastic displacement of railway tracks can also be expressed in terms of the spring stiffness at the rail supporting point (equation (4) in Table 8.2) [114].

8.3 Field measurements

8.3.1 Overview of test site

Field measurements of the dynamic response of a test track (i.e., the dynamic wheel load, rail and sleeper displacement, and rail bending stress) were conducted. The subgrade modulus was also estimated using the proposed subgrade modulus map and the conventional empirical equation, equation (1) in Table 8.2 [114]. The results were compared with the empirical results and those obtained using the FE model to assess the validity of the model.

A section of an in-service ballasted railway line in the Republic of Korea was used for this study. The test section was a straight and continuously welded rail track weighing 60 kg. The design subgrade modulus was quoted according to the Korean standard KS F2310 for subgrade materials, which was adopted at the time of the construction [101–103]. The parameters and photographs of the test site are shown in Table 8.3 and Fig. 8.2 (a) and (b), respectively. The vehicle load compositions of the tests are shown in Fig. 8.2 (c).

Table 8.3 Parameters of test track

	Test section
Track curvature (R)	∞ (Straight)
Substructure	Earthwork
Rail	60 kg N, Continuous welded rail
Sleeper	Prestressed concrete sleeper
Sleeper spacing	625 mm
Fastening	Pandrol e-clip
Cant	0 mm
Ballast thickness	300 mm
Ballast mat	–
Subgrade modulus [a]	0.15 N/mm³
Annual tonnage	60 MGT
Operational speed	Average 120 km/h

[a] Obtained from design data determined by PLT (KS F2310), k_{30} > 0.11 N/mm³ (Korean standard)[101–103]

(a) View of test section (b) Test train (EMU)

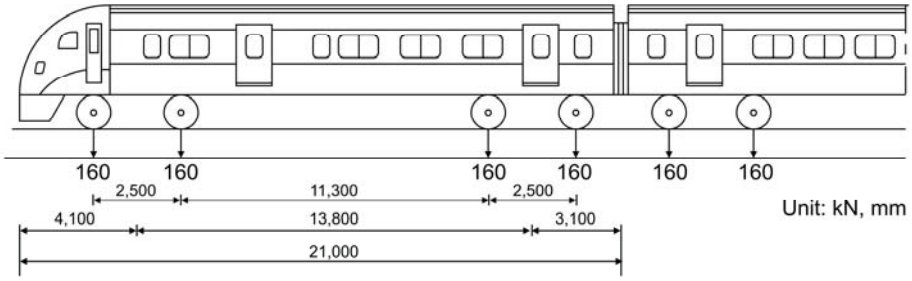

(c) Vehicle load composition of EMU (Electric Multiple Unit)

Fig. 8.2 Photographs of test track and train

8.3.2 Dynamic track response measurement

The dynamic wheel load acting on the track segment subjected to a passing train load was measured by installing a two-axis strain gauge on the rail web between the two test sleepers [55]. The measured signal was recorded on a data acquisition system (MGC-Plus) and was analyzed using the Origin™ program. To eliminate interference from other passing trains and obtain a reliable measure of the dynamic wheel load for the current passing train, measurements were performed using a wheel load gauge wired to eight strain gauges at an angle of 45° and attached along the neutral axis of the rail web at a distance of 100 mm from the center of the sleepers, as shown in Fig. 8.3(a).

The vertical wheel loads were measured using shear strain gauges coupled to a full Wheatstone bridge circuit [79]. The strain gauge bridges were calibrated using a hydraulic ram and load cell to obtain measurements with an accuracy of 2% [55, 79]. In order to prevent data distortion and loss, the sampling rate was set to more than 1 kHz.

The rail bending strain on the test track was measured using a one-axis strain gauge attached longitudinally to the bottom flange of the rail at the centre of the sleepers, as shown in Fig. 8.3(a) [55].

The empirical subgrade modulus of the test track can be calculated from the conventional equation using the measured vertical displacement of the track subjected to a passing train load and by comparing these results with the FEA results for the track. The dynamic displacement of two consecutive sleepers was measured relative to a reference frame anchored 2.0 m below the top of the sleepers, as shown in Fig. 8.3(b) [55]. The beam was assembled to measure the absolute vertical displacement of the two sleepers on each side of the instrumented track as the train passed over it.

Vertical rail displacements were measured using displacement transducers such as linear variable differential transformers (LVDTs) mounted on a jig anchored under the ballast layer of the track, as shown in Fig. 8.3(b).

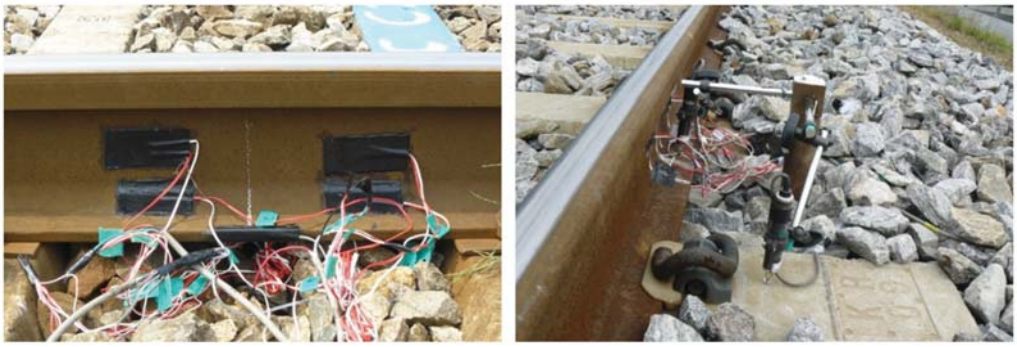

(a) Wheel load and rail bending stress (b) Rail and sleeper displacement

Fig. 8.3 Photographs of wheel load sensor, strain gauges, and LVDTs

Fig. 8.4 shows variations in the dynamic response of the ballasted test track. It can be seen that the dynamic wheel load and rail displacement was affected by an increase in the train speed (Fig. 8.4 (a)–(b)). Fig. 8.4 (c) and (d) show that the sleeper displacements and the rail bending stresses are slightly increased with the increase in the train speed.

These measurement results were applied to the conventional equation for the estimation of subgrade modulus. Then, the measured results were compared with the FEA results for two subgrade modulus values from the design and prediction value.

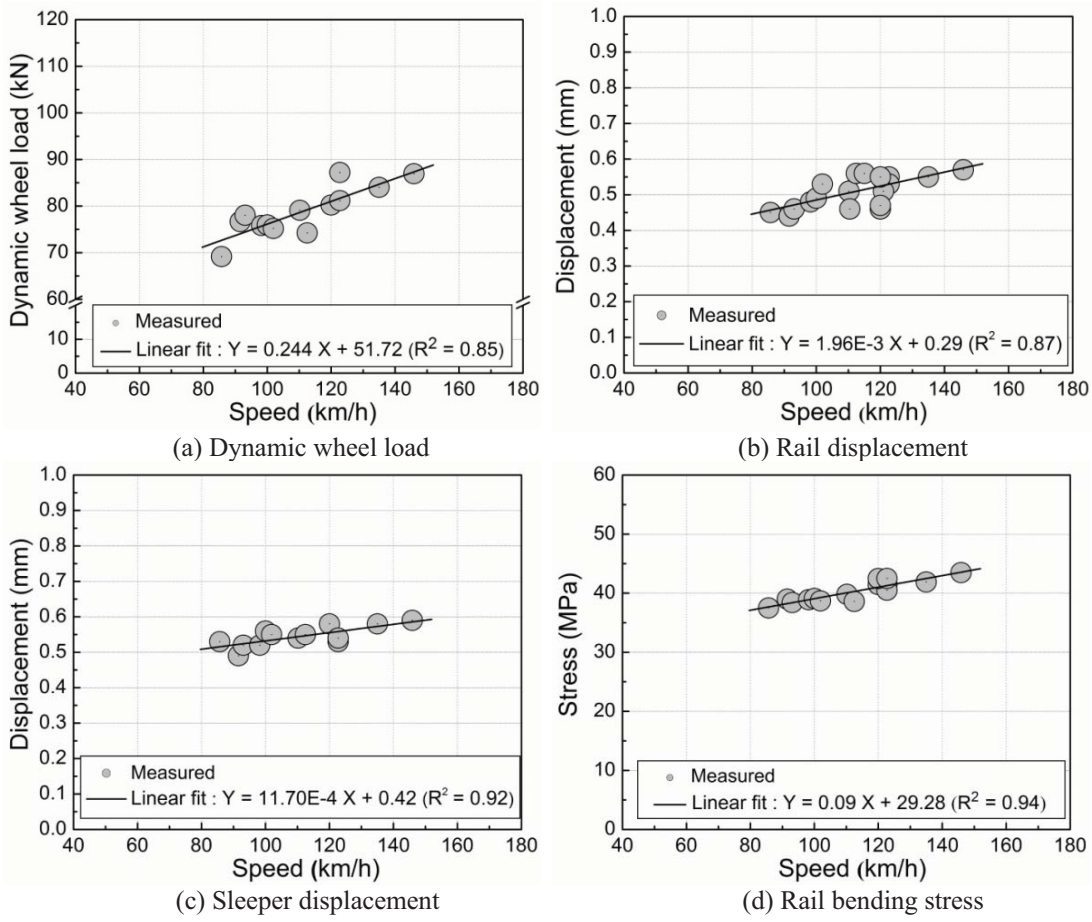

(a) Dynamic wheel load (b) Rail displacement

(c) Sleeper displacement (d) Rail bending stress

Fig. 8.4 Variations in dynamic response of ballasted test track

8.4 Prediction of subgrade modulus by qualitative analysis

8.4.1 Subgrade modulus map using field measurements

For simplicity, let us assume that "qualitative" implies non-numerical data or an explanation based on the attributes of a range of data. Qualitative analysis is often used in chemistry, heat mechanics, and the social sciences because it can be used to answer certain important questions more efficiently and effectively than a quantitative approach, which focuses on numbers [56, 196].

Track structures are built from various materials and are subjected to various environmental conditions, which make inspection and maintenance more difficult. However, the application of quantitative analysis does not allow for the study of track design and maintenance under in-service conditions because of many uncertain factors such as track deterioration and rail surface roughness. Nevertheless, the qualitative description of track response can use multiple colors and discrete space areas, rather than single values, to represent several uncertain variables. In this study, basic

qualitative analysis was used to estimate and predict the subgrade modulus of a real field, which is presented as a subgrade modulus map.

The measured dynamic wheel load and rail displacement for the field test train speed of 120 km/h were prepared as reference data (i.e., indicating the range of the discrete space area). The subgrade modulus was defined as a dependent variable of the qualitative analysis. The following parameter values were adopted based on the results of the field test and design values [101–103]: wheel load of 75–95 kN, sleeper spacing of 62.5 mm, KR 60 rail type, half-sleeper support surface area of 3,021 cm^2, and rail displacement of 0.3–1.0 mm.

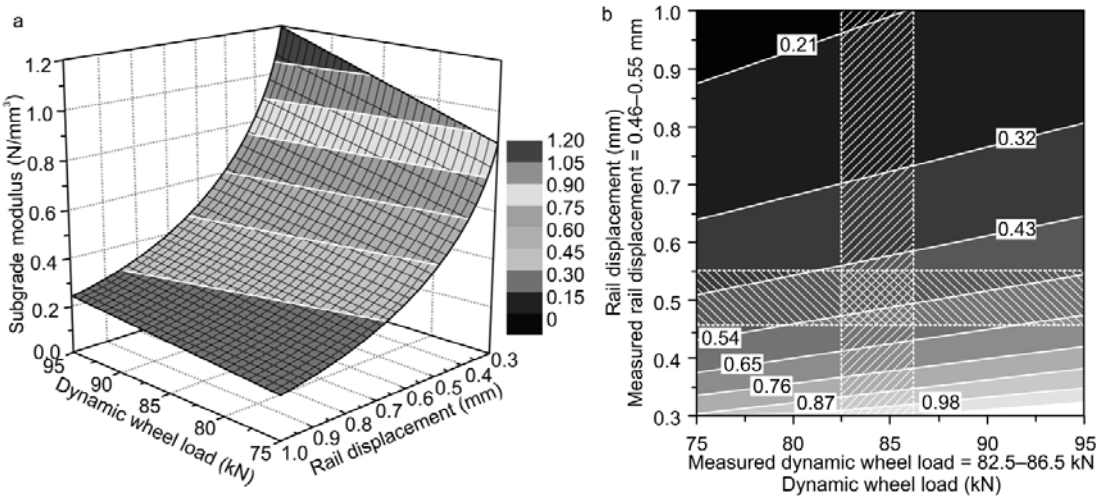

(a) Subgrade modulus vs. dynamic wheel load and rail displacement

(b) Diagram of subgrade modulus vs. dynamic wheel load and rail displacement with measured data

Fig. 8.5 Example of subgrade modulus map; subgrade modulus as a function of dynamic wheel load and vertical rail displacement

Fig. 8.5 shows the variation of the subgrade modulus with the rail displacement and dynamic wheel load for a vehicle speed of 120 km/h. Fig. 8.5 (a) is a subgrade modulus diagram (i.e., qualitative analysis map) that portrays the subgrade modulus as a function of the dynamic wheel load and rail displacement.

The subgrade modulus map was drawn using the empirical equation based on the assumed range of the dynamic wheel loads and rail displacements. The subgrade modulus of the in-service ballasted track could be predicted from the intersection region of the subgrade modulus map shown in Fig. 8.5 (b) and the range of the measurement results in both the vertical and horizontal directions. In other words, the intersection

region of a duplicated zone between the vertical and horizontal directions in Fig. 8.5 (b) represented the predicted subgrade modulus of the in-service ballasted track. As shown in Fig. 8.5, the discrete space area of the subgrade modulus decreased with increasing rail displacement and dynamic wheel load. For a rail displacement of less than 0.5 mm, the rate of increase in the subgrade modulus was high. It had a maximum value of 1.2 N/mm^3 for a dynamic wheel load of 95 kN and rail displacement of 0.3 mm. As can also be seen from Fig. 8.5, the rail displacement had a greater effect on the subgrade modulus than the dynamic wheel load.

Because the test section of the track was newly constructed (approximately 2 years old) [103] and the conventional empirical values were taken into account [33, 114], the subgrade modulus could be between 0.3 and 0.4 N/mm^3. However, the results of the predictions based on the measured data ranged between 0.43 and 0.76 N/mm^3 (the intersection region of a duplicated zone shown in Fig. 8.5 (b)). This means that the subgrade modulus of the in-service ballasted track was higher and more roughly distributed over a wider range than the design value used for the construction. To ensure an in-service value comparable to the design value, the rail displacement, which is affected by the vertical track stiffness, was kept constant at 0.7 mm while the dynamic wheel load was varied.

8.4.2 Validation of subgrade modulus of test track predicted

The ballasted track model used for numerical simulation, developed using the commercial FEA package LUSAS, was configured as shown in Fig. 8.6 [23, 31, 116, 155]. To investigate the train-induced track displacement of the test track, a time-history FE analysis was performed and the results were compared with those of the field test [23].

In the case of the electric multiple unit (EMU), one motor car and five passenger cars traveling at 120 km/h were considered in the analysis [23]. The two types of cars exerted different wheel loads. Multiple concentrated loads with variable element lengths that were dependent on the impact load shapes were used for the analysis [23]. The time-history train load compositions are illustrated in Fig. 8.2 (c).

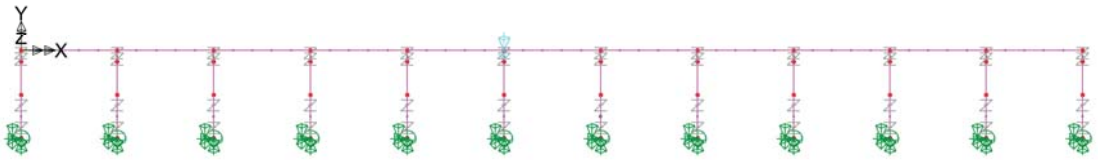

Fig. 8.6 Finite element analysis model

The rails and sleepers comprised frame elements, whereas the rail pad, ballast, and subgrade comprised spring elements [23, 31, 114]. The nodal points between the rail and sleeper elements were connected by spring damper elements with the same properties as those of the rail pad [23, 31, 37, 38]. The ballast conditions under the sleeper base were simulated by a spring element with the same properties as those of the ballast [23, 37, 31, 38]. The subgrade conditions under the ballast layer were simulated by a spring element with the properties listed in Table 8.5. The spring stiffness of the rail pad was 400 kN/mm, and the damping coefficient was 15.683 kN/m; the corresponding properties of the ballast were 200 kN/mm and 77.877 kN/m [23], respectively, according to the design data of the track [102, 103]. The FE model properties of the rails and sleepers are listed in Table 8.4 [102, 103].

Table 8.4 Properties of rails and sleepers in FEA model

	Properties	Rail (60 kg N)	Prestressed concrete sleeper
Section Properties	Cross-sectional area (cm^2)	77.5	516.75
	Moment of inertia (cm^4)	3,090	16,375
Material Properties	Elastic modulus (kN/cm^2)	21,000	4,000
	Weight density (kN/cm^3)	7.85×10^{-5}	2.5×10^{-5}
	Poisson's ratio (υ)	0.30	0.18

Table 8.5 Comparison of subgrade stiffness calculated by different methods

Methodology	Subgrade modulus (N/mm^3)	Subgrade stiffness (kN/mm)
Design value[a]	0.15	104.0
Proposed subgrade modulus map[b]	0.53–0.58 (average 0.56)	388.3

[a] Design value obtained by PLT (refer to Table 8.3)
[b] Using Eq. (1) in Table 8.2 and the proposed subgrade map with measured data (refer to Fig. 8.5(b))

The spring stiffness of the subgrade for the modulus shown in Table 8.5 was calculated, assuming the hypothetical load-bearing area to be 7.628×10^5 mm^2; this value was obtained using the formula $[b + (d - 15) \times 2] \times [\ell + (d - 15) \times 2]/2$, where b denotes the sleeper width of 265 mm, d denotes the ballast thickness of 300 mm, and ℓ denotes the sleeper length of 2,400 mm [23, 81, 101–103]. A wheel load of 82–86 kN and a train speed of 120 km/h were used. This was based on the dynamic wheel load, rail displacement, and general train speed in the field test. The boundary conditions of the FE model were imposed at the base of the horizontal subgrade [23, 31, 37, 38].

8.5 Results and discussion

Table 8.6 compares the subgrade modulus and vertical rail displacement of the test track obtained by different methods. The measured dynamic rail displacements are compared with those of the FEA for the different subgrade moduli listed in Table 8.6.

Table 8.6 Comparison between some FEA, empirical, and experimental results

Applied load (kN)	Subgrade modulus (N/mm³)		Rail displacement (mm)		
	Design value[a]	Proposed value[b]	Measured	FEA (1)[c]	FEA (2)[d]
82	0.15	0.58	0.461	0.604	0.456
86	0.15	0.53	0.507	0.634	0.476

[a] Design value (refer to Table 8.3 [103])
[b] Obtained using proposed subgrade modulus map
[c] Obtained using design value of subgrade modulus
[d] Obtained using proposed value determined from proposed subgrade modulus map

It is interesting to note that the displacements corresponding to the design subgrade moduli obtained by the PLT were greater than those corresponding to the moduli estimated from the proposed subgrade modulus map. Consequently, the analytically obtained displacement based on the design subgrade modulus (FEA (1)) underestimated the behavior of the in-service track. Moreover, the analytically obtained displacement based on the subgrade modulus estimated from the proposed subgrade modulus map (FEA (2)) was less than that of FEA (1).

The design subgrade modulus was approximately 70% less than that estimated from the proposed subgrade modulus map. It is therefore considered that the subgrade

modulus directly affects the displacement of an in-service track. Furthermore, the difference between the experimental and FEA (2) displacements was less than that between the experimental and FEA (1) displacements. The FEA (1) displacement was approximately 1.2 times the experimental displacement, whereas the FEA (2) and experimental displacements were in good agreement with only approximately 5% discrepancy. It is supposed that the FEA results obtained using the subgrade modulus estimated from the proposed subgrade modulus map are sufficiently reliable indicators of the behavior of an in-service track.

8.6 Conclusions

The subgrade modulus of an in-service ballasted track was assessed by performing field measurements using actual vehicles running along service lines. For comparison with the design value, the modulus was predicted using a proposed subgrade modulus map (i.e., qualitative analysis map) developed from the results of field measurements and empirical equations. The rail displacement of the ballasted track was predicted by an FE model that considers the spring stiffness at the rail support point, which includes the predictive subgrade stiffness. In addition, the rail displacement was compared with the data obtained through field measurements.

The analytical and experimental results obtained in this study are summarized below.

(1) The rail displacement obtained by FEA using the design subgrade modulus was greater than that obtained by the proposed subgrade modulus map. The design subgrade modulus was approximately 70% less than that estimated by the proposed subgrade modulus map. The numerical model employing the design subgrade modulus underestimated the rail displacement of the in-service track. The effect of the rail displacement on the subgrade modulus is greater than that of the dynamic wheel load.

(2) Relative to the experimentally determined rail displacement, the deviation of the displacement obtained by FEA using the design subgrade modulus was greater than that obtained using the subgrade modulus estimated from the proposed subgrade modulus map. The displacements obtained by FEA using the proposed subgrade

modulus map and by the field test results were in good agreement with only approximately 5% discrepancy.

(3) A comparison was performed between results obtained from conventional theory and results of the field measurement, and the comparison results contributed toward the development of simple estimation methods (not requiring expensive experiments and sophisticated equipment) for the subgrade modulus of an in-service ballasted track. The subgrade modulus of an in-service track can thus be qualitatively predicted by the proposed subgrade modulus map and a simple field test.

9 QUALITATIVE ANALYSIS FOR DYNAMIC RESPONSE OF BALLASTED TRACKS

9.1 Introduction

In this study, the qualitative analysis was defined by the prediction method of the track response using the analytical matrices functions which was validated by FEA and field measurement, i.e., related in the empirical theory for dynamic track mechanics, and the results of qualitative analysis showed as the discrete surface area (herein referred to as space solution). The analysis for dynamic track response of ballasted track was need to variable parameters of track components and track force related in the behaviors of ballasted track referred in section 9.2. Therefore it was performed that the numerical model by conventional theory of track dynamics and then it was compared with the finite element analysis results and the measured results in real field. These results of track response that was investigated by the qualitative analysis has validate by the measured results.

Track stiffness (track support stiffness) is a basic parameter of track design which influences the bearing capacity of track, the dynamic behavior of vehicle, and, in particular, the quality of track geometry and the life of track components. In general, relatively high track stiffness is beneficial as it provides sufficient track resistance to applied loads and results in decreased track deflection, which reduces track deterioration [31, 41, 114]. However, very high track stiffness leads to increased dynamic forces in the wheel–rail interface as well as on sleepers and ballast, which may cause wear and fatigue of track components [21, 22, 31, 41, 77, 114, 191]. Also, a particular problem is changes in track stiffness along the track, which causes variations in vehicle–track interaction forces and leads to differential settlement and therefore differential track geometry deterioration and potentially vibration problems [31, 41, 55, 110–112, 114].

Track stiffness is also known as a basic parameter that refers to the essential requirement ‘technical compatibility’. Hence, further research and studies are required in order to develop a rational approach to the track design and construction so that the track stiffness and its variations are within an acceptable range of values, or ideally, to achieve an optimum track stiffness [31, 110–112, 196, 197]. Also, it is important to be able to measure track stiffness using techniques that give accurate, repetitive, and

reproducible results so that the track performance of existing lines can be evaluated and appropriate decisions regarding track maintenance may be made. A recently research has been conducted in this area done by Fröhling, and Wu and Thompson, and also others reviewed and summarized by Hunt [55, 57, 86–92, 95, 110–112, 191].

Compared with previous studies, a new effort is made to use the spatially varying ballast/subgrade stiffness derived directly from the results measured by non-destruction method [88, 95, 195] and rolling stiffness measurement vehicle (RSMV) as input data in simulations [6, 110, 111]. Determining input data for ballast/subgrade has been a very complex task for simulating vehicle–track interaction problems.

Current standards and assessment methods, without any consideration to the dynamic responses according to the variation of the rail pad and ballast stiffness and related in the other parameters, may not be sufficient for track maintenance and train speed settings. Safety, maintenance costs, and passenger comfort are highly determined by the track components dynamics [31, 41, 55, 77, 110, 111]. Accordingly, track maintenance planning can be based on the combined consideration of the track geometry inspection and the dynamic track responses [55, 110, 111, 129, 172, 185]. Among published articles, the works by Bonaventura et al. and Li et al., Sun et al. and Vermeij et al. are referred to [17, 31, 108, 110, 111, 114, 172, 185]. The dynamic modeling of track–vehicle and track–vehicle interactions is discussed in detail in the literature surveys by Knothe and Grassie, Popp et al., Nielsen et al., and Polach et al. [31, 41, 98, 114, 129, 130, 140, 141].

However, according to the results of this study (Section 4–8), the prediction and assessment results for track response obtained from the measured data were distributed in the wide range. Thus, the dynamic response of the in-service ballasted track was relatively random or higher than the results of FE analysis. Further, the dynamic response of the in-service ballasted track was distributed more roughly and over a wider range than its initial design value (i.e., the value considered during track design and construction). Therefore, the dynamic response of in-service ballasted tracks does not depend on a single design value of track structure. To ensure that the track performance is similar to the initial value or the stable condition was confirmed that dynamic response of ballasted track take a real field condition into consideration.

From the results of this study (Section 4–8), the principal parameter was the rail pad and ballast stiffness that was related in the track support stiffness. It was mainly affected in the track response and the entire system of the ballasted track. Therefore, these parameter could be adjust and maintain, and make an estimate of the properties or performance by the simple field test, i.e., the rail and sleeper displacement and dynamic wheel load. This study focus has allowed for the inclusion of a high number of variables and constraints to determine the parameters and response of ballasted track and has placed its principal objective on the track design and maintenance made with the elastic materials of track components focused on the rail pad and ballast.

These parameters were defined by the matrices of dynamic properties of track components and it was calculated by the complex matrices. Thus it was display the solution of track response as the range of discrete space solution. The variation in track response was performed and measured as a function of the variations in the vertical track stiffness related in rail pad and ballast stiffness and rail surface roughness, track impact factor, train velocity, etc.

In this section, the behavior of ballasted track was evaluated by the dynamic response of test track measured (i.e., dynamic wheel load, rail displacement, sleeper displacement and rail bending stress) and the empirical theory (adopted from conventional equations) was compared with both the results of qualitative analysis. Therefore dynamic behavior of ballasted track was qualitatively estimated and predicted by numerical model, i.e., the ballasted track including the spring-damper element (2DOF) which was considered the range of spring stiffness according to actual and design parameters. Further, in this study, the results of qualitative analysis for dynamic response of track matrices which was the commonness solution of over three different empirical equations according to Winkler beam theory and Zimmermann theory at different range of rail pad and ballast stiffness as a function of the discrete space area of response for tracks. Therefore, the predictive results were evaluated using the dynamic wheel load and the rail displacement measured and it provides the empirical prediction range of dynamic responses in the service ballasted tracks.

Using the qualitative analysis, dynamic track responses are suitable for predicting by a constraint parameter which was chosen by the field measurement and should be of practical use in track maintenance. If the some kinds of measured track response were presented, it was possible to predicting the other response and parameters of the

ballasted track by represented in the space solution which was defined by the range. This study presents a statistical analysis of the measured results and gives a good understanding about ballasted track response and its variations. Such information is very useful when the decision on what is acceptable track support stiffness ranges, i.e., related in the rail pad and ballast stiffness. Therefore it was possible to predicting to the field condition and suitable for maintaining the ballasted track.

9.2 Mathematical modeling of track dynamics

In this section mathematical models used to simulate the train-track dynamic interaction will be presented. This section mainly focuses on models describing the track deflection in the vertical plane [31]. The following topics will be discussed [31]:

- Beam (rail) on continuous elastic foundation (Section 9.2.1),

- Beam (rail) on discrete supports (Section 9.2.2),

- Beam (rail) on discrete supports including ballast model (Section 9.2.3), and

- Beams (rails) on sleepers embedded in continuum, including three-dimensional

FEM models (Section 9.2.4).

9.2.1 Beam on continuous elastic foundation (Winkler beam)

The railway track structure consists of the rails, sleepers, rail pads, fastenings, ballast and subgrade. Depending on what one wants to investigate, these components may be modeled in a simpler or a more sophisticated manner [31]. The rail may be modeled either as an ordinary Euler-Bernoulli beam (the conventional beam theory is used) or as a Rayleigh-Timoshenko beam [31]. The Rayleigh-Timoshenko beam theory includes the rotational inertia of the beam cross section and beam deformations due to the shear force. Also a longitudinal (axial) force in the rail may be included in this model [31].

A beam (the rail) laid on a continuous elastic foundation, i.e., modeled by distributed linear spring stiffness, and occurred to proportionally deflection by acted on the distributed force [31]. The model is need to calculatd for the track parameters; the beam bending stiffness EI (Nm^2) and the foundation stiffness (the ballast bed modulus), k (N/m^2, i.e. N/m per unit meter rail) [31]. The rail deflection w(x) (x is the length coordinate) is obtained from the differential equation (9-1) [31].

$$EI\frac{d^4w(x)}{dx^4}+kw(x)=q(x) \tag{9-1}$$

Where, q(x) is the distributed load on the rail.

This model is used for static analysis for the tracks on soft supports with not account for dynamic effects because it contains no mass [31]. On the other hand, using this model the track is uplifted between the points of wheel load as shown in Fig. 9.1 [31]. Fig. 9.1 shows the beam, i.e., have a bending stiffness and laid on elastic foundation, loaded with a point force [31]. This model assumed that there is a tensile force between the rail and the foundation [31].

The discrete rail support model, a continuous model, reproduces the pinned-pinned frequency on distributed layers and reviewed by Grassie and Cox [31, 63]. They investigated the track support behavior and it was concluded that poorly damped sleeper resonances lead to higher sleeper stress [31, 63]. The influence of the rail pads stiffness as a varied support condition was found that a softer rail pad ensures the sleeper stability more effectively and it will significantly reduce the sleeper stress [31, 63].

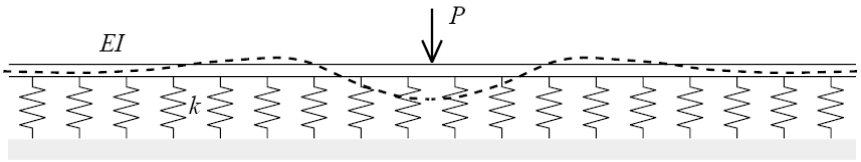

Fig. 9.1 Beam on elastic foundation [31]

9.2.2 Beam on discrete supports

The continuous discrete supported rail can be produced the pinned-pinned frequency in the track model [31]. The discrete supports, i.e., a series of a spring and a damper element, could be discrete spring-damper systems or spring-mass-spring system, and it is consisted of rail pads, sleepers and ballast bed as shown in Fig. 9.2 [31].

The rails, sleepers, and rail pads (and ballasts) are modeled by a beam (Euler-Bernoulli or Rayleigh-Timoshenko beam), a rigid mass and a spring-damper, respectively [31, 98, 130]. Therefore, the rail is linked with the sleeper by spring-damper element (rail pad)

and the between sleeper and elastic foundation also connected by spring-damper element (ballast).

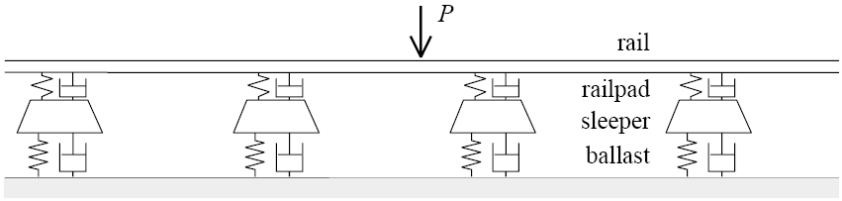

Fig. 9.2 Rail on discrete supports [31]

Using this track model, the three resonance frequencies have produced that the sleeper vibration on the ballast, the rail and sleeper vibration on the rail pad and the pinned-pinned frequency at each spring between the two masses [31]. The beam can be improved the dimension extension such as the three-dimensional track model.

9.2.3 Discretely supported track including ballast mass

Several researchers have investigated that a resonance frequency at low frequency (below 40 Hz) of the track model by considering to more masses into the simple model as shown in Fig. 9.3 [31, 98, 114, 151, 154]. A resonance at low frequency can be produced by considering the mass of ballast and subgrade is much larger than those of sleeper and rail, and by adjusting the subgrade stiffness [31, 63, 98, 114]. The ballast-subgrade masses vibrate on the subgrade stiffness [31].

As shown in Fig. 9.3, there are connections between the ballast and subgrade masses and a deflection at one point on sleeper) lead to affect the deflection at the adjacent sleepers such as an actual field track [31].

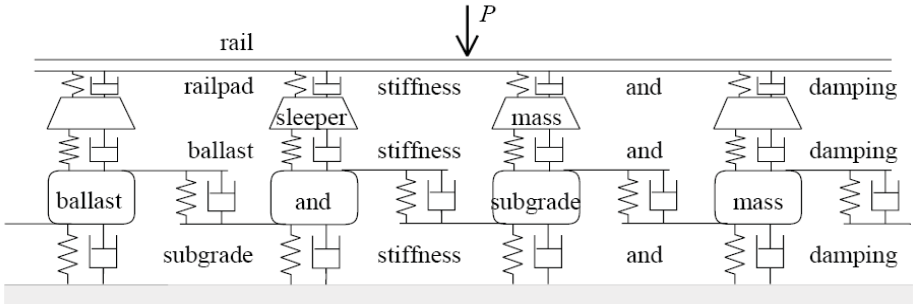

Fig. 9.3 Rail on discrete supports with rigid masses modelling the sleepers [31]

As shown in Fig. 9.3, rigid masses below the sleepers represent the mass of the ballast and the subgrade [31]. This model can be produced the four resonance vibration modes, i.e., embankment vibration, track-on-the-ballast vibration, rail-on-rail pad vibration and pinned-pinned vibration [31].

9.2.4 Three-dimensional finite element models

Recently, using the commercial computer package programs, the railway track can be modeled by more detailed (three-dimensional finite elements model, 3D FE model) and various elements (shell, solid, beam, spring-damper with linear or non-linearity) regarding to a real track properties. In 3D track model, as shown in Fig. 9.4, the sleepers are embedded in a continuous medium as a subgrade (track bed, i.e., modeled by 3D FE model) [31].

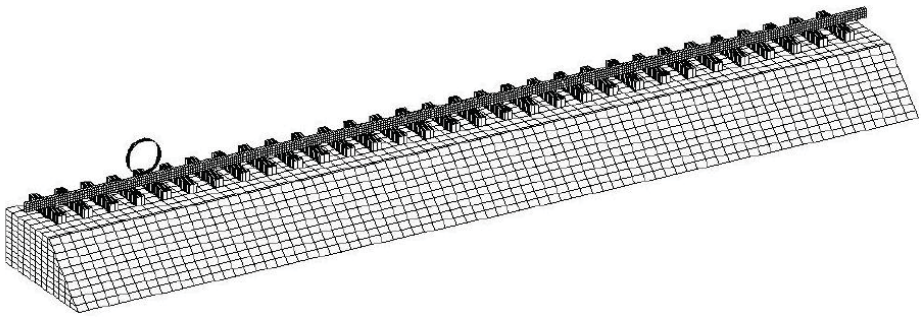

Fig. 9.4 3D track model (rail and sleepers in a continuous ballast and subgrade) [31]

Using 3D FE model, i.e., conducting a larger part of the surroundings element, the wave propagation from the track to the surroundings can be simulated, and then, wave reflections at the boundaries can be prevented by using the non-reflecting boundary conditions [31, 114, 154]. Further, the only half of the track is possible to conduct a track model by considering to symmetry condition at the track centre [31].

9.3 Qualitative analysis for ballasted track

9.3.1 Qualitative reasoning with engineering uncertainties

Any engineering design and maintenance work can usually be broken down into a set of relationships and constraints [122, 179, 196, 197]. A track design and maintenance

problem may be broken down into functional response such as the structural life at the according conditions of track components [31, 41, 114, 122, 179, 196, 197]. These static and dynamic responses can be easily represented in terms of inequalities [31, 41, 77]. Since the application of relevant geometric and engineering principles is always carried out within the scope of such functional response, most important engineering decision-making involves judgments regarding inequalities [122, 179, 196, 197]. Inequality constraints define solutions in the form of solution spaces [122, 179, 196, 197]. Single point solutions are sought in engineering due to the fact that complete solution spaces are too difficult to compute and qualitative reasoning is capable of deriving the complete solution space from a set of constraints [122, 179, 196, 197].

The principal technique of qualitative reasoning is constraint satisfaction [56, 117, 122, 196]. Engineering tasks are well suited to the formulation as Constraint Satisfaction Problems (CSP), which are defined by a set of variables subject to constraints [29, 179, 196]. The variables correspond to the relevant parameters of the design formulas [29, 179, 196]. The constraints express design criteria by equalities or inequalities [29, 179, 196]. As shown in Fig. 9.5, the CSP approach uses search methods that detect single variable assignments that satisfy all the constraints, and then provides a description of solution spaces, therefore allowing the identification of the optimum design solution range [117, 123, 196, 197].

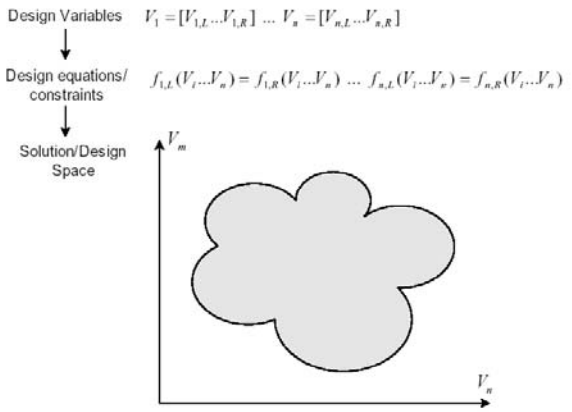

Fig. 9.5 Interval constraint and space solution of qualitative analysis [196]

Interval constraints were first introduced by J. G. Cleary [76, 179]. The initial goal was to address the error of floating-point numerical computations in the Prolog programming language, while placing formal arithmetic into a closer relation to the

formal language model [196, 197]. Interval constraint processing combines propagation and search techniques developed from artificial intelligence with methods from interval analysis, i.e., as interval propagation [196, 197]. Given a set of constraints C involving variables V_1 … V_n and a set of floating-point intervals V_1… V_n representing the domains of possible values, a reasoning procedure isolates a set of regions R_1…R_n approximating the constraint system solution [56, 134, 196, 197]. To compute such a set, a search procedure navigates through the initial intervals V_1…V_n, alternating pruning and branching steps [196, 197]. The pruning step, also called interval narrowing or interval propagation, is a numeric implementation of local arc consistency [134, 196, 197]. The typical space solution algorithm for a pruning step (the pseudo-code) is essentially making all the constraints specified satisfies to the input domain, as shown in Fig. 9.6 [29, 76, 117, 122, 123, 134, 196, 197].

```
function NC3 (S : constraint set, B : domain) : domain
% Output domain is necessarily included in the input domain
begin
    Queue all constraints from S in Q
    repeat
        Select a constraint c from Q
        B' ← narrow(B,c)   % Narrrow down B with respect to c
        if B' = Θ then return Θ   % Inconsistency of the constraint system
        Let S' = {c ∈ S | ∃v ∈ Var(c), B'_v ⊂ B_v }
          % Queue the constraints whose variables' domains have changed
        Q ← (Q ∪ S') \ {c}   % Delete c from Q
        B ← B'
    until Q is empty
    return B
end
```

Fig. 9.6 Domain narrowing algorithm enforcing consistency [196]

A system of constraint interval arithmetic consists of three distinct layers [196]. The top layer is concerned with the conversion from the external source to an internal data structure or constraint network [196]. The middle layer treats the interval iteration and relates the properties of the primitive calculations to that of the entire constraint data [196]. The bottom layer is a simple abstract theory for the implementation of primitive functions such as addition, subtraction, multiplication, etc [76, 117, 196]. The focus is placed on solving engineering design problems using numerical qualitative reasoning, i.e. numerical constraint satisfaction techniques [196]. The advantage of using CSP in this field is that consistency techniques represent an approximation of both input variables and solution spaces instead of single point values [29, 179, 196].

Track structure built in various materials and structural members that are subjected to cyclical loading and then it could not easily check and maintenance. Therefore, track engineers must use a combination of experience and analysis techniques in order to design details that achieve good and predictable performance [196]. This usually involves starting with a regulation or design code check of responses and allowable displacement and stress limits [196]. Often the code cannot cover all of the particular details under consideration because of the limits in scope, in which case the engineer may decide to extend the analysis into an investigation of local responses using finite element tools to better observe the dynamic response of track system. Even after this level of analysis, the design and maintenance can still not be considered "real field-proof" because many essential factors (such as deterioration of rail pad and ballast, rail surface roughness and the other defects) simply cannot be revealed by any analysis [196].

A low reliability of the input variables and parameters used in ballasted track analysis can have a potentially large effect on the solution due to the complex relationships between the equations [196]. If the uncertainty in the input data could be taken into account by allowing input variables to be presented as a range of values as opposed to a single value, it would enable the representation of the solution as a design space, therefore allowing engineers to realize a more reliable design and maintenance that satisfies the entire range of input values [179, 196, 197].

All variables and equations are described as objects consisting of properties and behaviors [179, 196, 197]. Also the constraints and average values are elementary to the calculation [179, 196, 197]. Recently, primary design standards suggest the use of conventional empirical theories that have their basis in the beam on continuous elastic foundation theory. However, it is difficult to calculate the dynamic response and parameter of complicated structural track components using the current calculation methods which use a single value as there is a significant difference between the input (design) variables and field measurement results. Nevertheless by using qualitative analysis, it is possible to easily portray the irregularity of input variables and also the diverse nature of the constraints range [179, 196, 197].

This study focus has allowed for the inclusion of a high number of variables and constraints to determine the parameters and response of ballasted track and has placed

its principal objective on the track design and maintenance made with the elastic materials of track components focused on the rail pad and ballast [179, 196, 197].

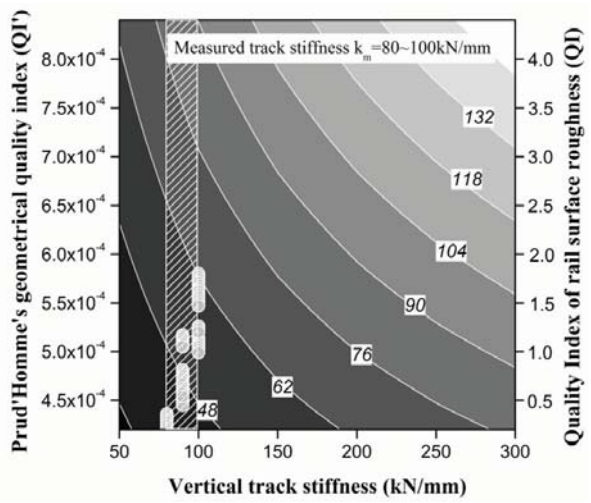

(a) Peak dynamic force P2 map; comparison of P2 with the other of measured track parameters

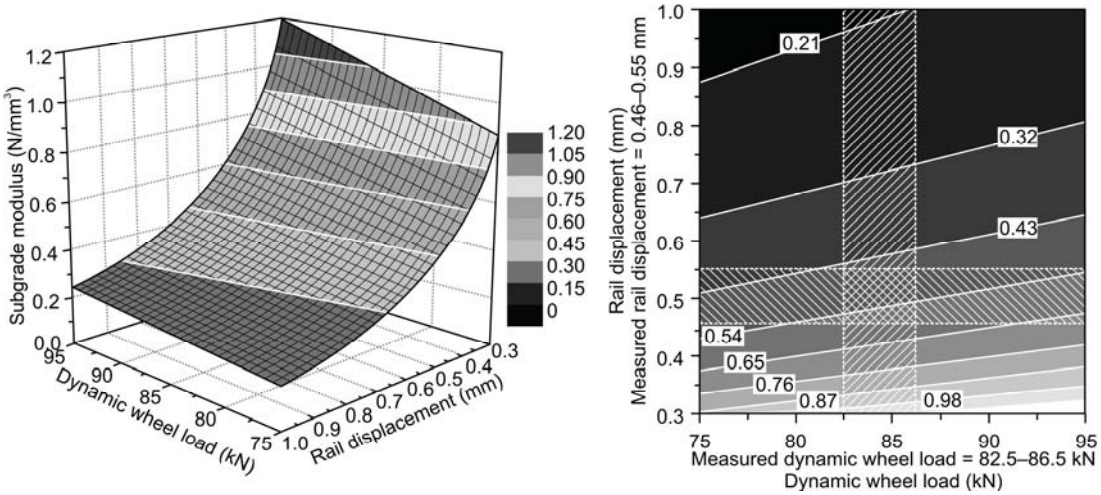

(b) Subgrade modulus map; comparison of subgrade modulus with the other of measured track parameters

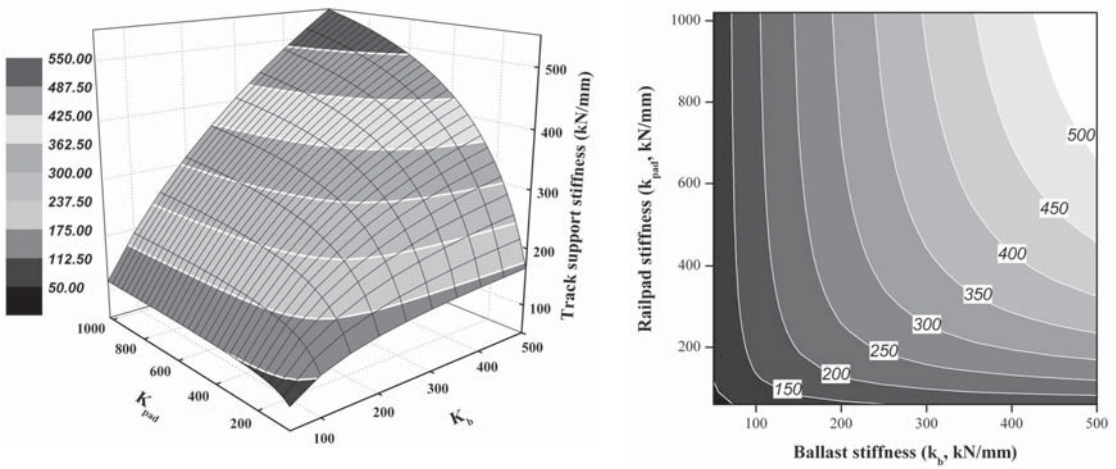

(c) Dynamic track support stiffness map; comparison of TSS as a function of track components properties (rail pad and ballast stiffness)

Fig. 9.7 Example of qualitative analysis maps for ballasted track

Fig. 9.7 shows examples of space solutions, i.e., the proposed prediction model, produced the assessment of track responses using the qualitative analysis and taking into account variation of track components properties and dynamic track response.

This proposed prediction model, i.e., a qualitative analysis–based dynamic behavior prediction model for ballasted tracks (qualitative prediction model), provides that the qualitative analysis map, and it should be portrayed as a range rather than as a single value. The result would therein be displayed as space or area, meaning that the result would be more reliable and would also greatly reduces the inaccuracies consistent with the input of single values [179, 196]. The proposed prediction model can be solves the various track response and parameters which are a part of the input variable and ranges of variable properties using data acquired from a field measurement, not only a single value.

9.3.2 Application of beam on continuous elastic foundation theory

In this section, track dynamics theory (i.e., beam on continuous elastic foundation as defined by Zimmermann) used to simulate by using qualitative analysis the track dynamics will be presented.

The qualitative analysis was defined by the method for display the analytical matrices with the results of discrete surface area (herein referred to as space solution) [25, 26, 34]. The analysis for dynamic track response of ballasted track was need to variable parameters of track components and track force related in the behaviors of ballasted track referred in Section 8.2. Therefore it was performed that the numerical model by conventional theory of track dynamics and then it was compared with the finite element analysis results and the measured results in real field. These results of track response that was investigated by the qualitative analysis has validate by the measured results.

However, the prediction results for track response obtained from the measured data were distributed in the wide range. Thus, the dynamic response of the in-service ballasted track was relatively random or higher than the results of FE analysis. Therefore the dynamic response of the in-service ballasted track was distributed more roughly and over a wider range than its initial design value (i.e., the value considered during track construction). Therefore, the dynamic response of in-service ballasted tracks does not depend on a single design value of track structure. To ensure that the

track performance is similar to the initial value or the stable condition was confirmed that dynamic response of ballasted track take a real field condition into consideration.

These parameters were defined by the matrices of dynamic properties of track components and it was calculated by the complex matrice [25, 30, 32]. Thus it was display the solution of track response as the range of discereteley space solution [25, 30, 32]. The variation in track response was performed and measured as a function of the variations in the vertical track stiffness related in rail pad and ballast stiffness and rail surface roughness, track impact factor, train velocity, etc.

Using the qualitative analysis, dynamic track responses are suitable for predicting by a constraint parameter which was chosen by the field measurement and should be of practical use in track maintenance. If the some kinds of measured track response were presented, it was possible to predicting the other response and parameters of the ballasted track by represented in the space solution which was defined by the range. Therefore we could be predicting to the field condition and suitable for mainteining the ballasted track.

In this study, the qualitative analysis mainly focuses on track dynamics theory describing the track stiffness, i.e., related on the rail pads, ballast stiffness and subgrade stiffness, track impact factor and that of depends on the response for track stress, displacement and resonance performance in the vertical plane.

Track support stiffness k (precisely global vertical track stiffness) can be defined as the ratio between the vertical force Q on rail and the vertical track displacement w as [110]:

$$k(t) = \frac{Q(t)}{w(t)} \quad or \quad k(f) = \frac{Q(f)}{w(f)} \tag{9-2}$$

Therefore, the dynamic track stiffness is dependent on the applied load or a function of excitation frequency f and time t domain [110]. Conventional track calculations are based on a static approach developed by Zimmermann [110]. For the static approach, it was considered an infinite long beam (rail) with a bending stiffness EI, which is loaded by a vertical force Q at x=0 and is supported by a continuous elastic foundation with distributed stiffness k_c ($k_c = k_s/a$) [31, 41, 110, 114]. Where, a is the sleeper spacing and k_s is the total of support stiffness in series of rail pad, ballast, and subgrade as shown in

Fig. 9.8 [31, 41, 110, 114]. Fig. 9.8 show the modern track model, were represented by Sato, Ripke and Oscarson, using the spring damper element for track component [114].

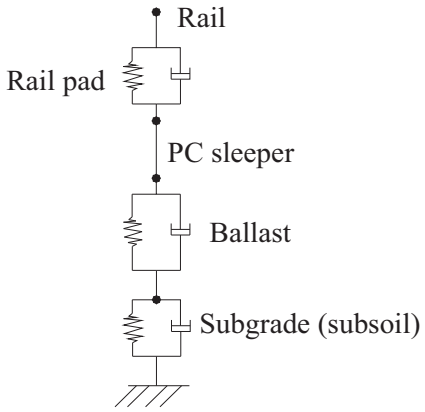

Modern track model [Sato, Ripke, Oscarson]

- Rail pad : spring & damper
- Ballast : spring & damper, mass
- Subgrade (subsoil) : spring & damper

Fig. 9.8 Modern track model using the spring damper element for track component

Governing differential equation for the problem combining with boundary conditions derives the solutions for rail displacement w, sectional moment of the rail M, and pressure load on sleeper F as follows [110]:

$$w(x) = \frac{QL^3}{8EI} e^{-(x/L)} \left(\cos\frac{x}{L} + \sin\frac{x}{L} \right) \tag{9-3}$$

$$M(x) = \frac{QL}{4} e^{-(x/L)} \left(\cos\frac{x}{L} - \sin\frac{x}{L} \right) \tag{9-4}$$

$$F(x) = \frac{Qa}{2L} e^{-(x/L)} \left(\cos\frac{x}{L} + \sin\frac{x}{L} \right) \tag{9-5}$$

Where, L is the characteristic length of the track and is determined by [41, 110]:

$$L = \sqrt[4]{\frac{4EI}{k_c}} = \sqrt[4]{\frac{4EIa}{k_s}} \tag{9-6}$$

And, k_s is determined as the series stiffness of pad stiffness k_{pad} and ballast/subgrade stiffness k_{bs} by [41, 110]:

$$\frac{1}{k_s} = \frac{1}{k_{pad}} + \frac{1}{k_{bs}} \tag{9-7}$$

Therefore, from the definition of equation (9-2), the global static track stiffness according to Zimmermann's theory can be obtained as [41, 110]:

$$k = \frac{8EI}{L^3} = 2\sqrt{2}\sqrt[4]{EIk_c^3} \tag{9-8}$$

The global track support stiffness is a function of the structural properties of the rail, rail pad, sleeper, and ballast/subgrade [41, 110].

9.3.3 Application of track dynamics with qualitative analysis

Recently, most of the track models presented for dynamic vehicle–track interaction have demonstrated and used for investigating the global vertical dynamic track stiffness [110, 111]. In the previous study, the finite element (FE) model for tracks consists of one rail of finite length and discretely supported rail pads by sleepers on ballast were conducted by using the commercial program DIFF [110, 111].

The FE model is conducted by the half of track model, and the rail is modelled by Rayleigh–Timoshenko beam element and the sleepers are considered as rigid masses [110, 111]. In this study, the computer program LUSAS [116] and MIDAS [119] were used to validate the qualitative analysis results with the measured and theoretical dynamic response of the ballasted tracks. The FE model for ballasted tracks used in this study consists of one rail of finite length, discretely supported via rail pads by sleepers on ballast/subgrade [31, 154]. The rail pad and ballast/subgrade is also modelled as an in series of elastic spring and viscous damper [110, 111]. The structural dynamic equations can be derived as:

$$\boldsymbol{M}\ddot{u} + \boldsymbol{C}\dot{u} + \boldsymbol{K}u = F \tag{9-9}$$

Where, *M*, *C*, and *K* are the mass, damping, and stiffness matrices of the track, respectively, and *F* is the applied load vector [110]. In the frequency domain, the equation (9-10) can be derived as [110]:

$$(-\omega^2 \boldsymbol{M} + i\omega \boldsymbol{C} + \boldsymbol{K}) \cdot U(\omega) = F(\omega) \tag{9-10}$$

By assuming *F* be a unit load vector acting at an excitation position on the rail, the track receptance is the solution of *U* at the loading position [110]. And, the global dynamic track stiffness is calculated by inverse of the track receptance [110]. Further details about numerical models and solutions of DIFF can be found in reference [110].

The dynamic interaction problem is solved by using an extended state-space vector approach and a complex modal superposition. The rail is consisted with the Young's modulus *E*, shear modulus *G*, density ρ, cross-sectional area *A*, second moment of area of section *I*, and shear coefficient κ [111]. The bending stiffness is represented by $B=EI$ and the shear stiffness by $K=GA\kappa$ [111]. The sleeper is conducted by mass m_s, whereas the rail pad and the ballast are modelled by stiffness and loss factor k_{pad} and η_{pad}, k_{bal} and η_{bal}, respectively [111]:

$$\tilde{k}_{pad} = k_{pad} + i\eta_{pad}, \qquad \tilde{k}_{bal} = k_{bal} + i\eta_{bal} \tag{9-11}$$

Both of the wheel force and point force exerted on each support of the rail [111]. The dynamic stiffness (impedance) $S(\omega)$ is introduced to the relationship between the force $\hat{F}_n$ at each support point and corresponding displacement $\hat{u}_n$ [111]:

$$\hat{F}_n = -S(\omega) \cdot \hat{u}_n \tag{9-12}$$

$$S(\omega) = \frac{\tilde{k}_{pad} \cdot (\tilde{k}_{bal} - \omega^2 m_s)}{\tilde{k}_{pad} + \tilde{k}_{bal} - \omega^2 m_s} \tag{9-13}$$

The global system of equations is completely defined after the assembly of the individual matrices of each element and the definition of the boundary conditions. The results obtained after solving the system of equations are in the transformed domain,

requiring a double inverse Fourier transform, in order to define a solution in the space/time domain [111]. The advantage of the method in relation to the fully three-dimensional finite element method is evident: instead of solving a system of equations with a high number of degrees of freedom. The adopted formulation is the most usual for this type of problems; nevertheless, the comparison between computed and experimental results proved to be satisfactory [98, 191].

On the 2DOF system, a system identification of the ballasted track is important on account of the actual global track vibration of the ballasted track may not be identical to the model assumed [89, 95, 98, 99]. According to previous studies, the 2DOF model of ballasted tracks has been proved by the field tests [88–92, 95]. Therefore, the ballasted track was simplified as a model of 2DOF discretely supported rail. According to Kaewunruen S and Remennikov A, the 2DOF model has been developed based on the FFT and Mode Superposition (MS) methods which are given in equations (9-14) and (9-15), respectively [89, 95, 132].

$$H_{11}(f)=\frac{\sqrt{[k_1+k_2-4\pi^2 f^2]^2+[2\pi f(c_1+c_2)]^2}}{\sqrt{\begin{matrix}[(k_1-4m_1\pi^2 f^2)(k_2-4m_2\pi^2 f^2)-4\pi^2 f^2(k_1m_1+c_1c_2)]^2\\ +4\pi^2 f^2[k_1c_2+k_2c_1-(m_1(c_1+c_2)+c_1m_2)4\pi^2 f^2]^2\end{matrix}}} \tag{9-14}$$

$$H_{11}(f)=\left|\begin{matrix}\dfrac{1}{m_1}\dfrac{4\pi^2\left(\dfrac{m_1}{k_1}\right)f^2}{\sqrt{\left[1-4\pi^2\left(\dfrac{m_1}{k_1}\right)f^2\right]^2+\left[4\pi^2\left(\dfrac{m_1}{k_1}\right)\left(\dfrac{c_1^2}{k_1m_1}\right)f^2\right]}}+\\ \dfrac{1}{m_2}\dfrac{4\pi^2\left(\dfrac{m_2}{k_2}\right)f^2}{\sqrt{\left[1-4\pi^2\left(\dfrac{m_2}{k_2}\right)f^2\right]^2+\left[4\pi^2\left(\dfrac{m_2}{k_2}\right)\left(\dfrac{c_2^2}{k_2m_2}\right)f^2\right]}}\end{matrix}\right| \tag{9-15}$$

where, m_1 and m_2 are masses of rail and sleeper, k_1 and c_1 represent stiffness and damping coefficients of the rail pad and k_2 and c_2 represent stiffness and damping coefficients of ballast [89, 95, 132]. The parameters in equation (9-14) represent the actual stiffness, actual damping and actual mass value [89, 95, 132]. On the contrary, those of equation (9-15) were represented the modal stiffness, modal damping and

modal mass based on the MS method [89, 95, 132]. These equations are to be used in least square method for the evaluation of the dynamic parameters of track components [89, 95, 132].

Previous study were reviewed the dynamic properties by field impact test and performed the analysis for frequency response function using equations (9-14) and (9-15) [89, 95, 132]. Dynamic properties of ballasted track were so rough and distributed widely [31, 41, 89, 95, 132]. Therefore to ensure the accuracy of dynamic property, it should be decided that the suitable parameter for the target track section, however it is difficult. Therefore, in present study, equations (9-14) and (9-15) (i.e., introduced in Section 4.2) were conducted in the qualitative analysis as a formulated in terms of modal and actual stiffness, damping and mass which was represented in the matrix formation. Further the results of these equations were represented in some range of parameters and response of track dynamics. The constitutive track model is applied to define the continuous equivalent stiffness properties on the longitudinal direction based on an anisotropic formulation, since the sleepers are usually contacted with the ballast by a link element. The selected Euler–Bernoulli beams provide the results for frequencies up to 500 Hz [31], and the Euler–Bernoulli beam model is easier to implement in a numerical code [6, 31, 89, 90]. Some simplifications are assumed that the connection between the rail and the sleepers is a single vector response on the rail, and only corresponding to the vertical displacement as explained in equation (9-16) [6, 31, 110]. The motion of the rail in the transformed domain is expressed by [6, 31]:

$$\left(\underbrace{\begin{bmatrix} EIk_1^4 & -k_p^* \\ -k_p^* & k_p^* \end{bmatrix}}_{[K]_{rail}} - \omega^2 \underbrace{\begin{bmatrix} m_r & 0 \\ 0 & 0 \end{bmatrix}}_{[M]_{rail}} \right) \underbrace{\begin{Bmatrix} u_{rail} \\ u_{sleeper} \end{Bmatrix}}_{u} = \underbrace{\{P\}}_{f} \tag{9-16}$$

Where, EIk_1 is the bending stiffness of the rail, k_p is the complex stiffness of the rail pad, m_r is the mass per unit length of the rail, and the vectors u and f are the vectors of displacements and loads on the rail, respectively [6]. The superscript symbol * in k_p represents complex stiffness ($\mathrm{k}_\mathrm{p}^* = \mathrm{k}_\mathrm{p} + \mathrm{i}\omega\mathrm{c}_\mathrm{p}$) due to taking the damping properties of rail pad into account [6, 31, 98, 99]. Where, c_p is the viscous damping factor and k_p is

the stiffness of the rail pad [6, 31, 98]. The stiffness and mass matrices of the rail are then assembled to the global dynamic system functions [6, 31, 98, 99]. The properties of the rails and sleepers and parameters of target track in the qualitative analysis are listed in Table 9.1 and Table 9.2, respectively.

Table 9.1 Properties of track components for qualitative analysis

	Properties	Rail (60 kg N)	Prestressed concrete sleeper
Section Properties	Cross-sectional area (cm^2)	77.5	516.75
	Moment of inertia (cm^4)	3,090	16,375
	Section modulus (cm^3)	396	–
	Supported area of half-sleeper (cm^2)	–	3,021
Material Properties	Elastic modulus (kN/cm^2)	21,000	4,000
	Weight density (kN/cm^3)	7.85×10^{-5}	2.5×10^{-5}
	Poisson's ratio (υ)	0.30	0.18

Table 9.2 Parameters of ballasted track for qualitative analysis

	Properties
Track curvature (R)	∞ (Straight)
Cant	0 mm
Substructure	Earthwork
Subgrade modulus [a]	0.15 N/mm³
Rail	60 kg N, Continuous welded rail
Sleeper	Prestressed concrete sleeper
Sleeper spacing	600 mm
Sleeper mass [a]	80 kg
Fastening type	Pandrol e-clip
Rail pad [a]	TPU pad
Rail pad stiffness [a]	400 kN/mm
Rail pad damping coefficient [b]	12.934 kNs/m
Ballast stiffness [a]	200 kN/mm
Ballast damping coefficient [b]	223.130 kNs/m
Ballast thickness (depth)	300 mm
Ballast mat	–
Train type	EMU (Electric Multiple Unit)
Wheelset mass (M_w)	1,025 kg
Static wheel load Q	80 kN
Operational speed	Average 130 km/h

[a] Value obtained from the design data book (Korean standard) [introduced in Section 8]
[b] Value obtained from the field measurement (impact hammer test) in Section 4

9.4 Result and discussion

9.4.1 Assessment of the track parameters using qualitative analysis

In the present analysis, a tangent track was considered. The effect of (vertical) track support stiffness, the influence of the rail pad and ballast stiffness variation on the track support stiffness and associated with the track responses were investigated. Some of the other values for the numerical simulations were obtained from previous numerical and experimental studies [31, 88–92, 95, 98, 99, 110, 152, 191]. The track response would be affected by several parameters such as rail pad and ballast stiffness, rail surface roughness, track components condition and the other things. Among of these parameters, the principal parameter was the rail pad and ballast stiffness that was related in the track support stiffness. It was mainly affected in the track response and the entire system of the ballasted track. Therefore, these parameter could be adjust and maintain, and make an estimate of the properties or performance by the simple field test, i.e., the rail and sleeper displacement and dynamic wheel load. As the result of previously on this section, the principal parameter was chosen by the rail pad and ballast stiffness for the qualitative analysis as shown in Fig. 9.9. The correlation between the variation of rail pad and ballast stiffness and the corresponding track response was evaluated from the qualitative analysis.

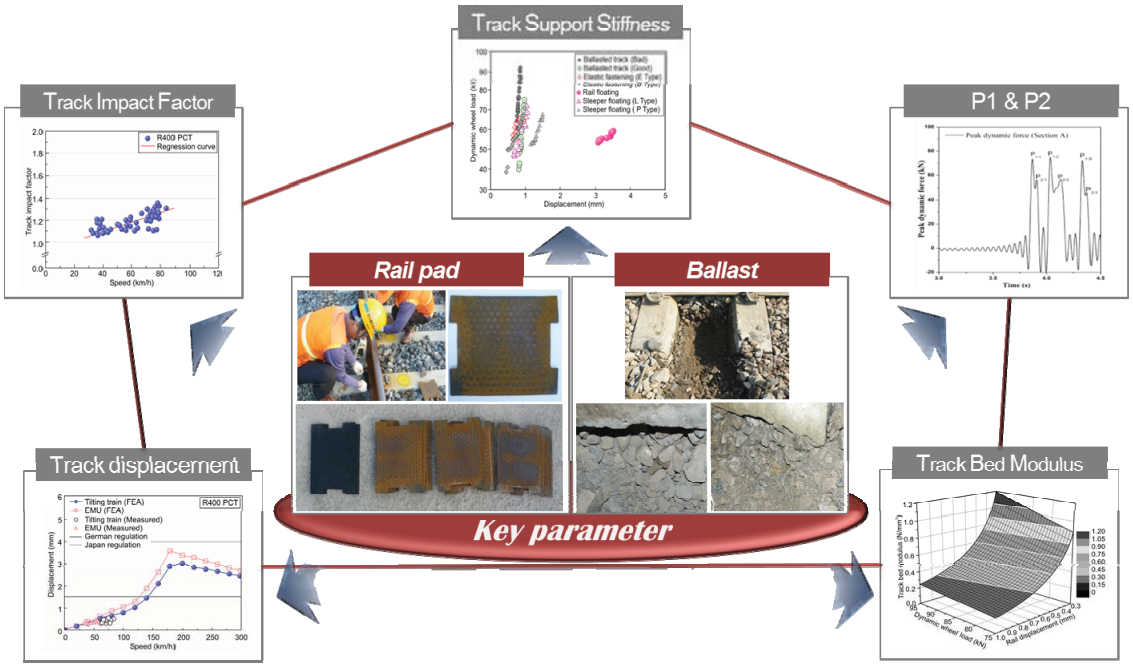

Fig. 9.9 Key parameters of qualitative analysis for in-service ballasted track

The rail support stiffness could be directly affects the track displacement, rail support pressure and track support stiffness. Therefore, it is considered that the rail support stiffness directly depends on the rail pad and ballast stiffness.

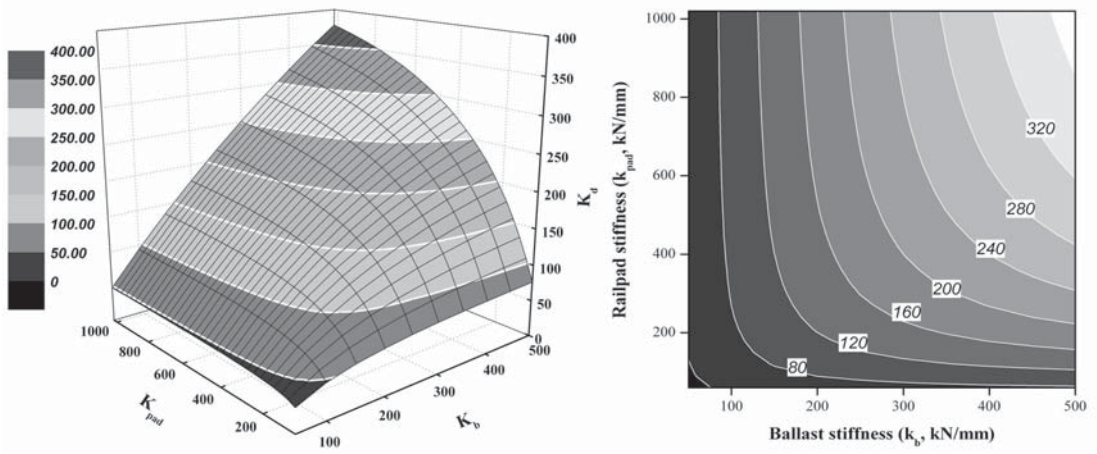

Fig. 9.10 Example of dynamic rail support stiffness map for ballasted track; rail support stiffness as a function of rail pad and ballast stiffness

Fig. 9.10 shows that rail support stiffness increased with an increase in the rail pad and ballast stiffness. The discrete space area of rail support stiffness increased with an increase in the rail pad stiffness and ballast stiffness (Fig. 9.10 (b)). For a constant rail pad stiffness of 400 kN/mm, i.e., normal TPU pad used in the Korean conventional ballasted railway line, the high ballast stiffness caused the rail support stiffness to increase.

Therefore, it was investigated that the rail support stiffness was more affected by the rail pad stiffness than the ballast stiffness at the ballast stiffness of over 200 kN/mm. For instance, at the ballast stiffness of 300 kN/mm, the rail support stiffness at a rail pad stiffness of 600 kN/mm was much larger than that at a rail pad stiffness of 400 kN/mm, i.e., larger by a factor of approximately 1.2.

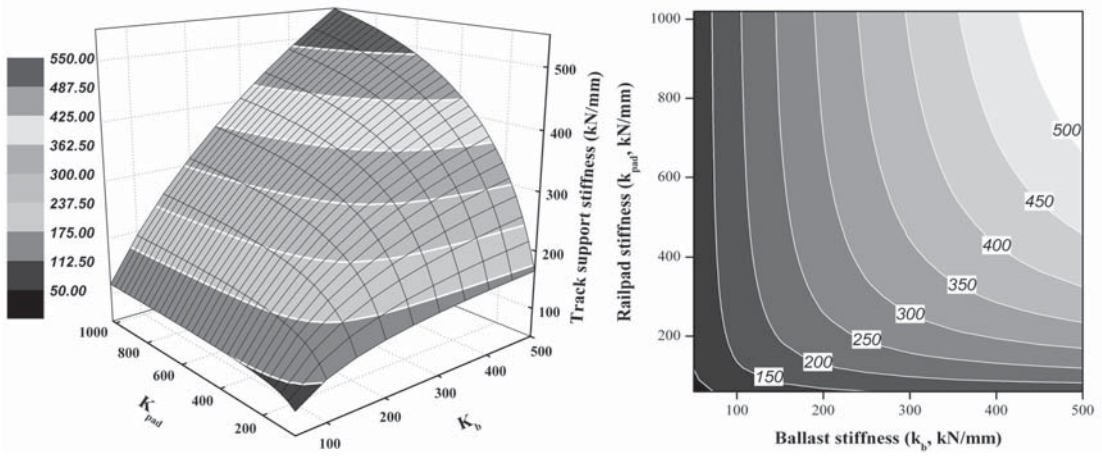

Fig. 9.11 Example of dynamic track support stiffness map for ballasted track; track support stiffness as a function of rail pad and ballast stiffness

Fig. 9.11 shows that track support stiffness increased with an increase in the rail pad and ballast stiffness. For a constant rail pad stiffness of 400 kN/mm, the high ballast stiffness also caused the track support stiffness to increase. Therefore, it was investigated that the track support stiffness was more affected by the rail pad stiffness than the ballast stiffness at the ballast stiffness of 300 kN/mm.

For instance, at the ballast stiffness of 300 kN/mm, the track support stiffness at a rail pad stiffness of 600 kN/mm was much larger than that at a rail pad stiffness of 400 kN/mm, i.e., larger by a factor of approximately 1.4. For instance, at the ballast stiffness of 200 kN/mm, the track support stiffness at the rail pad stiffness of both 400 and 600 kN/mm was the same discrete area of the track support stiffness, i.e., the deviation between rail pad stiffness was less than that for a case of the ballast stiffness of 300 kN/mm.

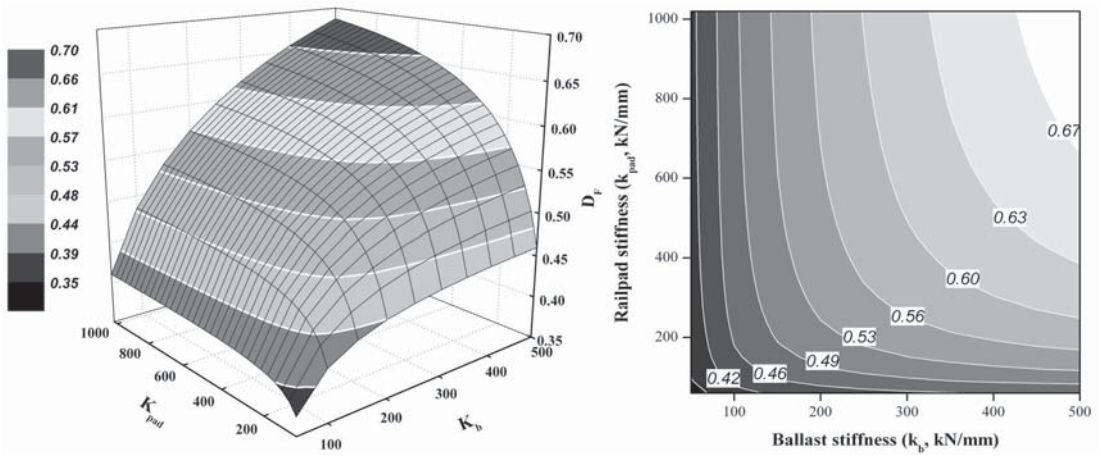

Fig. 9.12 Example of dynamic force distribution factor map for ballasted track; force distribution factor as a function of rail pad and ballast stiffness

Fig. 9.12 shows that force distribution factor increased with an increase in the rail pad and ballast stiffness. In the Korean track design standard, it was recommended by 0.52–0.58 for the conventional ballasted track. The force distribution factor could be directly affects the track displacement, rail support pressure and sleeper reaction force. Therefore, it is considered that the force distribution factor directly depends on the bending stiffness of rail, sleeper spacing and rail support stiffness.

For a constant rail pad stiffness of 400 kN/mm, the high ballast stiffness also caused the force distribution factor to increase. However, in that case, most force distribution factor could be ensuring that of the Korean standard regardless of increasing the ballast stiffness. Therefore, allowing for an increasing stiffness of rail pad, to ensure that the force distribution factor is satisfied with the Korean standard, the ballast stiffness was held constant at 200–300 kN/mm while varying the rail pad stiffness.

The characteristic length of the track could be directly affects the track displacement and rail bending stress. Therefore, it is considered that the characteristic length of track directly depends on the bending stiffness of rail and rail support stiffness. The characteristic length of the track also could be directly affects the secondary track settlement and rail corrugation. However, it was difficult to measure and investigate experimentally.

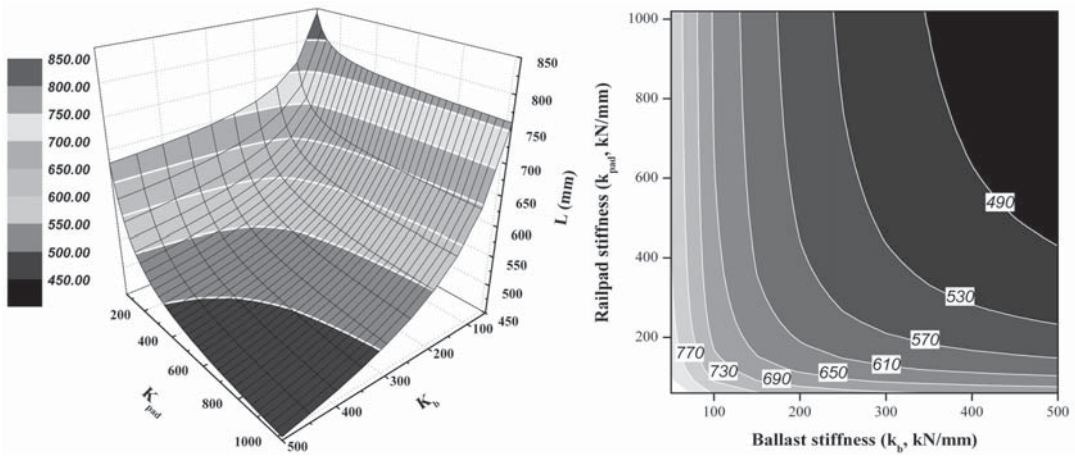

Fig. 9.13 Example of characteristic length of the track map for ballasted track; characteristic length of track as a function of rail pad and ballast stiffness

Fig. 9.13 shows that characteristic length of the track decreased with an increase in the rail pad and ballast stiffness. For a constant rail pad stiffness of 400 kN/mm, the high ballast stiffness also caused the characteristic length of the track to decrease. Therefore, allowing for an increasing stiffness of rail pad, to ensure that the characteristic length of track is similar to the sleeper spacing, i.e., the Korean conventional ballasted track of 588–625 mm, the ballast stiffness was held constant at 200~300 kN/mm while varying the rail pad stiffness.

The subgrade modulus is an important parameter in the investigation of track deterioration, track maintenance, track settlement, and critical speed of ballasted tracks [33, 39, 77, 114, 142, 155, 159]. Subgrade modulus, as reviewed in Section 8, which is similar to the coefficient of ballast, the ballast modulus and the coefficient of subgrade reaction calculated from the measured modulus of deformation, is estimated by performing a plate load test during the construction of railway tracks; the same method has been used for roads and railways [33, 39, 77, 114, 142, 155, 159, 173]. Subgrade modulus is very high, such as in the vicinity of bridges and slab tracks, the dynamic forces exerted on tracks increase [33, 77, 114]. This leads to a reduction in the lifetime of track components, thus reducing the maintenance period [77, 114]. It has been shown that reduction in subgrade modulus variations at a railway level crossing results in improved railway performance and reduced maintenance [33, 77, 114].

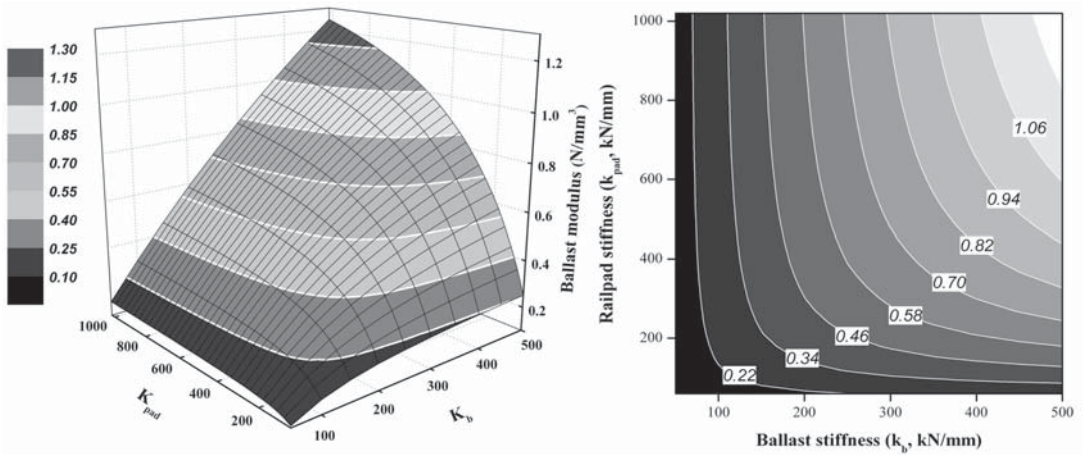

Fig. 9.14 Example of dynamic subgrade modulus map for ballasted track; subgrade modulus (ballast modulus) as a function of rail pad and ballast stiffness

Fig. 9.14 shows that subgrade modulus (ballast modulus) increased with an increase in the rail pad and ballast stiffness. As seen in Fig. 9.14, the ballast stiffness affects subgrade modulus more strongly than the rail pad stiffness. In case of the Korean track design standard, the proposed optimum subgrade modulus is within a very narrow and single value of 0.15 N/mm³ (k_{30} > 0.11 N/mm³, KS F2310) for the conventional ballasted track.

However, according to section 8 in this study, the subgrade modulus of in-service ballasted tracks does not depend on a single design value of subgrade modulus. To ensure that the subgrade modulus is similar to the initial value, the ballast stiffness was held constant at 200–300 kN/mm while varying the rail pad stiffness.

For a constant rail pad stiffness of 400 kN/mm, the high ballast stiffness also caused the subgrade modulus to increase. However, in that case, most subgrade modulus could be exceeding that of the Korean standard regard of increasing the ballast stiffness. Therefore, the numerical model (which was referred in the conventional empirical track theory) with the subgrade modulus estimated from the design value of subgrade modulus underestimated the behavior of the in-service track.

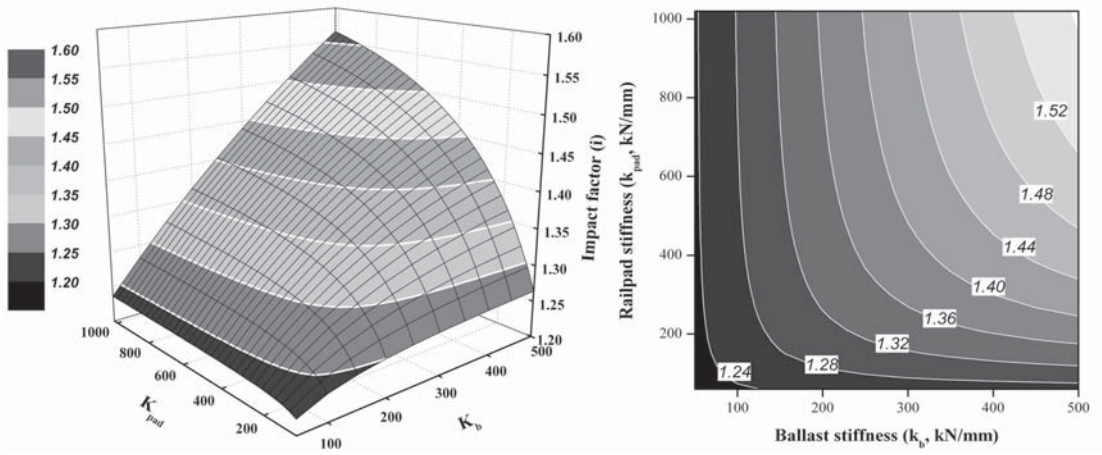

Fig. 9.15 Example of track impact factor map for ballasted track; impact factor as a function of rail pad and ballast stiffness

Fig. 9.15 shows that track impact factor increased with an increase in the rail pad and ballast stiffness. As seen in Fig. 9.15, the ballast stiffness affects track impact factor more strongly than the rail pad stiffness. In case of the Korean track design standard, the proposed track impact factor is within a very narrow range of 1.410–1.513 (train speed of 80–100 km/h) for the conventional railway track. However, according to section 5 and 6 in this study, the track impact factor of in-service ballasted tracks does not depend on a single design value of track impact factor. To ensure that the track impact factor does not exceed to the initial design level, the ballast stiffness was held constant at 200–300 kN/mm while varying the rail pad stiffness, track condition and rail surface roughness. For a constant rail pad stiffness of 400 kN/mm, the high ballast stiffness also caused the track impact factor to increase.

For instance, the ballast track in good condition was affected by the wheel-rail contact surface roughness more strongly than the rail pad and ballast stiffness. The ballast is the only elastic spring material in a ballasted track, and its elasticity reduces with time. Therefore, the deterioration of the ballast affected the performance of the ballasted track, and therefore, the dynamic wheel load was not distributed effectively over the ballasted track in bad condition. Therefore, it was concluded that the appropriate track support stiffness (which is affected by the rail pad and ballast stiffness) was important to prevent exceeding the track impact factor over the design specifications.

9.4.2 Assessment of the dynamic track responses using qualitative analysis

Fig. 9.16–Fig. 9.21 shows the variation in dynamic track response plotted against the variation in the rail and ballast stiffness at a vehicle speed of 120 km/h (i.e., the general train speed in test site).

The sleeper reaction force could be directly affects the track displacement, rail support pressure and track deterioration. Therefore, it is considered that the sleeper reaction force directly depends on the track support stiffness, rail displacement and rail bending stiffness.

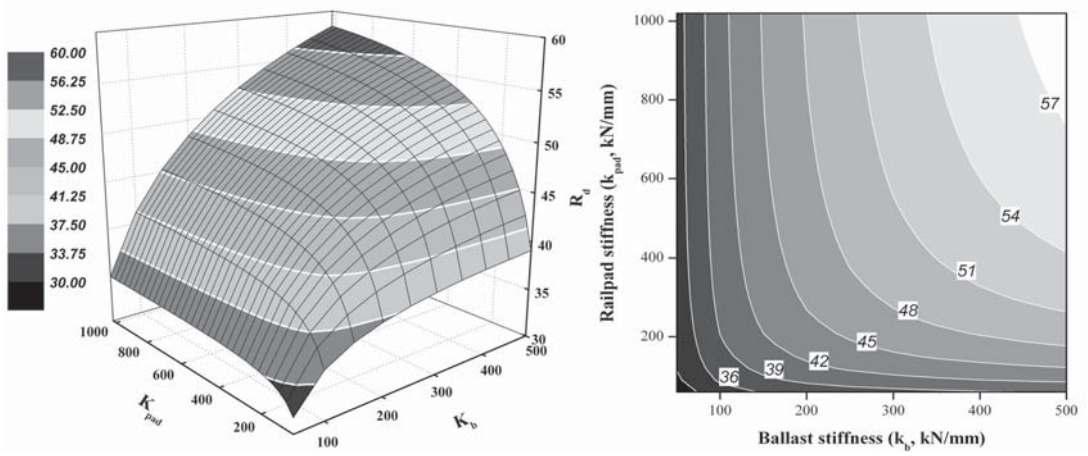

Fig. 9.16 Example of dynamic sleeper reaction force map for ballasted track; sleeper reaction force as a function of rail pad and ballast stiffness

Fig. 9.16 shows that sleeper reaction force increased with an increase in the rail pad and ballast stiffness. The discrete space area of sleeper reaction force increased with an increase in the rail pad stiffness and ballast stiffness.

For a constant rail pad stiffness of 400 kN/mm, the high ballast stiffness caused the sleeper reaction force to increase. Therefore, it was investigated that the sleeper reaction force was more affected by the ballast stiffness than the rail pad stiffness. For instance, at the rail pad stiffness of 400 kN/mm, the sleeper reaction force at a ballast stiffness of 300 kN/mm was much larger than that at a ballast stiffness of 200 kN/mm, i.e., larger by a factor of approximately 1.1.

In a general concept, the sleeper reaction forces were 60% of the dynamic wheel load [31, 55, 114]. However, in that case, most sleeper reaction force could be ensuring that 60% of the dynamic wheel load at the ballast stiffness of 400 kN/mm.

The rail displacement could be directly affects the track displacement, passenger comfort and track deterioration. Therefore, it is considered that the rail displacement directly depends on the track support stiffness, characteristic length of the track, dynamic wheel load and rail bending stiffness.

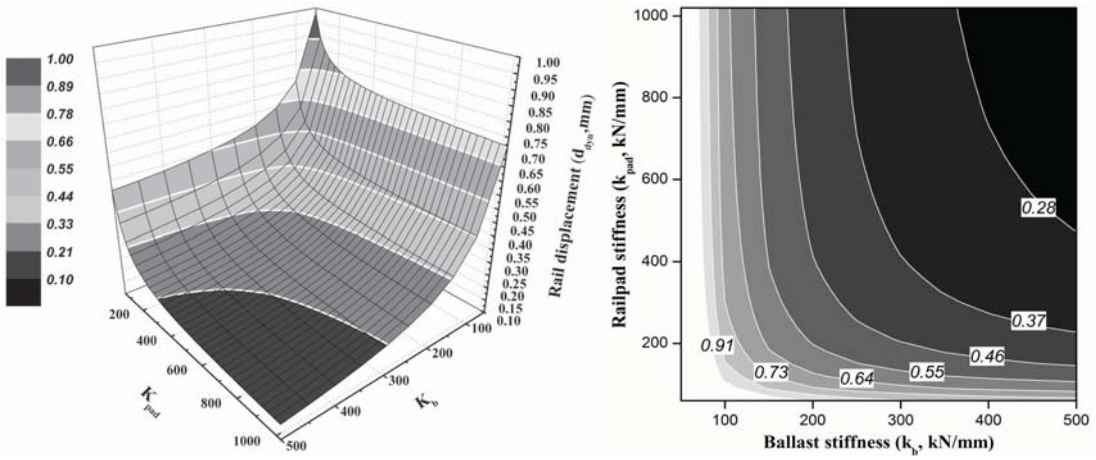

Fig. 9.17 Example of dynamic rail displacement map for ballasted track; rail displacement as a function of rail pad and ballast stiffness

Fig. 9.17 shows that rail displacement decreased with an increase in the rail pad and ballast stiffness. As seen in Fig. 9.17, the ballast stiffness affects rail displacement more strongly than the rail pad stiffness. In case of the classic ballasted track, the general rail displacement was the low average displacement of only 0.3–0.4 mm under a wheel load of 100 kN, i.e., corresponds to a subgrade modulus of 0.3–0.5 N/mm³ [114]. In case of Korean and German regulation, the proposed rail displacement is within a very narrow range of 1.2–1.5 mm for the high speed railway (HSR) line.

However, according to section 6 in this study, the rail displacement of in-service ballasted tracks does depend on the track components and ballast condition. To ensure that the rail displacement does not exceed to the limit level of Korean regulation for maintenance that of the normal level (0.4–0.5 mm), the ballast stiffness was held constant at 200–220 kN/mm while varying the rail pad stiffness from 400 kN/mm to

600 kN/mm. For a constant rail pad stiffness of 400 kN/mm, the high ballast stiffness also caused the rail displacement to increase.

The rail bending stress could be directly affects the track displacement and track safety. Therefore, it is considered that the rail bending stress also directly depends on the track support stiffness, characteristic length of the track, dynamic wheel load and rail bending stiffness, i.e., similar to the rail displacement.

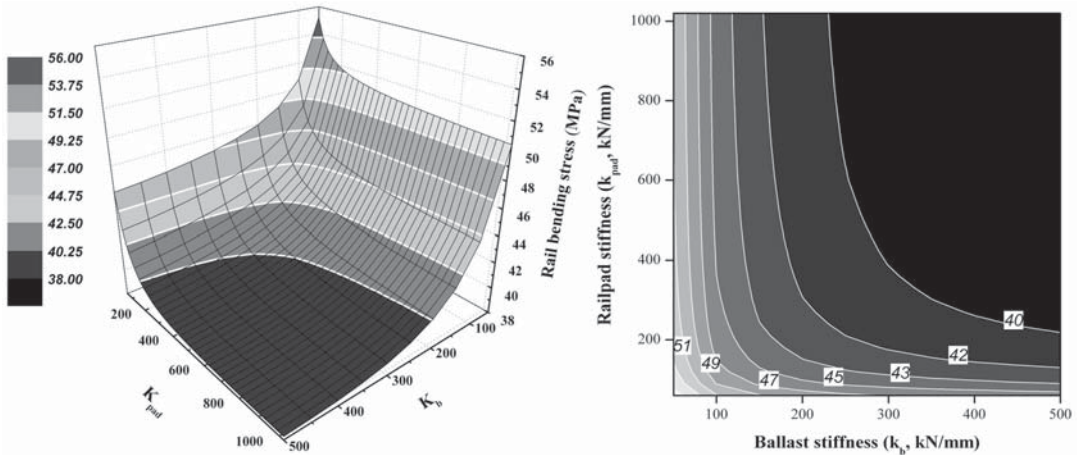

Fig. 9.18 Example of dynamic rail bending stress map for ballasted track; rail bending stress as a function of rail pad and ballast stiffness

Fig. 9.18 shows that rail bending stress decreased with an increase in the rail pad and ballast stiffness. As seen in Fig. 9.18, the ballast stiffness affects rail bending stress more strongly than the rail pad stiffness. In case of Korean and German regulation, the proposed rail bending stress of the continous welded rail (CWR) for the high speed railway (HSR) line was less than 92 MPa and 70 MPa, respectively. Therefore, according to Eisenmann [114], the rail bending stress of the required properties for a ballasted track on high speed lines was less than 60 MPa.

However, in that case, most rail bending stress could be ensuring that of the Korean and German regulation regardless of increasing the ballast and rail pad stiffness. Therefore, allowing for an increasing stiffness of rail pad and ballast, to ensure that the rail bending stress is satisfied with the Korean and German regulation, the rail displacement should be in controlled that of the regulation.

The rail support pressure could be directly affects the rail pad and track deterioration. Therefore, it is considered that the rail support pressure directly depends on the track support stiffness, rail displacement and effective surface area of the rail pad. In the present analysis, the following parameter values of rail pad, i.e., normal TPU pad used in the Korean conventional ballasted railway line, were adopted: the effective surface area of rail pad of 36,800 mm^2, rail pad length and width of 160 mm and 230 mm, respectively.

Fig. 9.19 shows the variation in rail support pressure plotted against the variation in the rail pad and ballast stiffness.

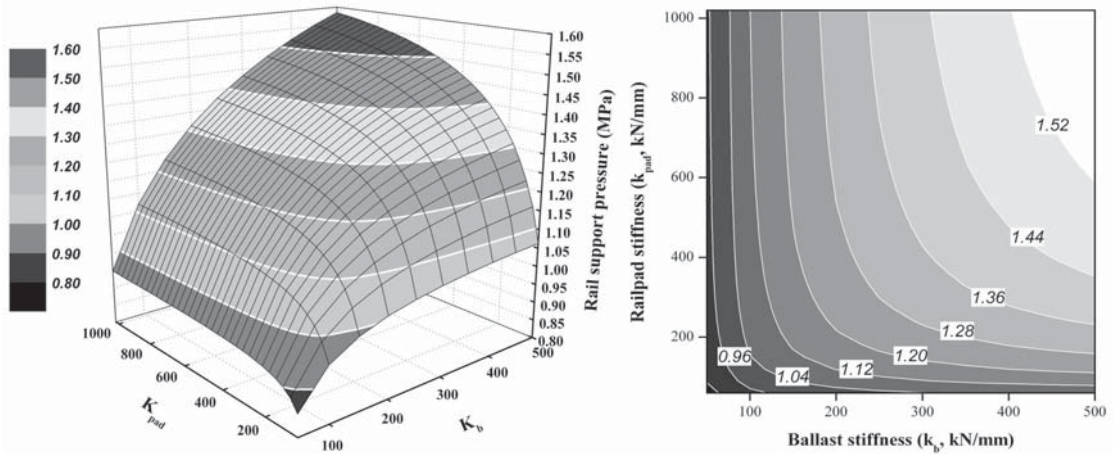

Fig. 9.19 Example of dynamic rail support pressure map for ballasted track; rail support pressure as a function of rail pad and ballast stiffness

Fig. 9.19 shows that rail support pressure increased with an increase in the rail pad and ballast stiffness. As seen in Fig. 9.19, the ballast stiffness affects rail support pressure more strongly than the rail pad stiffness. The rail support force does depend on the track support stiffness and then the rail support force was divided by the effective surface area of rail pad. Therefore, the rail support pressure directly depends on the ballast stiffness which was affect the track support stiffness. For a constant rail pad stiffness of 400 kN/mm, the high ballast stiffness also caused the rail support pressure to increase.

The natural frequency of track could be directly affects the entire system dynamics of the track, the resonance and track deterioration. Therefore, it is considered that the natural frequency of track directly depends on the track support stiffness, track and unsprung mass of vehicle and rail bending stiffness. Fig. 9.20 shows the variation in

natural frequency of track (1st vibration mode) plotted against the variation in the rail pad and ballast stiffness.

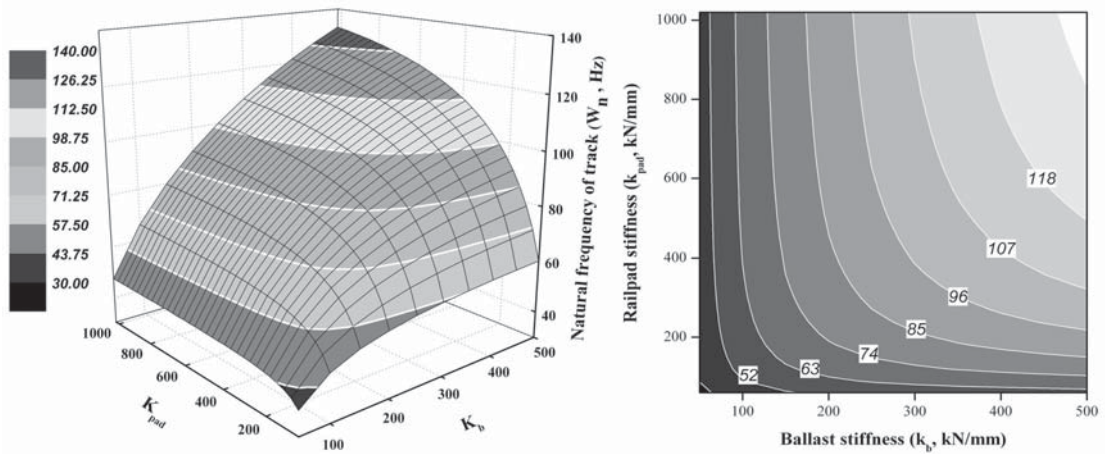

Fig. 9.20 Example of natural frequency of track map for ballasted track; natural frequency of track as a function of rail pad and ballast stiffness

Fig. 9.20 shows that natural frequency of track (1st vibration mode) increased with an increase in the rail pad and ballast stiffness. As shown in Fig. 9.20, the ballast stiffness affects natural frequency of track more strongly than the rail pad stiffness. Therefore, the natural frequency of track directly depends on the ballast stiffness which was affect the track support stiffness. For a constant rail pad stiffness of 400 kN/mm, the high ballast stiffness also caused the natural frequency of track to increase.

According to section 6 in this study, the 1st excitation frequency depends on the train speed and sleeper spacing. The results of the eigenvalue analysis in which the mass and stiffness of the rail-sleeper-ballast system and the frequency analysis of the time history responses showed that the natural frequency of the analytical model was approximately 74–76 Hz, though there are some differences depending on sleeper type [31, 98, 114].

The sleeper spacing (600 mm) gives the 1st excitation frequency (sleeper-passing frequency) as approximately 75 Hz in the 170–175 km/h speed range. Thus, resonance of the ballast track is induced because the sleeper-passing frequency and the natural frequency based on the mass and stiffness of the rail coincide in the frequency band of 70 Hz [31].

The track support stiffness of the ballasted track hard to be chosen to low as to prevent excitation by a train running at high speed of the natural frequency (1st vibration mode). The first natural frequency of the track must be sufficiently higher to prevent rapid track deterioration. Therefore, it was concluded that the appropriate track support stiffness (which is affected by the rail pad and ballast stiffness) was important to prevent the resonance of the track. To ensure that the natural frequency of track does not similar to the range of the 1st excitation frequency (sleeper-passing frequency), the ballast stiffness was held constant at 200–300 kN/mm while varying the rail pad stiffness.

In addition, since the difference between the results of section 6 (i.e., validated by the measured and analytical result) and the qualitative analysis (e.g, in the case of rail pad and ballast stiffness of 400 kN/mm and 200 kN/mm, respectively) was approximately 2%, the qualitative analysis results reflected the measured and the commercial FEA package results well. Therefore, it is considered that qualitative analysis results obtained using measured data such as rail pad stiffness are suitable for predicting the natural frequency of ballasted track and should be of practical use in track maintenance.

The resonance velocity (i.e., the critical speed at the 1st excitation frequency) could be directly affects the resonance performance and track deterioration [31, 41, 77, 114]. Therefore, it is considered that the resonance velocity directly depends on the natural frequency of the track. The so-called resonance velocity is the characteristic parameter of track system. The resonance velocity depends on the subgrade modulus, track support stiffness, bending stiffness of the track and mass of the track [31, 114]. The uncommon highest dynamic loads occur at resonance velocity.

The actual railway line speed has to be much lower than the resonance velocity. The calculation of the resonance velocity was inaccurate, because the bending stiffness of the track was unknown for the entire track grid, and it was hard to reflect that the elasticity and mass of the ballast bed. Therefore, in the present study, the resonance velocity was qualitatively estimated and limited to the critical speed at the 1st excitation frequency of the ballasted track based on the result of natural frequency of the track.

Fig. 9.21 shows the variation in resonance velocity plotted against the variation in the rail pad and ballast stiffness.

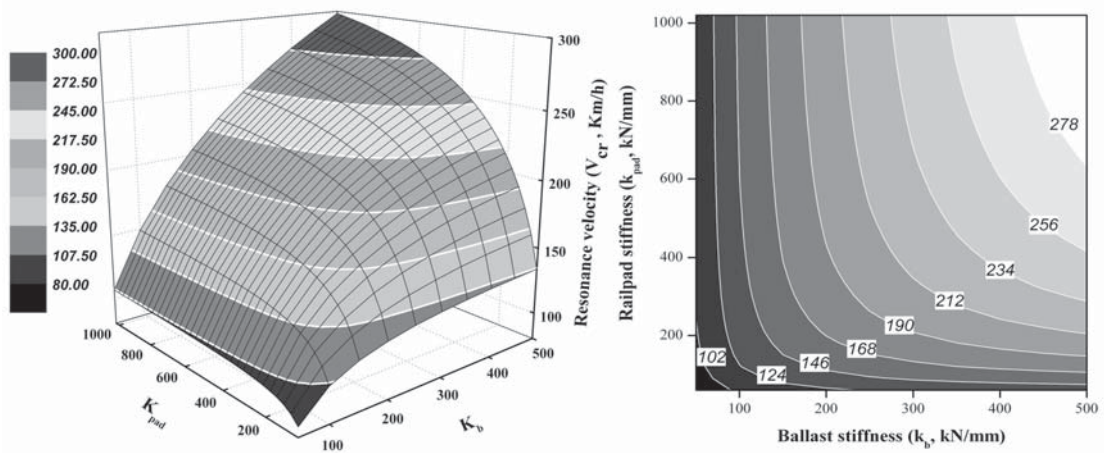

Fig. 9.21 Example of resonance velocity map for ballasted track; resonance velocity of track as a function of rail pad and ballast stiffness

Fig. 9.21 shows that resonance velocity increased with an increase in the rail pad and ballast stiffness. As shown in Fig. 9.21, the ballast stiffness affects resonance velocity more strongly than the rail pad stiffness. Therefore, the resonance velocity directly depends on the ballast stiffness which was affect the track support stiffness. For a constant rail pad stiffness of 400 kN/mm, the high ballast stiffness also caused the natural frequency of track to increase.

The first natural frequency of the track must be sufficiently higher to prevent the resonance velocity within the service speed of the conventional ballasted tracks. However, it should be take the other response of the track into consideration. Therefore, it was concluded that the appropriate track support stiffness was important to prevent the resonance of the track. However, in that case, most resonance velocity could be comprised in the service speed regardless of increasing the rail pad and ballast stiffness. Therefore, allowing for an increasing stiffness of rail pad and ballast, it is considered that qualitative analysis results are suitable for predicting the resonance velocity of in-service ballasted track and should be of practical use in track maintenance and monitoring. Thus, it would be make use of planning the train schedule and the service speed.

9.5 Validation of proposed qualitative prediction model

A qualitative analysis–based dynamic behavior prediction model for ballasted tracks (qualitative prediction model) was developed to predict and assess track performance as a function of dynamic vehicle loading and track support stiffness variation. The proposed prediction model consists of a two-degrees-of-freedom dynamic track model and modified track properties, which define the rail pad and ballast stiffness ranges, based on designed and measured values.

In section 8, field measurements were conducted to measure the dynamic response of a test track (i.e., dynamic wheel load, rail displacement, and rail bending stress). For instance, track support stiffness, rail displacement and rail bending stress assumed that the principal response of a ballasted track. These responses were qualitatively estimated and predicted by qualitative analysis using the empirical track dynamics theory. Then, the measured results were compared with the results of the qualitative analysis (the proposed prediction model, qualitative analysis map) to validate the ability of the model to predict track behaviors.

In the validation of present analysis, it was performed that the rail pad stiffness measured using the specimens from the test tracks, i.e., introduced in section 8.3. The normal pandrol rail pad used in the Korean conventional ballasted track was adopted in the rail pad stiffness test according to the Korean standard (KS F2310). A total of seven specimens of a rail pad used for the conventional ballasted track in South Korea were selected to measure the dynamic stiffness of rail pad. The state of each specimen was relatively good and the dynamic rail pad stiffness was measured to be 480–520 kN/mm.

Fig. 9.22 shows the procedure of qualitative analysis (the proposed qualitative prediction model) for the prediction of dynamic track response using the measured data of the test track. Using the basic information for test tracks (such as the measured rail pad stiffness, track support stiffness and prediction ballast stiffness), the dynamic response of in-service ballasted track could be predicted from the intersection region of the proposed qualitative analysis map shown in Fig. 9.22.

- ***Step 1***; Draw the measured data block (the rail pad stiffness, Fig. 9.22(①)) in horizontal direction on the qualitative analysis map (TSS map).
- ***Step 2***; Plot the measured TSS data (circles in Fig. 9.22(②)) in the qualitative analysis map (TSS map), and check the intersection region of a duplicated zone (Fig. 9.22(③)) in vertical direction between both of the measured data block and measured TSS data.
- ***Step 3***; Draw the blocks in both the vertical and horizontal directions on the qualitative analysis map (track response map), and Check the intersection region of a duplicated zone between the vertical and horizontal direction represented the predicted resonse of the in-service ballasted track.
- ***Step 4***; Verify the range of the prediction results (value in white box) using the real track response data obtained from the target track (circles in Fig. 9.22(④)).

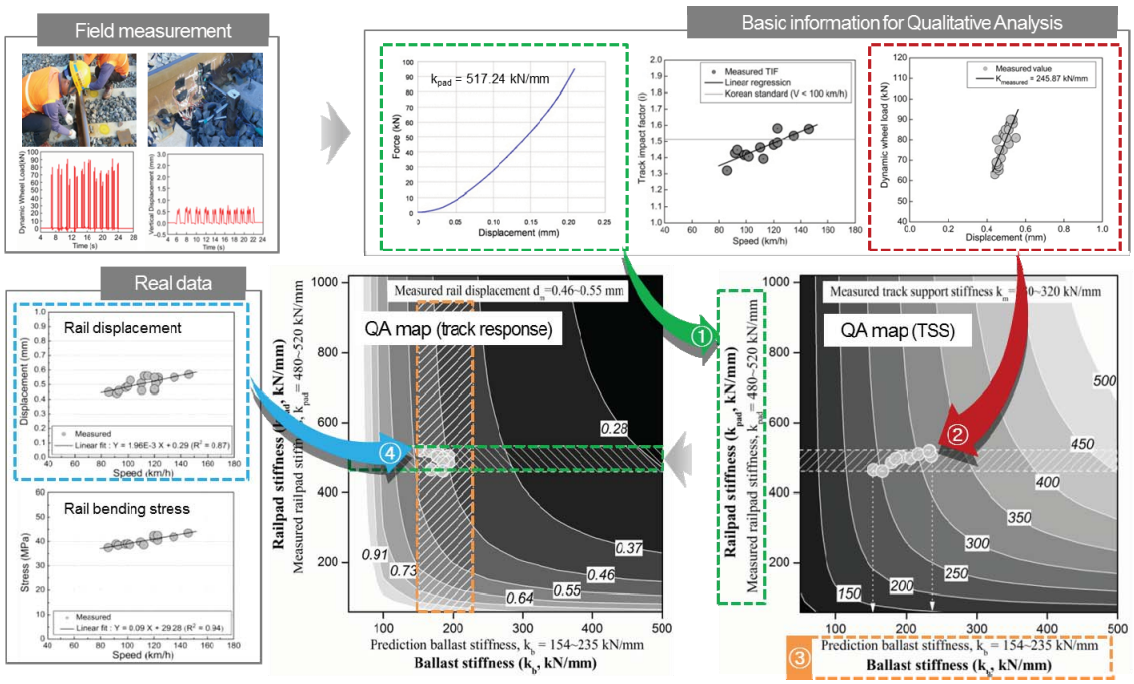

Fig. 9.22 Procedure of qualitative analysis for prediction of dynamic track response

In this study, the measured rail pad stiffness of 480–520 kN/mm, the vehicle speed of 120 km/h (i.e., the general train speed in test site), the measured track support stiffness and rail displacement were defined as reference or guide data (i.e., indicate that the

range of discrete surface area) and the track support stiffness, rail displacement and rail bending stress were defined as dependent variables of qualitative analysis.

Fig. 9.23 shows the variation in track support stiffness (TSS) plotted against the variation in the rail pad and ballast stiffness. The TSS of the in-service ballasted track was predicted from the intersection region of a duplicated zone between the vertical and horizontal direction represented the predicted resonse of the in-service ballasted track.

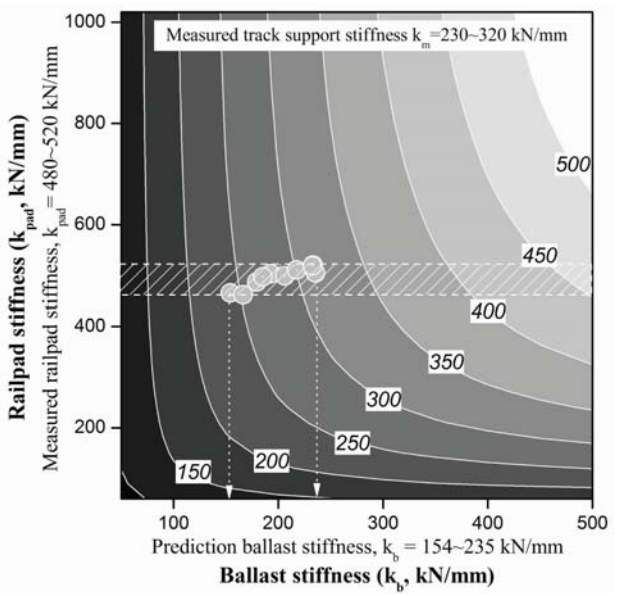

Fig. 9.23 Track support stiffness map for ballasted track

; Comparison of TSS estimated using field measurement (circles) with that estimated using qualitative analysis, measured rail pad stiffness, and prediction ballast stiffness

Fig. 9.24– Fig. 9.25 shows that the diagram (the proposed qualitative analysis map) of prediction rail displacement and rail bending stress vs. the measured rail pad stiffness with each of the measured data in section 8.

The qualitative analysis results for the rail displacement and rail bending stress showed good agreement within about 2–5% with the field measurement results. Therefore, it is considered that qualitative analysis results obtained using measured data such as rail pad stiffness and dynamic track support stiffness are suitable for predicting the dynamic responses acting on a ballasted track and should be of practical use in track maintenance.

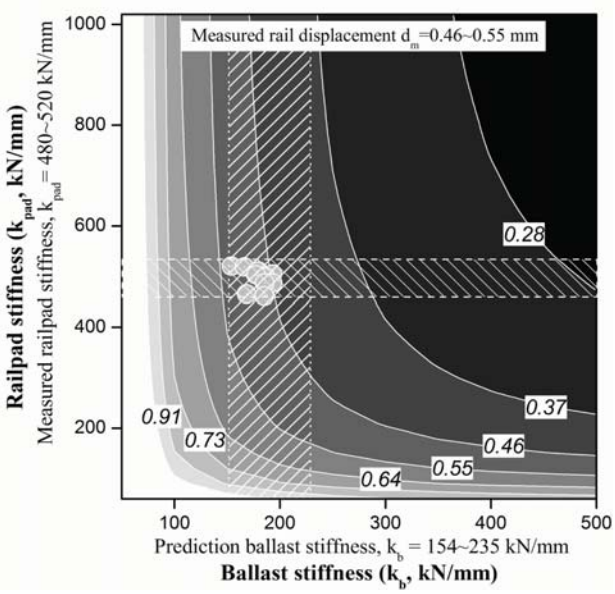

Fig. 9.24 Rail displacement map for ballasted track

; Comparison of rail displacement estimated using field measurement (circles; refered to Fig. 8.4) with that estimated using qualitative analysis, measured rail pad stiffness, and prediction ballast stiffness

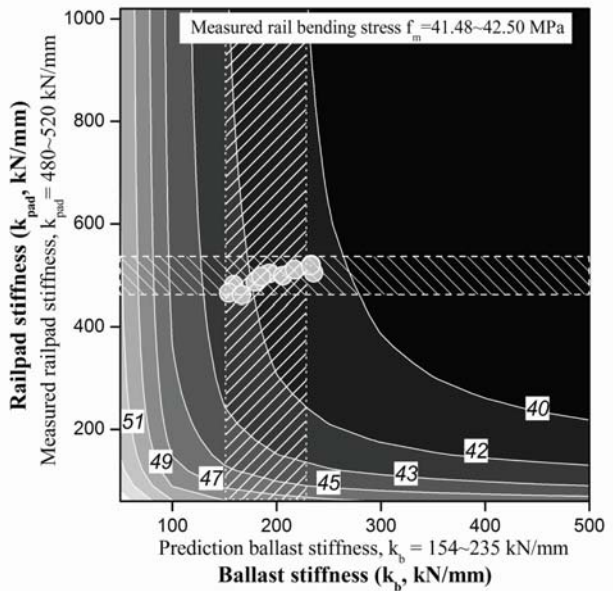

Fig. 9.25 Rail bending stress map for ballasted track

; Comparison of rail bending stress estimated using field measurement (circles; refered to Fig. 8.4) with that estimated using qualitative analysis, measured rail pad stiffness, and prediction ballast stiffness

9.6 Conclusions

A qualitative analysis–based dynamic behavior prediction model for ballasted tracks (qualitative prediction model) was developed to predict and assess track performance as a function of dynamic vehicle loading and track support stiffness variation.

The results obtained in this section are summarized below.

(1) The prediction model consists of a two-degrees-of-freedom dynamic track model and modified track properties, which define the rail pad and ballast stiffness ranges, based on designed and measured values. The qualitative prediction model for dynamic track behavior, capable of simulating the complex interaction between the track's component properties and track responses, was developed in this study.

(2) The ballast was set on 200–300 kN/mm is effective in reducing the track deterioration (track deflection and deformation) and dynamic resonse. Further, it was concluded that the appropriate track support stiffness was important to prevent exceeding the dynamic response of the in-service ballasted track, i.e., track forces, dynamic contribution, vibration behavior, over the design specifications. The qualitative analysis results showed good agreement within 2–5% with the field measurement results.

(3) The qualitative analysis results are presented as a discrete space area of various track responses and parameters, instead of single values. The dynamic behavior of in-service ballasted tracks can be qualitatively predicted by the proposed qualitative analysis map as a function of the rail pad and ballast stiffnesses, and a simple field test.

(4) This new approach is expected to facilitate track behavior assessment by owners based on more realistic track conditions, as well as reduce inaccuracies and deliver results that are consistent with the prediction results of in-service track responses using single design values.

10 CONCLUSIONS

The main aims of the research reported in this thesis are as follows:

• To identify track response evaluation methods that provide results reflecting the field performance of different ballasted track situations.

• To apply the mechanics of a ballasted track to qualitative analysis to understand its behavior and the variations in the track's component properties.

• To use the discrete space solution of the qualitative analysis method to calculate the parameters and responses of the ballasted track in terms of the rail pad and ballast stiffnesses or predict the dynamic response of ballasted tracks to study their behavior in actual tracks. Therefore, it was suggested that the method of assessing the actual track response should be evaluated and proposed.

• To predict the field condition and suitability for maintaining a ballasted track.

The following specific objectives have been achieved in order to meet these aims:

(1) A literature review has been performed to study the behavior of ballasted track, field measurement methods, track mechanics, numerical analysis and application of discrete space solution modeling using qualitative analysis in simulating track behavior.

(2) Various track components such as rail pad, ballast, sleeper, and rail that are widely used in the South Korea and represent a range of physical properties have been selected for this research. Current rail pad and subgrade modulus tests as specified in the Korea Specification (the European CEN standards or the KHRC standard for fastening systems; 2002 and KS F2310) have been conducted.

(3) Track impact factor (TIF) and track support stiffness (TSS), which can measure dynamic force as a function of track displacement and train velocity, has been investigated for seven tested tracks. In the case of the ballasted track, the condition of ballast (gravel) was found to directly affect the TSS. Moreover, the effects of slope of the wheel load-displacement curve, dynamic wheel load, and amplitude of initial-to-peak dynamic wheel load on this track were found to be significantly greater than those

on the slab tracks. Therefore, the deterioration of the ballast affected the performance of the ballasted track, and therefore, the dynamic wheel load was not distributed effectively over the ballasted track in bad condition.

The TIF was calculated for standard deviations of the measured dynamic wheel load. For a standard deviation of σ, all the seven track segments satisfied the design specifications. For a standard deviation of σ, the calculated TIF was generally lower level than the Korean standard. For a standard deviation of 2σ, the measured TIF of almost all the slab tracks was lower than the design specifications. Further, the TIF for the service line appeared to increase with the TSS, and therefore, it was inferred that the TSS directly affects the TIF. It is reasonable to consider the actual TSS, in addition to the structural and resilience characteristics, of various types of tracks for determining the design specifications of TIF. Therefore, it was concluded that the appropriate TSS was important to prevent exceeding the TIF over the design specifications.

(4) On-site measurements at four general railway service lines were conducted to calculate the empirical dynamic TIF for two different trains while taking into account the track condition and the track component, i.e., sleeper type including fastening, and to evaluate the train-induced track displacement, the derived time history function using the measured TIF were applied to a numerical analysis.

The analytical results reproduced the experimental results well within about 2–5% difference in the values. Therefore, applying the derived time history function based on the measured TIF are considered to give sufficiently reliable FEA results in investigating the behavior of the ballasted track. It showed that the derived time history function using the measured TIF which on a smaller track curvature with wooden sleepers is higher than other test section. Therefore, it would be advantageous to increase the weight of sleepers on existing lines to increase the train speed through the speedup effect without the improved track curvature.

(5) Theoretical, empirical, and statistical studies were performed to derive a prediction equation for the peak dynamic forces acting on railway tracks. The predicted values can be used for track maintenance and assessment of rail surface roughness, vertical track stiffness, and train velocity.

Numerical simulations and measurements of peak dynamic wheel-rail forces (P1 and P2) for an HSR line with an irregular rail surface showed that the vertical track stiffness affects P2 more strongly than P1. Hence, P1 is more affected by QI and train velocity than P2. The multiple regression analysis results, along with Prud'Homme's geometrical quality index (QI′) and the corresponding QI, were used to derive an empirical prediction equation for the dynamic forces. For a constant QI, an increase in the vertical track stiffness caused the peak dynamic force to increase. Therefore, it is obvious that keeping the vertical track stiffness of ballasted tracks constant is important to reduce P2.

The multiple regression analysis results showed good agreement within 2–5% with the space solution of Prud'Homme's equation. Therefore, it is inferred that the multiple regression analysis results obtained using measured data such as QI and P1 (or P2) can be used to predict the peak dynamic forces acting on ballasted tracks, and the prediction equation should be of practical use for track maintenance.

(6) The FEA result obtained using the subgrade modulus estimated from the design value (by PLT) was greater than that estimated from the empirical equation. The subgrade modulus estimated from design value was approximately 70% less than that estimated from the empirical equation. The numerical model with the subgrade modulus estimated from the design value underestimated the behavior of the in-service track. Therefore, it is thought that the subgrade modulus directly affects the displacement of the track.

The FEA and measurement results obtained using the subgrade modulus estimated from the empirical equation showed a good agreement within approximately 5%. Therefore, it is thought that the analysis results obtained using the subgrade modulus estimated from the empirical equation is sufficiently reliable for investigating the behavior of in-service tracks. The behavior of in-service tracks can be analyzed using the measured track response. Further, the behavior of in-service ballasted tracks can be easily predicted by FEA using the subgrade modulus estimated from the empirical equation and subgrade modulus map i.e., diagram of subgrade modulus in function of dynamic wheel load and vertical rail displacement.

(7) The parameters and dynamic response of the ballasted track determined through field measurements and qualitative analysis showed that the vertical TSS more strongly affects every parameter and is therefore affected to a greater extent by ballast stiffness than by rail pad stiffness. The ballast stiffness set at 200–300 kN/mm is found to be effective in reducing track deterioration (track deflection) and the impact damage level. In conclusion, appropriate TSS (which is affected by the rail pad and ballast stiffnesses) is important for preventing the TIF from exceeding the design specifications.

Using qualitative analysis, the predicted dynamic track response map can be derived and advantageously used to effectively deal with uncertainties and design variables. The results of the qualitative analysis showed good agreement with field measurement and FEA results. Therefore, the results of the qualitative analysis obtained using the measured data (such as rail pad stiffness and rail bending stress (or rail displacement)) can be used to predict the various dynamic responses of ballasted tracks.

(8) Field measurement, FEA and qualitative analysis results have been correlated and engineering practices have been proposed.

The conclusions that can be drawn from this research are:

(1) The dynamic behavior of ballasted track has been traditionally estimated by field measurement or the commercial finite element analysis program, both of which were could be considered as inappropriate because of the inaccurate simulation of the track component mechanics of ballasted track during train loading and the inappropriate rail pad and ballast properties used for the field test and numerical analysis respectively.

(2) It is necessary to have assessment method for the track response which assess the performance of different rail pad and ballast materials scientifically and provide results reflecting the field performance of different in-service ballasted track condition.

(3) It was found in the field measurement, finite element analysis and qualitative analysis that there is a stiffness effect on the rail pad and ballast, and the dynamic track response is dependent on the elastic material such as a rail pad and ballast.

(4) It was found that the theoretical TSS was calculated considering only the vertical stiffness of the tracks cannot be used to predict the TSS of actual tracks was estimated because the TSS of actual tracks is rail bending stiffness dependent and did not considering the longitudinal stiffness of the tracks. The measured value of TTS was 16–32% higher than the theoretical value. Thus, the theoretical TSS is not appropriate and it is important to consider the longitudinal stiffness used in the track.

(5) The TIF for the service line appeared to increase with the TSS, and therefore, it was inferred that the TSS directly affects the TIF. Therefore, it was concluded that the appropriate TSS was important to prevent exceeding the TIF over the design specifications.

(6) Applying the derived time history function based on the measured TIF are considered to give sufficiently reliable FEA results in investigating the behavior of the ballasted track. Therefore, the simulated process is considered as appropriate actual TIF because it was able to reflect the ballasted track performance that there was an increase in settlement and stiffness due to variation track condition and track components (i.e., rail, sleeper and rail fastening system), which is likely to represent the performance of the ballasted track in the field.

(7) The multiple regression analysis results using the measured QI and peak dynamic wheel-rail forces, along with Prud'Homme's geometrical quality index (QI′) and the corresponding QI, were used to derive an empirical prediction equation by qualitative analysis for the dynamic forces.

(8) Numerical simulations and measurements of peak dynamic wheel-rail forces (P1 and P2) for an HSR line with an irregular rail surface showed that the vertical track stiffness affects P2 more strongly than P1. Hence, P1 is more affected by QI and train velocity than P2.

(9) For a constant QI, an increase in the vertical track support stiffness caused the peak dynamic force to increase. Therefore, it is obvious that keeping the vertical TSS of ballasted tracks constant is important to reduce P2.

In case the vertical TSS is known approximately, the peak dynamic force could be predicted using the space solution and QI, which can be measured through a simple test using RAILPROF. Thus, the proposed equation is easy to implement using digital straightedges (such as RAILPROF).

(10) It can be seen that subgrade modulus decreased with an increase in the rail displacement. At a rail displacement of less than 0.5 mm, the rate of increase in subgrade modulus was high. The maximum value of prediction subgrade modulus was approximately twice that of the initial design value of subgrade modulus. The rail displacement affects subgrade modulus more strongly than the dynamic wheel load.

(11) The subgrade modulus of the in-service ballasted track was predicted from the intersection region of ranges of measurement results. As a result of qualitative analysis, the subgrade modulus of the in-service ballasted track was higher and was distributed more roughly and over a wider range than its initial design value (i.e., the value considered during subgrade construction).

(12) The subgrade modulus of in-service ballasted tracks does not depend on a single design value of subgrade modulus. To ensure that the subgrade modulus is similar to the initial value, the rail displacement (which is affected by the vertical track stiffness) was held constant at 0.7 mm while varying the dynamic wheel load.

(13) The track response and the entire ballasted track system are likely to be mainly affected by the rail pad and ballast stiffnesses, which are related to the track support stiffness. It is more difficult to appropriately secure the ballast stiffness (i.e., it is difficult to determine the gravel condition underneath the sleeper). Thus, a single value of the ballast stiffness is not likely to allow for efficient track analysis, and therefore, a range of values is preferred.

(14) The ballasted track response should ideally be a function of the degree of stiffness of the rail pad or ballast. A qualitative analysis, which calculates the range of these stiffnesses based on the measured and initial values, would be more suitable in simulating track behavior because the current assessment method uses a single value and there is a significant difference between the design variables and field measurement results.

Therefore, the rail pad and ballast stiffnesses could be adjusted and maintained to estimate the properties or performance of the ballasted track using simple field or specified laboratory tests incorporating a sample test track.

(15) Using qualitative analysis, it is also possible to easily portray the irregularity in input variables and the diverse nature of the range of constraints. Therefore, it would also significantly reduce inaccuracies and deliver consistent single-value inputs.

The results of this study interpret the various track responses and parameters that are a part of the input variables and variable properties, using a range of data acquired from field measurements, rather than using single design values.

(16) The dynamic track response obtained using qualitative analysis is suitable for predicting the constraint parameters determined by field measurements and should facilitate practical track maintenance operations. If certain kinds of measured track responses are available, it is possible to predict the other responses and parameters of the ballasted track by representing them in a space solution defined in a specific range. Therefore, it can be concluded that this study succeeded in predicting the field condition and suitability for maintaining a ballasted track.

REFERENCES

[1] Abdelkrim M., Bonnet G., and Buhan P. (2003), A computational procedure for predicting the long term residual settlement of a platform induced by repeated traffic loading, Computers and Geotechnics 30, 463–476.

[2] Al Shaer A., Duhamel D., Sab K., Foret G., and Schmitt L. (2004), Dimensionnement dynamique d'un banc d'essai de voie ferree a echelle reduite par le code CESAR-LCPC, XIV eme Colloque Vibrations, chocs et bruit, Ecully.

[3] Alaoui A., Naciri T. (1995), Les voies ballastees, Technical Report: Rapport EUROBALT, CERAM, ENPC.

[4] Allemang R. (1993), Modal Analysis – Where do we go from here?, International Journal of Analytical and Experimental Modal Analysis, 8(2), 79-91.

[5] Allemang R., Brown D. (1986), Multiple – Input experimental modal analysis – A survey, International Journal of Modal Analysis, January, 37-43.

[6] Alves Costa P., Calçada R., Cardoso A.S., and Bodare A. (2010), Influence of soil non-linearity on the dynamic response of high-speed railway track, Soil Dyn. Earthq. Eng. 30(4), 221–235.

[7] American Railway Engineering and Maintenance-of-Way Association (2012), Manual for Railway Engineering, Maryland 20706, US.

[8] Andersen L. (2002), Wave propagation in infinite structures and media, PhD Thesis, Aalborg University.

[9] Andersson M., Murray M., Ferreira L., and Lake N. (2004), Collection and use of railway track performance and maintenance data. In: Proceedings of CORE 2004—conference on railway engineering, Darwin, Australia.

[10] Balsan M. (1980), Un modele mathematique de la voie ferree moderne, These de l'Ecole Nationale des Ponts et Chaussees.

[11] Banverket. (1997), Spårlägeskontroll och Kvalitetsnormer – Central Mätvagn Strix, BVF587.02.

[12] Bathe K.J., Wilson E.L. (1976), Numerical Methods in Finite Element Analysis, Prentice-Hall, Englewood Cliffs, NJ.

[13] Berggren E.G., Kaynia A.M., and Dehlbom B. (2010), Identification of substructure properties of railway tracks by dynamic stiffness measurements and simulations, Journal of sound and vibration, 329, 3999–4016.

[14] Berggren E.G., Li M.X.D., and Spännar J. (2006), A new approach to the analysis and presentation of vertical track geometry quality and rail roughness with focus on train–track interaction and wavelength content. In Proceedings of the 7th International Conference on Contact Mechanics and Wear of Rail/Wheel Systems (CM2006), Brisbane, Australia, 24–27 September 2006.

[15] Bodare A., et al. (2009), Evaluation of track stiffness with a vibrator for prediction of train-induced displacement on railway embankments, Soil Dyn. Earthq. Eng. 29(8) 1187–1197.

[16] Bodin V. (2001), Comportement du ballast des voies ferrees soumises a un chargement vertical et lateral, These de l'Ecole Nationale des Ponts et Chaussees.

[17] Bonaventura C.S., Palese J.W., and Zarembski A.M. (2003), Real-time prediction of railway vehicle response to the interaction with track geometry. In Proceedings of the IHHA Special Technical Session, Fort Worth, Texas, USA, 5.1–5.9.

[18] Boresi A.P., Schmidt R.J. (2003), Advanced mechanics of materials, 6th Edition, John Wiley & Sons, New York, NY, 163–165, 357–371.

[19] Brown D. (1982), Keynote Speech Modal Analysis – Past, Present and Future, Proceedings of the 1st International Modal Conference, Union College, New York.

[20] Buddhima Indraratna., Wadud Salim, (2005), Mechanics of ballasted rail tracks: A geotechnical perspective, Taylor & Francis, London, UK.

[21] Cai Z. (1992), Modelling of rail track dynamics and wheel/rail interaction, Ph.D. Thesis, Department of Civil Engineering, Queen's University, Ontario, Canada.

[22] Choi J.Y. (2013), Influence of track support stiffness of ballasted track on dynamic wheel-rail forces, Journal of Transportation Engineering, 139, 709–718.

[23] Choi J.Y. (2013), Prediction of displacement induced by tilting trains running on ballasted tracks through measurement of track impact factors, Engineering Failure Analysis, 31, 360–374.

[24] Choi J.Y., et al. (2010), Applying precast slab panel track to replace timber track in an existing steel plate girder railway bridge, J. Rail Rapid Transit, 224, 159–167.

[25] Choi J.Y., Lee D.W., and Park Y.G. (2011), A Study on the Evaluation of Track Support Stiffness on the Various Track Type in Urban Transit, Journal of the Korean Society for Railway, 14(3), 262-270 (in Korean).

[26] Choi J.Y., Park Y.G., and Lee S.M. (2011), The Evaluation of Track Impact Factor on the Various Track Type in Urban Transit, Journal of the Korean Society for Railway, 14(3), 248-255 (in Korean).

[27] Clark R. (2004), Rail flaw detection: overview and needs for future developments. NDT&E Int, 37(2), 111–118.

[28] Clark R.A., Dean P.A., Elkins J.A., and Newton S.G. (1982), An investigation into the dynamic effects of railway vehicles running on corrugated rails, Journal of Mechanical Engineering and Science 24, 65–76.

[29] Cleary J.G. (1987), Logical Arithmetic, Future Computing Systems.

[30] Dahlberg T., Nielsen J. (1991), Dynamic behaviour of free–free and in-situ concrete railway sleepers, in: Proceedings of International Symposium on Precast Concrete Railway Sleepers, Madrid, Spain.

[31] Dahlberg Tore. (2003), Railway track dynamics - a survey, Linköping University, Sweden, (unpublished).

[32] DataFit. (2003), User's Manual. Oakdale, PA, USA: Oakdale Engineering.

[33] DB Netz AG. (2002), Requirements catalog for the construction of the permanent way 4th revised edition, Technical notification concerning the body of permanent way technology regulations, RO 03/2002, Version of 08/01/2002.

[34] De Man A.P. (1996), Determination of dynamic track properties by means of excitation hammer testing, Railway Engineering International 1996 Edition,(4), 8-9.

[35] De Man A.P. (2002), DYNATRACK: A survey of dynamic railway track properties and their quality, Ph.D. Thesis, Faculty of Civil Engineering, Delft University of Technology, The Netherlands.

[36] De Man A.P., Esveld C. (2000), Recording, estimating, and managing the dynamic behavior of railway structures, Proceedings of Symposium Leuven. The Netherlands.

[37] Desai C.S., Siriwardane A.M. (1982), Numerical models for track support structures, J. Geotech. Geoenviron. Eng., 108(GT3), 461–480.

[38] Dinkel J., Grundmann H. (1999), Winkler parameters for railway dynamics derived from 3-D half space analysis, Proceedings of EURODYN-99, 831–836.

[39] Ebersohn W., Trevizo M.C., and Selig E.T. (1993), Effect of low track modulus on track performance, International Heavy Haul Association, Proc. of Fifth International Heavy Haul Conference, 379-388.

[40] Esveld C. (1997), Track structures in an urban environment. In: Proceedings of symposium K.U. Leuchen, The Netherlands, 1–21.

[41] Esveld C. (2001), Modern Railway Track, 2nd edition, MRT-Productions, The Netherlands.

[42] Esveld C., Kok A.W.M., and De Man A.P. (1998), Integrated numerical and experimental research of railway track structures, Proceedings of the 4th International Workshop on Design Theories and their Verification of Concrete slabs for Pavements and Railroads, Portugal.

[43] Esveld C., Steenbergen M. (2006), Force-based Assessment of Rail Welds, WCRR, Montreal, Canada.

[44] Esveld C., Steenbergen M.J.M.M. (2005), Force-based Assessment of Weld Geometry, Proc. 8th International Heavy Haul Conference, Rio de Janeiro, Brazil.

[45] European Standard EN 14363. (2005), Railway applications – testing for the acceptance of running characteristics of railway vehicles – testing of running behaviour and stationary tests.

[46] European Standard EN, Official journal of the European communities. (2002), Technical Specification for Interoperability Relating to the Infrastructure Subsystem, L245/143.

[47] European Standard prEN 13848-5. (2007), Railway applications – track – track geometry quality – part 5: geometric quality levels.

[48] Ewins D.J. (1995), Modal Testing: Theory and Practice, Research Studies Press, Taunton.

[49] Fahey S.O'F., Pratt J. (1998), Frequency domain modal estimation techniques, Experimental Techniques, 22(5), 33-37.

[50] Fenander A. (1997), Frequency dependent stiffness and damping of rail pads, Proceedings of Institute of Mechanical Engineering Part F, 211, 51-62.

[51] Fenander A. (1998), A fractional derivative rail pad model included in a railway track model, Journal of Sound and Vibration, 212(5), 889-903.

[52] FIP Commission on Prefabrication. (1987), Concrete Railway Sleepers – FIP State of Art Report, Thomas Telford Ltd., London, UK.

[53] Ford R. (1988a), Modal analysis of a concrete railway sleeper, Research Note AVG/RN881122-1, School of Mechanical and Industrial Engineering, University of New South Wales, Australia.

[54] Ford R. (1988b), Vibration responses of systems comprising a concrete sleeper, rail section, and various types of rail pads, Research Note AVG/RN881122-2, School of Mechanical and Industrial Engineering, University of New South Wales, Australia.

[55] Fröhling R.D. (1997), Deterioration of railway track due to dynamic vehicle loading and spatially varying stiffness, Ph.D. Diss., University of Pretoria.

[56] Gedig M. H. (1995), A framework for qualitative and semi-quantitative analysis in engineering design and evaluation, Thesis (M.A. Sc.), University of British Columbia.

[57] Graduate School of Railway, Seoul National University of Science and Technology (2009), A study on the maintenance and estimate of fatigue life for used rail, Seoul Metro, Korea.

[58] Grassie S.L. (1987), Measurement and attenuation of load in concrete sleepers, Proceedings of Conference on Railway Engineering, Perth, September 14-16, 125-130.

[59] Grassie S.L. (1989), Resilient rail pads: Their dynamic behavior in the laboratory and on track, Proceedings of Institute of Mechanical Engineering Part F, 203, 25-32.

[60] Grassie S.L. (1989), Behavior in track of concrete sleepers with resilient rail pads, Proceedings of Institute of Mechanical Engineering Part F, 203, 97-101.

[61] Grassie S.L. (1995), Dynamic modelling of concrete railway sleepers, Journal of Sound and Vibration, 187, 799–813.

[62] Grassie S.L. (1996), Models of railway track and train-track interaction at high frequencies: Results of benchmark test, Vehicle System Dynamics, 25(Supplement), 243-262.

[63] Grassie S.L., Cox S.J. (1984), The dynamic response of railway track with flexible sleepers to high frequency vertical excitation, Proceedings of Institute of Mechanical Engineering Part D, 24, 77-90.

[64] Grassie S.L., Cox S.J. (1984), The dynamic response of railway track with flexible sleepers to high frequency vertical excitation, Proceedings of Institute of Mechanical Engineering, Part D 198, 117–124.

[65] Grassie S.L., Gregory R.W., Harriswon D., and Johnson K.L. (1982), The dynamic response of railway track to high frequency vertical excitation, Proceedings of the Institution of Mechanical Engineers, Part C, Journal of Mechanical Engineering Science, 24(2), 77-90.

[66] Grassie SL., Kalousek J. (1994), Rail corrugation: characteristics, causes and treatments, Proceedings of the Institution of Mechanical Engineers, Part F, Journal of Rail and Rapid Transit, 207(F1), 57-68.

[67] Gu G., Choi J. (2013), The dynamic response of rail support, Vehicle System Dynamics, doi: 10.1080/00423114.2013.778415.

[68] Guerin N., Sab K., and Moucheront P. (1998), Identification experimentale d'une loi de tassement du ballast, Canadian Geotechnical Journal, 36, 523–532.

[69] Gustavson R. (2000), Static and dynamic finite element analyses of concrete sleepers, Licentiate of Engineering Thesis, Department of Structural Engineering, Chalmers University of Technology, Sweden.

[70] Gustavson R., (2002), Structural behaviour of concrete railway sleepers. PhD Thesis, Department of Structural Engineering, Chalmers University of Technology, Sweden.

[71] Hall L. (2002), Simulations and analyses of train-induced ground vibrations in finite element models, Soil Dynamics and Earthquake Engineering, 23, 403–413.

[72] Hamet J.F. (1999), Railway noise: use of the Timoshenko model in rail vibration studies. Acustica, 85, 1–12.

[73] Hay W.M. (1982), Railroad Engineering, 2nd edition, John Wiley & Sons, Inc.

[74] He H., Fu Z. (2001). Modal Analysis, Butterworth – Heinemann Publishers, Great Britain. Indraratna, B. and Salim, W. (2005). Mechanics of Ballasted Rail Tracks A Geotechnical Perspective. Taylor & Francis, London.

[75] Heckl M.A. (1995), Railway noise: can random sleeper spacing help? Acustica, 81, 559–564.

[76] Hickey T. J., Qiu Z., and van Emden M. H. (2000), Interval Constraint Plotting for Interactive Visual Exploration of Implicitly Defined Relations, Reliable Computing, Vol 6, No. 1.

[77] Hunt G.A. (2005), Review of the effect of track stiffness on track performance, Research Project T372, AEATR-II-2004-018, Rail Safety and Standards Board.

[78] Ilias H. (1999), The influence of rail pad stiffness on wheelset/track interaction and corrugation growth, Journal of Sound and Vibration. 227, 935–948.

[79] International Union of Railways, Office for Research and Experiments (1965), Question D71, Stresses in the Track, Ballast and Formation as a Result of Rolling Loads, Stresses in Rails, Part 2: Calibration and Measuring Procedures, Report No.1, Utrecht, Holland.

[80] International Union of Railways. (2003), Testing and approval of railway 488 vehicles from the point of view of their dynamic behaviour–safety–track 489 fatigue–ride quality, UIC 518, 2nd Ed., Railway Technical Publications, Paris, France.

[81] International Union of Railways. (2008), Vertical elasticity of ballastless track, UIC project report, 15 rue Jean Rey – F75015 Paris.

[82] Iwnicki S., Grassie S., and Kik W. (1999), Track settlement prediction using computer simulation tools, Vehicle System Dynamics Supplement, 37–46.

[83] Johan Öberg. (2006), Track deterioration of ballasted tracks-marginal cost models for different railway vehicles. TRITAAVE Report 2006:88, Division of Rail Vehicles, Department of Aeronautical and Vehicle Engineering, Royal Institute of Technology (KTH), Stockholm, Sweden.

[84] Johnson K.L. (1992), Contact Mechanics, Cambridge University Press, Cambridge.

[85] Kaewunruen S. (2007), Experimental and numerical studies for evaluating dynamic behaviour of prestressed concrete sleepers subject to severe impact loading, PhD Thesis, School of Civil, Mining, and Environmental Engineering, University of Wollongong, NSW, Australia.

[86] Kaewunruen S., Remennikov A (2008), Dynamic properties of railway track and its components: a state-of-the-art review, http://ro.uow.edu.au/engpapers/493

[87] Kaewunruen S., Remennikov A. (2004), A state-of-the-art review report on vibration testing of ballasted track components, July-Dec Research Report, CRC Railway Engineering and Technology, Australia.

[88] Kaewunruen S., Remennikov A. (2005), Applications of experimental modal testing for estimating dynamic properties of structural components, In: Proceedings of Australian Structural Engineering Conference 2005, Newcastle, Australia.

[89] Kaewunruen S., Remennikov A. (2005), In-field dynamic testing and measurements of railway tracks in Central Queensland, March-June Research Report, CRC Railway Engineering and Technologies, Australia.

[90] Kaewunruen S., Remennikov A. (2005), Integrated field measurements and track simulation for condition assessment of railway tracks. In: Proceedings of the 1st international conference on structural condition assessment, monitoring, and improvement, Perth, Australia, 391–398.

[91] Kaewunruen S., Remennikov A. (2006), Non-destructive evaluation for dynamic integrity of railway track structure. In: Proceedings of international conference on structural integrity and failure—SIF2006, Sydney, Australia, 294–299.

[92] Kaewunruen S., Remennikov A. (2006), Non-destructive testing (NDT): a tool for dynamic health monitoring of railway track structures. Mater Aust, 39(6), 14–16.

[93] Kaewunruen S., Remennikov A. (2006), Sensitivity analysis of free vibration characteristics of an in-situ railway concrete sleeper to variations of rail pad parameters. J Sound Vib, 298(1–2), 453–461.

[94] Kaewunruen S., Remennikov A. (2007), Effect of improper ballast tamping packing on dynamic behaviors of on-track railway concrete sleeper. Int J Struct Stability Dyn, 7(1), 167–177.

[95] Kaewunruen S., Remennikov A. (2007), Field trials for dynamic characteristics of railway track and its components using impact excitation technique. NDT&E International, 40(7), 510-519.

[96] Kaewunruen S., Remennikov A. (2008), Nonlinear transient analysis of railway concrete sleepers in track systems. International Journal of Structural Stability and Dynamics, in press.

[97] Khordehbinan M.W. (2009), Sensitive analysis of granular layers of rail support system in the ballasted railway tracks of Iran, Master of Science dissertation, University of Tehra.

[98] Knothe K., Grassie S.L. (1993), Modelling of railway track and vehicle/track interaction at high frequencies. Vehicle System Dynamics, 22, 209–262.

[99] Knothe K., Wu Y. (1998), Receptance behaviour of railway track and subgrade, Archive of Applied Mechanics, 68, 457-470

[100] Knothe K., Yu M., and Ilias H. (2003), Measurement and Modelling of Resilient Rubber Rail-Pads. In: K. Popp und W. Schiehlen (Ed.), System Dynamics and Long-term Behaviour of Railway Vehicles, Track and Subgrade, Springer Verlag, Berlin Heidelberg, Germany, 265-274.

[101] Korea Rail Network Authority (2011), Railroad Track Design Standard, Part: Subgrade. (in Korean).

[102] Korea Rail Network Authority (2011), Railroad Track Design Standard, Part: Track. (in Korean).

[103] Korea Railroad Research Institute (2009), Evaluation for stability of track-subgrade by improving speedup in the Gyeongchun Line, Korea Rail Network Authority (KR) (in Korean).

[104] Kumaran G., Menon D., and Krishman Nair K. (2003), Dynamic studies of rail track sleepers in a track structure system, Journal of Sound and Vibration, 268, 485–501.

[105] Kutner M.H., Nachtsheim C.J., and Neter J. (2004), Applied Linear Regression Models, 4th ed., McGraw-Hill/Irwin, Boston, Massachusetts, USA.

[106] Lackenby J. (2006), Triaxial behaviour of ballast and the role of confining pressure under cyclic loading, PhD Thesis, School of Civil, Mining, and Environmental Engineering, University of Wollongong, NSW, Australia.

[107] Lalanne C. (1999), Vibrations Sinusoidales, Hermes Science Publication.

[108] Li D., Ernest T. (1995), Wheel/track dynamic interaction—track substructure perspective, Vehicle Syst. Dynamics, 24, 183–196.

[109] Li D.Q., Salahifar T., Malone J., and Kalay S.F. (2005), Implementation of performance-based track geometry inspection on North American railroads. In Proceedings of the 8th International Heavy Haul Conference, Rio de Janeiro, Brazil, 553–560.

[110] Li M.X.D., Berggren E.G. (2010), A study of the effect of global track stiffness and its variations on track performance: simulation and measurement. Proceedings of the Institution of Mechanical Engineers, Part F: Journal of Rail and Rapid Transit, 224, 375–382

[111] Li M.X.D., Berggren E.G., and Berg M. (2009), Assessment of vertical track geometry quality based on simulations of dynamic track-vehicle interaction. Proceedings of the Institution of Mechanical Engineers, Part F: Journal of Rail and Rapid Transit, 223, 131–139

[112] Li M.X.D., Ekevid T., and Wiberg N.E. (2003), An integrated vehicle–track-ground model for investigating the wheel/rail dynamic forces due to high axle loads. In Proceedings of the 6th International Conference on Contact Mechanics and Wear of Rail/Wheel Systems (CM2003), Gothenburg, Sweden, 10–13 June 2003, 295–300.

[113] Liang B., Zhu D. (2001), Dynamic analyisis of the vehicle-subgrade model of a vertical coupled system, Journal of Sound and Vibration, (245), 79-92.

[114] Lichtberger B. (2010), Track compendium, Eurail Press.

[115] Lombard P.J. (1978), Track structure-optimization of design, Heavy Haul Railway Conference, Institute of Engineers, Australia, Perth.

[116] LUSAS. (2005), LUSAS finite element analysis system user manual, version 13.8, FEA Ltd., Kingston upon Thames, Surrey, UK.

[117] Mackworth A. (1977), Consistency in networks of relations, Artificial Intelligence.

[118] Metrikine A.V., Popp K. (1998), Vibration of a periodically supported beam on an elastic half-space, European Journal of Mechanics and Solids 18, 679–701.

[119] MIDAS Information Technology Co. Ltd. (2009), MIDAS/FEA user manual, Joongwon-gu, Seongnam, Gyeonggi-do, Korea.

[120] Ministry of Land, Transport and Maritime Affairs. (2011), Korean standard of railway design, Part: Subgrade.

[121] Mitchell L. (1986), Signal processing and the Fast Fourier Transform (FFT) Analyser: A survey, International Journal of Modal Analysis, January, 24-36.

[122] Montanari U. (1974), Networks of constraints: fundamental properties and applications to picture process, Information Science.

[123] Moore R. E. (1966), Interval Analysis, Prentice-Hall, Englewood cliffs.

[124] Na S.H., et al. (2007), Experimental study on the variation of track stiffness between earthwork and bridge, Proceedings of the Korean society for railway autumn conference, 281-288 (in Korean).

[125] Narayanan R.M., Jakub J.W., Li D., and Elias S.E.G. (2004), Railroad track modulus estimation using ground penetrating radar measurements. NDT&E Int, 37(2), 141–151.

[126] Naudé F.P. (2005), Development of a methodology for calculating stresses in track components, Master of Engineering (Mech) Thesis, University of Pretoria.

[127] Naudé F.P., Frohling R.D., and Theron N.J. (2005), Development of a methodology to calculate stresses in track components, Journal of rail and rapid transit, Proceedings of the institution of mechanical engineering, vol. 219, No. F4, 213-224

[128] Neilsen J.C.O. (1991), Eigenfrequencies and eigenmodes of beam structures on an elastic foundation, Journal of Sound and Vibration, 145, 479–487.

[129] Nielsen J.C.O. (2006), High-frequency vertical wheel–rail contact forces – validation of a prediction model by field testing. In Proceedings of the 7th International Conference on Contact Mechanics and Wear of Rail/Wheel Systems (CM2006), Brisbane, Australia, 24–27 September 2006, 41–48.

[130] Nielsen J.C.O., Lundén R., Johansson A., and Vernersson T. (2003), Train–track interaction and mechanisms of irregular wear on wheel and rail surfaces. Vehicle System Dynamics, 40(1–3), 3–54.

[131] Nordborg A. (1995), Vertical rail vibrations: noise and structureborne sound generation. PhD Thesis, Department of Technical Acoustics, KTH, Stockholm.

[132] Oakdale Engineering. (2005), DataFit User's Manual, Oakdale Engineering, Oakdale, PA, USA.

[133] Okada K., Ghataora G.S. (2002), Use of cyclic penetration test to estimate the stiffness of railway subgrade, K. Okada, NDT&E international, 35, 65–74.

[134] Older W. J., Velino A. (1993), Constraint Arithmetic on Real Intervals, Constraint Logic Programming: Selected Research, 175-196, MIT Press.

[135] OriginLab Corporation. (2003), Origin manual, Version 7.5, One Roundhouse Plaza, Northampton, MA.

[136] Oviedo-Marlot X. (2001), Etude du comportement du ballast par un modele micromecanique, These de l'Ecole Nationale des Ponts et Chaussees.

[137] Pandrol. (2003), Tests on studded rubber rail pads to establish a technique for measurement of high frequency dynamic stiffness of rail pads. Report no.41369-1.

[138] Persson I. (2006), Using GENSYS.0603, (DEsolver, Östersund).

[139] Plenge M., Lammering R. (2003), The dynamics of railway track and subgrade with respect to deteriorated sleeper support. In: K. Popp und W. Schiehlen (Ed.), System Dynamics and Long- term Behaviour of Railway Vehicles, Track and Subgrade, Springer Verlag, Berlin Heidelberg, Germany, 295-314.

[140] Polach O., Berg M., and Iwnicki S. (2006), Simulation. In Handbook of railway vehicle dynamics (Ed. S. Iwnicki), ch. 12, 359–421 (Taylor & Francis Group).

[141] Popp K., Kruse H., and Kaiser I. (1999), Vehicle–track dynamics in the mid-frequency range. Vehicle System Dynamics, 31, 423–464.

[142] Priest J. A., Powrie W. (2009), Determination of Dynamic Track Modulus from Measurement of Track Velocity during Train Passage. Journal of Geotechnical & Geoenvironmental Engineering, Volume 135, Issue 11, 1732–1740

[143] Oostermeijer K.H., Kok A.W.M. (2000), Dynamic behavior of railway superstructure, HERON, vol.45, No.1 / ISSN 0046-7316, 25–34.

[144] Rail Safety & Standards Board. (2005), Review of the effect of track stiffness on track performance, Evergreen House, 160 Euston Road, London NW1 2DX, UK, February.

[145] Rail Safety and Standards Board. (1993), Permissible Track Forces for Railway Vehicles, London, Group Standard GM/TT0088, Issue 1, Revision A (Online http://www.rgsonline.co.uk).

[146] Rail Safety and Standards Board. (1995), Commentary on Permissible Track Forces for Railway Vehicles, London, Technical Commentary GM/RC2513, Issue 1 (Online http://www.rgsonline.co.uk).

[147] RAILPROF Manual (2011), Esveld Consulting Services BV, Zaltbommel, The Netherlands (www.esveld.com).

[148] Railway Technical Research Institute. (1997), Design Standard and Manual for Railway Structure (Ballasted Track), Japan.

[149] Ravishankar N., Dey D.K. (2002), A First Course in Linear Model Theory, Chapman and Hall/CRC, Boca Raton, Florida, USA.,101

[150] Raymond G.P. (1978), Design for railroad ballast and subgrade support, Journal of the Geotechnical Engineering Division ASCE, 104(1), 45-60.

[151] Remennikov A., Kaewunruen S. (2005), Investigation of vibration characteristics of prestressed concrete sleepers in free-free and in-situ conditions. In: Proceedings of Australian structural engineering conference 2005, Newcastle, Australia.

[152] Remennikov A., Kaewunruen S. (2007), A review on loading conditions for railway track structures due to train and track vertical interaction. Structural Control and Health Monitoring, in press.

[153] Remennikov A., Kaewunruen.S (2006), Experimental Investigation on Dynamic Railway Sleeper/Ballast Interaction, Experimental Mechanics,46, 57–66

[154] Sadeghi J. (1997), Investigation of characteristics and modeling of railway track system, PhD Thesis, School of Civil, Mining, and Environmental Engineering, the University of Wollongong, Australia.

[155] Sadeghi J. (2009), Fundamentals of analysis and design of railway ballasted track, Iran University of Science and Technology Publication, Tehran, Iran.

[156] Sahlin S., Sundquist H. (2001), Banmekanik.Kompendium I brobyggnad ,TRITA-BKN Report, number 62, Brobyggnad.

[157] Sato Y. (1995), Japanese studies on deterioration of ballasted track, Vehicle System Dynamics 24 (suppl.), 197–208.

[158] Sauvage G. (1993), Railway track vertical static behavior, Research Report, INRETS/LTN.

[159] Selig E.T., Li D. (1994), Track modulus: its meaning and factors influencing it, Transportation Research Record 1470, 47-54, USA.

[160] Selig E.T., Waters, J.M. (1994), Track geotechnology and substructure management, 1st Ed., Technology Development and Application Committee, on behalf of the Railways of Australia.

[161] Sheng X., Jones C.J.C., and Petyt M. (1999), Ground vibration generated by a load moving along a railway track, Journal of Sound and Vibration, 228, 129–156.

[162] Shenton M.J. (1978), Deformation of railway ballast under repeated loading conditions, Pergamon Press, Oxford.

[163] Sjoberg M. (2002), On dynamic properties of rubber isolators, Ph.D. Thesis, Department of Vehicle Engineering, Kungl Teknisa Hogskolan Royal Institute of Technology, Stockholm, Sweden.

[164] Smutny J. (2004), Measurement and analysis of dynamic and acoustic parameters of rail fastening, NDT&E International, 37, 119-129.

[165] Standards Australia. (2001), AS1085.19-2001 Railway track material - Part 19: Resilient fastening assemblies, Standards Australia.

[166] Standards Australia. (2003), AS1085.14-2003 Railway track material - Part 14: Prestressed concrete sleepers, Standards Australia.

[167] Steenbergen M.J.M.M., Esveld C. (2004), Proposal for New Rail Weld Geometry Standards (in Dutch), Report 7-04-220-7, ISSN 0169-9288, TU Delft, Delft.

[168] Steenbergen M.J.M.M., Esveld C. (2006), Rail Weld Geometry and Assessment Concepts, Vol. 220, J. of Rail and Rapid Transit, 257–271.

[169] Steenbergen M.J.M.M., Esveld C. (2006), Relation between the Geometry of Rail Welds and the Dynamic Wheel–Rail Response: Numerical Simulations for Measured Welds, Vol. 220, J. of Rail and Rapid Transit, 409–423.

[170] Steenbergen M.J.M.M., Esveld C., and Dollevoet R.P.B.J. (2005), New Dutch Assessment of Rail Welding Geometry, European Railway Review,11, 71–79.

[171] Steffens D.M. (2005), Identification and development of a model of railway track dynamic behavior, M.Eng. Thesis, School of Civil Engineering, Queensland University of Technology, QLD. Australia.

[172] Sun Y.Q., Dhanasekar M., and Roach D. (2004), Effect of track geometry irregularities on wheel–rail impact forces. In: Proceedings of the Conference on Railway Engineering, Darwin, 20–23 June 2004.

[173] Teodoru I.B., TOMA I.O. (2009), Numerical analysis of plate loading test, Bul. Inst. Polit. Iasi, Tomul, LV (LIX), f. 1.

[174] Thompson D.J., van Vliet W.J., and Verheij J.W. (1998), Developments of the indirect method for measuring the high frequency dynamic stiffness of resilient elements, Journal of Sound and Vibration, 213(1), 169-188.

[175] Thompson D.J.,Jones C.J.C, Wu T.X., and France G.de (1999), The influence of the non-linear stiffness behaviour of rail pads on the track component of rolling noise, Proceedings of the Institution of Mechanical Engineers, Part F: Journal of Rail and Rapid Transit, 213, 233-241

[176] Timoshenko S. (1926), Method of analysis of statistical and dynamical stresses in rail. In: Proceedings of second international congress for applied mechanics, Zurich, 407–418.

[177] Track Design Technical Report (2005), Structural technical report (Track division), Shinbundang Line, Korea (in Korean).

[178] Track Design Technical Report (2006), Structural technical report (Track division), Seoul City Metro Line 9, Korea (in Korean).

[179] Tsang Edward. (1993), Foundation of Constraint Satisfaction, Academic Press, San Diego, CA, USA.

[180] TWINS (Track Wheel Interaction Noise Software). (1999), Theoretical and user's manual version 3.0, (TNO Institute of Applied Physics, Delft, The Netherlands).

[181] UIC project report. (2008), Vertical elasticity of ballastless track, International Union of Railways, 15 rue Jean Rey – F75015 Paris.

[182] UIC, ORE (1965), Question D71, Stresses in the Track, Ballast and Formation as a result of Rolling Loads, Stresses in Rails, Part 2: Calibration and Measuring Procedures. Report No.1, Utrecht, Holland.

[183] Van't Z. (1993), Assessment of dynamic characteristics of rail pads, Railway Engineering International 1994 Edition, 23(4), 15-17.

[184] Verheij J.W. (1982), Multi-path sound transfer from resiliently mounted shipboard machinery, Ph.D. Thesis, TNO Institute of Applied Physics, Delft University of Technology, the Netherlands.

[185] Vermij I., Graaf H.J., and Ginkel W.J. (2006), Evaluation of the track geometry using vehicle dependent assessment filters. NedTrain Consulting (internal report).

[186] Vincent G. (2001), Modal analysis and numerical modeling of a concrete railway sleepers, M.Eng. Thesis, Department of Structural Engineering, Chalmers University of Technology, Göteborg, Sweden.

[187] VTI report 595A (2007), Tilting Trains–Description and Analysis of the Present Situation (A Literature Study), Sweden.

[188] Wang J. (2002), The influence of track and vehicle properties on dynamic impact forces, Spoornet, submitted to Spoornet Engineering.

[189] Weaver Jr W., Timoshenko S.P., and Young D.H. (1990), Vibration Problems in Engineering, fourthed, Wiley, New York.

[190] Wolf J.P. (1994), Foundation Vibration Analysis using Simple Physical Models, Prentice-Hall, Englewood Cliffs, NJ.

[191] Wu T.X., Thompson D.J. (1999), The effects of local preload on the foundation stiffness and vertical vibration of railway track, Journal of Sound and Vibration, 219(5), 881-904.

[192] Wu T.X., Thompson D.J. (2004), The effects of track nonlinearity on wheel/rail impact, Proceedings of the Institution of Mechanical Engineers Part F: Rail and Rapid Transit; 218(1), 1-15.

[193] Zarembski A.M., Palese J. (2003), Transitions eliminate impact at crossings, Railway Track and Structures. August.

[194] Zaveri K. (1985), Modal Analysis of Large Structures – Multiple Exciter Systems, Naerum Offset, Denmark.

[195] Zhai W.M., Wang K.Y., and Lin J.H. (2004), Modelling and experiment of railway ballast vibrations, Journal of Sound and Vibration, 270, 673–683.

[196] Zhou Ye. (2003), Engineering Qualitative Analysis and Its Application on Fatigue Design Steel Structures, PhD Thesis, University of British Columbia.

[197] Zhou Ye., Stiemer S. F. (1998), Qualitative and Semi-Quantitative Analysis of Welding Distortion, Proceeding of Structural Specialty Conference of CSCE.